AD-A041 095 SYSTEMS CONTROL INC PALO ALTO CALIF F/G 17/7
AN OPERATIONAL EVALUATION OF OMEGA FOR CIVIL AVIATION OCEANIC N--ETC(U)
FEB 77 F KARKALIK, E WISCHMEYER DOT-FA75WA-3662
UNCLASSIFIED FAA-RD-77-65 NL
1 OF 3
AD A041 095

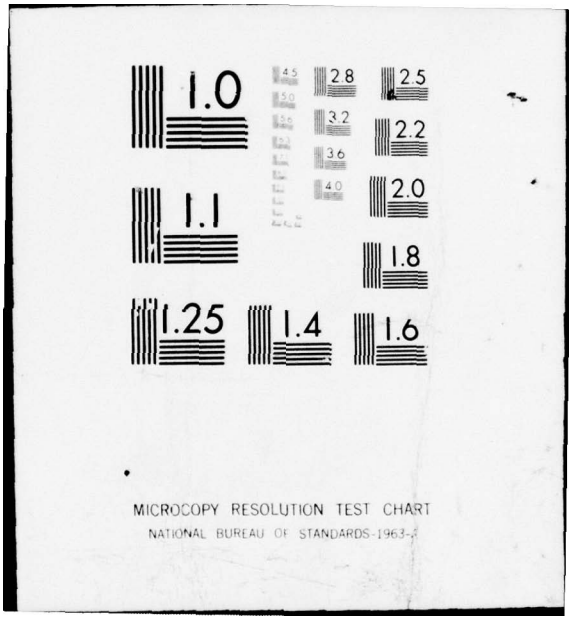
1.0
1.1
1.25
1.4
1.6
1.8
2.0
2.2
2.5
2.8
3.2
3.6
4.0
4.5
5.0
5.6
MICROCOPY RESOLUTION TEST CHART
NATIONAL BUREAU OF STANDARDS-1963-A

AD A041095

Report No. FAA-RD-77-65

2
NW

AN OPERATIONAL EVALUATION OF OMEGA FOR CIVIL AVIATION OCEANIC NAVIGATION

DISTRIBUTION STATEMENT A
Approved for public release;
Distribution Unlimited

DDC
JUN 30 1977
B

FEBRUARY 1977

FINAL REPORT

Document is available to the U.S. public through
the National Technical Information Service,
Springfield, Virginia 22161.

Prepared for

U.S. DEPARTMENT OF TRANSPORTATION
FEDERAL AVIATION ADMINISTRATION
Systems Research & Development Service
Washington, D.C. 20590

AD No.____
DDC FILE COPY

Technical Report Documentation Page

1. Report No.	2. Government Accession No.	3. Recipient's Catalog No.
FAA-RD-77-65		

4. Title and Subtitle	5. Report Date
An Operational Evaluation of Omega for Civil Aviation Oceanic Navigation.	February 1977 (12) 278 p.
	6. Performing Organization Code
7. Author(s) F. Karkalik, E. Wischmeyer	8. Performing Organization Report No.
9. Performing Organization Name and Address Systems Control, Inc. (Vt) 1801 Page Mill Road Palo Alto, California 94304	10. Work Unit No. (TRAIS)
	11. Contract or Grant No. DOT-FA75WA-3662
12. Sponsoring Agency Name and Address U.S. Department of Transportation Federal Aviation Administration Systems Research and Development Service Washington, D.C. 20590	13. Type of Report and Period Covered Final Report. Covering Aug, 1975 — Feb, 1977
	14. Sponsoring Agency Code ARD-333

15. Supplementary Notes

16. Abstract

Interest in Omega navigation for satisfying oceanic air navigation requirements is rapidly increasing. In particular, Omega is under serious consideration by major airlines as a Loran-A replacement. This report describes a flight evaluation program performed from August 1975 to September 1976 on oceanic routes to Central and South America, and over the Atlantic and Pacific Oceans. The primary objective of this work was to determine the operational reliability and suitability of Omega navigation for satisfying oceanic air navigation requirements. More than 300 hours of data were gathered, including data on the new stations Liberia, La Reunion, and Argentina. Omega was found to be a satisfactory Loran-A replacement, with adequate signal strengths and geometries in most areas evaluated.

17. Key Words	18. Distribution Statement
Omega Navigation Oceanic Navigation Civil Aviation Navigation Systems	**Document is available to the U.S. public through the National Technical Information Service, Springfield, Virginia 22161.**

19. Security Classif. (of this report)	20. Security Classif. (of this page)	21. No. of Pages	22. Price
UNCLASSIFIED	**UNCLASSIFIED**	**273**	

Form DOT F 1700.7 (8-72) Reproduction of completed page authorized

389 333

METRIC CONVERSION FACTORS

Approximate Conversions to Metric Measures

Symbol	When You Know	Multiply by	To Find	Symbol
	LENGTH			
in	inches	*2.5	centimeters	cm
ft	feet	30	centimeters	cm
yd	yards	0.9	meters	m
mi	miles	1.6	kilometers	km
	AREA			
in^2	square inches	6.5	square centimeters	cm^2
ft^2	square feet	0.09	square meters	m^2
yd^2	square yards	0.8	square meters	m^2
mi^2	square miles	2.6	square kilometers	km^2
	acres	0.4	hectares	ha
	MASS (weight)			
oz	ounces	28	grams	g
lb	pounds	0.45	kilograms	kg
	short tons (2000 lb)	0.9	tonnes	t
	VOLUME			
tsp	teaspoons	5	milliliters	ml
Tbsp	tablespoons	15	milliliters	ml
fl oz	fluid ounces	30	milliliters	ml
c	cups	0.24	liters	l
pt	pints	0.47	liters	l
qt	quarts	0.95	liters	l
gal	gallons	3.8	liters	l
ft^3	cubic feet	0.03	cubic meters	m^3
yd^3	cubic yards	0.76	cubic meters	m^3
	TEMPERATURE (exact)			
°F	Fahrenheit temperature	5/9 (after subtracting 32)	Celsius temperature	°C

*1 in = 2.54 (exactly). For other exact conversions and more detailed tables, see NBS Misc. Publ. 286, Units of Weights and Measures, Price $2.25, SD Catalog No. C13.10:286.

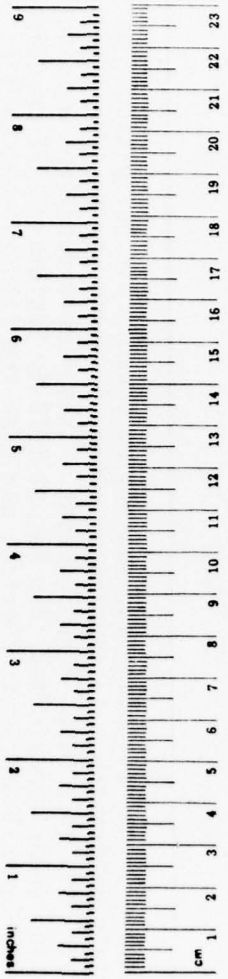

Approximate Conversions from Metric Measures

Symbol	When You Know	Multiply by	To Find	Symbol
	LENGTH			
mm	millimeters	0.04	inches	in
cm	centimeters	0.4	inches	in
m	meters	3.3	feet	ft
m	meters	1.1	yards	yd
km	kilometers	0.6	miles	mi
	AREA			
cm^2	square centimeters	0.16	square inches	in^2
m^2	square meters	1.2	square yards	yd^2
km^2	square kilometers	0.4	square miles	mi^2
ha	hectares (10,000 m^2)	2.5	acres	
	MASS (weight)			
g	grams	0.035	ounces	oz
kg	kilograms	2.2	pounds	lb
t	tonnes (1000 kg)	1.1	short tons	
	VOLUME			
ml	milliliters	0.03	fluid ounces	fl oz
l	liters	2.1	pints	pt
l	liters	1.06	quarts	qt
l	liters	0.26	gallons	gal
m^3	cubic meters	35	cubic feet	ft^3
m^3	cubic meters	1.3	cubic yards	yd^3
	TEMPERATURE (exact)			
°C	Celsius temperature	9/5 (then add 32)	Fahrenheit temperature	°F

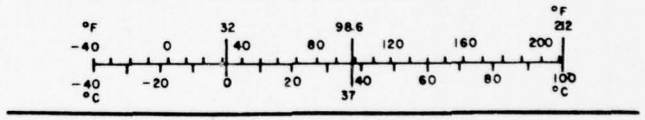

CONTENTS

White Section
Buff Section
DISTRIBUTION/AVAILABILITY CODES
Dist. AVAIL. and/or SPECIAL
A1

CONTENTS (Continued)

FIGURES

FIGURES (Continued)

TABLES

SUMMARY AND CONCLUSIONS

An evaluation of Omega navigation was conducted over most of Pan Am's routes, including flights over the North Atlantic, the Pacific, and flights to South America. Data were collected on revenue flights from August 1975 through September 1976 to evaluate the operational reliability and suitability of Omega, particularly 3.4 kHz difference frequency Omega, for bounding the errors of self-contained navigation systems such as Doppler radar and inertial navigation. This evaluation was intended to provide information on the acceptability of Omega as a Loran-A replacement. Data were acquired on more than 300 operational flight hours.

It is concluded in general that Omega is suitable for bounding the errors of self-contained navigation systems, and should be a satisfactory Loran-A replacement. In addition, full three frequency Omega was observed to exhibit better accuracy than the 3.4 kHz difference frequency operating mode, particularly in weaker signal environments. The conclusions are based upon: the flight records, including numerical data on Omega system performance; numerical comparisons of Omega performance referenced to other position sensors; the evaluation of Omega performance by the inflight observer; and information provided by the inflight observer on flight conditions.

Specific conclusions are:

(1) Omega signal availability appears to be adequate over the oceanic routes evaluated, which were: North Atlantic, South America to Africa over the South Atlantic, East Coast routes to South America, and routes over the South and Western Pacific.

(2) The reliability of the Omega transmitters appears to be satisfactory for oceanic air navigation. Only one unscheduled transmitter off-air period which resulted in an inadequate number of signals being available was noted.

(3) System accuracy was generally observed to be 1-2 nm. However, position comparisons between Omega and other navigation systems showed disagreements larger than 2 nm. The overall position discrepancy between Omega and other on-board sensors showed roughly a 6 nm standard deviation, based on about one hundred observations.

(4) Omega should be a satisfactory replacement for Loran-A in the role of bounding the errors of self-contained navigation systems, based on the accuracy and reliability observed in the flight evaluation. Omega will also provide a new long-range navigation system capability for bounding self-contained navigation system errors in many areas which do not presently have Loran-A service.

(5) Omega signal availability in some regions may be marginal, especially if one or more transmitters are not operating. These problem areas include North America, especially coastal waters to the west, and certain areas near the West Indies and Australia. The commissioning of the Australian station will help signal availabilities in the southwest Pacific, but decommissioning of the Trinidad station will reduce signal availability to a marginal level over some areas of CONUS and CONUS off-shore, including the Gulf of Mexico.

(6) The theoretical advantages of 3.4 kHz difference frequency Omega -- primarily reduced sensitivity to anomalous propagation -- were not directly observable in this evaluation program. The 3.4 kHz difference frequency operating mode was observed to be less accurate than the full three frequency operating mode, as indicated both by receiver RMS position error estimates and by off-line statistical comparisons with other navigation sensors.

RECOMMENDATIONS

(1) Analysis of data gathered on different days over the same routes showed that a single flight over a given route would not provide sufficient data for a thorough evaluation of Omega coverage and signal-to-noise ratios on that route. Therefore, it is recommended that more data be acquired on routes already flown. Analysis of data gathered over the North Atlantic suggests that a minimum requirement is ten flights on each route of interest in each direction.

(2) For completeness of the data base, it is recommended that data be gathered on oceanic routes other than those evaluated during this program. Specifically, Omega data should be gathered on polar routes and North Pacific routes.

(3) It is recommended that flight comparisons of different makes of Omega receivers be made to assess the position location dispersion of the receivers under identical signal conditions. The characteristics of different Omega receivers using the same airspace must be understood in order to properly integrate Omega navigation into the airspace system.

(4) A flight evaluation of four frequency Omega is recommended to determine its performance characteristics, including;

- Probability of successful lane ambiguity resolution in the 288 nm wide lanes of four frequency Omega.
- Accuracy improvement (if any) attributable to the inclusion of the fourth frequency.

- Probability of receiving at least one of four Omega frequencies from a given transmitter, compared to the probability of receiving at least one of three Omega frequencies from a given transmitter.

(5) It is recommended that monitor station evaluations be performed to supply four frequency Omega performance characteristics as measured in the simpler case of a fixed, rather than moving, Omega receiver. Fixed monitor data can inexpensively provide information on:

- Accuracy of different four frequency Omega signal processing schemes.
- Probabilities of successful lane resolution.
- Response of different signal processing schemes to varying propagation phenomena, such as SIDs, PCAs, and diurnal variations.
- Required modifications to propagation correction models.

I. INTRODUCTION

As a result of increasing interest in the use of Omega for air navigation, the FAA has initiated a number of programs to evaluate the suitability of Omega for meeting specific civil air navigation requirements. Oceanic air navigation requirements in particular are of immediate interest due to the scheduled shutdown of Loran-A. This report details the findings of an evaluation of Omega in an operational environment for satisfying oceanic requirements. This work as conducted by Systems Control, Inc. (Vt) [SCI (Vt)] as part of its navigation systems support contract with the FAA.

Three objectives were pursued in the flight evaluation program, which evaluated both 3.4 kHz difference frequency Omega and full three frequency Omega operation. The objectives were:

- To evaluate 3.4 kHz difference frequency Omega for operational suitability and reliability as a civil navigation aid for oceanic routes.
- To evaluate 3.4 kHz difference frequency Omega as a system for bounding the errors of self-contained navigation systems such as Doppler radar and non-redundant inertial.
- To evaluate full three frequency Omega for operational suitability and reliability, and for error bounding, with particular attention paid to signal quality and availability.

The flight evaluation program was not designed specifically to evaluate the performance of the Omega receivers used, but rather the receivers were used as engineering tools (e.g., to collect system data). Precise determination of Omega

accuracy was not a primary objective because no calibrated position reference was available. Statistics were generated, however, which compare Omega to other on-board navigation systems.

A candidate for bounding the errors of self-contained navigation systems is 3.4 kHz difference frequency Omega. 3.4 kHz difference frequency Omega refers to a technique for processing the raw Omega phase data. Using this technique, measurements of signal phase from each station at 13.6 kHz and 10.2 kHz are subtracted to form 3.4 kHz difference frequency measurements. These difference frequency measurements may be processed directly into a position estimate, instead of separately processing the 10.2 kHz and 13.6 kHz measurements. A significant theoretical advantage of this method is the attendant greater distance between adjacent lines of position with the same phase measurement (i.e., wider lanes). Additionally, since propagation anomalies (sudden ionospheric disturbances (SIDs), for example) have correlated effects at 10.2 kHz and 13.6 kHz, the subtraction in the difference frequency scheme can reduce the effect of these anomalies. 3.4 kHz difference frequency Omega can be less accurate because the 3.4 kHz phase measurement is less sensitive to changes in position, and it can be more sensitive to effects of additive noise. A further disadvantage is the requirement for receiving two signals from an individual transmitter in order that the transmitter be usable for navigation.

Full three frequency Omega is also under consideration for oceanic and long-range air navigation. Analysis of data gathered on early flights showed that 3.4 kHz difference

frequency Omega and full three frequency Omega have similar characteristics, including similar accuracies and susceptibilities to Omega propagation effects. This study collected valuable information on Omega operational suitability and reliability, and signal quality and availability. The flight evaluation program was extended to allow more information to be gathered. This ensured that a broader data base would be obtained on normal Omega operation along with more opportunities to observe any anomalous propagation effects. Since Omega is being evaluated as a Loran-A replacement, the capability of Loran-A as applied to air navigation was considered as part of the evaluation criteria.

The Omega evaluation program was conducted by SCI (Vt) with the cooperation and assistance of Pan American World Airways and the Canadian Marconi Company (CMC). Pan Am furnished the Boeing 707 evaluation aircraft, the receiver installations, and trained navigators who operated the receiver, gathered data on scheduled flights, and supplied the data to SCI (Vt) for analysis. CMC provided installation support and technical information on hardware operation. SCI (Vt) processed the collected data to satisfy the program objectives listed above. The first data collection flight was performed on August 19, 1975, and the last data collection flight of this program was performed on September 20, 1976. During this time interval, Omega flight data was acquired over the North Atlantic, the Pacific, and on routes to Central and South America.

The flight evaluation program was formally divided into Phases A and B, as described in Table 1.1. Note particularly that in Phase A and the first part of Phase B, the

TABLE 1.1 - CHARACTERISTICS OF PHASES A AND B DATA COLLECTION

PHASE	DATES	RECEIVER	ANTENNA	DATA RECORDING	ROUTES EMPHASIZED	AIRCRAFT
A	8/75-9/75	CMC 740P	E-Field	Manual	North Atlantic	Boeing 707, N872PA
B	3/76-5/76	CMC 740P	H-Field	Manual & Automatic	Pacific, South America	Boeing 707, N427PA
B	6/76-9/76	CMC 740	H-Field	Manual	South America	Boeing 707, N427PA

receiver used was a Canadian Marconi 740P. This prototype receiver had additional software to allow it to operate in both the 3.4 kHz difference frequency mode and a conventional three frequency mode. In the second part of Phase B, the receiver used was a production model 740, which did not have the difference frequency capability.

Table 1.2 shows the Omega transmitter complement during Phases A and B. Of the eight Omega transmitters presently operating (this includes Trinidad but not the Australian station), the five most northerly stations were usable during Phase A. This station complement utilized in the Phase A flights gave essentially the same signal coverage over the North Atlantic as that expected from the final Omega station configuration. Phase B flight evaluations exploited the availability of new stations as they became operational.

Data collection was accomplished by an Omega observer/operator who maintained logs on flight conditions and Omega receiver parameters. This information, along with a limited amount of automatically recorded data in Phase B, was processed into plots of signal-to-noise (S/N) ratios for each station on each flight. Comparisons of Omega-indicated position with the outputs of other navigation sensors were used to compute statistical data.

The remainder of the report is organized into the following chapters:

- Chapter II briefly discusses 3.4 kHz difference frequency Omega.
- Chapter III describes the hardware used in the evaluation.
- Chapter IV describes the data collection and reduction processes.

TABLE 1.2 - OMEGA STATION COMPLEMENT IN PHASES A AND B

TIME SLOT	OMEGA STATION USING TIME SLOT (PHASE A)	OMEGA STATION USING TIME SLOT (PHASE B)	DATE NEW STATION USABLE IN TIME SLOT
A	Norway	Norway	Dec. 73
B	Trinidad	Liberia	18 Feb. 76
C	Hawaii	Hawaii	Jan. 75
D	North Dakota	North Dakota	Oct. 72
E	---	La Reunion	1 Mar. 76
F	---	Argentina	1 July 76 - Test Status from Sept. 75
G	---	Trinidad	1 Feb. 76
H	Japan	Japan	Apr. 75

- Chapter V presents the results of the flight evaluation program. Separate subsections of this chapter discuss results obtained in individual geographic regions.

The following four appendixes are included:

- Appendix A discusses composite Omega, a special case of which is 3.4 kHz difference frequency Omega.
- Appendix B contains S/N ratio plots of all stations received during the flight evaluation program.
- Appendix C presents comparative analysis of Loran-C, VLF communications, and Omega transmitter performance, based upon U.S. Naval Observatory Time Series data.
- Appendix D reviews previous Omega tests and evaluations.

II. COMPOSITE OMEGA AND DIFFERENCE FREQUENCY CONCEPTS

Composite Omega, a special case of which is 3.4 kHz difference frequency Omega, is a technique for taking optimal or suboptimal linear combinations of Omega phase data from the same Omega station at two or three different frequencies. Composite Omega can be useful for reducing the effects of both predictable and unpredictable propagation anomalies. It is much simpler to implement than full predicted propagation correction programs. In addition, composite Omega can be used for lane ambiguity resolution. The primary disadvantages of composite Omega are a requirement for Omega signals to be available at two frequencies from each station used and a greater sensitivity to phase measurement noise. Composite Omega is derived and discussed in detail in Appendix A. This section discusses the special case, 3.4 kHz difference frequency Omega, in general terms.

3.4 kHz difference frequency Omega operates by differencing the phase measurements at 10.2 and 13.6 kHz in order to form the following 3.4 kHz "phase measurement":

$$\varphi_{3.4} = \varphi_{13.6} - \varphi_{10.2} \tag{2.1}$$

The 3.4 kHz phase measurements are then processed for navigation in the same way as other phase measurements. The "3.4 kHz signals" are considered to propagate at roughly the same speed as the 10.2 and 13.6 kHz signals.

The advantages of 3.4 kHz difference frequency Omega are greater lane width and reduced sensitivity to anomalous propagation, as compared to full three frequency operation. The lanes of the 3.4 kHz difference frequency have a spacing of 24 nm along the baseline, as opposed to 8 nm for 10.2 kHz and 6 nm for 13.6 kHz. This greater lane width results in a higher tolerance to errors in the external position estimates used to initialize receiver position. In addition, the wider lane operation can accommodate a longer duration of signal interruption without slipping a lane. Because the phase measurements at the two frequencies are subtracted, any errors correlated between the two phase measurements (phase errors due to Sudden Ionospheric Disturbances, Polar Gap Absorptions, surface conductivity, diurnal variations) will tend to be subtracted out. Thus, accuracy may be enhanced under some conditions of anomalous propagation. Lastly, when 10.2 kHz operation is possible as well as 3.4 kHz operation, the 3.4 kHz mode may be used to perform resolution of the 10.2 kHz lanes.

The advantages of 3.4 kHz difference frequency Omega are due to the joint processing of the 10.2 kHz and 13.6 kHz Omega signals. However, if signals are not available at both 10.2 and 13.6 kHz from a given station, then any receiver using only the 3.4 kHz difference frequency mode in the strictest sense will not be able to use any information from that station. With separate phase-locked loops for measuring the 10.2 and 13.6 kHz signals, if either phase-locked loop (PLL) slips a lane, the result in a simple receiver implementation will be that the receiver will slip a 3.4 kHz lane of 24 nm, rather than a 6 nm or 8 nm lane. Further, the 3.4 kHz phase measurement will be quite sensitive to phase noise, and for this reason, receiver time constants are often increased for 3.4 kHz operation.

III. EVALUATION EQUIPMENT

3.1 INTRODUCTION

This section describes the particular Omega navigation systems used in the flight evaluations, including the Omega set's operating features, installation, and interface with the aircraft and flight crew. The Canadian Marconi 740P Omega navigation system is discussed in some detail, including a comparison with the production model Canadian Marconi 740. The installation and use of these systems on the Boeing 707 are also discussed.

3.2 EVALUATION HARDWARE

3.2.1 General Description

The Canadian Marconi 740P Omega Navigation System is a fully automatic, computerized, three frequency Omega Navigation System suitable for transport aircraft. The receiver consists of three units: an antenna, a receiver/processor unit (RPU), and a control/display unit (CDU). The antenna can be either an E-field antenna or a steerable H-field antenna. The H-field antenna has a typical weight of about 4 lb, and is approximately 7" square and 2" high. The RPU is packaged in a 1/2 ATR box, weighs approximately 19 lb, and requires 400 Hz, 115v power. The RPU contains the receiver front end, H-field antenna steering matrix, and a general purpose processor which emulates the H-P 2100 minicomputer. The processor utilizes an 8K core memory with 16 bit words. The CDU closely resembles the CDUs used on inertial navigation systems, and presents the Omega data in

similar formats. The particular receiver used was purchased by the FAA for flight evaluation purposes, and contains additional features for use as a flight evaluation tool.

The Canadian Marconi 740P includes many features making it suitable for transport aircraft. The receiver is fully automatic, and requires initialization only of latitude, longitude, GMT, and date. Synchronization is performed automatically, as is station selection. All principal navigation parameters are computed and displayed in standard formats.

3.2.2 Receiver Operating Theory

The majority of the navigation system functions are performed by a general-purpose digital processor. The processor supplies outputs to the control display unit (CDU) and an external data stream output. It can also supply autopilot output signals. The information displayed is derived from measurements made by the RF section of the receiver and the aircraft air data system. These measurements can be processed in the normal three frequency mode or in the 3.4 kHz difference frequency mode.

The processor supplies information to the CDU both in the normal modes and also in a test mode. The normal operating modes of the CDU are described in the next section, and correspond closely to the operating modes of ARINC 561 inertial units. The test mode, however, provides to the operator information on the internal status of the processor which would otherwise not be available. Table 3.1 shows some of the primary parameters of interest available through the test mode.

TABLE 3.1 - CANADIAN MARCONI CMC-740P MEMORY LOCATIONS OF PRIME INTEREST AVAILABLE THROUGH TEST MODE

FORMAT	CONTENT	LOCATION	NOTE
3	S/N Ratios (A) to (F)	140 to 147 150 to 157 160 to 167 170 to 177	3.4 KHz 10.2 KHz 13.6 KHz 11.3 KHz
0	Frequency Switch	660	Cumulative Coding: "1" deselect 3.4 KHz "2" deselect 10.2 KHz "4" deselect 13.6 KHz "10" deselect 11.3 KHz Thus: "1" means "No 3.4 KHz" "16" means "Only 3.4 KHz" "0" means "Use All"
0	Diurnal Predict-ion Model	660	"1XXXXX" is "Pierce Model" " XXXXX" is "Navoceano Model" (Note: "XX..." is "Don't Care")
0	Choice of Stations (Cumulative Dis-play)	662	0 = Allow all Stations Eliminate H G F E D C B A 200 100 40 20 10 4 2 1
0	General Failure Flag	667	1 = A/D Failure 2 = TAS —— 4 = HDG —— 10 = N/A 20 = Osc. Drift 40 N/A 200 = Mag Tape Failure
0	Stations Log	737	Cumulative Display 3 Right-Most Digits: H G F E D C B A 200 100 40 20 10 4 2 1
0	Status Log	737	Cumulative Display "10XXXX" means "AMBIGUITY" " 4XXXX" means "DR" " 3XXXX" means "3.4 KHz Mode Note: "X" means "Don't Care"
1	Position Error (Estimated)	736	Nautic Miles 3: "AMBIGUITY" Status 10: "DR" Status 5: Do not use 3.4 KHz Mode
2 4 4 4	True Airspeed Heading From Synchro True Heading Computed Drift Angle, Computed	723 725 641 643	Knots Degrees ÷10
4 1 1	Magnetic Variation Distance to Stns (A to H) Stns Bearings (A to H)	1032 13440 13450	Degrees ÷ 10 In Naut. Miles In Degrees

Receiver software on the CMC 740P is capable of operating in the normal three frequency mode, the 3.4 kHz difference frequency mode, or in both modes simultaneously. Frequency-mode selection is manual with an automatic override. Included in Table 3.1 is the format of word 660, the "Frequency Switch" of the CMC 740P. By inputting an appropriate value into word 660, the Omega operator can select the desired Omega frequencies for the receiver to use. By deselecting the 10.2 kHz, 13.6 kHz, and 11.3 kHz frequencies, the receiver operates in the 3.4 kHz difference frequency mode. However, if the estimated position error (word 736) becomes greater than 5 nm, receiver software automatically reverts to the full three frequency mode of operation.

The processor derives a position estimate from a set of phase measurements combined with the air data and heading inputs. The phases of the Omega signals are determined in the processor, which closes three phase-tracking loops, one for each frequency. The phase measurements are combined to form lines-of-position (LOPs), and a least squares estimate of position is obtained by combining the LOP information with the previous position estimate, as updated by aircraft heading and true airspeed.

Propagation predictions are applied by the processor to correct phase measurements. These propagation corrections are obtained from a full propagation model, with solar illumination, surface conductivity, and magnetic field effects calculated.

The processor also supplies a data output signal in a pulse code modulated format for automatic data recording. Table 3.2 shows the parameters available on this data output. This data was recorded only in the Phase B flights with the CMC 740P. Use of the automatically recorded data is discussed below in Section 3.3.

TABLE 3.2 - CANADIAN MARCONI CMC-740P PARAMETERS AVAILABLE ON DATA OUTPUT STREAM

WORD NAME	WORD NO.	CONTENT	FORMAT	UNITS	RANGE
BLOCK NO. #1	1	SAMPLE NO.	16 BITS INTEGER	10 SEC STEPS	-32768 TO +32767
DATE	2 3 4	DAY MONTH YEAR	16 BITS INTEGER	DAY MONTH YEAR	0 31 0 12 0 94
HOUR	5 6	MINUTES HOURS	16 BITS INTEGER	0.1 MIN HOUR	0 599 0 23
TIME	7	SEE WORD DESCRIPTION	16 BITS INTEGER	0.1 SEC	0 99
XNB	8	USER CODE	16 BITS CODED		16 BITS
POSITION	9, 10 11, 12	LATITUDE LONGITUDE	FLOATING POINT	RADIANS N, E = + S, W = -	
GROUND SPEED VECTOR	13, 14 15, 16	SPEED TRACK	FLOATING POINT	KNOTS RADIANS	0 999 0 2
WIND VECTOR	17, 18 19, 20	SPEED DIRECTION	FLOATING POINT	KNOTS RADIANS	0 999 0 2
SYNCHRO INPUTS	21, 22 23, 24	HEADING TAS	FLOATING POINT	RADIANS KNOTS	0 2 0 999
RMS	25	RMS ERROR (ESTIMATED)	16 BITS INTEGER	NM	0 TO +32767
TX LOG	26	SEE WORD DESCRIPTION	16 BITS CODED		SEE WORD DESCRIPTION
FRSW	27	FREQ. SWITCH & DIURNAL MODEL	16 BITS CODED		SEE WORD DESCRIPTION
DISCR	28	DISCRETE INPUT SIGNALS	16 BITS CODED		SEE WORD DESCRIPTION
BITE SYNCHRO	29	SEE WORD DESCRIPTION	16 BITS CODED		SEE WORD DESCRIPTION
BITE SYSTEM	30	SEE WORD DESCRIPTION	16 BITS CODED		SEE WORD DESCRIPTION
BITE WARNINGS	31	SEE WORD DESCRIPTION	16 BITS CODED		SEE WORD DESCRIPTION
PHASES	32 TO 47	32 VALUES	8 BITS INTEGER	CECS	-99 +99
SNR	48 TO 63	32 VALUES	8 BITS INTEGER	SEE WORD DESCRIPTION	0 99
COR	64 TO 79	32 VALUES	8 BITS INTEGER	CECS *2	-128 +127
BLOCK NO. #2	80	SAMPLE NO	16 BITS INTEGER	10 SEC STEPS	-32768 TO +32767
CKSUM	81	CHECKSUM	16 BITS INTEGER		SEE WORD DESCRIPTION

3.2.3 System Operation

Figure 3.1 shows the CMC 740P CDU. Prominent in this figure are the mode select knob in the lower left, the numeric keyboard in the lower right, and two numeric display windows across the top. Additional devices are a series of ten annunciator lights across the top of the numeric display windows, an "Insert" pushbutton in the center of the CDU, "From/To" waypoint number display windows, an unlabeled waypoint number display, leg-change and waypoint definition pushbuttons, manual/automatic leg-change toggle switch, and a dimmer knob.

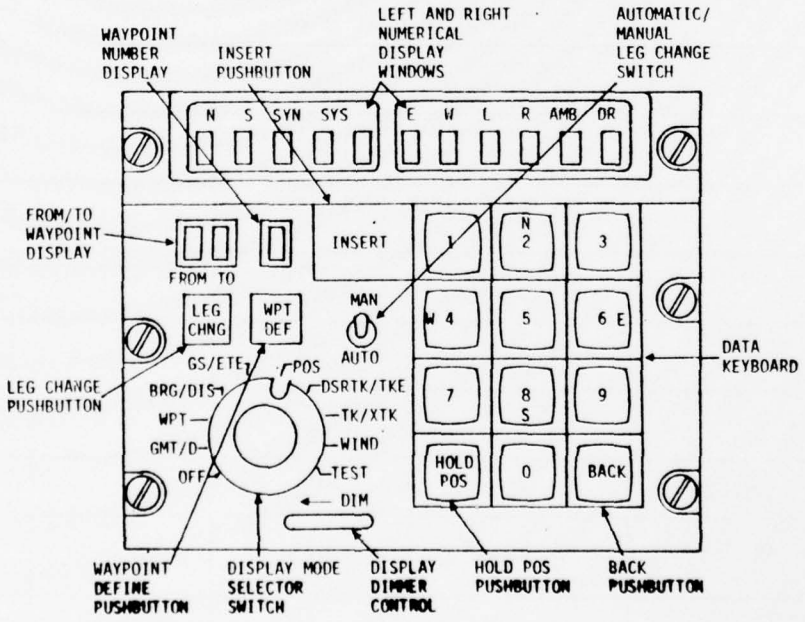

FIGURE 3.1 - CMC 740P CONTROL DISPLAY UNIT

Receiver initialization requires entering only the date, time, and present position. The Greenwich Mean Time is entered on the keyboard in hours, minutes, and tenths of minutes. Data format for latitude and longitude is degrees, minutes, and tenths.

With the receiver initialized, the principal navigation parameters can be read by turning the mode selector knob to the desired parameter and reading the results from the two display windows. Table 3.3 shows the parameters available, the units of the parameters, and the resolution of the display.

The test position on the mode select knob is used for reading internal receiver parameters. However, the procedure for reading these parameters is somewhat more involved than the procedure for reading the normal navigation parameters.

3.2.4 Receiver Checkout Tests and Installations

Over the course of the flight evaluation program, care was taken in receiver checkout and installation so that the data acquired would be quantitative and usable. Receiver checkouts were performed at the Canadian Marconi facilities in Montreal, using a computerized test system. The receiver checkout procedure involved exercising the Omega receiver in a flight simulated by a computerized test system. This evaluation procedure included checking of the synchronization time of the receiver, correct antenna steering, proper heading and air-data interface operation, and a number of other checks during the simulated flight. This detailed checkout procedure served to detect and isolate any faults in the receiver before flight evaluations began.

TABLE 3.3 - LIST OF DISPLAYED OUTPUTS FOR CMC-740P

Function Selector	Left Hand Display				Right Hand Display			
	Output	Range	Resolution	Up-Date	Output	Range	Resolution	Up-Date
OFF	Blank	-	-	-	Blank	-	-	-
GMT/D	Greenwich Mean Time	24 hours	0.1 min	6 sec	Calendar	100 years	1 day	6 sec
WPT	Latitude of Stored Waypoints (10)	± 90° N/S	0.1 min	-	Longitude of Stored Waypoints (10)	± 180° E/W	0.1 min	-
BRG/DIS	Great Circle Bearing to Destination	0° to 360°	1°	10 sec	Great Circle Distance to Destination	999.9 n.m.	1 n.m.	10 sec
GS/ETE	Aircraft Groundspeed	0 to 9999 knots	1 knot	10 sec	Estimated Time Enroute	0 to 9999 min	1 min	10 sec
POS	Latitude of Present Position	± 90° N/S	0.1 min	1 sec	Longitude of Present Position	± 180° E/W	0.1 min	1 sec
DSRTK/TKE	Great Circle Desired Track to Destination	0° to 360°	1°	10 sec	Great Circle Track Angle Error	0° to 180° L/R	1°	10 sec
TK/XTK	Great Circle Actual Track	0° to 360°	0.1°	10 sec	Cross Track Deviation	999.9 n.m. L/R	0.1 n.m.	10 sec
WIND	Wind Direction	0° to 360°	1°	10 sec	Wind Velocity	9999 kts	1 knot	10 sec
TEST	Displays all 8's Lamp test, N/S, SYS, SYN				Displays all 8's Lamp test, E/W, L/R, AMB, DR			

A total of three receiver installations were made in two different aircraft. Precautions were exercised in the installations to minimize any interference which might be generated on board the aircraft. These included skin mapping the aircraft when an H-field antenna was used. In the Phase A flights with the CMC 740P Omega navigation system, the 740P replaced a CMC 719 Omega navigation system which had previously been evaluated. By using the existing antenna and cabling, a debugged installation was available in a very short time, facilitating the initiation of the data collection procedure. The antenna used was a capacitive plate E-field antenna mounted in a spare radar-altimeter well on the underside of the aircraft. This antenna installation was susceptible to precipitation static, which is common to all E-field antennas. For the Phase B flights, a different Boeing 707 was used, and a steerable H-field antenna was installed. The aircraft was skin mapped to determine a good location for installation, so that interference from harmonics of 400 Hz skin currents would be minimized. The H-field antenna is fairly immune to precipitation static, but is somewhat more expensive than the E-field antenna. The steerable H-field antenna utilized additional software to control the antenna steering matrix and two preamplifiers at the antenna, rather than just one preamplifier as required by E-field antennas.

3.2.5 Description of Production Hardware

In the last part of the Phase B flight evaluations, the prototype Canadian Marconi 740P was replaced by a production model Canadian Marconi 740. The major differences were that the 740 did not have the 3.4 kHz difference frequency mode, nor did it have the data output signal for automatic data recording. Operation of the 740 was virtually identical to operation of the 740P.

3.3 BOEING 707 AND FLIGHT CREW

The platform for the flight evaluations of the Omega receivers was a Pan American Boeing 707 in scheduled passenger service. A full-time observer was present on the evaluation flights in order to operate the Omega equipment and to record quantitative and qualitative data.

Evaluation of the Omega receiver in regular, scheduled passenger service provided the most realistic operational test possible, and considerably reduced the cost of the flight evaluation. In scheduled service on regular oceanic routes, the Omega receiver was exposed to the environmental conditions of the avionics bay, including heat soaking at low-latitude ground stops. The Omega equipment was operated from the actual 400 Hz aircraft and ground power supplies, and exposed to on-board interference sources such as galleys. The duties performed by the Omega receiver operators included Omega set initialization and waypoint programming, quantitative data collection from both the normal Omega parameters and those parameters available through the test mode, and data collection from other on-board sensors. In addition, the observers recorded qualitative data regarding on-board conditions, external meteorological conditions, and abnormal Omega behavior. For example, the response of the Omega set to operation of the aircraft electrical system, landing-induced jumps of the position indicated by the Omega set, correlation of low S/N ratios with flights through clouds, and receiver overheating symptoms were all noted by the observers in flight. This information was of great importance in the evaluation of flight data.

IV. DATA COLLECTION AND DATA REDUCTION

4.1 INTRODUCTION

This section describes the data collection and data reduction procedures used on Phase A and Phase B flights. Data sources consisted of flight observer logs, magnetic tape recordings of the Omega receiver data output signal, and flight plans. The collected data was used to generate plots of S/N ratios observed in flight, to compare Omega to other data sources, and to provide information for determination of signal availabilities and other system characteristics of interest.

4.2 PHASE A DATA COLLECTION AND DATA REDUCTION

4.2.1 Analysis of Flight Observer Logs

The most important source of information on the Phase A flights was the log compiled on each flight by the Omega operator/observer. The log contained observations of flight conditions and Omega receiver performance in general, as well as numerical information obtained from the various displays of the Omega receiver. These observations included correlation of observed precipitation static with flights in clouds, observation of auroral activity, and records of such events as switching generators on the electrical bus powering the Omega receiver and testing the fire warning alarm. Additional information included readouts of Doppler radar parameters, air data indications, and waypoint passage. The use of these observations permitted development

of conclusions about many observed Omega system operational phenomena. Virtually none of the nonnumerical information provided by the flight observer would have been available with a fully automatic Omega data recording system.

Complete numerical information was also provided by the Omega operator/observer. These data were furnished on data sheets, and included the following parameters:

- Flight Number
- Data and Time
- Omega position
- Distance to go (Omega and DME or Doppler)
- Reference position (VOR/NDB overflight or Doppler position)
- S/N ratios on all stations at all frequencies
- Stations in use
- Warning flags (if any)
- Ground speed and track (Omega and Doppler)
- Wind estimate
- Flight conditions
- Receiver operating mode

Most of these parameters were read from the CDU using the mode select knob, but the S/N ratios and the receiver operating modes were read from the computer memory using the "Test" mode. Other data, such as VOR and NDB overflights or Doppler position, were read from the appropriate instruments. Nominally, manual data-recording intervals were 20 minutes.

The flight plans of the various flights were a useful supplement to the flight notes. Figure 4.1 shows the flight plan of a Phase A flight, specifically Flight 66, August 21, 1975. Although much of the information on the flight plan

.NYCWMPA 211959 CIDXNPA

PA 06621 N872 300C/A IAD FRA DRUMMEY
330/
SKD LV IAD 2155Z AR FRA 0540Z CRZ TAS 467

POSN	FL	ZTM/TTME	POSN	ETA / ATA	AW/TRK / DEV	DST	DTGO	MNO	TAS	WIND / TRKSET	GS / VAR	TODFL / DRFT	OAT / SPOT
IAD	CLB	033/0033	TOC		VAR	212		CLB	369		384	85.0	
TOC	330	008/0041	HAMPTON		VAR	061	3259	806	478	31046	496	72.6	
HTO	330	012/0053	NANTUCKT		DRCT	107	3198	806	477	31060	512	71.0	
ACK	370	020/0113	DAVES		J585	150	3091	805	465	31077	463	68.2	
DAVE	370	010/0123	YARMOUTH		J585	082	2941	805	465	31077	468		
YQI	370	016/0139	HALIFAX		HL575	133	2859	805	464	31086	490	61.8	
YHZ	370	020/0159	SYDNEY		HL575	160	2726	805	465	31076	491	58.5	
YQY	370	017/0216	RAMEA		HL577	136	2566	805	467	30054	484	54.5	
RZ	360	035/0251	49N50W		M099.8	309	2430	806	470	26052	520	51.2	
50W	360	043/0334	50N40W		M107.6	394	2121	806	470	23093	547	44.2	
40W	360	042/0416	51N30W		M104.6	386	1727	805	471	24095	557	35.9	
30W	360	043/0459	52N20W		M100.3	378	1341	804	468	28061	524	28.1	
20W	360	022/0521	52N15W		M105.8	185	963	802	465	31064	512	20.3	
15W	360	029/0550	CORK		M105.1	241	778	799	464	33069	498	16.4	
CRK	370	016/0606	MERLIN		UR37	134	537	802	467	32050	501	11.4	
MRL	410	016/0622	IBSLEY		UR37	126	403	806	469	28019	488	8.6	
IBY	410	014/0636	DOVER		UR37	119	277	807	468	21031	491	5.7	
DVR	410	006/0642	KOKSY		UG1	049	158	807	466	20046	482	3.3	
KOK	410	014/0656	TOD		UG1	109	109	807	463	20053	465	2.3	
TOD	DES	023/0719	FRANKFRT		VAR	139		DES	364		361	0.0	

TOGW	BURN	LGW	DESFL	TIME	COMP	AVTAS/GS	AIRMILES/GND	COST
286.0	87.7	198.3	2.7	0719	P38	455/493	3332/3610	

ADDITIONAL FLTPLAN INFO
TRK CRZ TOGW FUEL TIME COST LEVELS
LRC 286.0 89.2 0725 64 330 RZ/340 CRK/330

PZ ED 212155 MET 211200

FIGURE 4.1 - FLIGHT PLAN FOR PAN AMERICAN FLIGHT 66, AUGUST 21, 1975

was not used in the analysis of each flight, the availability of this data often allowed fine points in Omega system performance to be resolved. The columns of information on the flight plan are, from the left: "From" waypoint, flight level, segment time enroute/total time enroute, "To" waypoint, route segment, segment length, total distance to go, Mach number, true airspeed, wind, groundspeed, and estimated percent of fuel until top of descent.

4.2.2 Generation of S/N Ratio Plots

A number of S/N ratio plots were generated for each of the Phase A flights. The plots followed the same format for all of the Phase A flights, and for the entire flight evaluation program.

On the Phase A flights, five plots were generated for each flight. These plots documented S/N ratios of the five Omega stations transmitting during Phase A (Norway, Trinidad, Hawaii, North Dakota, and Japan). Figure 4.2 shows a typical plot. The vertical axis is S/N ratio observed through a 50 Hz bandwidth, and the horizontal scale is Greenwich Mean Time. Plots were made of the S/N ratios at 10.2 kHz, 13.6 kHz, and 3.4 kHz. The 3.4 kHz S/N ratio is nominally the lower of the 10.2 kHz and the 13.6 kHz S/N ratios. 11-1/3 kHz data was also collected, but not processed.

Generating the S/N ratio plots required conversion of the internal S/N parameter to S/N ratio in dB through 50 Hz. Figure 4.3 shows the graph which contains the conversion information. A set of polynomials were fitted piecewise to this graph and programmed on a Univac 1108. The numerical information on S/N ratios from each station was keypunched, entered into the computer, converted using the polynomial curve-fit, and plotted using a standard plotting routine.

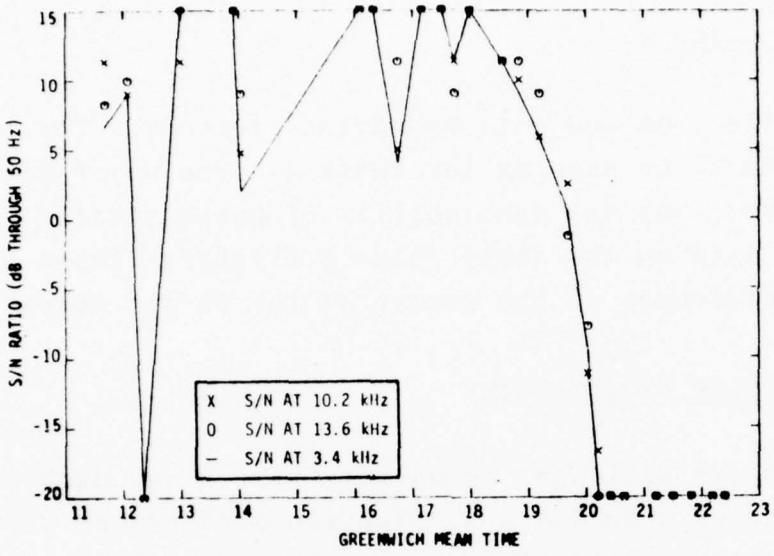

FIGURE 4.2 - S/N PARAMETERS, STATION A, FRANKFURT-CHICAGO, FLIGHT 59, AUGUST 28, 1975

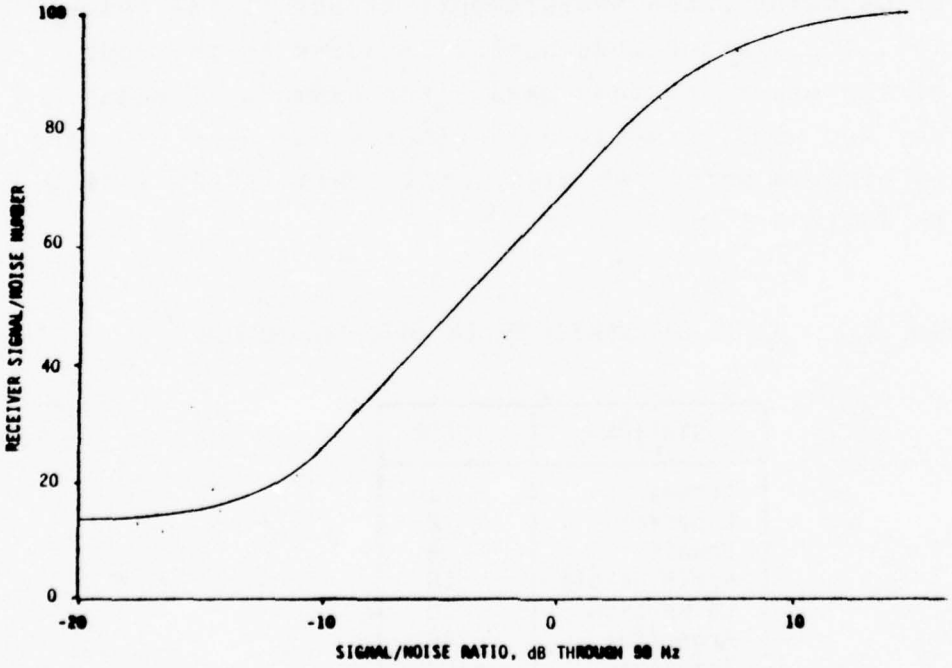

FIGURE 4.3 - CONVERSION OF S/N NUMBER TO S/N IN dB THROUGH 50 Hz

4.3 PHASE B DATA COLLECTION AND DATA REDUCTION

4.3.1 Introduction

Data collection and data reduction procedures for Phase B were much the same as for Phase A. The major difference, however, was the availability of automatically recorded flight data on the early Phase B flights. There were also minor differences in the format of the flight notes.

4.3.2 Analysis of Flight Notes

The analysis of flight notes for Phase B was much the same as the analysis in Phase A. The two differences were different formats for flight notes in Phase B and the use of special numerical data recording forms in the latter part of Phase B with the CMC 740. Table 4.1 shows the code for the stations in use. If a station was used in the position solution using phase measurements at any of the three frequencies, the station code number is added to the code numbers of the other stations used. For example, 1 means only Norway was used, 2 means only Liberia was used, 3 means Norway and Liberia were both used, etc. This is the same code as in Table 3.1.

TABLE 4.1 - CODE OF STATIONS IN USE PARAMETER

STATION	CODE
Norway	1
Liberia	2
Hawaii	4
North Dakota	10
La Reunion	20
Argentina	40
Trinidad	100
Japan	200

4.3.3 Software for Reading Data Tapes

The philosophy of the automatic data collection was that the automatic data collection be a supplement to, and not a replacement for, the flight notes. As well as recording the required numerical information, the observer was capable of recording many phenomena that could not be recorded automatically. Further, the amount of data that could be automatically recorded was limited by the capabilities of the cassette recorder.

The main software problem to be solved was one of reformatting. Table 3.2 shows the data available on the data output signal, which was recorded in its entirety on magnetic tape. Note that the output parameters are fixed point, floating point, and logical (individual bits set or cleared). The floating point numbers required the most processing to convert from the Omega receiver format (identical to the HP 2100 minicomputer format) to the format of the computer on which the data reduction was being done, either a Univac 1108 or PDP-11. Fixed point parameters were fairly easily converted from one machine to another, and logical parameters were treated using bit-test instructions on the data reduction computer.

Table 4.2 lists the major programs written for the Phase B data collection. There are several differences between the various programs. The most obvious differences are in language and machine; FORTRAN programs were run only on the Univac 1108, and BASIC programs were run only on a PDP-11. Most of the programs shared common routines to the extent possible. For example, the BASIC

TABLE 4.2 - MAJOR DATA REDUCTION PROGRAMS USED IN PHASE B

PROGRAM NAME	MACHINE USED	LANGUAGE	USES AND OUTPUTS
OUTPUT	1108	FORTRAN	General purpose tape print program-date, time, lat, lon, selected S/N ratios, stations in use, etc.
OUTPUT	PDP-11	BASIC	Similar to FORTRAN OUTPUT
FANG	1108	--	Octal dump of raw data on magnetic tape
MTBDMP	PDP-11	BASIC	Octal dump of raw data on magnetic tape
WRTLOS	PDP-11	BASIC	Four options: (1) all 32 S/N ratios, (2) all 32 predicted propagation corrections, (3) all 32 raw phase measurements, and (4) everything else.

programs used common tape-read routines, floating-point conversion routines, output routines, and much of the same logical data conversions. All of the PDP-11 programs were written to print either on the line printer or on a user console. The programs developed provide a comprehensive and complete software package.

4.4 MANUAL DATA PROCESSING

Manual data processing refers to the analysis of the flight notes, S/N plots, computer printouts, and flight plans to determine what of significance occurred during each evaluation flight. Manual data processing was usually concerned with determination of signal availability, observation of incidents, and correlation of results with other sources.

Determination of signal availability was a major objective in the flight evaluation program. Signal availability was determined on each flight from both S/N ratio plots and recorded information on stations in use by the receiver. These sampled data sources were compared to each other and with the flight notes to determine a good estimate of that point beyond which signals were not, in general, usable. This task was complicated by the sampling of the parameters, and by the erratic dropout of signals. Sometimes signals would not be definitely above or definitely below the threshold of usability for several hours of flight time, making determination of a clear cut boundary difficult. When multiple flights along the same route were performed, comparisons of results on different flights were made to provide a more valid distinction. These multiple flights provided information on signal variations from day to day; because of limited data, however, time-of-day trends were not observable.

Observation of in-flight incidents was another major effort of the manual data processing. These incidents included occurrence of precipitation static, occurrence of auroras, and comparisons of 3.4 kHz difference frequency Omega with three frequency Omega. Generally, flight notes, numerical data, and the S/N ratio plots were all used for observation of incidents involving the response of the Omega receiver to external influences. 3.4 kHz difference frequency Omega was most easily compared to three frequency Omega at times when the operator manually changed receiver operating modes.

The results obtained were compared with published predictions and other results. These comparisons were made to extend the results of the flight evaluation program to

expected performance of the Omega system as a whole. The flight evaluation program was designed to evaluate Omega system performance in terms of operational reliability and utility, and was not designed to focus on any particular phenomena. However, when these phenomena occurred, comparisons with independently-derived results allowed a more meaningful conclusion to be made as to the significance of the phenomena observed. This was particularly true when only one or two occurrences were observed, and it was important not to make an erroneous prediction based upon a limited data base. Most significantly, signal availabilities observed on isolated flights were compared with predictions to estimate whether the performance observed on the particular flight(s) was typical of expected system performance.

4.5 STATISTICAL DATA PROCESSING

Statistical information was generated as comparisons of Omega to other navigation sensors. These data were gathered from the flight notes, and included comparisons of:

a. Omega groundspeed with Doppler groundspeed,

b. Omega distance to go with Doppler distance to go and DME, and

c. Omega latitude and longitude with Doppler latitude and longitude, VOR and NDB overflights, and surveyed positions measured with the aircraft on the ground.

Standard statistics were generated on these position comparisons, including means, standard deviations, and where applicable, correlation coefficients and regression lines.

For comparative evaluation of the distance-to-go calculations, the differences between Omega readings and the reference sensor were calculated, and mean and standard deviations of these

comparisons were generated. Statistics were generated for Phase A flights with the receiver in the 3.4 kHz difference frequency mode and the three frequency mode separately, and both modes together. In Phase B, statistics were generated for each of the major flight regions, namely the Pacific and South America.

Comparisons of Omega latitude and longitude with other position information were the most interesting statistics to compute. The objectives of the data processing of latitude and longitude were not only to compute standard deviations and means of latitude and longitude, but also to determine any correlation between these errors. Statistics were generated for the Phase A flights in both receiver modes independently, and with all data combined. Statistics were also generated for the Pacific flights and the South America flights.

Conventional means and standard deviations of position comparisons were generated as well as regression coefficients. The regression coefficients attempt to fit the latitude errors y and the longitude errors x to each other by

$$y = a_1 x + a_o \tag{4.1}$$

where a_o and a_1 are given by

$$a_1 = \frac{\Sigma xy - \frac{\Sigma x \Sigma y}{n}}{\Sigma x^2 - \frac{(\Sigma x)^2}{n}} \tag{4.2}$$

$$a_o = \bar{y} - a_1 \bar{x} \tag{4.3}$$

and

$$\bar{y} = \frac{\Sigma y}{n} \tag{4.4}$$

$$\bar{x} = \frac{\Sigma x}{n} \tag{4.5}$$

and n is the number of measurements.

The slope parameter a_1 is an estimate of the major axis of the error ellipse. The coefficient of determination r^2 was also calculated to determine how well the data fit the straight line approximation. The formula for the coefficient of determination is given by

$$r^2 = \frac{\left(\Sigma xy - \frac{\Sigma x \Sigma y}{n}\right)^2}{\left(\Sigma x^2 - \frac{(\Sigma x)^2}{n}\right)\left(\Sigma y^2 - \frac{(\Sigma y)^2}{n}\right)} \tag{4.6}$$

In general, the coefficients of determination were close to zero, indicating that the latitude and longitude errors were not significantly correlated.

V. RESULTS

5.1 GENERAL RESULTS

This section presents a broad overview of Omega system performance. Results from flights over the Atlantic Ocean, the Pacific Ocean, and North and South America indicate satisfactory Omega system performance with generally good signal availabilities.

The general results include a comparative analysis of 10.2 kHz and 13.6 kHz Omega signal strengths and availabilities. A comparative analysis of 3.4 kHz difference frequency Omega and full three frequency Omega was also performed. Each of these analyses is discussed in a separate section below.

Signal availability and reliability in general was good. During the evaluation flights, very few occasions were observed when an Omega station was off the air on all three frequencies. Signals were generally adequate except in the South Pacific and over North America. The addition of the Australian station to the Omega transmitter complement should alleviate the problems of signal availability in the South Pacific, but not over North America.

Early data collection flights indicated that the performance of full three frequency Omega was somewhat better than the performance of 3.4 kHz difference frequency Omega. In order to obtain data on the best Omega performance, most of the data were collected in the three frequency mode. Data collection in the 3.4 kHz difference frequency mode

was usually accomplished by selecting the 3.4 kHz difference frequency mode, waiting for the receiver to stabilize, recording the results, and then switching back to the three frequency mode. Much of the data items collected were similar or identical in both modes, making the exact choice of operating mode less critical.

5.1.1 3.4 kHz Difference Frequency Omega vs. Three Frequency Omega

3.4 kHz difference frequency was found to have limited utility compared to three frequency Omega. This result was obtained under the constraints of an operational evaluation and the use of a single receiver software implementation.

One of the main theoretical advantages of 3.4 kHz difference frequency Omega is the ability to perform lane ambiguity resolution. In practice, it was found in some weak signal conditions that the receiver would not navigate as well in the 3.4 kHz difference frequency mode as it would navigate in a full three frequency mode. This was manifested in larger RMS position error estimate values in the 3.4 kHz mode, as well as greater incidence of Ambiguity and Dead Reckoning warning lights. For the receiver to operate in the 3.4 kHz difference frequency mode, signals from three or more stations must be received at both 10.2 and 13.6 kHz. In fringe signal areas, where the lane resolution capability is most desirable, the usable signal level is determined by the weaker of the 10.2 and 13.6 kHz signals. Thus, when only one of these two signals is usable from a station in use, the navigation information from the other signal and, hence, from that station, is not usable in a strict 3.4 kHz difference frequency mode of operation. In contrast, the full three frequency mode would obtain and use navigational information from the station under these same circumstances.

Because 3.4 kHz difference frequency Omega takes a linear combination of the 10.2 kHz and 13.6 kHz Omega signals with opposite algebraic signs, any common propagation anomalies (such as SIDs) will tend to be of diminished effect in the position solution. This benefit is achieved at the expense of greater sensitivity of the position solution to phase noise. This benefit, however, was not observed during the evaluation.

When reinitializing the Omega receiver position from an external position reference, 3.4 kHz difference frequency Omega can tolerate greater errors in the external position reference than can full three frequency Omega. 3.4 kHz difference frequency Omega has nominal lane widths of 24 nm, as opposed to the nominal 8 nm lane widths associated with 10.2 kHz Omega. In the more sophisticated Omega receivers, the position which is entered for reinitialization is used as an initial position estimate. From this initial estimate, a best estimate of position is derived based on the phase of the Omega signals received. External position references may have appreciable errors when used for reinitializing Omega position, especially at jet speeds of nearly 500 kt. In the wider 3.4 kHz difference frequency Omega lanes, greater errors in these external position references can be tolerated when reinitializing the receiver. This advantage was exploited in operational use by reinitializing the receiver in the 3.4 kHz difference frequency mode. After allowing the receiving software to derive a position estimate based on the reinitialization, operation was continued in the normal three frequency mode.

During the flight evaluation program, three frequency Omega was observed to perform better than 3.4 kHz difference frequency Omega, as indicated by the smaller RMS position error estimates, and comparable or better position comparison errors when referenced to other on-board navigation equipment (discussed in Section 5.2.5 below). Therefore, full three frequency Omega may be preferable to the 3.4 kHz difference frequency Omega for performing the error bounding function.

5.1.2 10.2 kHz and 13.6 kHz Signal Quality

In the Phase A flights and the Phase B flights with the CMC 740P, the 13.6 kHz S/N ratios were usually higher than the 10.2 kHz S/N ratios, which is consistent with propagation theory. However, on the Phase B flights with the CMC 740, the 10.2 kHz S/N ratios were often much higher than the 13.6 kHz S/N ratios.

A possible explanation for the higher S/N ratios of the 10.2 kHz signals is 400 Hz interference from sources on the aircraft to which the H-field antenna is susceptible. 13.6 kHz is a multiple of 400 Hz, while 10.2 kHz is not a multiple. The 400 Hz is automatically maintained to a tolerance of ± 4 Hz, but is usually set by the flight engineer to $\pm 1/4$ Hz. For a receiver with a bandwidth of 50 Hz, or 25 Hz to each side of the center frequency, the 400 Hz signal would have to drift more than 7 Hz for the harmonic to fall in the receiver pass band at 10.2 kHz, but normally a harmonic would be present at 13.6 kHz. Thus, it is conceivable that the lowered 13.6 kHz S/N ratios, which were well correlated among the different stations on Phase B flights with the CMC 740, are a result of local interference.

Figures 5.1 and 5,2 show two sample S/N ratio plots, the former generated from CMC 740P data, the latter from CMC 740 data. These plots give clear indications of the 10.2 kHz and 13.6 kHz S/N ratio trends. On some flights, however, the 10.2 kHz and 13.6 kHz S/N ratios were nearly equal, with some occurrences of each signal being higher. Figure 5.3 is an example of this phenomenon, with the CMC 740P used.

On both frequencies, the S/N ratios showed more scatter about low S/N ratios than about higher S/N ratios. Figures 5.1 through 5.3 illustrate this effect, which was noted throughout the flight program.

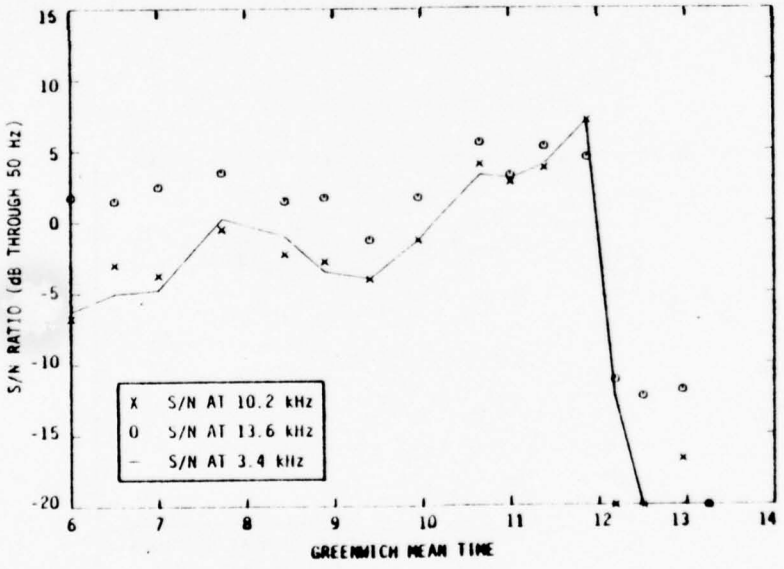

FIGURE 5.1 - S/N RATIOS, STATION E, TAHITI-LOS ANGELES, FLIGHT 816, APRIL 29, 1976

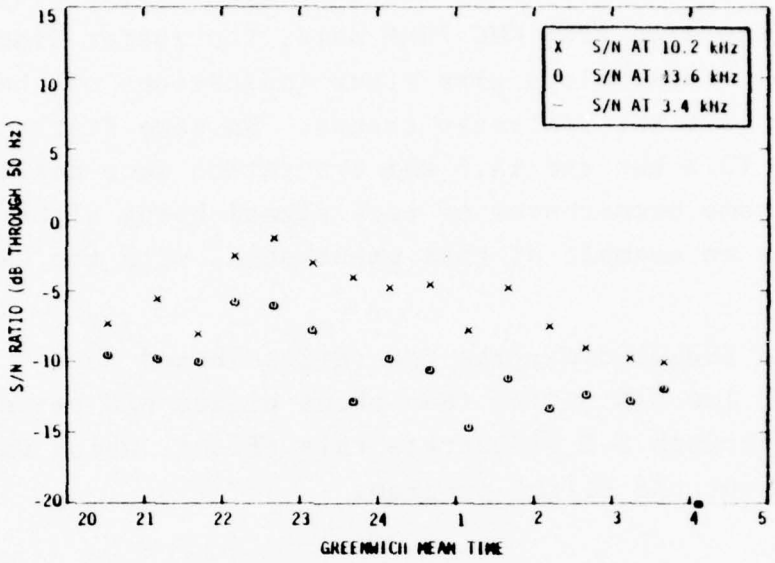

FIGURE 5.2 - S/N RATIOS, STATION G, JOHANNESBURG-RIO DE JANEIRO VIA CAPETOWN, FLIGHT 202, JULY 7, 1976

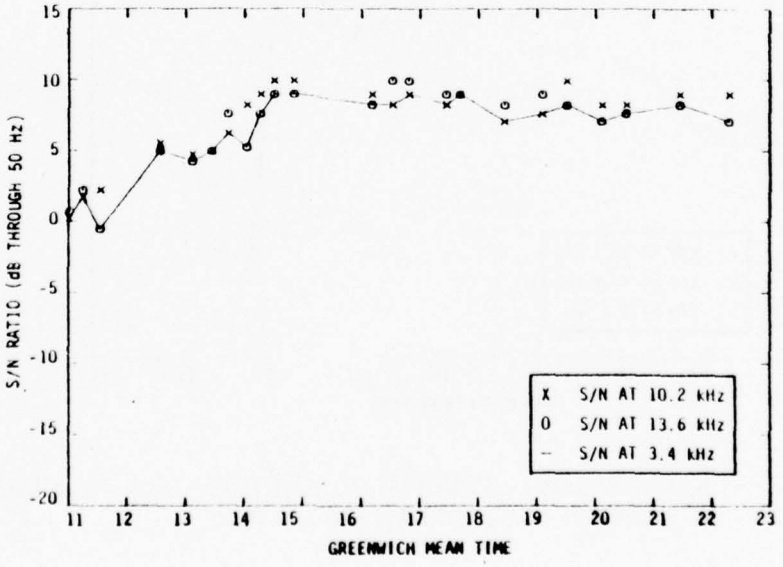

FIGURE 5.3 - S/N RATIOS, STATION E, HONG KONG-SYDNEY VIA DJAKARTA, FLIGHT 812, MAY 19, 1976

5.2 NORTH ATLANTIC FLIGHTS

5.2.1 Introduction

The North Atlantic data collection flights consisted of the eleven Phase A flights and two Phase B flights, as shown in Table 5.1. However, data from Flight 66, March 22, 1976, does not appear to be correct and is not considered in the discussions below. Thus, roughly 100 hours of good data were collected, almost all of it from Phase A. Figure 5.4 shows the detailed flight paths of the Phase A North Atlantic crossings, which give a representative coverage of the North Atlantic. On these flights, the eastbound departures generally were at approximately 2300 GMT, while the westbound flights departed at approximately 0100 GMT. Thus, the eastbound flights were generally at night and the westbound flights in daytime. Usually the westbound flights took the more northerly routes, and the eastbound flights flew the more southerly routes shown in Figure 5.4.

TABLE 5.1 - NORTH ATLANTIC FLIGHTS

FLIGHT	DATE	ORIGIN	DESTINATION	PHASE
44	Aug 19, 1975	New York	Copenhagen	A
59	Aug 20, 1975	Frankfurt	Chicago	A
67	Aug 21, 1975	Frankfurt	Washington	A
66	Aug 21, 1975	Washington	Frankfurt	A
59	Aug 23, 1975	Frankfurt	Chicago	A
58	Aug 23, 1975	Chicago	Frankfurt	A
44	Aug 26, 1975	New York	Copenhagen	A
59	Aug 28, 1975	Frankfurt	Chicago	A
58	Aug 28, 1975	Chicago	Frankfurt	A
59	Sept 1, 1975	Frankfurt	Chicago	A
59	Sept 2, 1975	Frankfurt	Chicago	A
66	Mar 22, 1976	New York	Frankfurt	B
67	Mar 26, 1976	Frankfurt	New York	B

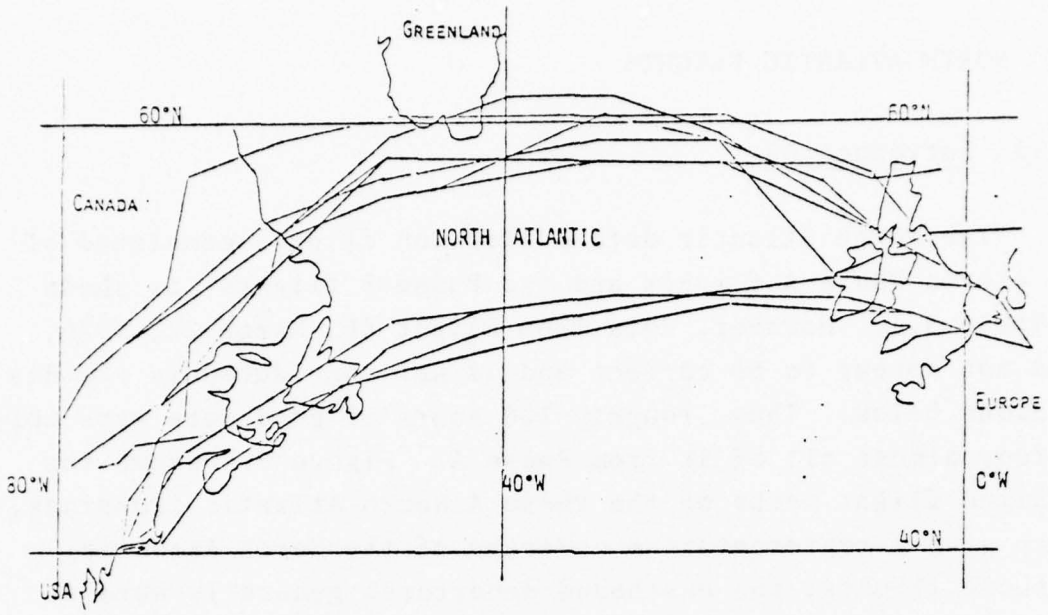

FIGURE 5.4 - PHASE A NORTH ATLANTIC CROSSINGS

5.2.2 Signal Availability

Omega was found to give adequate coverage over the North Atlantic. Figure 5.5 shows the availability regions observed on the Phase A flights, including Stations A, C, D, H, and B (Trinidad). Of the remaining stations, Stations B (Liberia) and F should be of major utility for navigation over the North Atlantic, but Stations E and G (Australia) should be of limited value.

Station A provides strong signals over the North Atlantic, but these signals are, of course, subject to the Greenland Shadow. This phenomenon is the strong attenuation of signals propagating over the Greenland ice cap, and limits the availability of Station A signals in the western portions of the Atlantic. Figure 5.6 illustrates the effect of the Greenland Shadow, with the typical sharp edge of signal availability. Note that over most of the flight, Station A was available with strong signals.

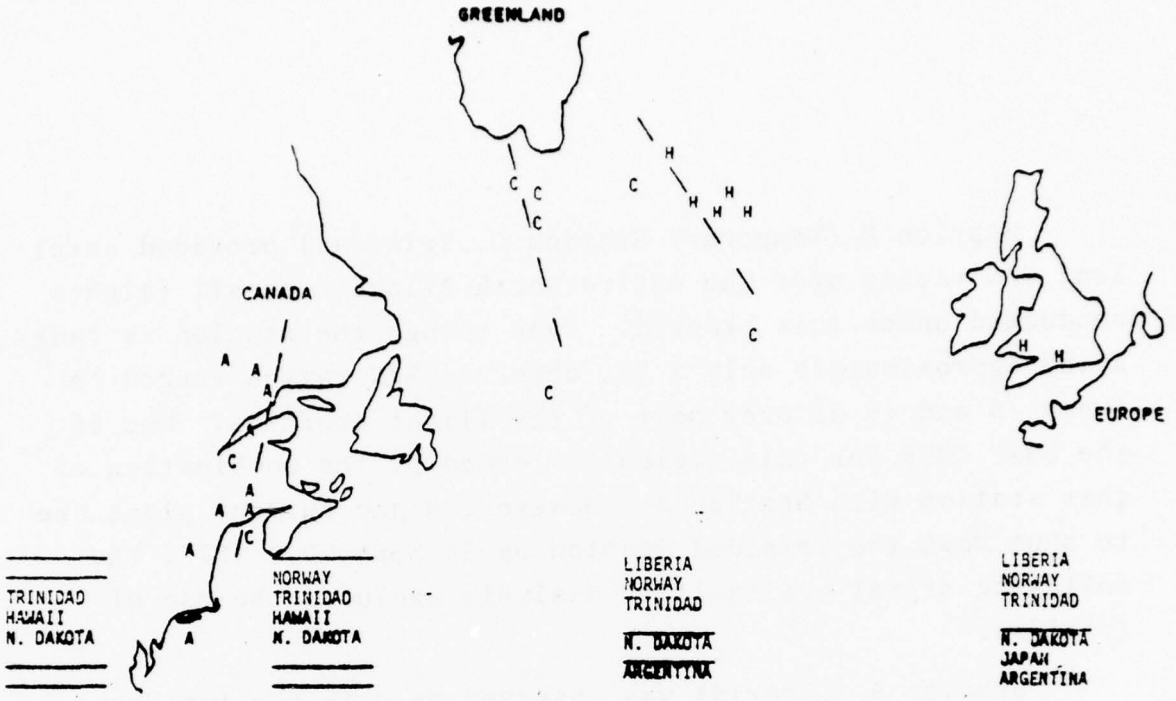

FIGURE 5.5 - OBSERVED OMEGA SIGNAL AVAILABILITY DURING PHASE A

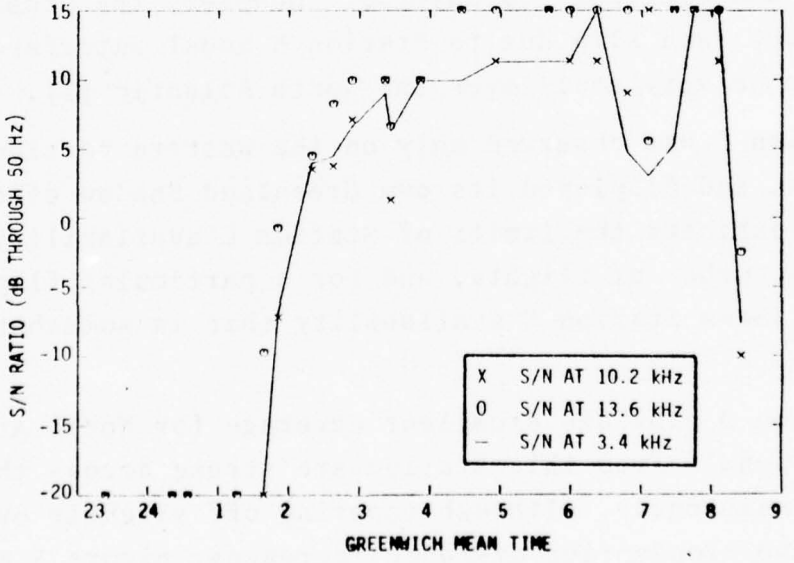

FIGURE 5.6 - S/N RATIOS, STATION A, CHICAGO-FRANKFURT, FLIGHT 58, AUGUST 28, 1975

Station B (Temporary Station G, Trinidad) provided excellent S/N ratios over the entire North Atlantic on all flights conducted under this program. Even though the station is radiating approximately only 1 KW, observed S/N ratios ranged between -5 and +5 dB over most of the flight profiles. One of the best LOPs for this region is formed by the combination of this station with Station A. However, since current plans are to shut down the Trinidad Station on 30 September 1977, the following signal availability analysis excludes the use of Trinidad.

Station B (Liberia) was observed on only the two Phase B flights, but showed excellent S/N ratios over the flight. During the day, Station B should provide stable signals over the entire North Atlantic route structure. However, modal interference is expected at night, primarily west of a great circle arc through Greenland and Liberia. Modal interference effects as observed from a moving platform would be highly stochastic and difficult to observe. However, the probability of a 10.2 kHz lane slip due to Station B modal interference is expected to be very small over the North Atlantic [1].

Station C was observed only on the western portions of the flights, and displayed its own Greenland Shadow effects. Figure 5.5 exhibits the limits of Station C availability observed on a number of flights, and for a particular flight, Figure 5.7 shows Station C availability that is somewhat above average.

Station D provides excellent coverage for North Atlantic flights. Signals from this station are strong across the Atlantic consistently, although tapering off slightly over Europe as the propagation distance increases; Figure 5.8 illustrates this effect.

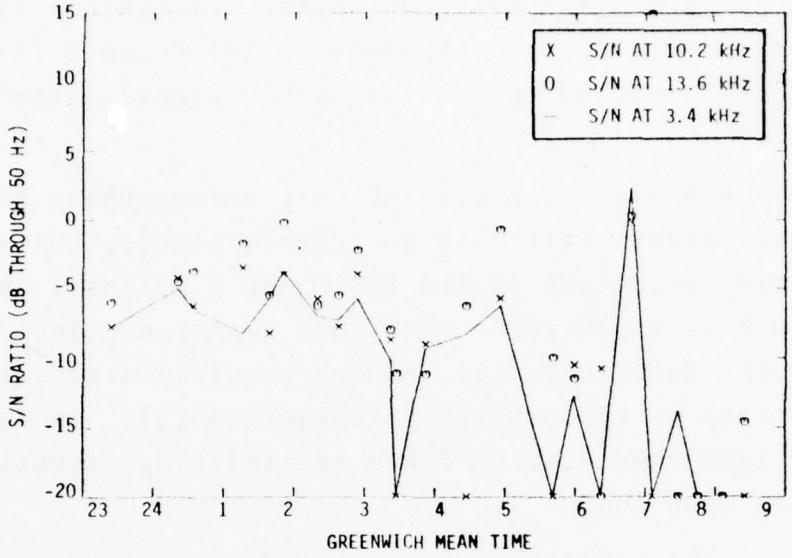

FIGURE 5.7 - S/N RATIOS, STATION C, CHICAGO-FRANKFURT, FLIGHT 58, AUGUST 28, 1975

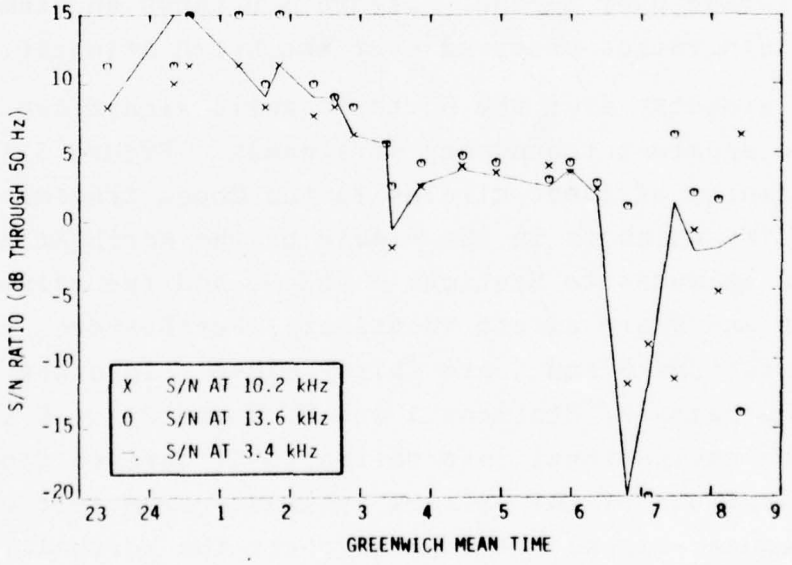

FIGURE 5.8 - S/N RATIOS, STATION D, CHICAGO-FRANKFURT, FLIGHT 58, AUGUST 28, 1975

Station E was not transmitting during the Phase A flights, and was observed over Europe only once in the Phase B flights; Station E is not expected to provide usable signals over the North Atlantic.

Station F was also transmitting only during Phase B North Atlantic flights (although not commissioned), but was receivable only during one of the two Phase B flights. However, Station F is expected to give good signal availability over most of the North Atlantic, except possibly over Europe during conditions of all daylight propagation [2]. In fact, on the one flight when Station F was transmitting, signal availabilities were good.

Station G (Australia) is not expected to be usable over the North Atlantic due to the extreme propagation path lengths.

Station H was observed only over the eastern part of the North Atlantic, and appeared to have its own Greenland Shadow. This station will therefore be useful only for redundant coverage over Europe. Figure 5.9 shows an example of Station H S/N ratios observed over the North Atlantic.

Station geometry over the North Atlantic significantly decreases the apparent redundancy of signals. Figure 5.10 shows the azimuths of great circles to the Omega transmitters from 44°N, 40°W, which is in the middle of the North Atlantic. Note that the azimuths to Stations A and H, and the azimuths to Stations C and D are almost identical. Furthermore, the azimuths to Stations B and E are fairly close. In other words, for any of the pairs of Stations A and H, C and D, or B and E, most of the navigational information to be derived from having both stations of the pair is available from just one station. Adequate signal availability over the North Atlantic will require the availability of at least one station from each of the three pairs, or at least one station from two of

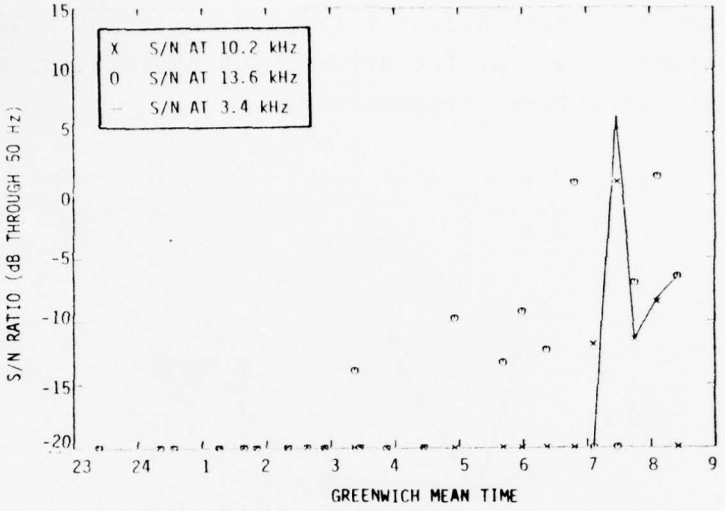

FIGURE 5.9 - S/N RATIOS, STATION H, CHICAGO-FRANKFURT, FLIGHT 58, AUGUST 28, 1975

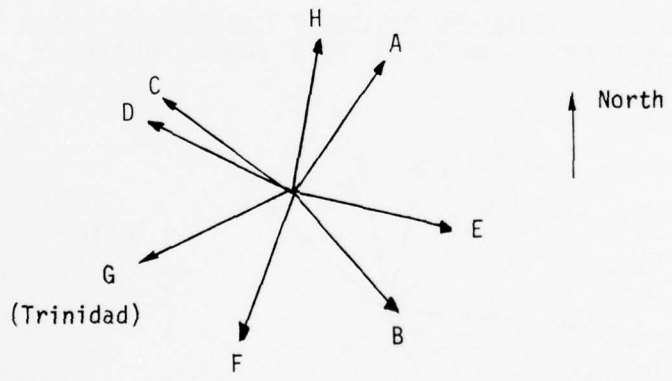

FIGURE 5.10 - AZIMUTHS OF GREAT CIRCLES TO OMEGA TRANSMITTERS FROM 44°N, 40°W (MID-ATLANTIC)

the pairs if Station F is available. Although the signal geometries vary over the North Atlantic (Figures 5.11 and 5.12), this generalization is useful for determining the effects of lost signals from individual transmitters.

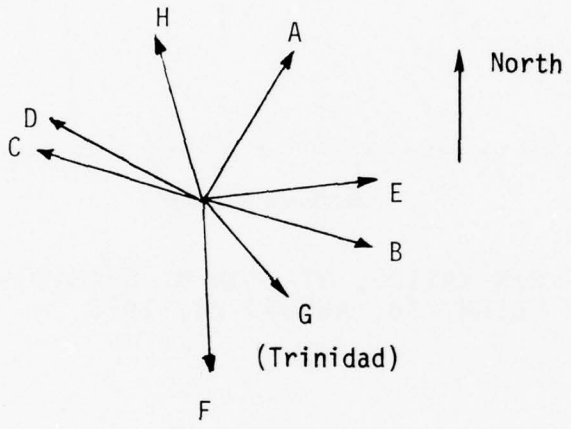

FIGURE 5.11 - AZIMUTHS OF GREAT CIRCLES TO OMEGA TRANSMITTERS FROM 41°N, 72°W (LONG ISLAND)

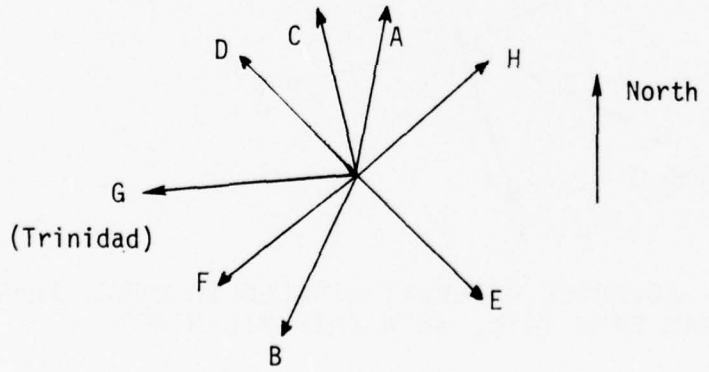

FIGURE 5.12 - AZIMUTHS OF GREAT CIRCLES TO OMEGA TRANSMITTERS FROM 50°N, 8°E (FRANKFURT A.M.)

At the high latitudes of some of the North Atlantic crossings, auroral effects are frequently observed. In fact, Figures 5.6 through 5.9 show S/N ratio degradations at about 0330 GMT which occurred at the same time as an aurora. It is not expected that auroral activity will degrade the stronger Omega signals, but weaker signals may not be usable during an aurora.

In summary, Stations A, B (Liberia), D, and F will be of major utility over the North Atlantic. Stations C, E and H will serve supporting roles, due to their supplying information redundant to that supplied by the stronger signals.

5.2.3 Omega System Performance Without the Trinidad Station

Because the Trinidad Omega station is temporary and scheduled for decommissioning, the present performance of the Omega system with the Trinidad station operational must be interpreted in order to obtain a reasonable expectation of the future performance of the Omega system in its final configuration, which will not utilize Trinidad. Based on the North Atlantic crossings in Phase B, predicted Omega signal coverage [2] and analysis of transmitter geometries over the North Atlantic, it is expected that the loss of the Trinidad Omega station will have little effect on Omega system coverage in the North Atlantic.

When Station F is operating normally and adequate signals are receivable, the loss of the Trinidad station should not be particularly significant over the North Atlantic. Figure 5.10 shows that the great circle to the Trinidad station lies on an azimuth of 216°, or very nearly the same azimuth as Station F. Thus, Stations F and G will supply redundant information. When Station F is not available, as might happen

over the eastern part of the North Atlantic, adequate signals should be available from enough other stations that no serious loss of navigational capability would be encountered.

The replacement of the Trinidad Omega station by the Liberia Omega station appears overall to give an improvement in Omega system performance over the North Atlantic. The Liberia station will consistently provide strong signals to the North Atlantic area and modal interference is not expected to be a problem. The Liberia station thus completes the favorable geometry of one strong station in every quadrant of the compass.

5.2.4 Flight-to-Flight Repeatability of Results

Flight data collected over the North Atlantic shows that Omega S/N ratios have considerable variations from day to day, as well as the well-known diurnal variations. The flights over the North Atlantic provided a good opportunity to observe these variations, as many flights were accomplished over very similar routes. On these flights, signal availability regions were observed, as discussed above. Referring to Figure 5.5, note that Stations A, C, and H have considerable variation in the location of the thresholds of signal availability. For example, even when compensation is made for day and night effects, the Station A threshold of signal availability (the Greenland Shadow) varies from Long Island to Newfoundland, with differences of over 100 miles east to west. Similarly, Station H was usually available as far west as Greenland, but sometimes was not available west of England. Thus, Omega signals show considerable day-to-day variation.

5.2.5 Position Comparison Statistics

Although determination of Omega accuracy was not the primary objective of the flight evaluation program, a limited number of comparisons were made between the Omega-indicated position and other position references. Errors in latitude and longitude were largely uncorrelated, and the overall position discrepancy between Omega and other on-board sensors showed roughly a 6 nm standard deviation, based on about one hundred observations.

Statistics were generated comparing the Omega-indicated navigation parameters to parameters as indicated by other on-board sensors. The statistics were computed for Omega operation in both the difference frequency and full three frequency modes of operation. Position indications of Omega were compared to Doppler radar positions, positions measured with the aircraft on the ground, and overflights of NDBs and VORs. Groundspeed references were obtained from the Doppler radar, and distance-to-go references were supplied by Doppler radar and DME.

Table 5.2 shows position comparisons of Omega-indicated positions and Doppler radar-indicated positions, VOR and NDB overflights and positions of the aircraft on the ground. Minutes of longitude were converted to nm at a mean latitude of 51° for the North Atlantic. All the mean errors are small, less than 1 nm, but the standard deviations are all at least 4 nm. These are position comparisons, however, not position errors measured from a calibrated reference. The three frequency standard deviation in longitude is roughly twice the difference frequency standard deviation. This is due to a small number of data points with large latitude discrepancies. The squares of the correlation coefficients are all very small, indicating negligible correlation between latitude and longitude errors.

TABLE 5.2 - POSITION COMPARISONS, OMEGA REFERENCE TO VOR, NDB, AND DOPPLER RADAR CHECKPOINTS

	DIFFERENCE FREQUENCY OMEGA	THREE FREQUENCY OMEGA	DIFFERENCE FREQUENCY & THREE FREQUENCY OMEGA
Latitude (nm)			
Mean	0.9 South	0.1 North	0.3 South
Std. Dev.	4.8	4.0	4.4
Longitude (nm)			
Mean	0.7 West	0.1 West	0.4 West
Std. Dev.	2.8	5.0	4.2
$(\text{Corr. Coeff.})^2$	0.01	0.04	0.03
No. of Points	34	39	73

Table 5.3 shows comparisons of Omega and on-board sensors in distance to go and groundspeed. In these comparisons, the three frequency mode was found to be in better agreement with on-board sensors than was the difference frequency mode.

Distance-to-go comparisons showed roughly equivalent standard deviations and means for both the three frequency and difference frequency modes of operation. The three frequency mode was found to be slightly more accurate, but this difference is not significant.

Groundspeed comparisons showed better results with three frequency Omega than with the difference frequency Omega. In fact, the standard deviations of difference

TABLE 5.3 - OMEGA REFERENCED TO DOPPLER RADAR AND DME GROUNDSPEED AND DISTANCE TO GO

	DIFFERENCE FREQUENCY OMEGA	THREE FREQUENCY OMEGA	DIFFERENCE FREQUENCY OMEGA & THREE FREQUENCY OMEGA
Distance to Go (nm)			
Mean	-2.5	-1.8	-2.1
Std. Dev.	6.2	5.8	5.9
No. of Points	25	40	65
Groundspeed (kts)			
Mean	1.6	-1.6	-0.3
Std. Dev.	18.1	12.3	15.0
No. of Points	41	58	99

frequency Omega were found to be roughly 50% greater than the standard deviations of three frequency Omega. This may be a result of the greater sensitivity of the 3.4 kHz difference frequency Omega mode to measurement noise.

The standard deviations in latitude and longitude can be compared with the standard deviation of distance to go in order to check the validity of the observed statistics. If the 3.4 kHz difference frequency standard deviations in latitude and longitude are combined in a sum-of-squares manner, the resulting value is about 6 nm. This value of 6 nm corresponds well with the 6 nm standard deviations observed in the distance-to-go statistics. If the few large errors observed in computing the three frequency Omega longitude statistics are eliminated from consideration, a similar result is obtained for three frequency Omega. This provides a useful validity check on the observed statistics.

5.3 PACIFIC OCEAN FLIGHTS

5.3.1 Introduction

A total of 21 flights were conducted in the Pacific, all of these using the Canadian Marconi 740P. These flights, documented in Table 5.4 and Figure 5.13, were representative of the region. Four or more stations were usable for route segments in all regions evaluated except three: in the East Indies around Djakarta, between Auckland and Tahiti, and on the western portion of routes from Los Angeles. The addition of the Australian station to the Omega transmitter complement should make reception of four or more Omega stations feasible throughout the Pacific area, with the possible exception of the North American coastline and adjacent waters.

5.3.2 Signal Availability

Flights in the Pacific indicate good signal availabilities in the region, even without the Australian station. Stations C, E, and H provide the strongest signals in the area. Figure 5.14 shows the approximate coverage areas provided by the different stations as observed on various flights. The coverage area boundaries show signal availabilities at the time of day when the aircraft was at the given location, and are not corrected for diurnal variations in signal strength, nor necessarily averaged over a large number of samples for each location.

Station A (Norway) availability was satisfactory only in the western Pacific, with significant diurnal variations. Station A was available in the Guam-Tokyo-Hong Kong triangle, but was not usable again until past Djakarta on the flight

TABLE 5.4 - PACIFIC OCEAN FLIGHTS

FLIGHT	DATE	ORIGIN	DESTINATION	VIA
825	Apr 8, 1976	New York	Honolulu	Dallas
818	Apr 10, 1976	Honolulu	San Francisco	Los Angeles
815	Apr 11, 1976	San Francisco	Tahiti	Los Angeles
816	Apr 12, 1976	Tahiti	San Francisco	Los Angeles
815	Apr 25, 1976	San Francisco	Auckland	Los Angeles, Tahiti
816	Apr 29, 1976	Auckland	San Francisco	Tahiti, Los Angeles
803	May 17, 1976	Tokyo	Guam	
802	May 17, 1976	Guam	Tokyo	
003	May 18, 1976	Tokyo	Hong Kong	
812	May 19, 1976	Hong Kong	Sydney	Djakarta
812	May 20, 1976	Sydney	Honolulu	Pago Pago

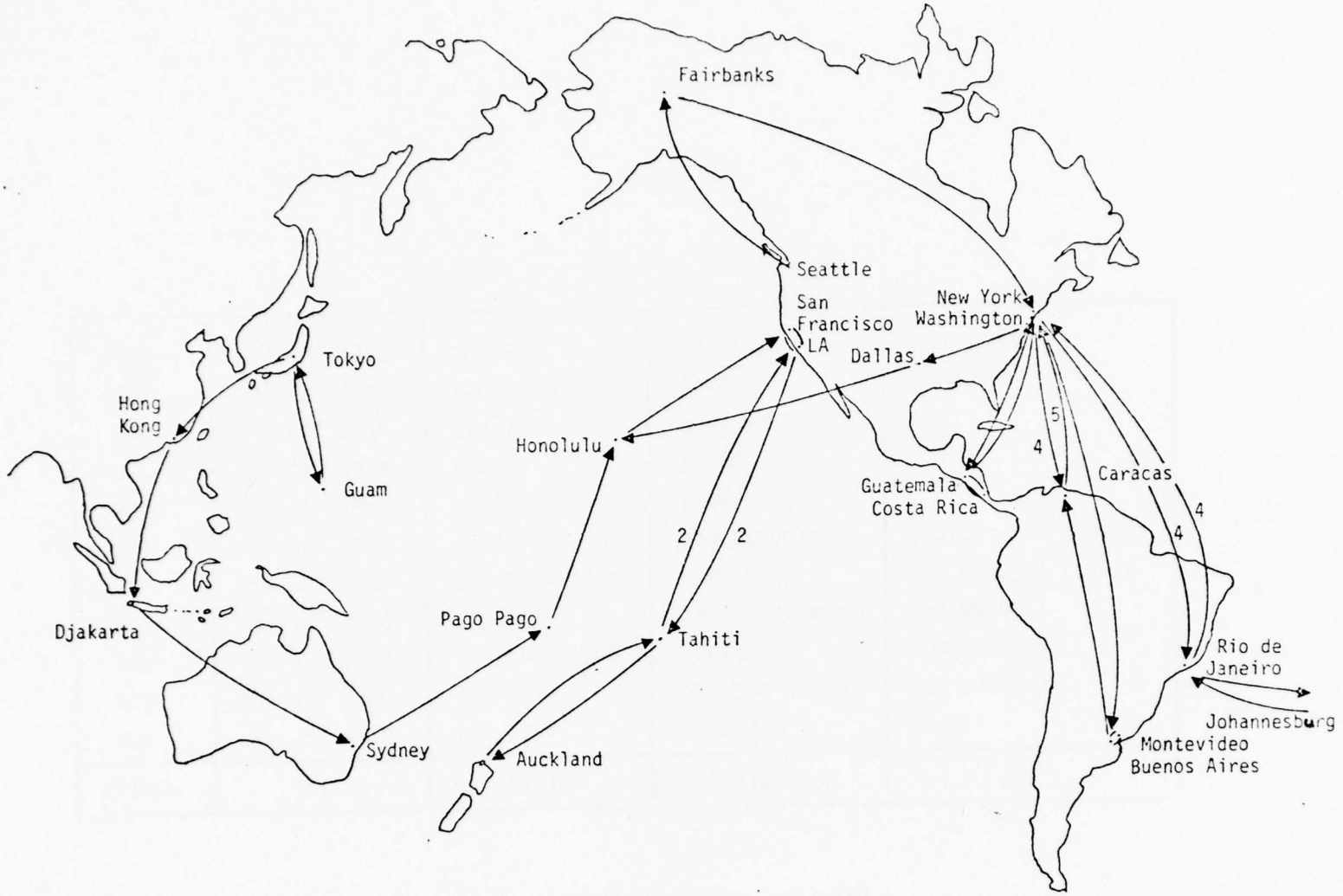

FIGURE 5.13 - PHASE B DATA COLLECTION FLIGHTS

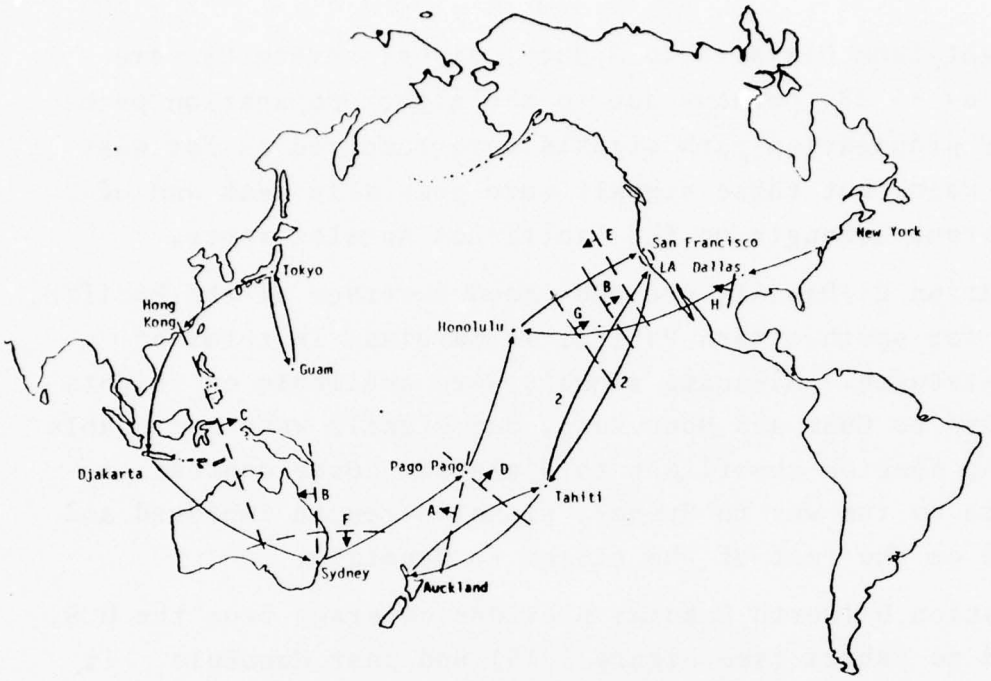

FIGURE 5.14 - SIGNAL AVAILABILITY IN THE PACIFIC

to Sydney. This station was weak but usable over Australia until sunrise, when signals were no longer receivable. Signals were again received halfway between Sydney and Pago Pago, and continued to be usable on the flight into Honolulu. The propagation path during this period of availability was daylight at the transmitter and night at the receiver.

Station B (Liberia) provides usable signals in the western Pacific with an easterly propagation path, and usable signals in the eastern Pacific with a westerly propagation path. However, these signals in the eastern Pacific were not used due to receiver software excluding westerly propagation signals at ranges greater than 5,000 nm. Station B signals on flights from Tokyo to Guam and Hong Kong were weak but usable, and somewhat stronger south to Djakarta. On

the flight from Djakarta to Sydney, signal strengths were as high as +5 dB, perhaps due to the night propagation path. Westerly propagation-path signals were received as far west as Pago Pago, but these signals were generally weak and of inconsistent strength on the Tahiti-Los Angeles route.

Station C (Hawaii) provides good coverage of the Pacific, but the far southwestern Pacific is marginal in terms of signal strength. Adequate signals were available on flights from Tokyo to Guam and Hong Kong, but signals were not usable past Hong Kong on the flight to Djakarta. Over central Australia on the way to Sydney, signal strength improved and was good on the rest of the flight to Honolulu.

Station D (North Dakota) provides coverage from the U.S. mainland to Tahiti (see Figure 5.15) and past Honolulu. It is weak but usable on the Tokyo-Guam segments. On the Tokyo-Sydney flight, Station D was occasionally available but was not used for position calculation due to the range of the westerly propagation path being greater than 5,000 nm. However, signal strength improved passing Pago Pago, and signals were incorporated into the position solution.

Station E (La Reunion) supplied coverage over almost the entire Pacific, with good signal strengths consistently available, despite propagation paths of around 10,000 nmi. However, signal availability stops abruptly at about 130°W, or roughly 10°W of Los Angeles. This very abrupt signal cutoff is shown in Figure 5.16, as observed on a flight from Los Angeles to Tahiti. This is apparently not due to H-field antenna mis-steering near the Station E antipode (located in the Pacific off Baja, California) because a similar cutoff in signals has been observed with a receiver using an E-field antenna [3].

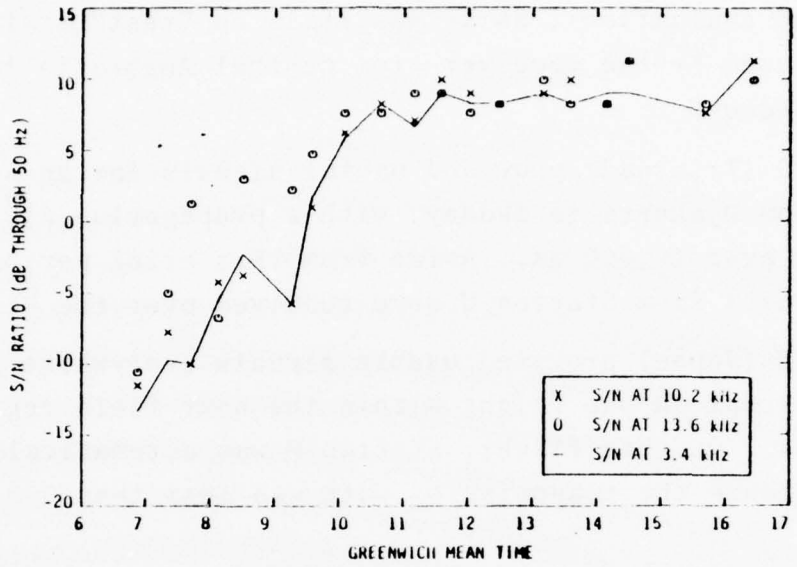

FIGURE 5.15 - S/N RATIOS, STATION D, TAHITI-SAN FRANCISCO VIA LOS ANGELES, FLIGHT 816, APRIL 12, 1976

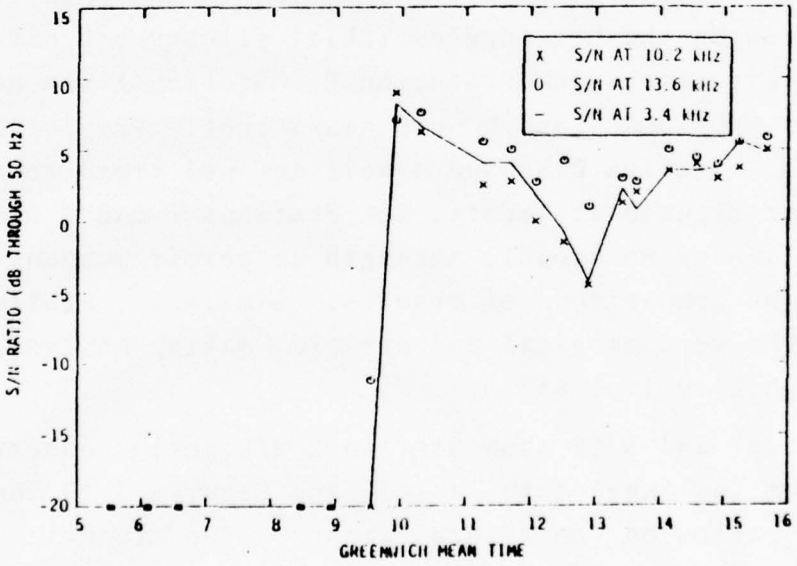

FIGURE 5.16 - S/N RATIOS, STATION E, SAN FRANCISCO-TAHITI VIA LOS ANGELES, FLIGHT 815, APRIL 11, 1976

Station F (Argentina) was not consistently available during the flight evaluations, as it was still on "test" status. Signals were used by the receiver from central Australia to Pago Pago, however.

Station G (Trinidad) provided useful signals for an hour and a half from Djakarta to Sydney, with a propagation distance of just over 10,000 nm. Aside from this brief period, no usable signals from Station G were received over the Pacific.

Station H (Japan) provided usable signals everywhere in the Pacific except on one flight within the near-field region of the antenna. On that flight, Station H was automatically deselected because the transmission path was less than 300 nm.

5.3.3 Flight-to-Flight Repeatability of Results

The flights in the Pacific covered an extremely large area with little duplication of flights. However, the Los Angeles-Tahiti segment was covered four times, twice in each direction. Effects observed on the Los Angeles-Tahiti flights are discussed below, with emphasis on Station E. Station A was never available, and Stations C and H were consistently very strong on the flights. Station D showed a well defined trend towards somewhat weaker signals at Tahiti, but Stations F and G were not available in any noticeable strength to permit meaningful flight-to-flight comparisons of results. Similarly, Station B signal strengths were marginal and erratic, making analysis of any repeatability impossible.

Figures 5.17 and 5.18 show Station E S/N ratios observed on flights from Los Angeles to Tahiti, and Figures 5.19 and 5.20 show S/N ratios on the return flights. The dramatic transition in Station E S/N ratios on all flights is notable, with Figure 5.17 showing the cleanest transition and Figure

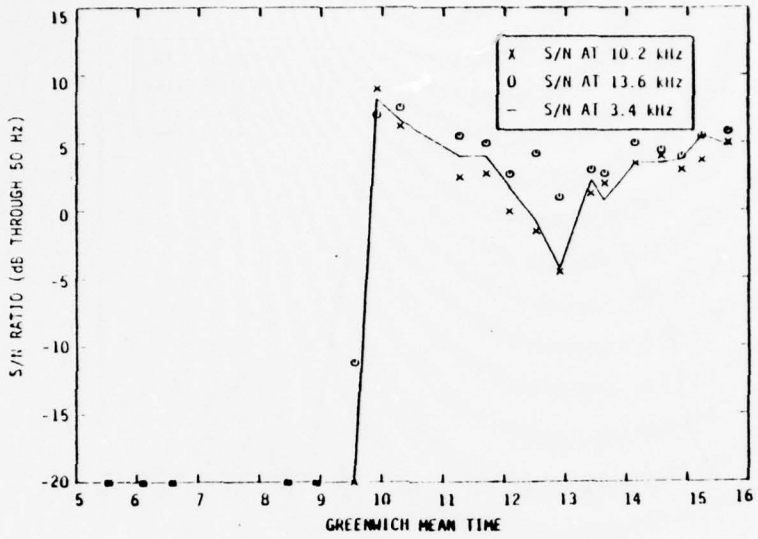

FIGURE 5.17 - S/N RATIOS, STATION E, SAN FRANCISCO-TAHITI VIA LOS ANGELES, FLIGHT 815, APRIL 11, 1976

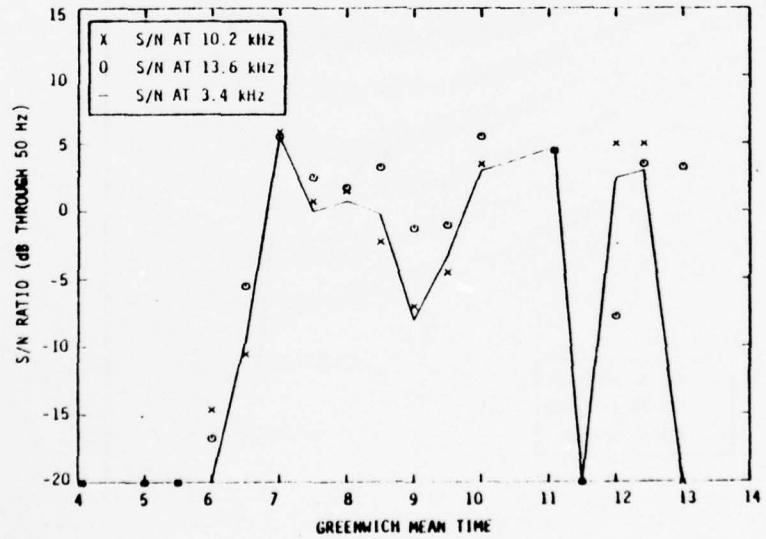

FIGURE 5.18 - S/N RATIOS, STATION E, SAN FRANCISCO-TAHITI VIA LOS ANGELES, FLIGHT 815, APRIL 25, 1976

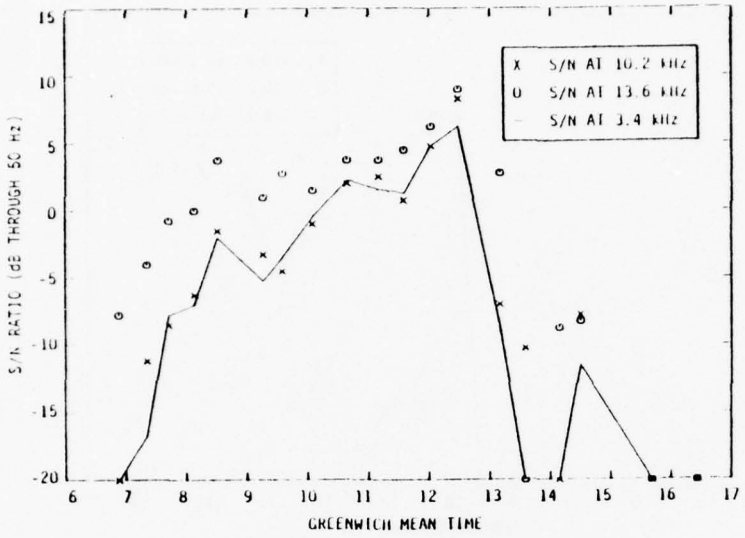

FIGURE 5.19 - S/N RATIOS, STATION E, TAHITI-SAN FRANCISCO VIA LOS ANGELES, FLIGHT 816, APRIL 12, 1976

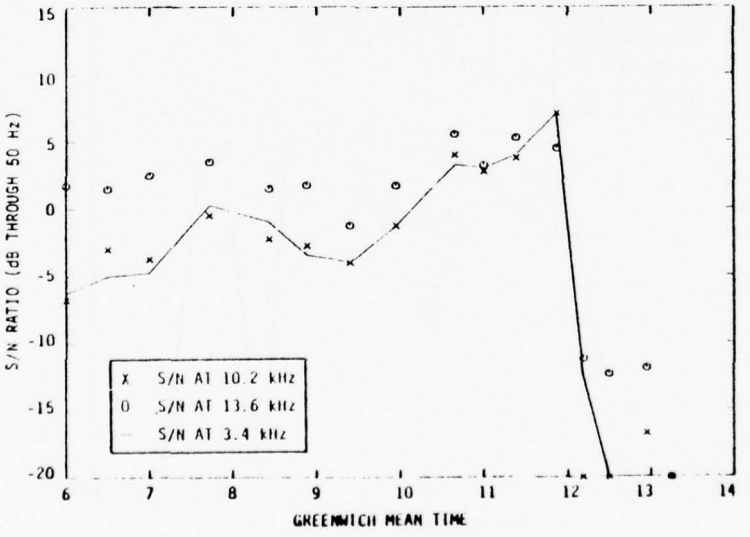

FIGURE 5.20 - S/N RATIOS, STATION E, TAHITI-LOS ANGELES FLIGHT 816, APRIL 29, 1976

5.19 showing the least abrupt S/N transition. Table 5.5 shows the locations of the aircraft during the middle of the transition from good signals to bad. Note that all of these points are fairly close together, perhaps because of the similarity in time of day; predicted propagation conditions [2] indicate that the threshold of available signals from Station E should be fairly invariant with time of day between Los Angeles and Tahiti.

5.3.4 Position Comparison Statistics

Statistics were generated comparing the indicated position of the CMC 740P to various position references. These included 90 data points, of which 35 were measured with the aircraft on the ground, 30 after takeoff, and the rest during cruise. Excluded from consideration were points taken immediately after landing, as the Omega receiver position on at least two occasions jumped 8 or 10 miles when the aircraft actually touched down.

The statistics generated are shown in Table 5.6. Note that the standard deviation of latitude is smaller than the standard deviation of longitude, and there is very little correlation between the latitude and longitude position-comparisons. The circular error probability (CEP) is approximately 2', or 2 nm.

5.3.5 Crosstrack Drift Incident

On Flight 816, 13 April 1976, the Omega-indicated position drifted approximately 16 nm relative to the Doppler radar and Loran-A positions. This unusual incident is discussed below, but no satisfactory explanation has been found.

TABLE 5.5 - MIDPOINTS OF STATION E S/N TRANSITIONS

FLIGHT	DATE	ORIGIN	DESTINATION	GMT	FIGURE	LAT.	LON.
815	April 11, 1976	San Francisco	Tahiti	0930	5.17	21°53'N	128°06'W
816	April 12, 1976	Tahiti	San Francisco	1310	5.19	24°02'N	126°37'W
815	April 25, 1976	San Francisco	Tahiti	0630	5.18	23°11'N	127°21'W
816	April 29, 1976	Tahiti	San Francisco	1200	5.20	25°45'N	125°27'W

TABLE 5.6 - POSITION COMPARISONS, PACIFIC FLIGHTS.
OMEGA REFERENCED TO GROUND POSITIONS

Latitude, Mean Error	0.5'N
Latitude, Std. Dev.	1.9'
Longitude, Mean Error	0.2'W
Longitude, Std. Dev.	2.5'
Correlation Coefficient	0.2
Number of Points	90

On Flight 816, 13 April 1976, a divergence between Omega-indicated position and Doppler and Loran-A positions was first noted at about 0900 (GMT), when the aircraft was at about 2°S, 141°W. At 0945 (1°N, 140°W), the Omega receiver was reset 16' to the east to compensate for the apparent drift. However, at 1230 (20°N, 129°W), the drift had started to fade, and the 16' update of the Omega set was removed.

Figure 5.21 shows the station geometry observed at 1229 (GMT), when the aircraft was at about 20°N, 129°W. The azimuths of great circle paths to the four stations with usable signal strengths were within 144° of each other, and three of these were within 54° of each other. Thus, the station geometry undoubtedly contributed to the crosstrack drift. However, the long duration of the crosstrack drift suggests that a propagation anomaly or an erroneous propagation prediction may have contributed to the error. Note that the addition of an Australian Omega station would not have substantially improved station geometry. Even the addition of an atomic time standard to the Omega receiver might not have completely solved the drift problem if, in fact, propagation anomalies were present.

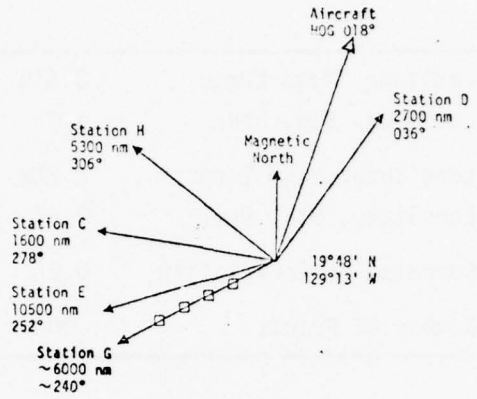

FIGURE 5.21 - GEOMETRY OF USABLE SIGNALS OBSERVED ON FLIGHT 816, 13 APRIL 1976, 1229 GMT

5.3.6 Expected Pacific Signal Quality with the Australian Station

The Australian station will make a valuable contribution to Omega navigation in the Pacific. The station will be especially important for navigation north and east of Australia, and will add redundant coverage to most of the rest of the Pacific.

The Australian station will be an important addition to the Omega signal complement in the East Indies and off the coast of Indochina. Presently, this area receives good signals from Station E to the east and Station H to the north. Stations B and C are often available, but the ranges to the transmitters are near the maximum limit of usability. With the Australian station operational, a third strong signal will be available in the region, with the two weaker signals available for increased reliability and accuracy.

In the Pacific as a whole, the Australian station will contribute signal redundancy to all but the North and South America western coasts. Stations C, D, E, and H already provide very good coverage of the Pacific except for the East Indies and Indochina, so that addition of the Australian station will not provide any new capabilities to most regions. However, the increased signal coverage will increase the redundancy available to the user.

5.4 CENTRAL AND SOUTH AMERICAN FLIGHTS

5.4.1 Introduction

A total of 21 flights to Central and South America were conducted. Table 5.7 documents these flights, which are divided into three groups: the Central American flights; the South American flights, including three round trips to Caracas and three round trips to Rio de Janeiro; and the South Atlantic flights, consisting of a round trip from Rio de Janeiro to Johannesburg, South Africa. The CMC 740P receiver was used on the Central American flights; the CMC 740 receiver was used on the South American and South Atlantic flights.

5.4.2 Signal Availability

5.4.2.1 South American Flights

Signal availability of the South American flights was generally good, with six stations (including Trinidad) usable on each flight. Figure 5.22 shows approximate signal availability areas.

TABLE 5.7 - CENTRAL AND SOUTH AMERICA DATA COLLECTION FLIGHT

	FLIGHT	DATE (1976)	ORIGIN	DESTINATION	DATA HOURS (GMT)
Central America	541	Mar 11	New York	San Jose, Costa Rica via Guatamala City	18-02
	541	Mar 12	San Jose	New York via Guatamala City & Washington, D.C.	13-24
South America	203	Jun 5	New York	Montevideo	01-13
	516	Jun 6	Montevideo	Caracas	13-18
	218	Jun 6	Caracas	New York	02-10
	201	Jul 6	New York	Rio de Janeiro	01-10
	202	Jul 7	Rio de Janeiro	New York	06-15
	217	Jul 22	New York	Caracas	12-20
	218	Jul 23	Caracas	New York	14-18
	201	Aug 2	New York	Rio de Janeiro	00-10
	202	Aug 3	Rio de Janeiro	New York	01-12
	217	Aug 12	New York	Caracas	13-19
	218	Aug 13	Caracas	New York	12-18
	201	Aug 18	New York	Rio de Janeiro	06-11
	202	Aug 19	Rio de Janeiro	New York	01-11
	217	Sep 9	New York	Caracas	14-18
	218	Sep 10	Caracas	New York	12-19
South Atlantic	201	Jul 6	Rio de Janeiro	Johannesburg	12-19
	202	Jul 7	Johannesburg	Rio de Janeiro via Capetown	12-15, 20-04

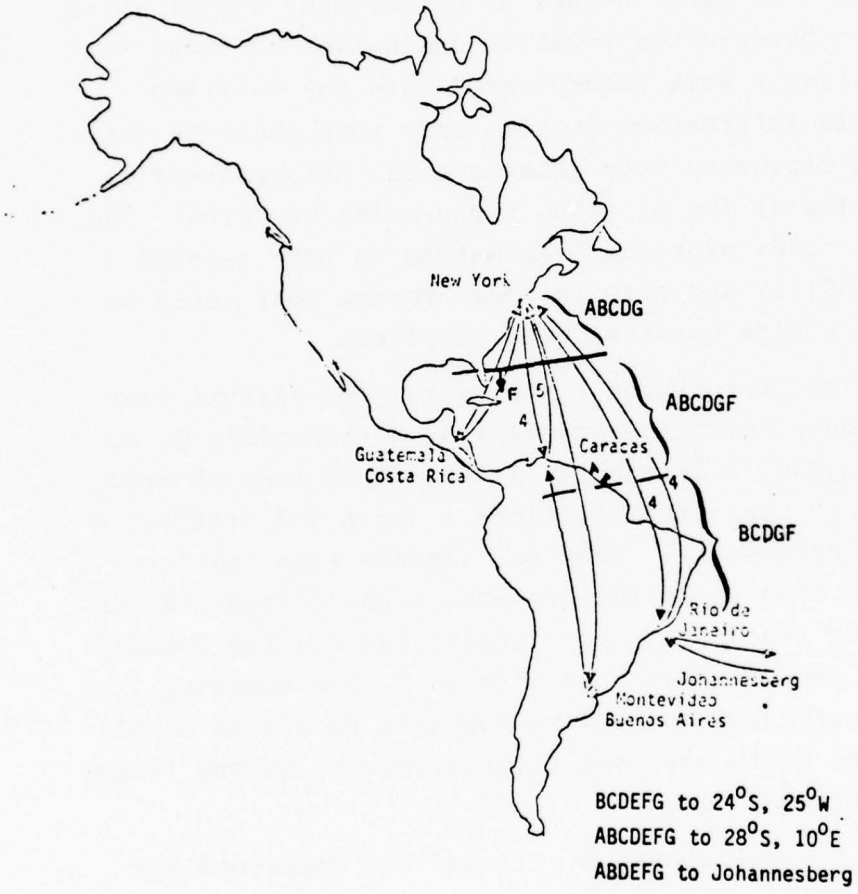

FIGURE 5.22 - OBSERVED OMEGA SIGNAL AVAILABILITIES ON SOUTH AMERICAN FLIGHTS

Data on signal availability was developed from two sources. In the first method, signal-to-noise ratio plots for each flight were generated from S/N ratios measured by the flight observer, and these plots were compared with plots from other flights to estimate signal quality, repeatability, and usability. The other method of determining signal availability was to observe the receiver indication of those stations whose signals were incorporated into the position solution. This information denotes only that phase measurements at some frequency were incorporated, not necessarily that information at two or three frequencies was used. The use of both methods provided information on both general signal availability and also the performance that could be expected from a high quality Omega receiver.

Six stations were found to be useful for flights from New York to South America: Stations A, B (Liberia), C, D, F, and G (Trinidad). Generally, it was found from observations of the S/N plots that Stations A and B and Stations D and F were complementary. That is, signals from Station A would begin to fade approximately when signals from Station B were becoming available, and signals from Station D would begin to fade when signals from Station F were becoming available. Stations C and G were found to be usable on all portions of the South American flights, except during flights too close to Station G.

Stations D and F showed a well-defined complementary signal availability pattern, but the complementary signal availability pattern of Stations A and B was less well defined. Station D usually showed a smooth, gradual, and well-defined decrease in S/N ratio on southbound flights. On these southbound flights, Station F showed a very similar increase in S/N ratios. This increase was also smooth, gradual, and well defined. Thus, signal availability of Stations D and F

was complementary, with one signal fading as the other grew stronger. Complementary signal availability of Stations A and B was stronger in the south. However, the signal strengths of these stations were erratic and less consistent than the signal strengths of Stations D and F.

On almost all of the South American flights, receiver software indicated that Stations B, C, D, F and G were used for nearly the entire flight. The CMC 740 flags a station as incorporated into the position solution if signals at any of the three frequencies were used. Thus, in marginal signal areas, the presence of signals at one particular frequency could mask the overall degradation of signal quality.

5.4.2.2 Central American Flights

The round trip to Central America did not display the same over-all signal availabilities as the flights to South America. Still, based on the one round trip, signal availabilities should be satisfactory over the Gulf of Mexico. Omega navigation will be of greatest value on this overwater segment of trips to Central America. From Florida southward, Stations C, D, F, and G were available, with Stations A, B and H intermittent. However, sufficient signals were available for the CMC 740P to operate in the difference frequency mode.

5.4.2.3 South Atlantic Flights

Signal availabilities on the South Atlantic flights were excellent. Generally, all stations except Station H were used on the flight from Rio de Janeiro to South Africa. Station A was usable only in the middle of the flight, and Station C was unusable over Africa. The other five stations, however, were available throughout the flight.

From the S/N plots, Stations B, E, and F show high S/N ratios, and Stations C, D, and G show fairly good S/N ratios. Station A was weak when available. Station H had good S/N ratios during the flight from South Africa to Rio de Janeiro, with usable signals obtained around local midlight.

5.4.3 Omega System Performance Without the Trinidad Station

In the western hemisphere, the effect of losing the Trinidad Omega station will vary from region to region, and will vary with receiver sensitivity and sophistication. Loss of Trinidad signals will have virtually no impact on Omega system performance in the South Atlantic, but may have an impact on signal availability over the Gulf of Mexico. Receivers which can process phase data independently at the various frequencies will have less performance loss than those which require signals to be present at two or three frequencies in order to navigate.

In the South Atlantic, Trinidad signals presently provide redundant coverage. With Stations B, C, D, E, and F available in this area, good signal quality and redundancy will exist even without the Trinidad station. Thus, the impact of losing this station should be minimal.

On South American flight routes, specifically New York to Caracas and Rio de Janeiro, the loss of the Trinidad station should be minimal for sensitive receivers in good installations, but may occasionally be significant for receivers of lower performance. The CMC 740 receiver usually was able to process data from Stations A, B, C, D, and F on South American flights. Thus, sufficient signal quality and redundancy for a high performance receiver should be available under most conditions of propagation media and transmitter availability. However,

Stations A and B and Stations D and F exhibit a complementary nature in signal availability, with Station C available over the entire route. If Station C is unavailable for any reason, and if the receiver sensitivity as installed is modest, then system performance may be unacceptable.

In the Gulf of Mexico, the situation is somewhat more sensitive to the availability of the Trinidad Omega station. Flight data shows that Stations C and D are of good quality in the Gulf, and Station F is near the threshold of availability during the day. Stations A, B, E, and H are not consistently available. Thus, the signal availability without Trinidad is only acceptable, with little margin for stations off the air or unreceivable.

5.4.4 Flight-to-Flight Repeatability of Results

The South American flights exhibited good repeatability of observed trends in S/N ratio for the stronger stations. Comparisons of Station A and Station F S/N ratios on flights from New York to Rio de Janeiro and Montevideo are discussed with supporting S/N ratio plots. Weaker stations showed little flight-to-flight repeatability of results.

On flights from New York to Rio de Janeiro and Montevideo, S/N ratio plots show good repeatability for Stations A and F. Station A S/N ratio plots for flights 203 (July 5, 1976), 201 (July 6, 1976), and 201 (August 2, 1976) are included as Figures 5.23 through 5.25. These plots consistently show good S/N ratios on Station A until signal cutoff. The cutoffs are shown in Table 5.8 and display good position correlation to the accuracy of the measurements, which is about 3° of latitude. Station F S/N ratios for these same three flights are included as Figures 5.26 through 5.28. The S/N ratios consistently increase on these flights.

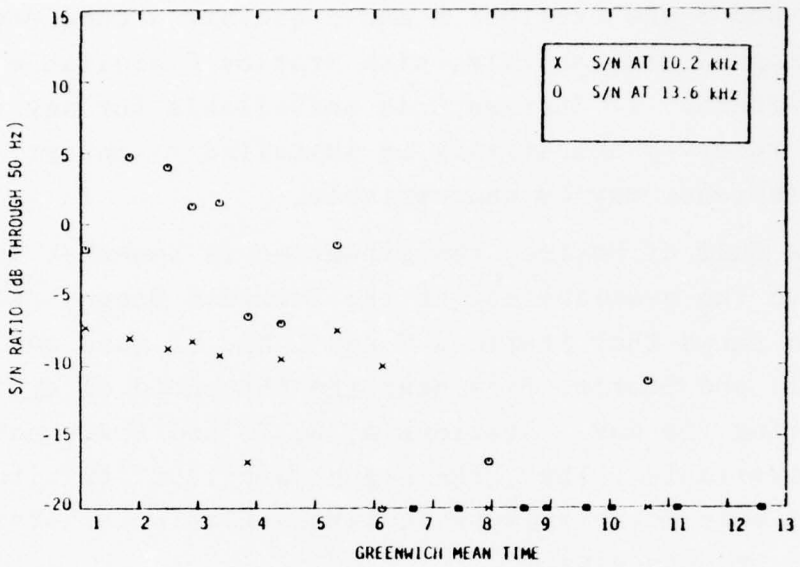

FIGURE 5.23 - S/N RATIOS, STATION A, NEW YORK-MONTEVIDEO, FLIGHT 203, JUNE 5, 1976

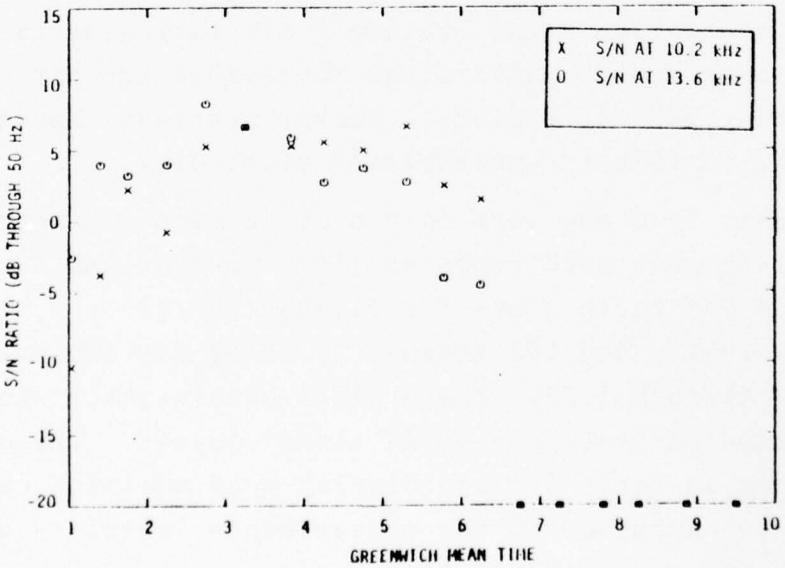

FIGURE 5.24 - S/N RATIOS, STATION A, NEW YORK-RIO DE JANEIRO, FLIGHT 201, JULY 6, 1976

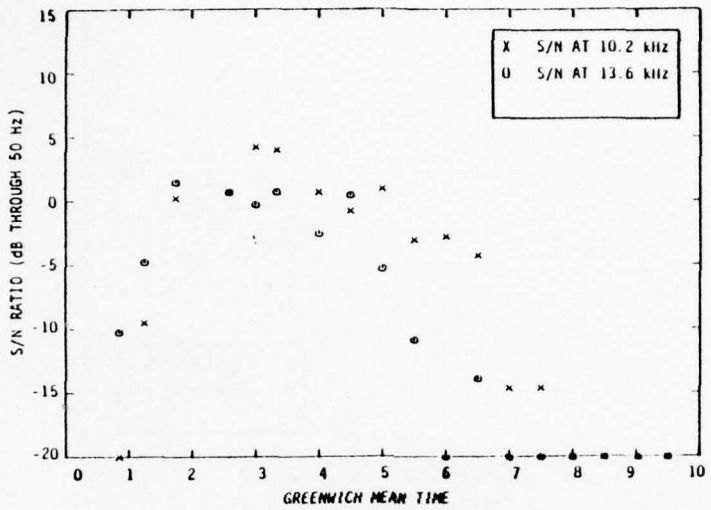

FIGURE 5.25 - S/N RATIOS, STATION A, NEW YORK-RIO DE JANEIRO, FLIGHT 201, AUGUST 2, 1976

TABLE 5.8 - LIMITS OF STATION A SIGNAL AVAILABILITY ON FLIGHTS TO SOUTH AMERICA

FLIGHT	DATE	LAT	LON	GMT
203	Jun 5, 1976	4°20'	3°03'	0608
201	Jul 6, 1976	3°03'	56°59'	0615
201	Aug 2, 1976	4°51'S	53°53'W	0730

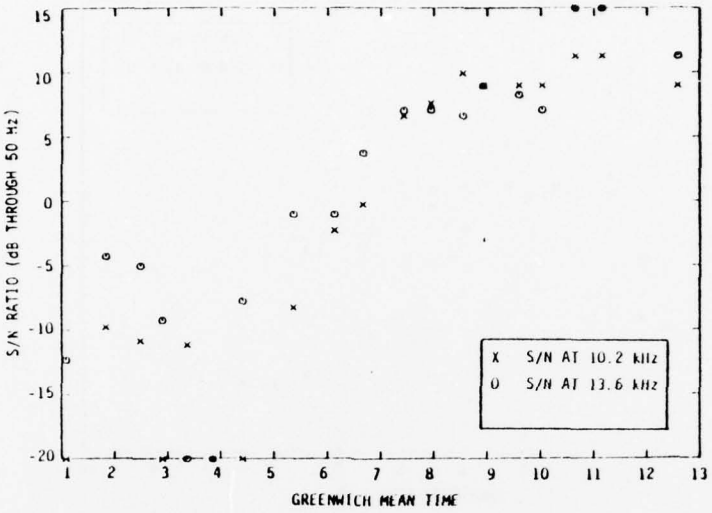

FIGURE 5.26 - S/N RATIOS, STATION F, NEW YORK-MONTEVIDEO, FLIGHT 203, JUNE 5, 1976

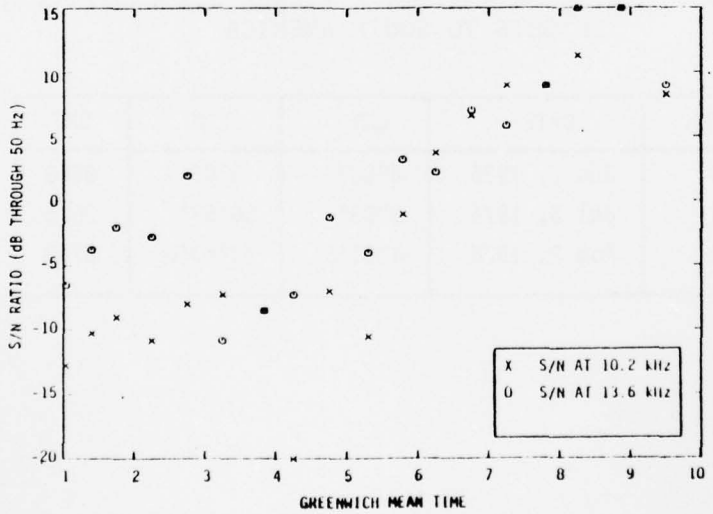

FIGURE 5.27 - S/N RATIOS, STATION F, NEW YORK-RIO DE JANEIRO, FLIGHT 201, JULY 6, 1976

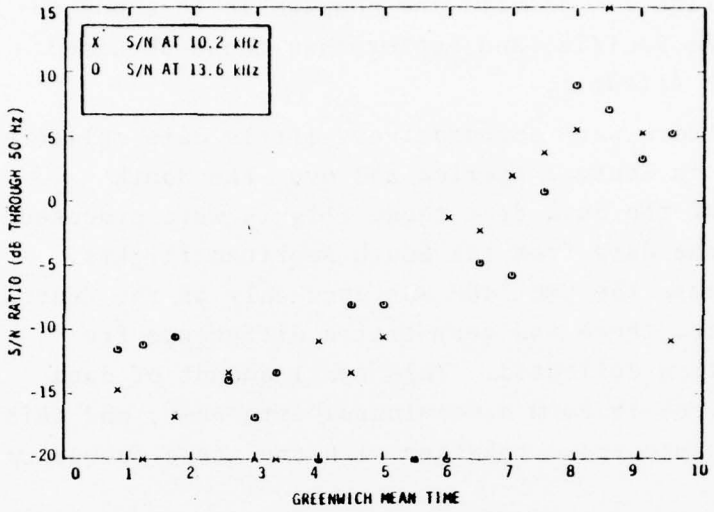

FIGURE 5.28 - S/N RATIOS, STATION F, NEW YORK-RIO DE JANEIRO, FLIGHT 201, AUGUST 2, 1976

Weaker stations, such as Station H, showed poor flight-to-flight repeatability of results. For a weaker station, any improvement or degradation of propagation medium characteristics can make the difference between signal availability or unavailability. Thus, the lack of correlation between signal availabilities on different days indicates fluctuations in propagation medium characteristics.

5.4.5 Position Comparison Statistics

Statistics were generated comparing the Omega-derived navigation parameters with navigation parameters obtained from other on-board sensors. The techniques used for the South American flight data processing were the same as used in the analysis of position-comparison data from the North Atlantic

and Pacific flights. Results are comparable to those obtained over the Pacific, and better than those obtained over the North Atlantic.

Because there were comparatively little data collected on the flights to Central America and over the South Atlantic, all of the data from these flights were processed together with the data from the South American flights. Similarly, because the CMC 740P was used only on the Central American flights, there was very little difference-frequency information collected. This small amount of data was not sufficient to form a meaningful data base, and this information was processed together with the three frequency Omega data.

Comparison of the CMC 740 position indications with the indications of traditional aircraft sensors was favorable. Table 5.9 shows the statistics generated. As in the results of previous sections, the standard deviations of longitude position comparison are larger than the standard deviations of latitude position comparison, even after allowing for the more closely spaced lines of longitude at high latitudes. The latitude and longitude position comparisons show only negligible correlation. Mean errors in both latitude and longitude are fairly small. In comparing the Omega position indications with Doppler radar position indications, note that the standard deviation in distance to go is greater than the root-sum-square of the latitude and longitude standard deviations of Omega relative to VOR, NDB, on-ground positions, and Doppler radar. In other words, the statistics suggest that the CMC 740 was somewhat more accurate than the Doppler radar.

TABLE 5.9 - POSITION COMPARISONS OF CMC 740 RELATIVE TO OTHER SENSORS

CMC 740 REFERENCED TO VOR, ADF, DOPPLER, POSITION FIXES, AND ON-GROUND FIXES	
Latitude, Mean Error	0.3 nm North
Latitude, Std. Dev.	1.5 nm
Longitude, Mean Error	0.1 nm East
Longitude, Std. Dev.	2.5 nm
Correlation Coeff.	0.3
CMC 740 RELATIVE TO DOPPLER RADAR	
Groundspeed, Mean Error	2.7 kt
Groundspeed, Std. Dev.	8.5 kt
Distance to go, Mean Error	-2.1 nm
Distance to go, Std. Dev.	4.7 nm

The cockpit observer felt that Omega was more accurate than the data of Table 5.9 would indicate. Errors in the Omega position comparisons would come from Doppler radar errors, imprecise knowledge of VOR locations in some parts of South America, and offset errors in overflying VORs and NDBs, in addition to Omega errors. The observer's subjective opinion was that Omega was accurate to one or two miles most of the time.

5.5 OTHER ROUTES

Additional flights accomplished included a round trip from New York to several cities in central Africa, and a flight from Seattle to New York via Fairbanks. Because the

receiver was not operating properly on the African trip, no results are presented from that trip.

5.5.1 Signal Availability Over North America

On the flight from Seattle to New York, signal availability was only adequate. In fact, signal availability over North America appears to be a major problem for Omega. Figure 5.29 shows the approximate route and signal availabilities observed on this flight. On the first leg of the flight, from Seattle to Fairbanks, Stations C and D were strong, H was marginal, and Station A was usable only after flying northward out of the Greeland Shadow. On the next leg of the flight, from Fairbanks to New York, Station A was usable only until the aircraft entered the Greenland Shadow. Station C showed signals at +5 dB on 10.2 kHz, but only at -10 dB on 13.6 kHz. Station D had very strong signals, but in flights near the transmitter, these signals would display near field effects and might not be usable. Station G (Trinidad) was weak but usable at the New York end on the flight east. In summary, Omega performance is marginal over this particular route.

5.5.2 Flights Through Auroras

Despite extensive auroral activity on the flight from Fairbanks to New York, little degradation in Omega system performance and signal characteristics were observed. Table 5.10 shows flight observer notes from this flight, along with position comparison statistics. Analysis of the S/N plots for this flight shows little if any degradation of S/N ratios during this flight. By comparison, in Figures 5.6 through 5.9, the correlation of S/N degradation with auroral activity was observed.

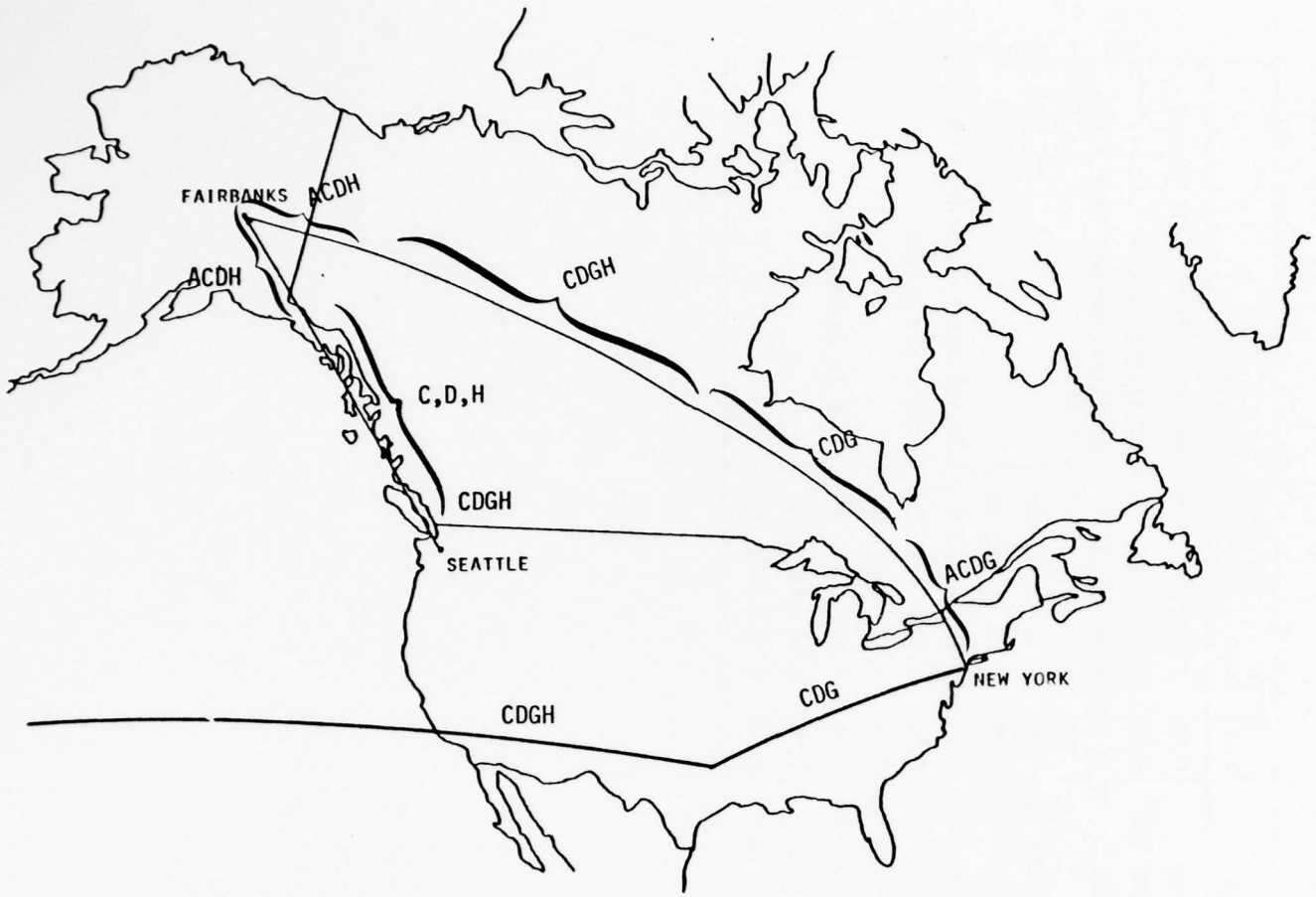

FIGURE 5.29 - OBSERVED SIGNAL AVAILABILITIES OVER NORTH AMERICA

TABLE 5.10 CONDENSED NOTES, FLIGHT 912, SEPTEMBER 20, 1976

GMT	Position	Error Lat.	Error Lon.	Stations In	Stations Use	Remarks
0503	Fairbanks	0.2N	1.6E	A CDE	H	An hour after local sunset
0518	Big Delta VOR	0.5S	2.7E	A CD	H	Brilliant aurora
0551	Mayo NDB	0.1N	3.0W	ABCDE	GH	Brilliant aurora both sides of track
0638	Ft. Simpson VOR	0.8N	3.9E	CD	GH	
0659	Hay River NDB	2.2N	2.0E	CDE	GH	
0755	Lynn Lake NDB	1.7S	2.1W	CDE	G	Occasional few seconds DR
0809	Thompson NDB	0.1S	1.1E	CDE	G	Aurora all around
0929	Kapuskasing NDB	0.1N	1.4E	BCD	GH	
0956	North Bay VOR	1.3N	0.8W	BCD	GH	Dawn in eastern sky
1034	Hancock VOR	1.5S	2.3E	ABCD	FGH	
1059	New York (JFK)	0.9N	1.2E	BCD	GH	

APPENDIX A
COMPOSITE OMEGA AND DIFFERENCE FREQUENCY CONCEPTS

A.1 INTRODUCTION

In this appendix, composite Omega [4, 5, 6] and 3.4 kHz difference frequency Omega are discussed. A new derivation of composite Omega is given, and 3.4 kHz difference frequency Omega is presented as a special case of composite Omega.

The appendix is concerned mainly with the theoretical discussions of combinations of 10.2 kHz and 13.6 kHz Omega signals. However, the concepts are applicable to any pair of frequencies.

A.2 DERIVATION OF COMPOSITE OMEGA

This section presents a derivation of composite Omega. In this derivation, the fundamental strengths and weaknesses of the composite Omega concept are clarified.

Let us consider the propagation time measured for an Omega signal traveling from the transmitter to the receiver. If the distance is d and the nominal propagation velocity is v, then at a specified frequency (say 10.2 kHz)

$$T_{10.2} = \frac{d}{v_{10.2}} + E_{10.2} \qquad (A.1)$$

In other words, the measured propagation time T is the quotient of the distance and the nominal (average) propagation speed, plus an error term $E_{10.2}$. Because $v_{10.2}$ is the average propagation speed, $E_{10.2}$ will be zero mean if there are no measurement biases. $E_{10.2}$ consists of propagation

anomalies, phase noise, and measurement errors. We can also write

$$T_{13.6} = \frac{d}{v_{13.6}} + E_{13.6} \tag{A.2}$$

Let us also assume that

$$v_{10.2} = v_{13.6} \tag{A.3}$$

Using Eq. (A.3), and subtracting Eq. (A.2) from Eq. (A.1), we obtain

$$T_{10.2} - T_{13.6} = E_{10.2} - E_{13.6} \tag{A.4}$$

Let us now consider the various components which together are lumped into E. These terms included predictable propagation anomalies (surface conductivity effects, magnetic field effects, diurnal variations, and seasonal variations), unpredictable anomalies (SIDs, PCAs, magnetic storms), and measurement errors. Note that multimodal propagation is assumed not to be a component of E, as in Eq. (A.3). The various components which affect $E_{10.2}$ will also affect $E_{13.6}$, and with the same algebraic sign (except possibly for measurement errors). Thus, we would expect some correlation between $E_{10.2}$ and $E_{13.6}$.

In general, for any probability distributions of $E_{10.2}$ and $E_{13.6}$, we can express $E_{13.6}$ as a linear combination of $E_{10.2}$ and a residue X, with X and $E_{10.2}$ uncorrelated. This result is derived in Section A.4. Thus, there exist a number c and a residue X such that

$$E_{13.6} = c\, E_{10.2} + X \tag{A.5}$$

In the case under consideration, $E_{13.6}$ and $E_{10.2}$ are zero mean and hence so is X. Combining Eqs. (A.5) and (A.4), we obtain

$$T_{10.2} - T_{13.6} = (1 - c)E_{10.2} - X \tag{A.6}$$

Since $E_{10.2}$ and X are uncorrelated, we can estimate $E_{10.2}$ by the optimal (minimum variance, minimum mean square error) linear estimate

$$\hat{E}_{10.2} = \frac{T_{10.2} - T_{13.6}}{1 - c} \tag{A.7}$$

and the error in this estimate of $E_{10.2}$ is

$$\hat{E}_{10.2} - E_{10.2} = \frac{-X}{1 - c} \tag{A.8}$$

We can use our estimate $\hat{E}_{10.2}$ to obtain an estimate of the propagation time if the propagation were at the nominal propagation speed

$$\hat{T}_{10.2} = T_{10.2} - \hat{E}_{10.2} \tag{A.9}$$

If we define

$$m = \frac{1}{1 - c} \tag{A.10}$$

and combine Eqs. (A.7), (A.9), and (A.10), we obtain

$$\hat{T}_{10.2} = m\, T_{13.6} - (m - 1)T_{10.2} \qquad (A.11)$$

This, of course, is the classic result obtained by Pierce [4].

Let us now discuss the limitations and implications of composite Omega, as illustrated in this derivation.

The first assumption made was that the propagation speeds were equal at 10.2 and 13.6 kHz. If, in fact, the average propagation speeds are not equal to each other, then there will be a bias term in Eq. (A.6) and hence in Eq. (A.8). Thus, The accuracy of our estimate $\hat{E}_{10.2}$ is degraded when the propagation speeds are not equal. Propagation speeds that are equal at the two frequencies but not equal to the nominal speed of propagation are components of $E_{10.2}$ and $E_{13.6}$, and not biases.

In composite Omega, the value of the correlation parameter c is very important. If c is near zero, composite Omega generates propagation corrections of low accuracy. If c is near one, however, composite Omega is extremely sensitive to measurement noise.

When $E_{10.2}$ and $E_{13.6}$ show little correlation (c near zero in Eq. (A.5)), the estimated propagation error $\hat{E}_{10.2}$ is comparatively poor. For an example, let us consider the special case of $c = 0$. The estimated propagation error $\hat{E}_{10.2}$ is, from Eqs. (A.4) and (A.7),

$$\hat{E}_{10.2} = E_{10.2} - E_{13.6} \qquad (A.12)$$

In other words, if the noise sources in each measurement show no correlation, and both measurements are required to estimate propagation errors, the linear estimator cannot reduce the

effects of the two noise sources by subtracting out that part of the noise common to both noise sources.

Let us now consider the special case of $c = 1$ in Eq. (A.5). Recall that c is not a correlation coefficient, and $c = 1$ does not mean $E_{13.6} = E_{10.2}$, nor does it mean $X = 0$. From Eqs. (A.7) and (A.8), it is clear that both our estimate $\hat{E}_{10.2}$ and the error in this estimate increase as c approaches 1. From Eq. (A.10), c near 1 implies m very large. Values of m greater than 4 or 5 are unusual, so values of c very close to 1 should not be observed in practice. However, Eq. (A.8) predicts that for c near 1, the error in the estimate $\hat{E}_{10.2}$ will increase. Because a component of the residue X in Eq. (A.8) is phase noise, composite Omega with c near 1 can be excessively sensitive to phase noise. For this reason, many 3.4 kHz difference frequency Omega receivers ($c = 0.75$) use longer receiver time constants in the 3.4 kHz difference frequency mode than in other modes.

Thus, composite Omega performs best when values of c are between 0 and 1--when c is close to 1, composite Omega is sensitive to measurement noise, and when c is close to 0, composite Omega provides little information. In the original paper [4], Pierce derived and showed experimental data that under most circumstances, $m = 2.25$. Substituting this value into Eq. (A.10) and solving for c, we find $c = 5/9$.

An easy way of using composite Omega without explicitly calculating propagation time is to use LOPs.

Differences of propagation time can be easily derived from phase measurements. The information supplied by the receiver will be the measured LOP

$$\text{LOP } (A\text{-}B)_{10.2} = \varphi_{A,10.2} - \varphi_{B,10.2} + 900 \qquad \text{(A.13)}$$

where $\varphi_{A,10.2}$ and $\varphi_{B,10.2}$ are the total phase delays encountered by the individual 10.2 kHz signals due to distance separation of the receiver and transmitters A and B. Since the Omega signals at 10.2 kHz make 10,200 complete sinusoidal oscillations per second, it follows that $\text{LOP (A-B)}_{10.2}$ is a measure of the difference of propagation times between signals from Station A and Station B. If $T_{A,10.2}$ is the propagation time for signals from Station A at 10.2 kHz, then

$$T_{A,10.2} - T_{B,10.2} = \frac{\text{LOP (A-B)}_{10.2} - 900}{10,200} \tag{A.14}$$

In a similar manner, we can obtain from the phase measurements

$$T_{A,13.6} - T_{B,10.2} = \frac{\text{LOP (A-B)}_{13.6} - 900}{10,200} \tag{A.15}$$

The time differences measured can be used to generate a composite Omega LOP if we assume the values c (or equivalently m) are equal for both stations. Let us suppose that we could measure $T_{A,10.2}$, $T_{A,13.6}$, $T_{B,10.2}$, and $T_{B,13.6}$ directly. Using Eq. (A.7), we obtain

$$\hat{E}_{A,10.2} = \frac{T_{A,10.2} - T_{A,13.6}}{1 - c} \tag{A.16}$$

and

$$\hat{E}_{B,10.2} = \frac{T_{B,10.2} - T_{B,13.6}}{1 - c} \tag{A.17}$$

AD-A041 095 SYSTEMS CONTROL INC PALO ALTO CALIF F/G 17/7
AN OPERATIONAL EVALUATION OF OMEGA FOR CIVIL AVIATION OCEANIC N--ETC(U)
FEB 77 F KARKALIK, E WISCHMEYER DOT-FA75WA-3662
UNCLASSIFIED FAA-RD-77-65 NL

2 OF 3
AD
A041 095

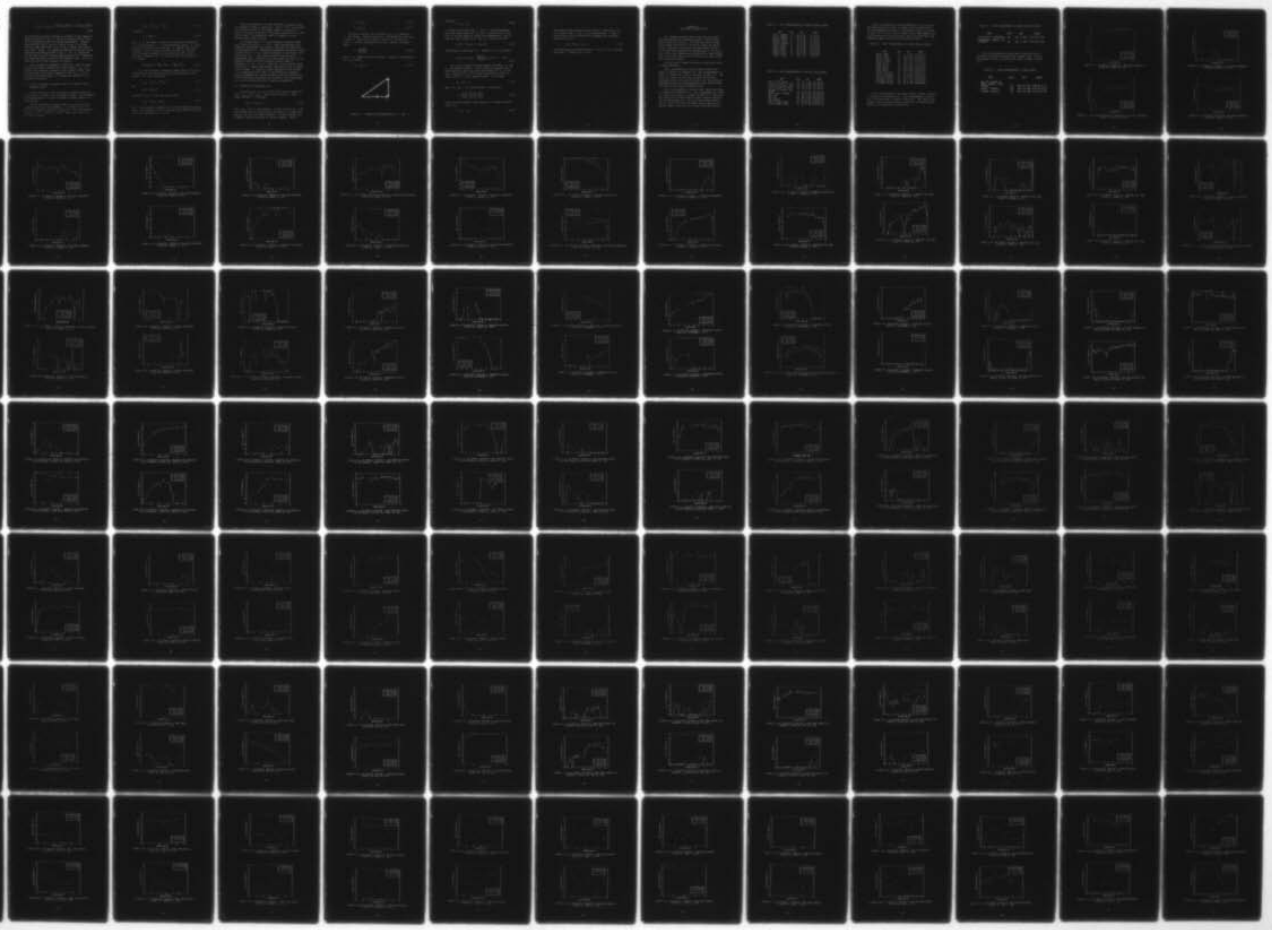

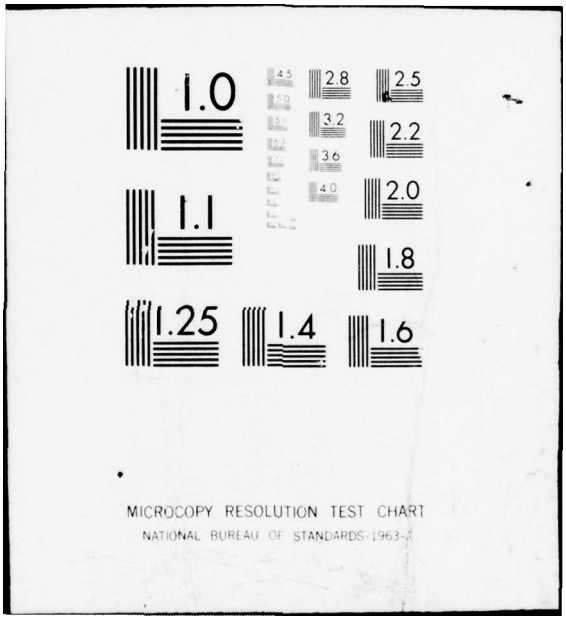
1.0
1.1
1.25
1.4
1.6
1.8
2.0
2.2
2.5
2.8
3.2
3.6
4.0
4.5
5.0
MICROCOPY RESOLUTION TEST CHART
NATIONAL BUREAU OF STANDARDS-1963-A

$$E_{A,10.2} - E_{B,10.2} = \frac{T_{A,10.2} - T_{B,10.2}}{1 - c} - \frac{T_{A,13.6} - T_{B,13.6}}{1 - c} \quad \text{(A.18)}$$

In other words, we have obtained an estimate of the composite Omega correction to the 10.2 kHz LOP, assuming that all four of the propagation times were known individually. However, comparing Eqs. (A.14) and (A.15) with (A.18), it is clear that the right hand side of Eq. (A.18) is known from the measured LOPs. Hence, the composite Omega LOP correction can be generated from measured LOPs if the c (or m) parameters are the same for both stations generating the LOP. Converting the composite Omega correction from seconds (in Eq. (A.18) to lanes (for use in the receiver) is trivial.

Under reasonable propagation conditions, composite Omega can be an extremely powerful yet simple concept. Eq. (A.7) captures the essential strength of the concept, namely, that the deviation from nominal propagation time $\hat{E}_{10.2}$ can be estimated from measurements of propagation time made at two different frequencies.

A.3 3.4 kHz DIFFERENCE FREQUENCY OMEGA AS A SPECIAL CASE OF COMPOSITE OMEGA

In this section, 3.4 kHz difference frequency Omega will be derived as a special case of composite Omega. The advantages and disadvantages of 3.4 kHz difference frequency Omega will be discussed.

3.4 kHz difference frequency Omega is a special case of composite Omega with the parameter c (from Eq. (A.5)) set to 0.75 for reasons that will be apparent. This corresponds to a value of $m = 4$ (from Eq. (A.10)). With this value of m, Eq. (A.11) becomes

$$\hat{T}_{10.2} = {}^{4}T_{13.6} - {}^{3}T_{10.2} \tag{A.19}$$

In general,

$$T_f = \varphi_f \lambda_f / v_f \tag{A.20}$$

where φ is the number of whole and fractional wavelengths, λ is the wavelength, v is the propagation speed, T is the propagation time, and the subscript f denotes a particular frequency. We have already assumed that the 10.2 kHz and 13.6 kHz signals propagate at the same speed (Eq. (A.3)). Therefore, combining Eqs. (A.19) and (A.20) and dividing out v, we obtain

$$\varphi_{10.2}\lambda_{10.2} = {}^{4}\varphi_{10.2}\lambda_{10.2} - {}^{3}\varphi_{10.2}\lambda_{10.2} \tag{A.21}$$

Let us now consider an imaginary Omega signal at 3.4 kHz, propagating at the same speed as the 10.2 kHz and 13.6 kHz signals. For this 3.4 kHz wave,

$$\lambda_{3.4} = {}^{3}\lambda_{10.2} = {}^{4}\lambda_{13.6} \tag{A.22}$$

and

$$\varphi_{3.4} = \varphi_{10.2}/3 \tag{A.23}$$

Equations (A.20), (A.22), and (A.23) yield

$$\hat{\varphi}_{3.4} = \varphi_{13.6} - \varphi_{10.2} \tag{A.24}$$

This is the classical equation for 3.4 kHz difference frequency Omega. The simplicity of this equation (both coefficients one) comes from the choice of $c = 0.75$.

The main advantage of 3.4 kHz difference frequency Omega over composite Omega is simplicity. In Eq. (A.24), an estimate for the phase of the 3.4 kHz Omega signal is expressed in terms of a simple difference of the phases measured at 10.2 kHz and 13.6 kHz. No propagation times are computed, and no multiplications are required.

Two disadvantages of 3.4 kHz difference frequency Omega arise from the choice of $c = 0.75$. These disadvantages are suboptimal propagation corrections, and excessive sensitivity to measurement noise. Suboptimal propagation corrections result from the use of $c = 0.75$, which in general is too large. This large value for c also causes excessive sensitivity to measurement noise. Equation (A.8) shows that the error of the composite Omega correction increases without bound as c approaches 1. For $c = 0.75$, the error in the composite Omega corrections is larger than optimal, and sensitive to increases in the residue X. Because a major component of the residue X is measurement noise, many 3.4 kHz difference frequency Omega implementations increase receiver time constants in the 3.4 kHz difference frequency mode to better filter measurement noise, with associated receiver tracking sluggishness.

A.4 DERIVATION OF EQUATION (A.5)

In Section A.2, Eq. (A.5) states that for any random variables $E_{13.6}$ and $E_{10.2}$, there exist a scalar c and a random variable X such that

$$E_{13.6} = cE_{10.2} + X \tag{A.25}$$

with $E_{10.2}$ and X uncorrelated. In this section, Eq. (A.25) will be derived first for the case of vectors in a plane, and then for the case of random variables. For this section, let us make a change of notation for easier reading. Define

$$E_1 = E_{10.2} \tag{A.26}$$

$$E_2 = E_{13.6} \tag{A.27}$$

Now let us consider the case where E_1, E_2, and hence X, are vectors. Observe Figure A.1. Our objective is to find a scalar c which will stretch or shrink E_1 so that the vector X will be perpendicular to E_1. Clearly, we should choose

$$c = \frac{\langle E_1, E_2 \rangle}{\langle E_1, E_1 \rangle} \tag{A.28}$$

where $\langle , \rangle$ denotes the inner product. Using our new notation, Eq. (A.5) becomes

$$E_2 = cE_1 + X \tag{A.29}$$

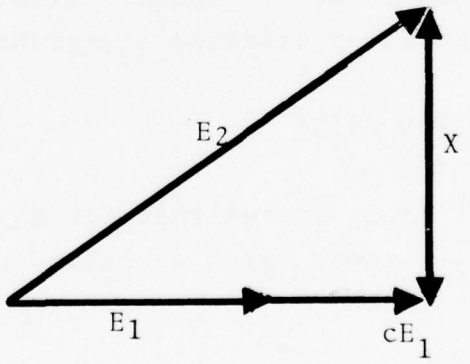

FIGURE A.1. GEOMETRICAL DETERMINATION OF c AND X

and hence

$$X = E_2 - cE_1 \tag{A.30}$$

It remains to be shown that X and E_1 are perpendicular. Since the inner product of E_1 and X will be zero if and only if the two (nonzero) vectors are perpendicular, let us take the inner product of X and E_1, using Eq. (A.24).

$$\langle X,E_1\rangle = \langle E_2,E_1\rangle - c\langle E_1,E_1\rangle \tag{A.31}$$

Substituting in the value of c from Eq. (A.22), we obtain

$$\langle X,E_1\rangle = \langle E_2,E_1\rangle - \frac{\langle E_1,E_2\rangle}{\langle E_1,E_1\rangle}\langle E_1,E_1\rangle = 0 \quad \text{Q.E.D.} \tag{A.32}$$

Let us now consider the more general case where E_1 and E_2 are random variables. We will make no assumptions as to distribution or mean, only that the variance of E_1 is not zero. Rewriting Eq. (A.5) in our new notation, we want to find a scalar c and a random variable X such that

$$E_2 = cE_1 + X \tag{A.33}$$

where E_1 and X are uncorrelated. If we define

$$c = \frac{\mathscr{E}[(E_1 - \bar{E}_1)(E_2 - \bar{E}_2)]}{\mathscr{E}[(E_1 - \bar{E}_1)(E_1 - \bar{E}_1)]} \tag{A.34}$$

where an overbar denotes mean value and $\mathscr{E}$ denotes expected value, and

$$X = E_2 - cE_1 \tag{A.35}$$

then these values give the desired results. Equation (A.33) is satisfied, and X and E_1 are uncorrelated. X and E_1 can be shown to be uncorrelated by expanding the left hand side of Eq. (A.36)

$$\mathcal{E}[(X - \overline{X})(E_1 - \overline{E}_1)] = 0 \qquad \text{(A.36)}$$

and substituting the expression for X by Eq. (A.35), and the value for c given by Eq. (A.34).

APPENDIX B
SELECTED S/N RATIO PLOTS

This appendix contains most of the S/N ratio plots generated during the evaluation program. Most omitted plots showed S/N ratios of -20 dB for the entire flight. A few showed S/N ratios of -20 dB for almost the entire flight, with only a few points that were above -20 dB. It is therefore reasonable to conclude that if S/N ratio plots for a given station were omitted for a given flight, that station was found to be of little or no value during that evaluation flight.

The plots are arranged according to region and route, as described below.

Plots corresponding to North Atlantic routes are shown in Figures B.1 through B.55. The correspondence of plots to a particular route is as shown in Table B.1. The first two flights in the table address the New York-Copenhagen route, the next four address the route between Frankfurt and the New York/Washington area, and the final five address the Chicago-Frankfurt route.

Plots corresponding to Pacific Ocean routes are shown in Figures B.56 through B.144. The correspondence of plots to a particular route is as shown in Table B.2. The first two flights in the table address routes between Honolulu and the continental U.S.; the next four flights address the U.S. West Coast-Tahiti-Auckland routes, and the remainder address routes in the western and South Pacific.

TABLE B.1 - PLOTS CORRESPONDING TO NORTH ATLANTIC ROUTES

ROUTE	FLIGHT	DATE	FIGURES
New York - Copenhagen	44	Aug. 19, 1975	B.1 thru B.5
New York - Copenhagen	44	Aug. 26, 1975	B.6 thru B.10
New York - Frankfurt	66	Mar. 22, 1976	B.11 thru B.13
Washington - Frankfurt	66	Aug. 21, 1975	B.14 thru B.18
Frankfurt - Washington	67	Aug. 21, 1975	B.19 thru B.23
Frankfurt - New York	67	Mar. 26, 1976	B.24 thru B.30
Chicago - Frankfurt	58	Aug. 23, 1975	B.31 thru B.35
Chicago - Frankfurt	58	Aug. 28, 1975	B.36 thru B.40
Frankfurt - Chicago	59	Aug. 28, 1975	B.41 thru B.45
Frankfurt - Chicago	59	Sept. 1, 1975	B.46 thru B.50
Frankfurt - Chicago	59	Sept. 2, 1975	B.51 thru B.55

TABLE B.2 PLOTS CORRESPONDING TO PACIFIC OCEAN ROUTES

ROUTE	FLIGHT	DATE	FIGURES
New York - Dallas - Honolulu	825	Apr. 8, 1976	B.56 thru B.63
Honolulu - Los Angeles - San Francisco	818	Apr. 10, 1976	B.64 thru B.70
San Francisco - Los Angeles - Tahiti	815	Apr. 11, 1976	B.71 thru B.77
Tahiti - Los Angeles - San Francisco	816	Apr. 12, 1976	B.78 thru B.84
San Francisco - Los Angeles - Tahiti - Auckland	815	Apr. 25, 1976	B.85 thru B.96
Auckland - Tahiti - Los Angeles	816	Apr. 29, 1976	B.97 thru B.110
Tokyo - Guam	803	May 17, 1976	B.111 thru B.117
Guam - Tokyo	802	May 17, 1976	B.118 thru B.123
Tokyo - Hong Kong	003	May 18, 1976	B.124 thru B.130
Hong Kong - Djakarta - Sydney	812	May 19, 1976	B.131 thru B.137
Sydney - Pago Pago - Honolulu	812	May 20, 1976	B.138 thru B.144

Plots corresponding to route between the U.S. East Coast and South America are shown in Figures B.145 through B.250. The correspondence of plots to a particular route is as shown in Table B.3. The first nine flights in the table address the route bewteen New York and Caracas, and on to Montevideo; the remainder address New York-Rio de Janeiro routes.

TABLE B.3 - PLOTS CORRESPONDING TO SOUTH AMERICAN ROUTES

ROUTE	FLIGHT	DATE	FIGURES
New York - Caracas	217	July 22, 1976	B.145 thru B.151
New York - Caracas	217	Aug. 12, 1976	B.152 thru B.158
New York - Caracas	217	Sept. 9, 1976	B.159 thru B.165
New York - Montevideo	203	June 5, 1976	B.166 thru B.173
Montevideo - Caracas	516	June 6, 1976	B.174 thru B.180
Caracas - New York	218	June 6, 1976	B.181 thru B.187
Caracas - New York	218	July 23, 1976	B.188 thru B.194
Caracas - New York	218	Aug. 13, 1976	B.195 thru B.201
Caracas - New York	218	Sept 10, 1976	B.202 thru B.207
New York - Rio de Janeiro	201	July 6, 1976	B.208 thru B.214
New York - Rio de Janeiro	201	Aug. 2, 1976	B.215 thru B.221
New York - Rio de Janeiro	201	Aug. 18, 1976	B.222 thru B.228
Rio de Janeiro - New York	202	July 7, 1976	B.229 thru B 236
Rio de Janeiro - New York	202	Aug. 3, 1976	B.237 thru B.243
Rio de Janeiro - New York	202	Aug. 20, 1976	B.244 thru B.250

Plots corresponding to the South Atlantic routes are shown in Figures B.251 through B.265. The correspondence of plots to a particular route is shown in Table B.4. The single South Atlantic route on which data were collected is between Rio de Janeiro and Johannesburg, South Africa.

TABLE B.4 - PLOTS CORRESPONDING TO SOUTH ATLANTIC ROUTES

ROUTE	FLIGHT	DATE	FIGURES
Rio de Janeiro - Johannesburg	201	July 6, 1976	B.251 thru B.257
Johannesburg - Capetown - Rio de Janeiro	202	July 7, 1976	B.258 thru B.265

Plots corresponding to other routes on which data was collected are shown in Figures B.266 through B.281. The correspondence of plots to a particular route is shown in Table B.5.

TABLE B.5 - PLOTS CORRESPONDING TO OTHER ROUTES

ROUTE	FLIGHT	DATE	FIGURES
New York - Nairobi via Dakar - Monrovia - Lagos - Kinshasa	190	March 16, 1976	B.266 thru B.272
Seattle - Fairbanks	903	Sept 20, 1976	B.273 thru B.276
Fairbanks - New York	912	Sept 20, 1976	B.277 thru B.281

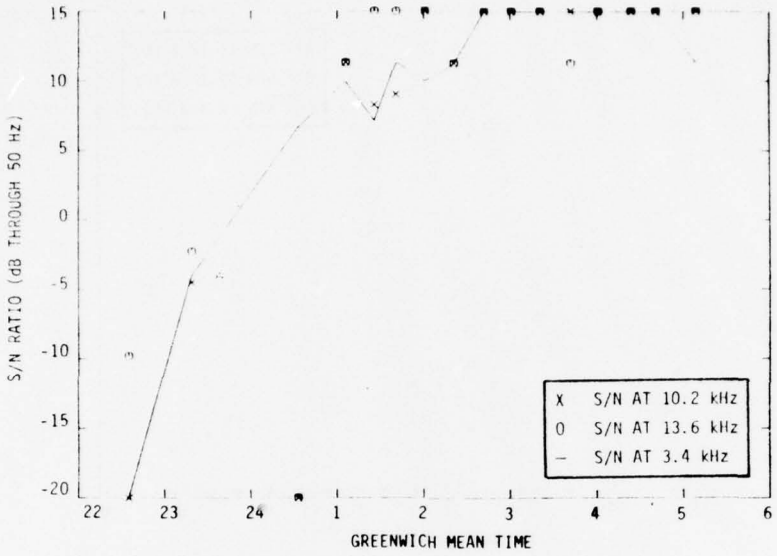

FIGURE B-1. S/N RATIOS, STATION A, NEW YORK COPENHAGEN FLIGHT 44, AUGUST 19, 1975

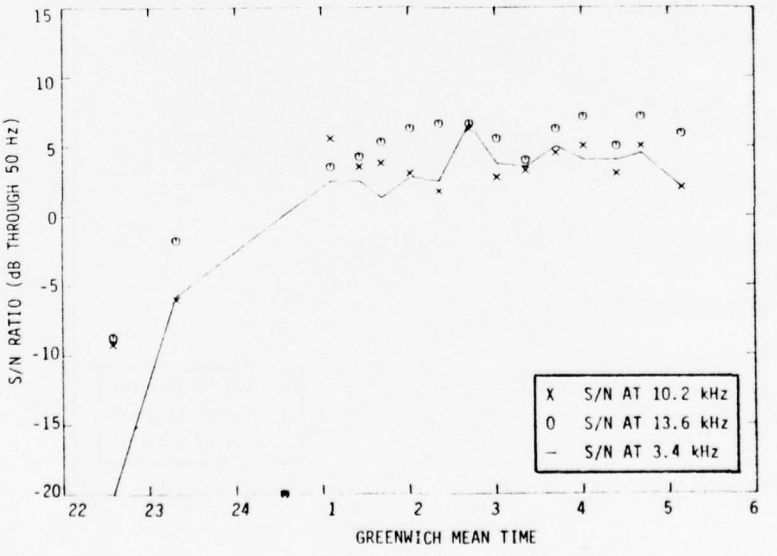

FIGURE B.2 S/N RATIOS, STATION B (TRINIDAD), NEW YORK-COPENHAGEN FLIGHT 44, AUGUST 19, 1975

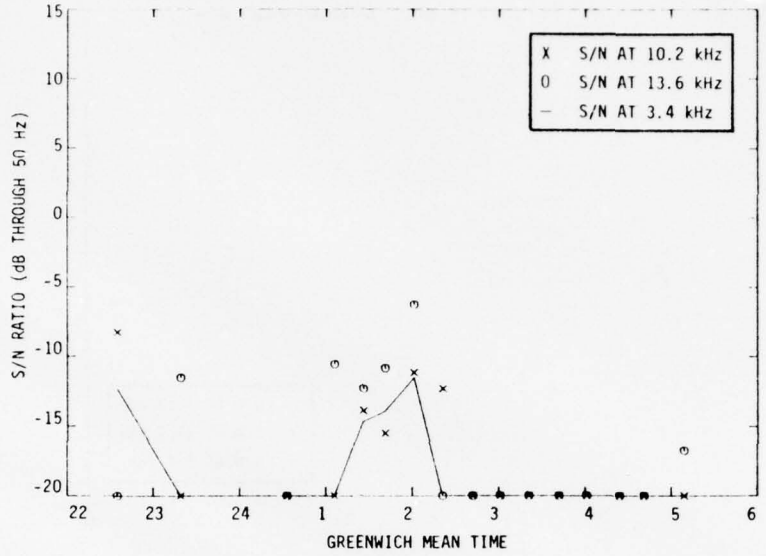

FIGURE B.3. S/N RATIOS, STATION C, NEW YORK-COPENHAGEN, FLIGHT 44, AUGUST 19, 1975

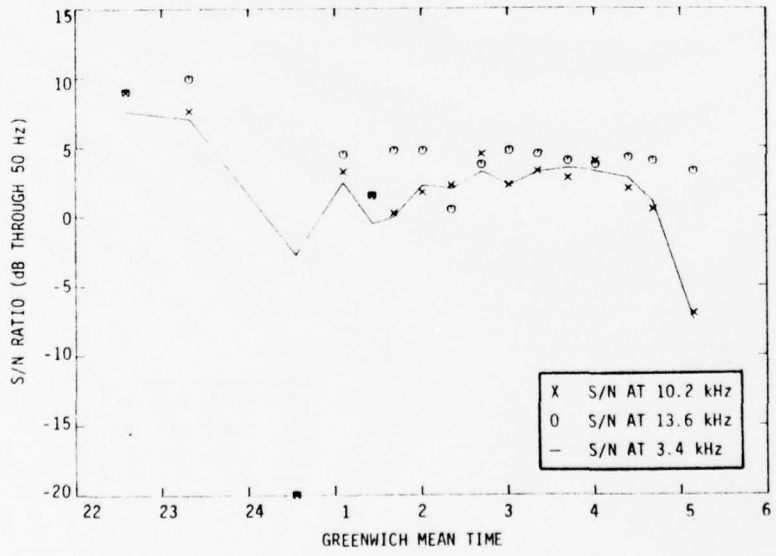

FIGURE B.4. S/N RATIOS, STATION D, NEW YORK-COPENHAGEN, FLIGHT 44, AUGUST 19, 1975

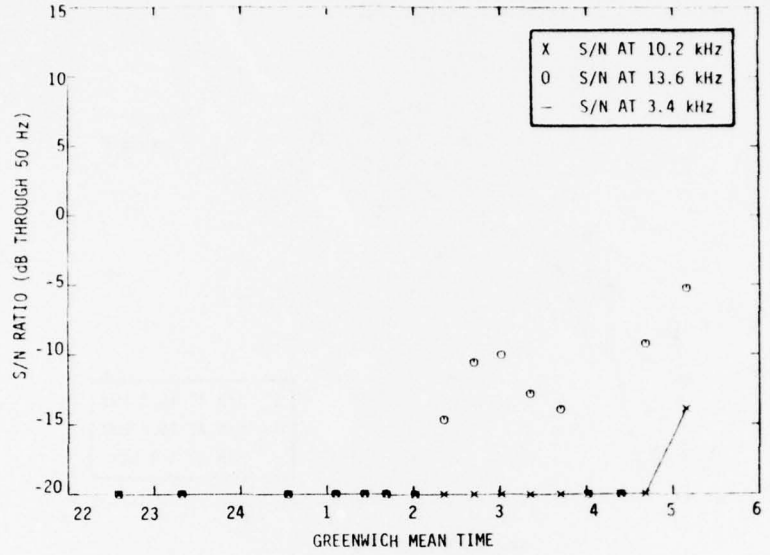

FIGURE B.5. S/N RATIOS, STATION H, NEW YORK-COPENHAGEN, FLIGHT 44, AUGUST 19, 1975

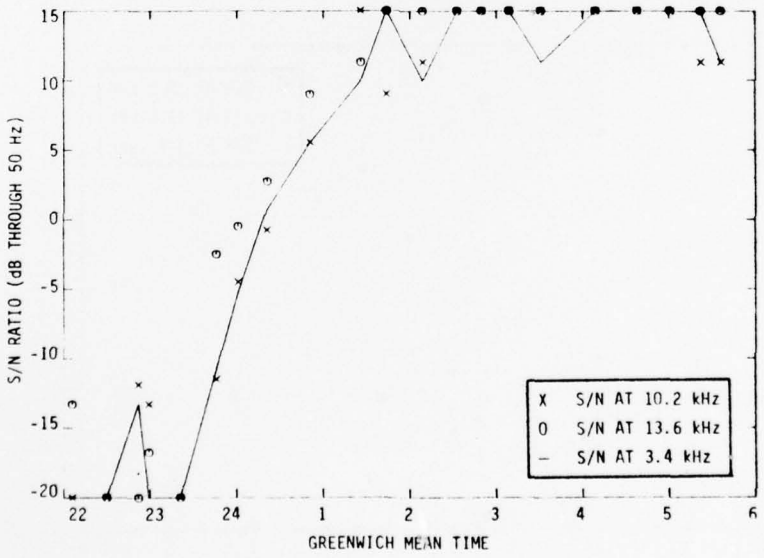

FIGURE B.6. S/N RATIOS, STATION A, NEW YORK-COPENHAGEN, FLIGHT 44, AUGUST 26, 1975

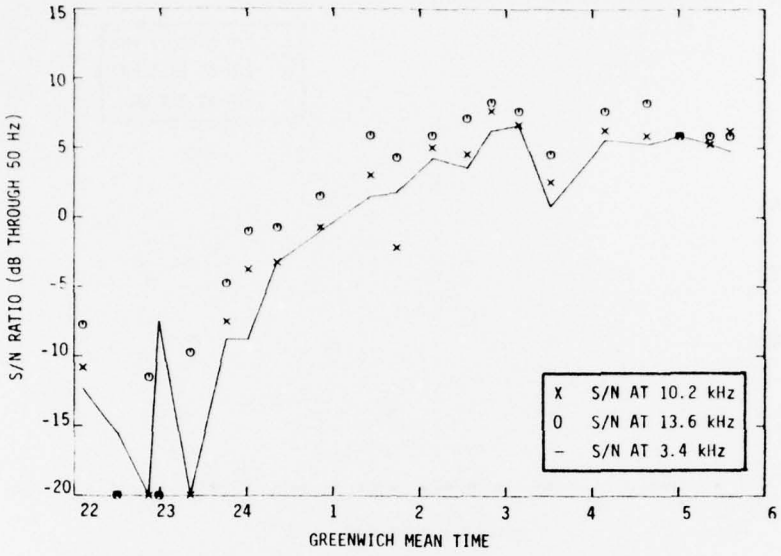

FIGURE B. 7. S/N RATIOS, STATION B (TRINIDAD), NEW YORK-COPENHAGEN FLIGHT 44, AUGUST 26, 1975

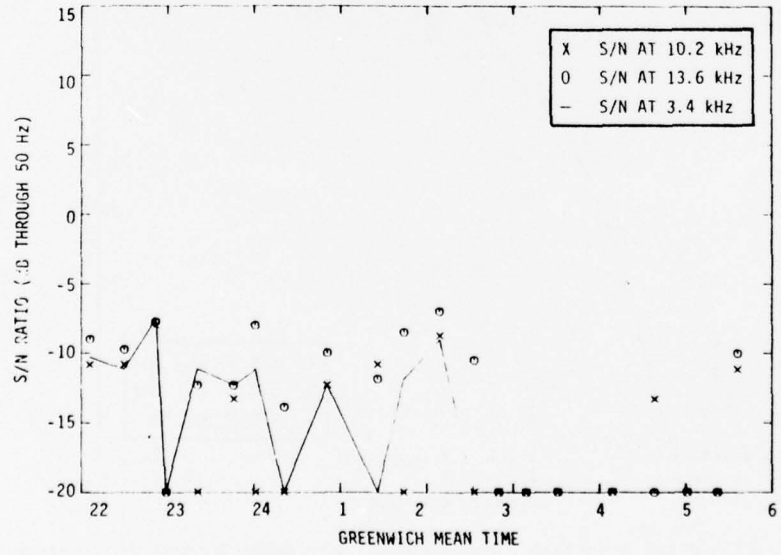

FIGURE B. 8. S/N RATIOS, STATION C, NEW YORK-COPENHAGEN, FLIGHT 44, AUGUST 26, 1975

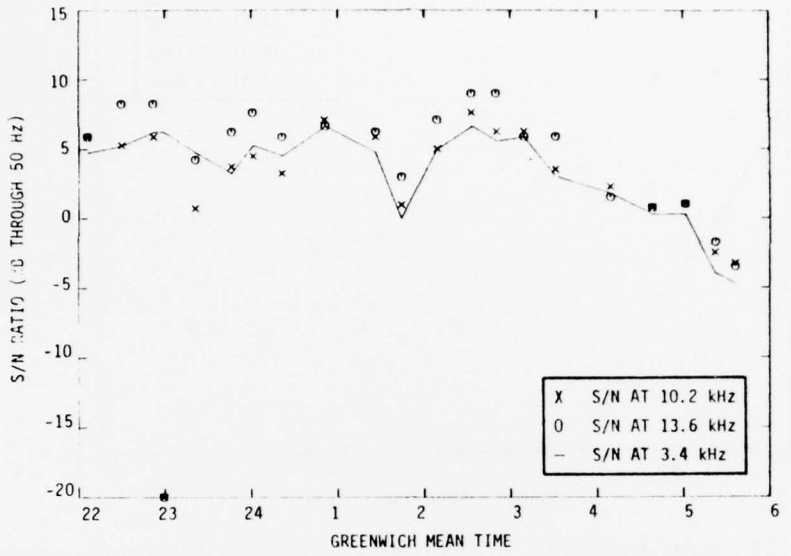

FIGURE B. 9 . S/N RATIOS, STATION D, NEW YORK-COPENHAGEN, FLIGHT 44, AUGUST 26, 1975

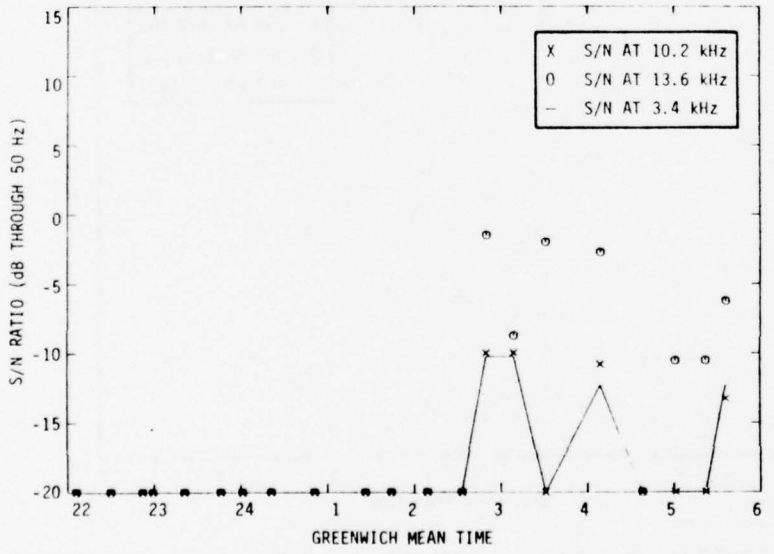

FIGURE B.10. S/N RATIOS, STATION H, NEW YORK-COPENHAGEN, FLIGHT 44, AUGUST 26, 1975

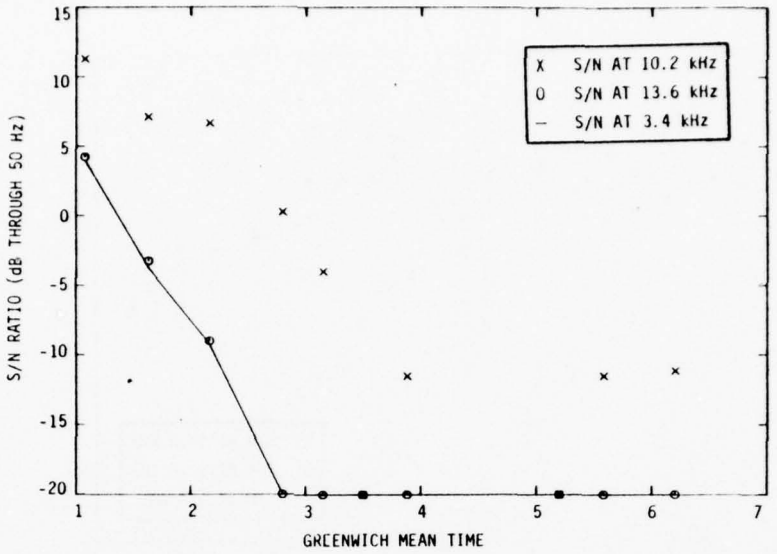

FIGURE B.11. S/N RATIOS, STATION D, NEW YORK-FRANKFURT, FLIGHT 66, MARCH 22, 1976

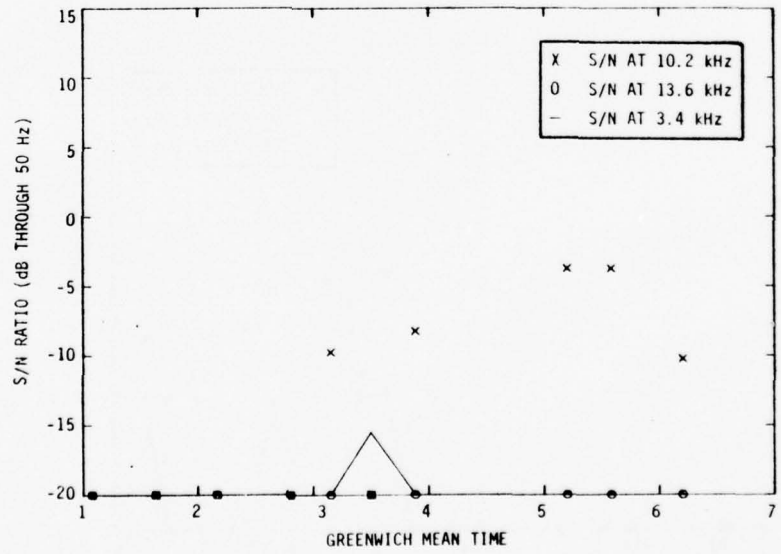

FIGURE B. 12. S/N RATIOS, STATION F, NEW YORK-FRANKFURT, FLIGHT 66, MARCH 22, 1976

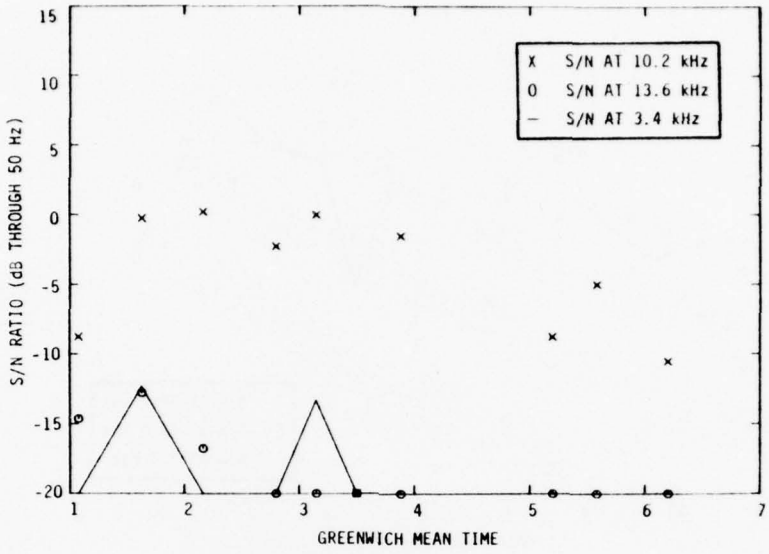

FIGURE B. 13. S/N RATIOS, STATION G, NEW YORK-FRANKFURT, FLIGHT 66, MARCH 22, 1976

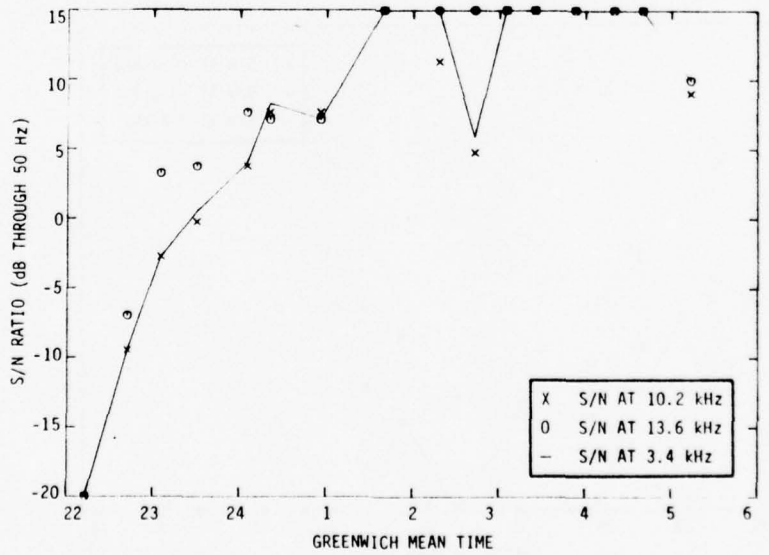

FIGURE B. 14. S/N RATIOS, STATION A, WASHINGTON-FRANKFURT, FLIGHT 66, AUGUST 21, 1975

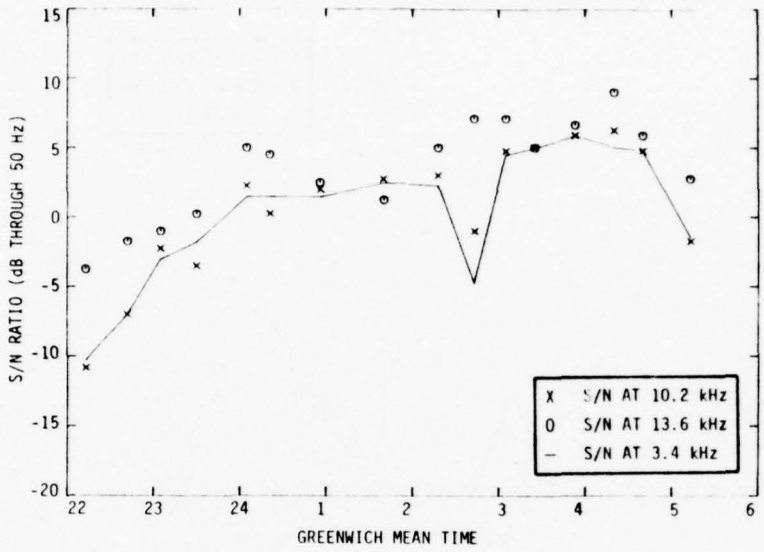

FIGURE B.15. S/N RATIOS, STATION B (TRINIDAD), WASHINGTON-FRANKFURT, FLIGHT 66, AUGUST 21, 1975

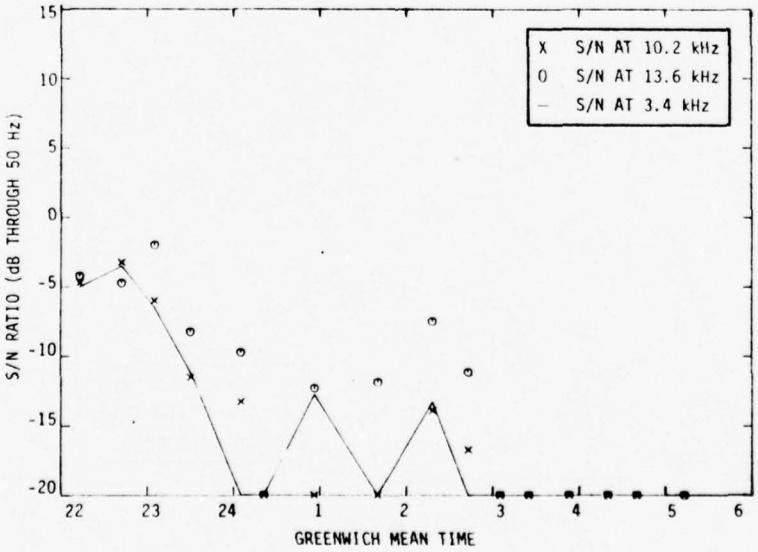

FIGURE B.16. S/N RATIOS, STATION C, WASHINGTON-FRANKFURT, FLIGHT 66, AUGUST 21, 1975

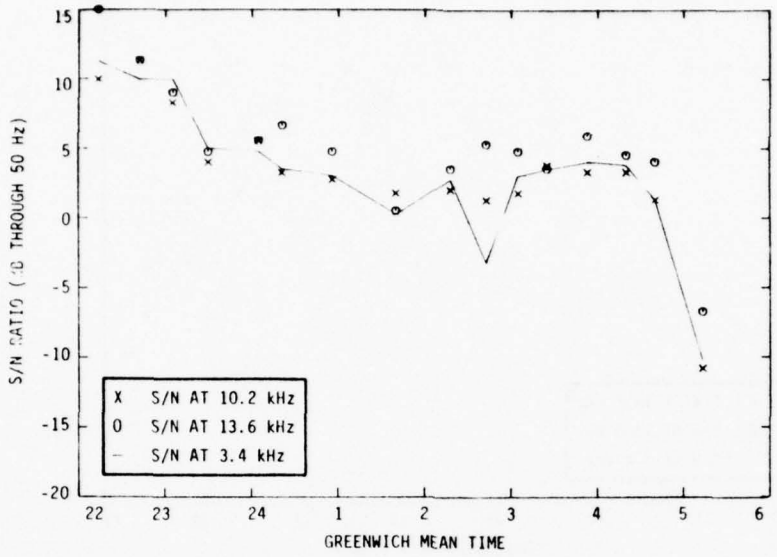

FIGURE B.17. S/N RATIOS, STATION D, WASHINGTON-FRANKFURT, FLIGHT 66, AUGUST 21, 1975

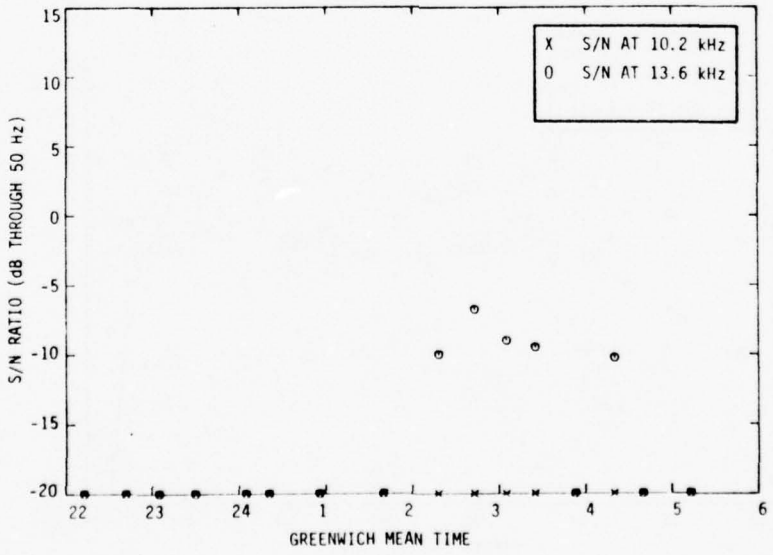

FIGURE B.18. S/N RATIOS, STATION H, WASHINGTON-FRANKFURT, FLIGHT 66, AUGUST 21, 1975

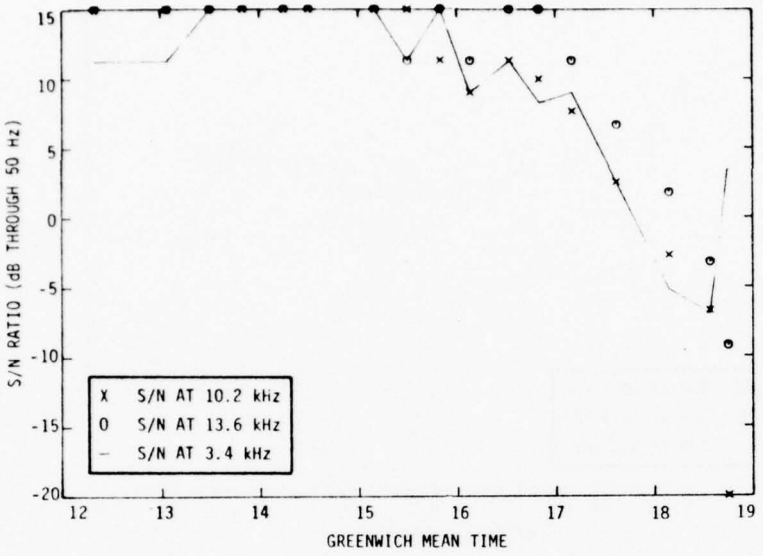

FIGURE B.19. S/N RATIOS, STATION A, FRANKFURT-WASHINGTON, FLIGHT 67, AUGUST 21, 1975

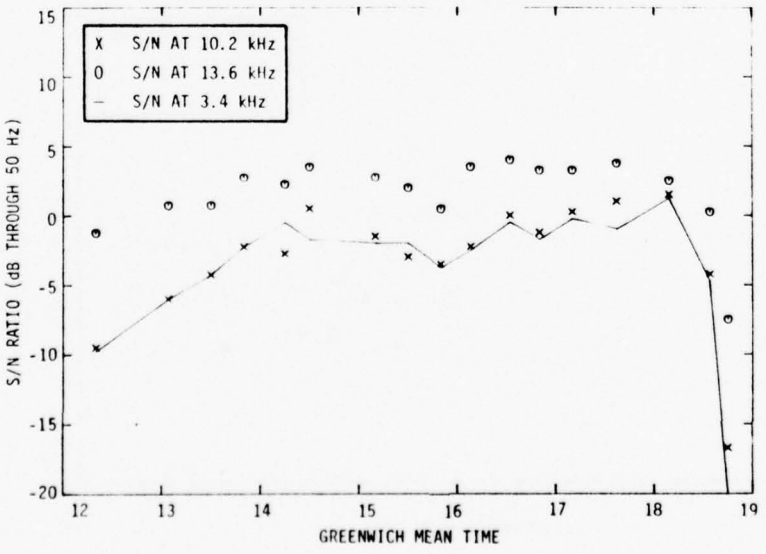

FIGJRE B.20. S/N RATIOS, STATION B (TRINIDAD), FRANKFURT-WASHINGTON FLIGHT 67, AUGUST 21, 1975

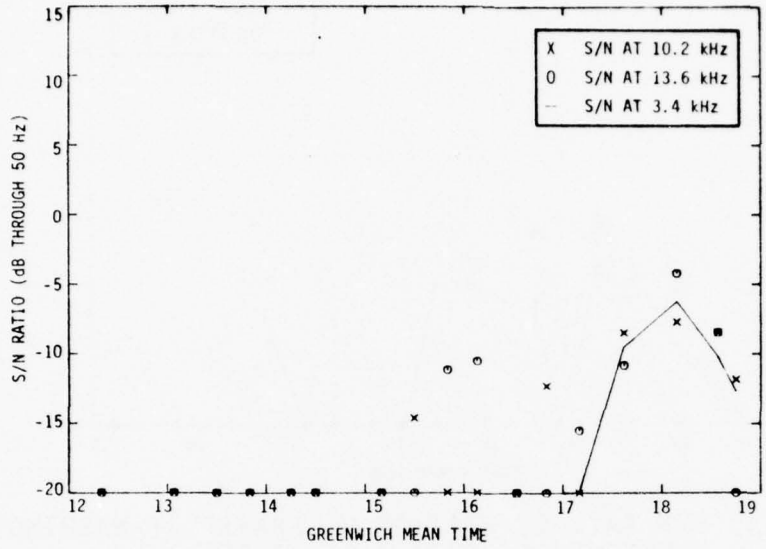

FIGURE B.21. S/N RATIOS, STATION C, FRANKFURT-WASHINGTON, FLIGHT 67, AUGUST 21, 1975

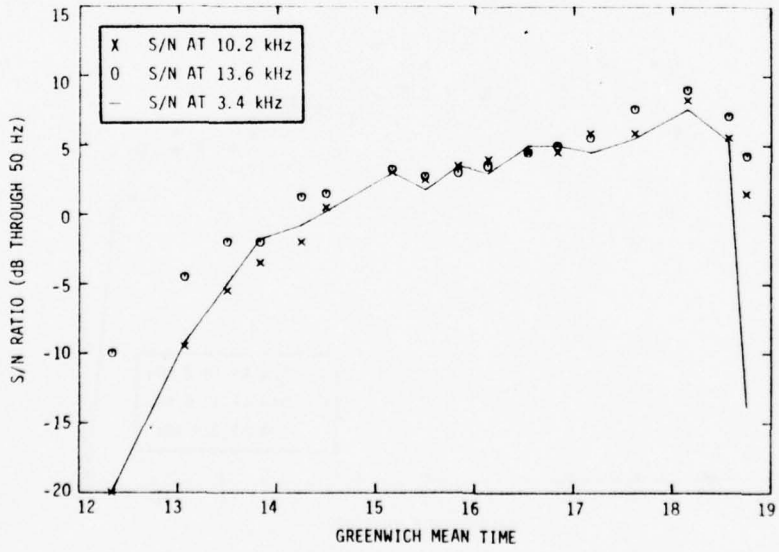

FIGURE B.22. S/N RATIOS, STATION D, FRANKFURT-WASHINGTON, FLIGHT 67, AUGUST 21, 1975

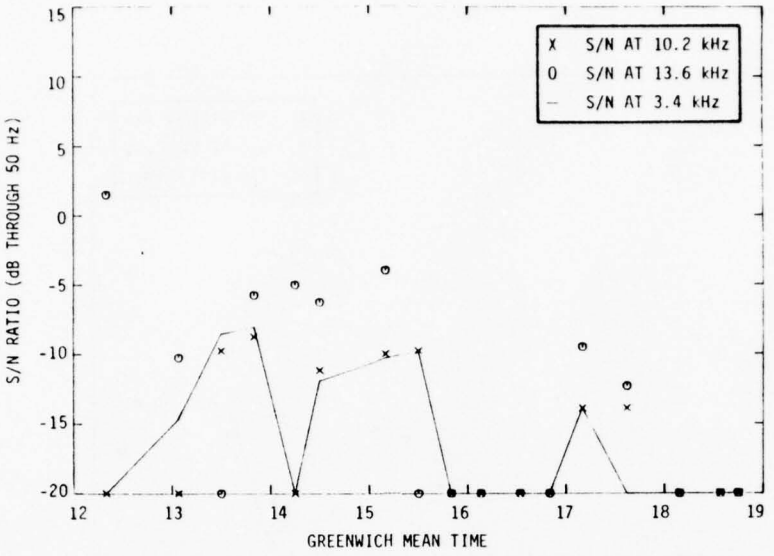

FIGURE B.23. S/N RATIOS, STATION H, FRANKFURT-WASHINGTON, FLIGHT 67, AUGUST 21, 1975

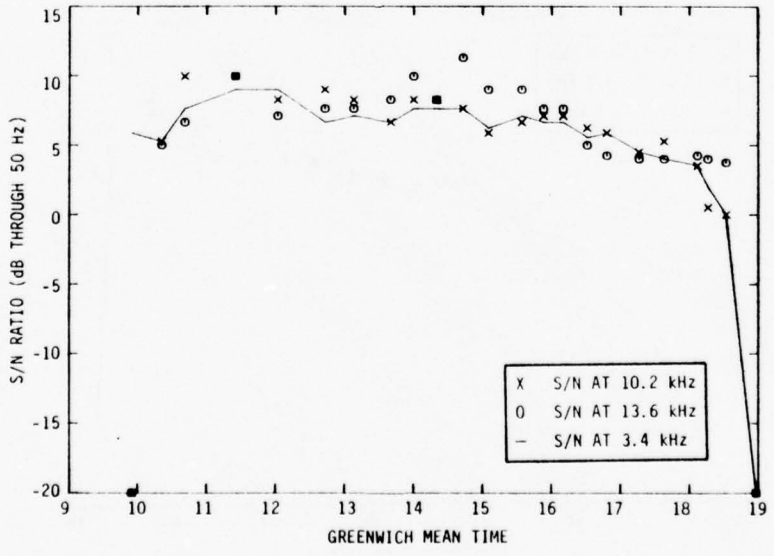

FIGURE B.24. S/N RATIOS, STATION B, FRANKFURT-NEW YORK, FLIGHT 67, MARCH 26, 1976

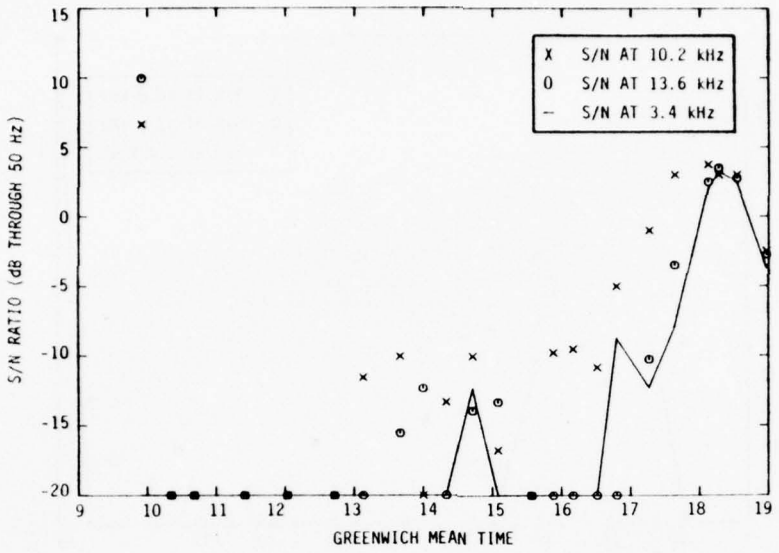

FIGURE B.25. S/N RATIOS, STATION C, FRANKFURT-NEW YORK, FLIGHT 67, MARCH 26, 1976

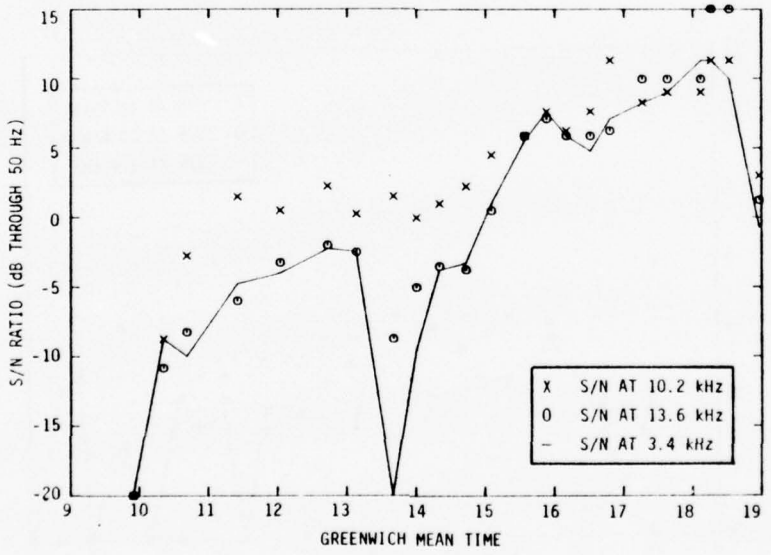

FIGURE B.26. S/N RATIOS, STATION D, FRANKFURT-NEW YORK, FLIGHT 67, MARCH 26, 1976

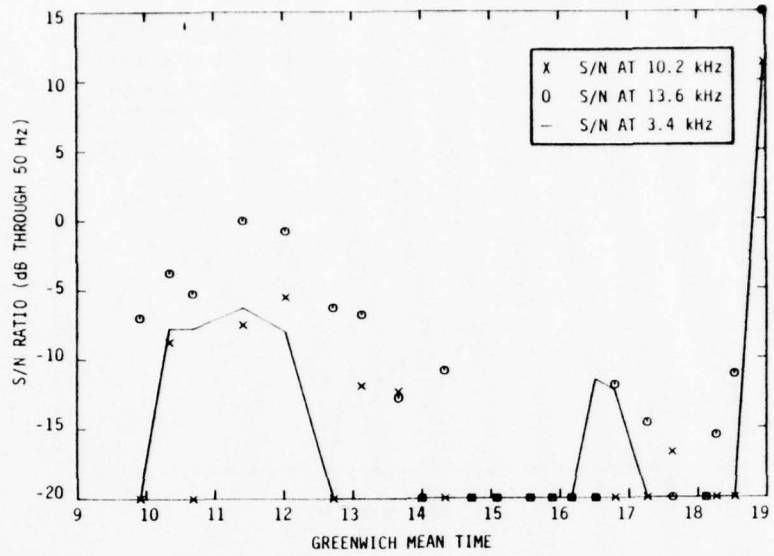

FIGURE B.27. S/N RATIOS, STATION E, FRANKFURT-NEW YORK, FLIGHT 67, MARCH 26, 1976

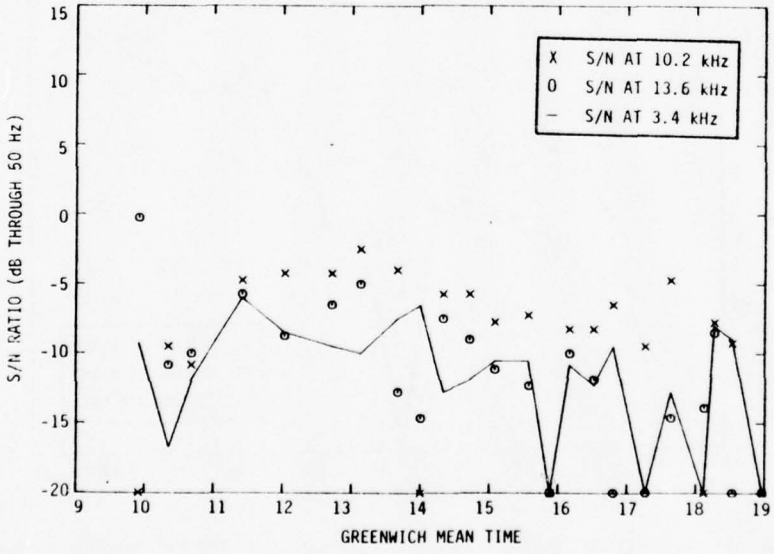

FIGURE B.28. S/N RATIOS, STATION F, FRANKFURT-NEW YORK, FLIGHT 67, MARCH 26, 1976

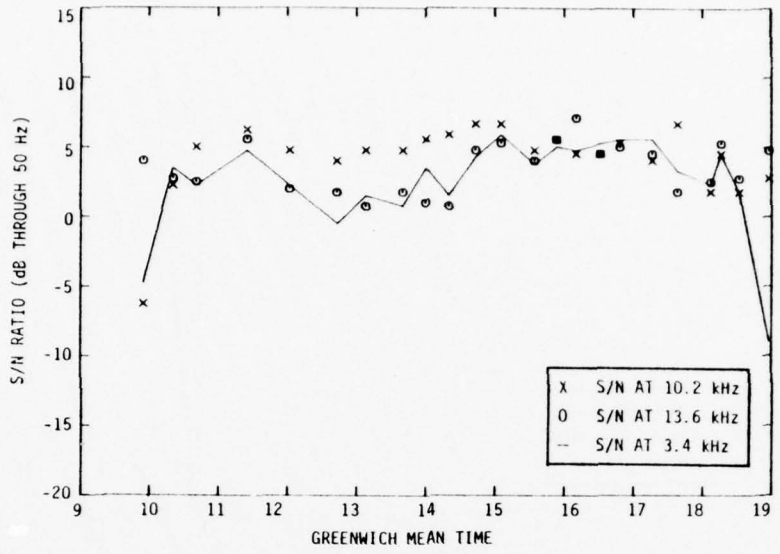

FIGURE B.29. S/N RATIOS, STATION G, FRANKFURT-NEW YORK, FLIGHT 67, MARCH 26, 1976

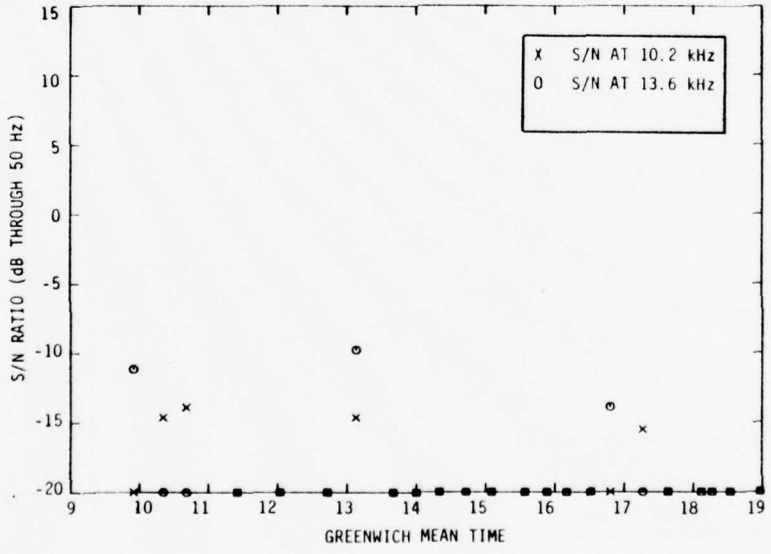

FIGURE B.30. S/N RATIOS, STATION H, FRANKFURT-NEW YORK, FLIGHT 67, MARCH 26, 1976

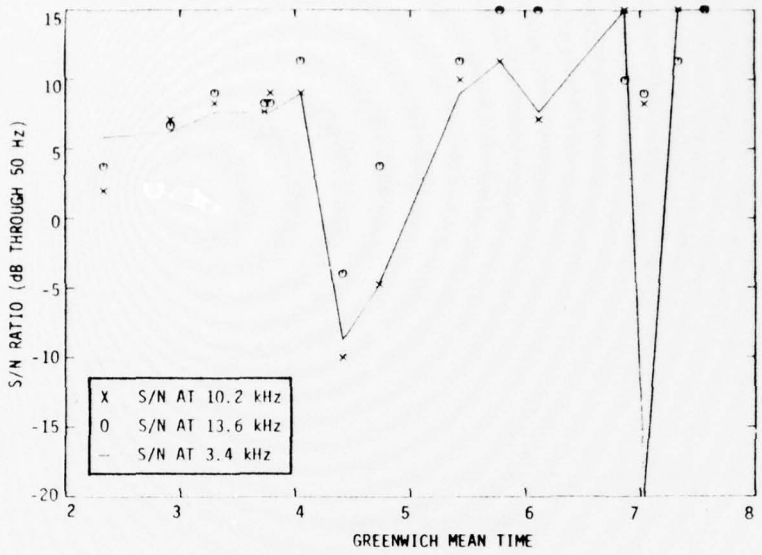

FIGURE B.31. S/N RATIOS, STATION A, CHICAGO-FRANKFURT, FLIGHT 58, AUGUST 23, 1975

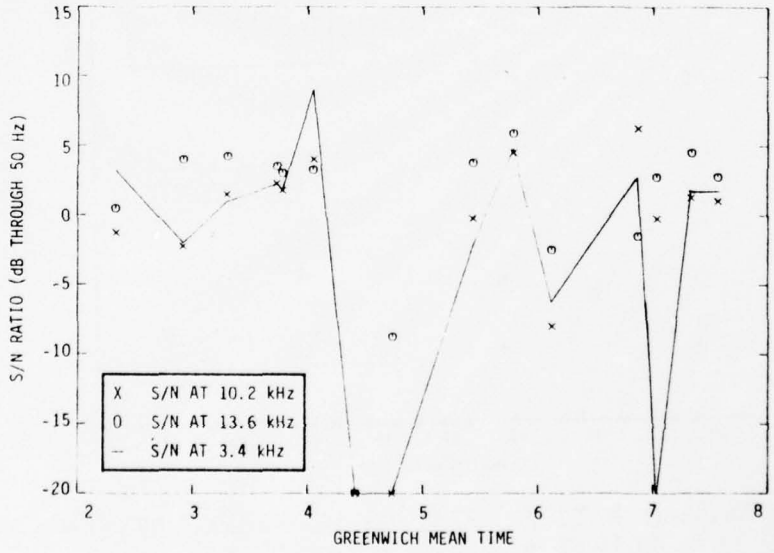

FIGURE B.32. S/N RATIOS, STATION B (TRINIDAD), CHICAGO-FRANKFURT FLIGHT 58, AUGUST 23, 1975

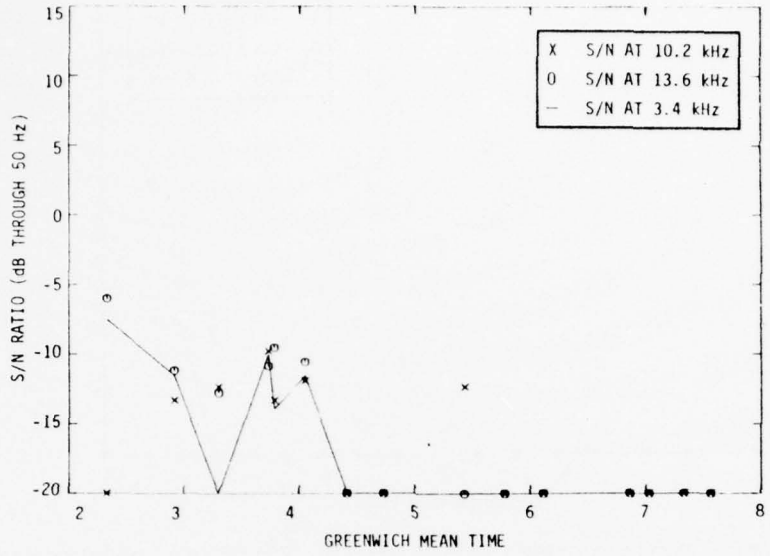

FIGURE B.33. S/N RATIOS, STATION C, CHICAGO-FRANKFURT, FLIGHT 58, AUGUST 23, 1975

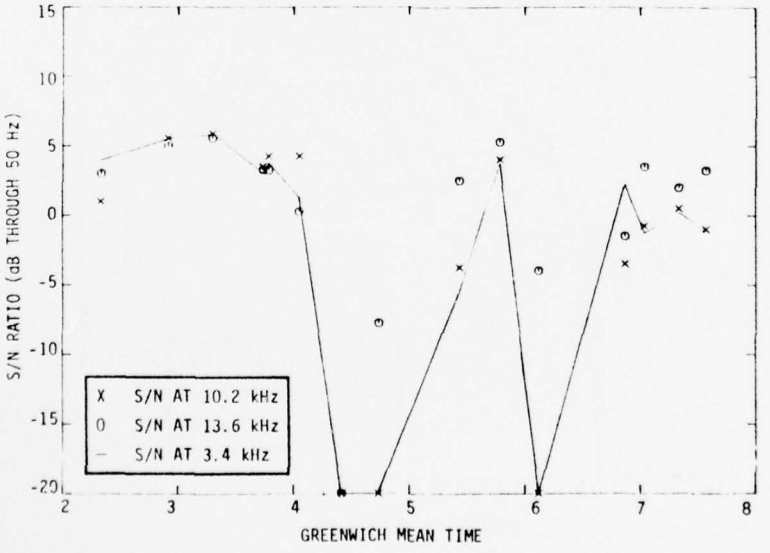

FIGURE B.34. S/N RATIOS, STATION D, CHICAGO-FRANKFURT, FLIGHT 58, AUGUST 23, 1975

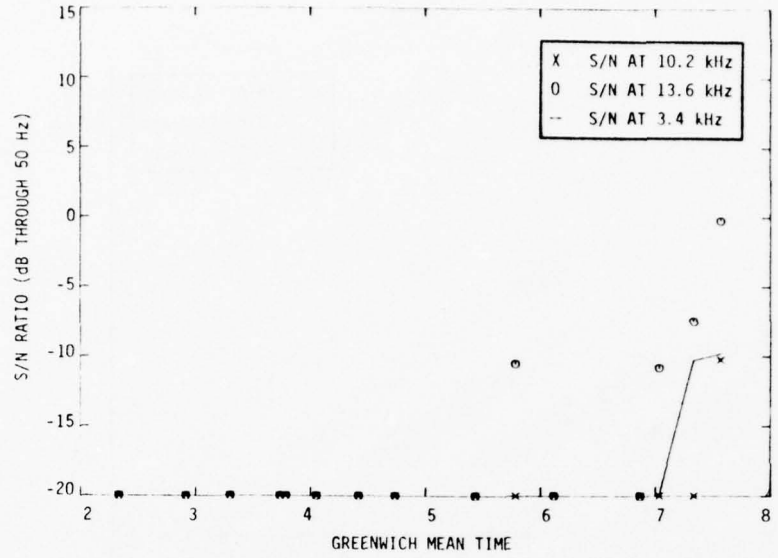

FIGURE B.35. S/N RATIOS, STATION H, CHICAGO-FRANKFURT, FLIGHT 58, AUGUST 23, 1975

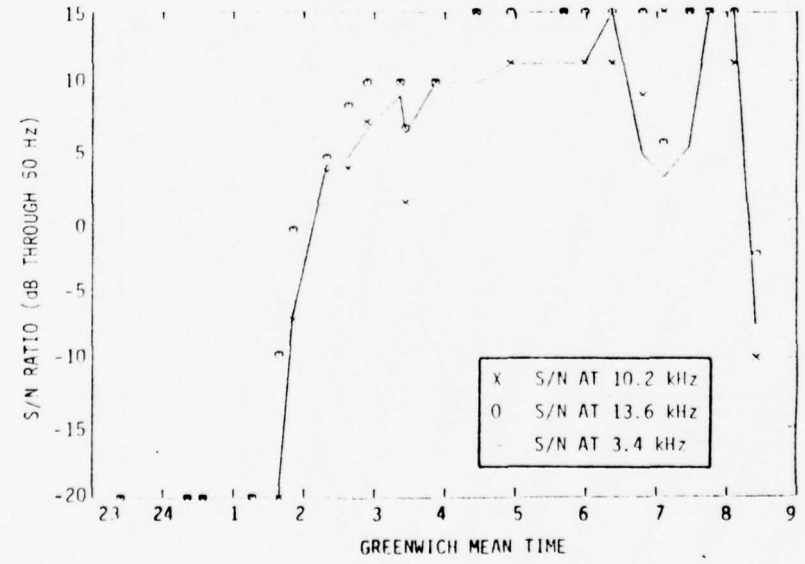

FIGURE B.36. S/N RATIOS, STATION A, CHICAGO-FRANKFURT, FLIGHT 58, AUGUST 28, 1975

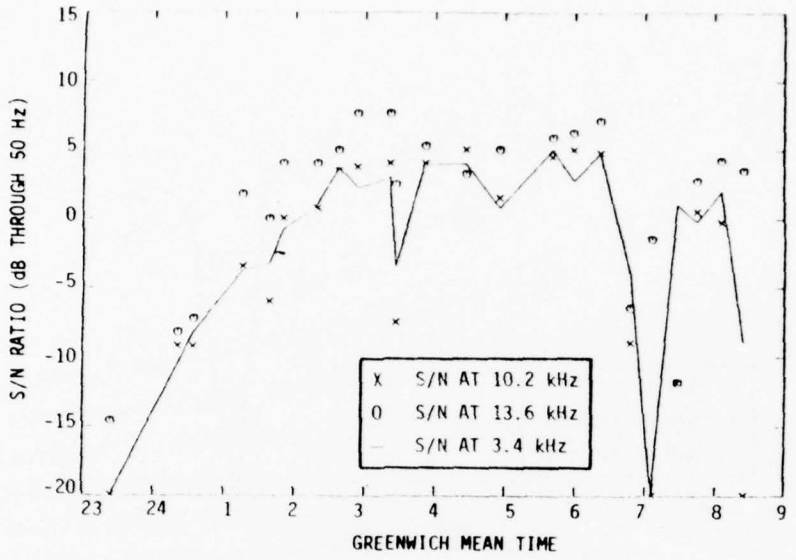

FIGURE B. 37. S/N RATIOS, STATION B (TRINIDAD), CHICAGO-FRANKFURT FLIGHT 58, AUGUST 28, 1975

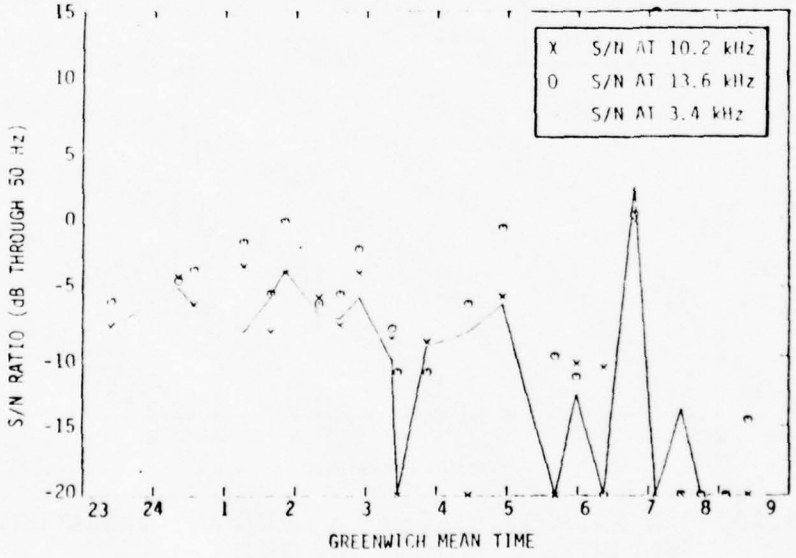

FIGURE B.38. S/N RATIOS, STATION C, CHICAGO-FRANKFURT, FLIGHT 58, AUGUST 28, 1975

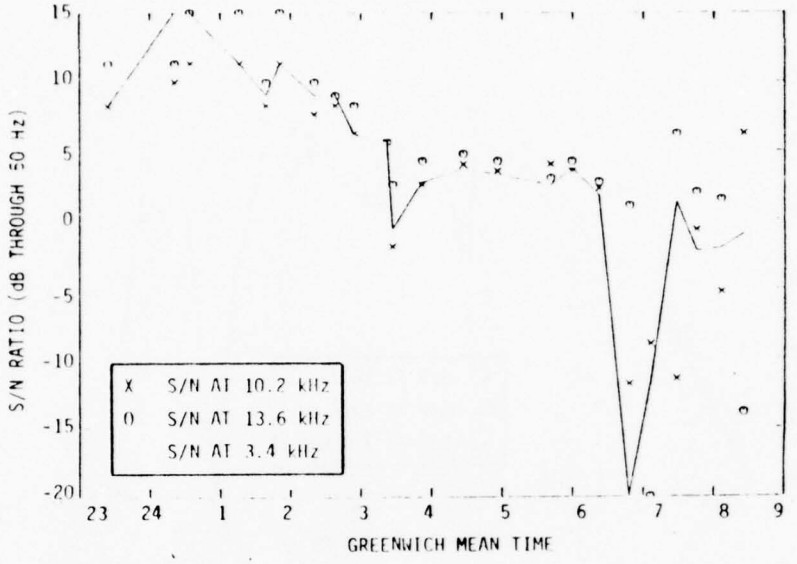

FIGURE B.39. S/N RATIOS, STATION D, CHICAGO-FRANKFURT, FLIGHT 58, AUGUST 28, 1975

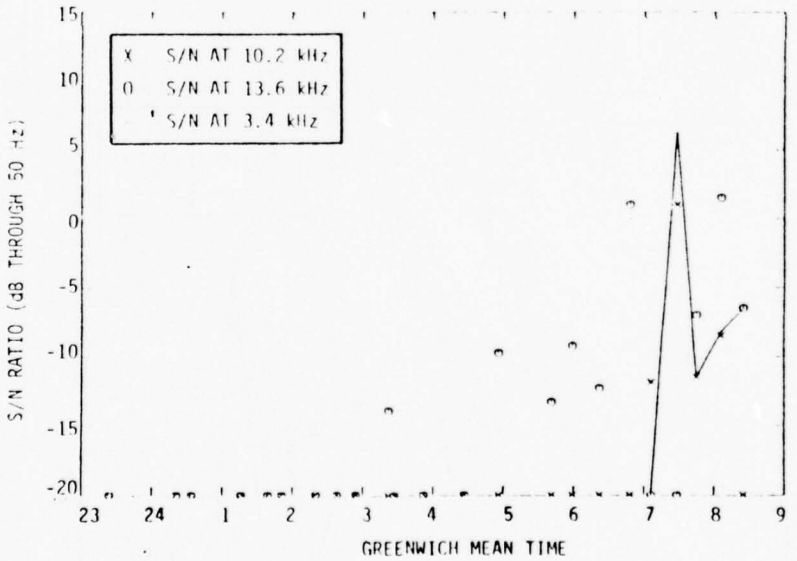

FIGURE B.40. S/N RATIOS, STATION H, CHICAGO-FRANKFURT, FLIGHT 58, AUGUST 28, 1975

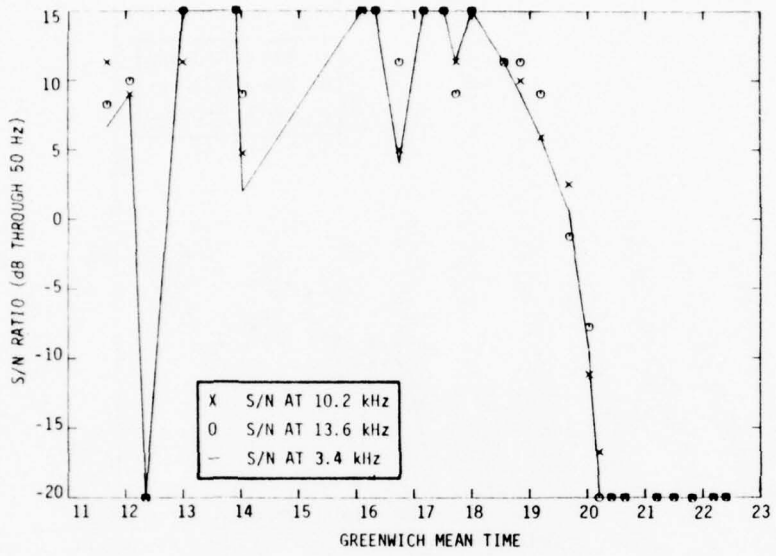

FIGURE B.41. S/N RATIOS, STATION A, FRANKFURT-CHICAGO, FLIGHT 59, AUGUST 28, 1975

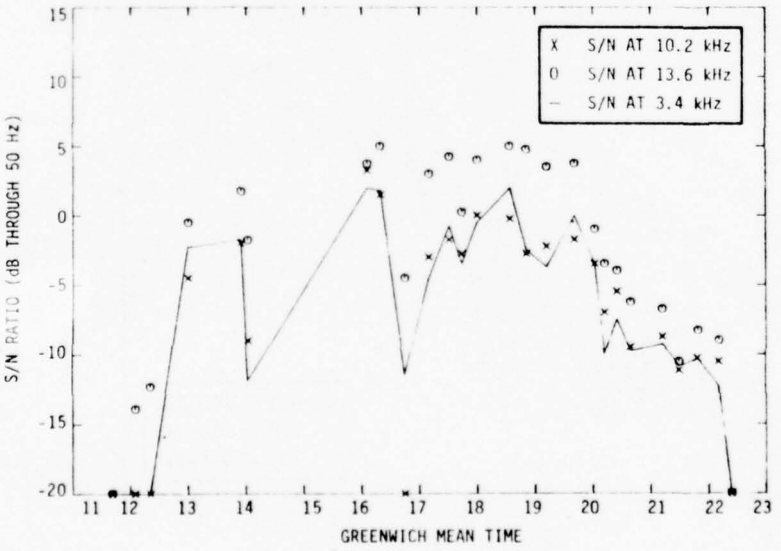

FIGURE B.42. S/N RATIOS, STATION B (TRINIDAD), FRANKFURT-CHICAGO FLIGHT 59, AUGUST 28, 1975

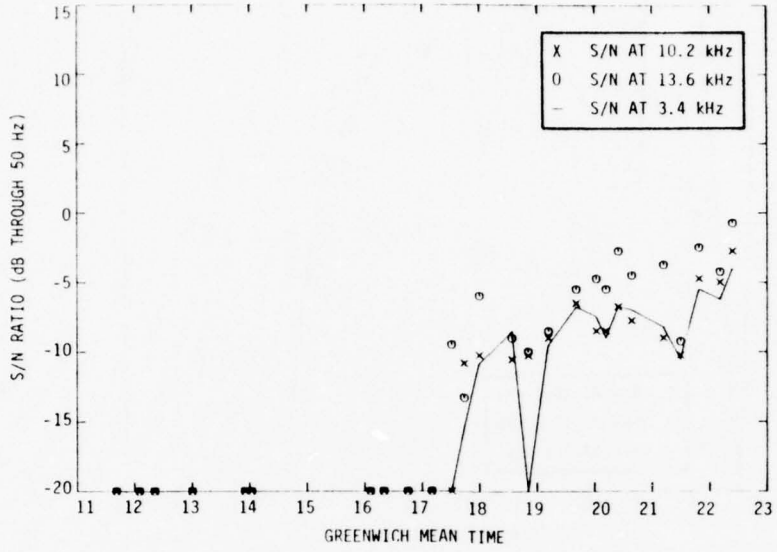

FIGURE B.43. S/N RATIOS, STATION C, FRANKFURT-CHICAGO, FLIGHT 59, AUGUST 28, 1975

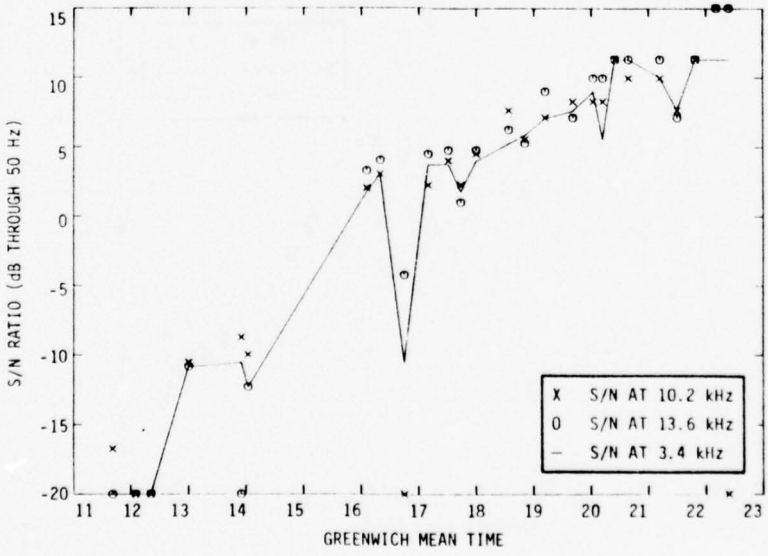

FIGURE B. 44. S/N RATIOS, STATION D, FRANKFURT-CHICAGO, FLIGHT 59, AUGUST 28, 1975

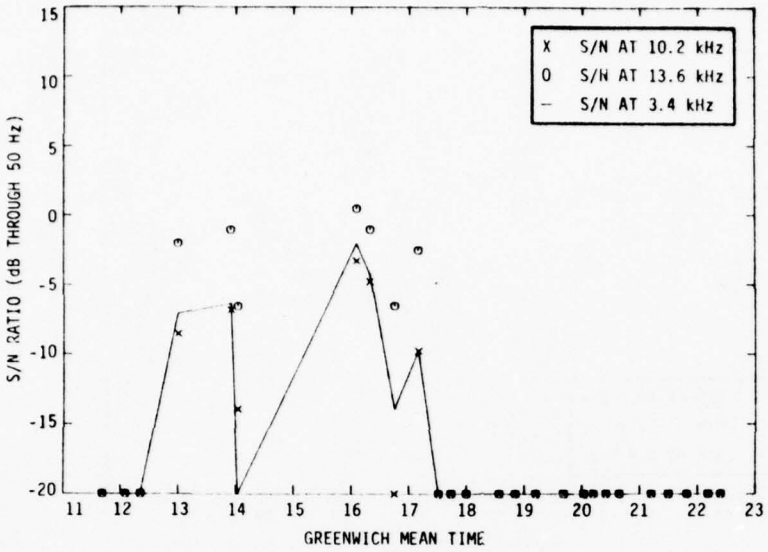

FIGURE B.45. S/N RATIOS, STATION H, FRANKFURT-CHICAGO, FLIGHT 59, AUGUST 28, 1975

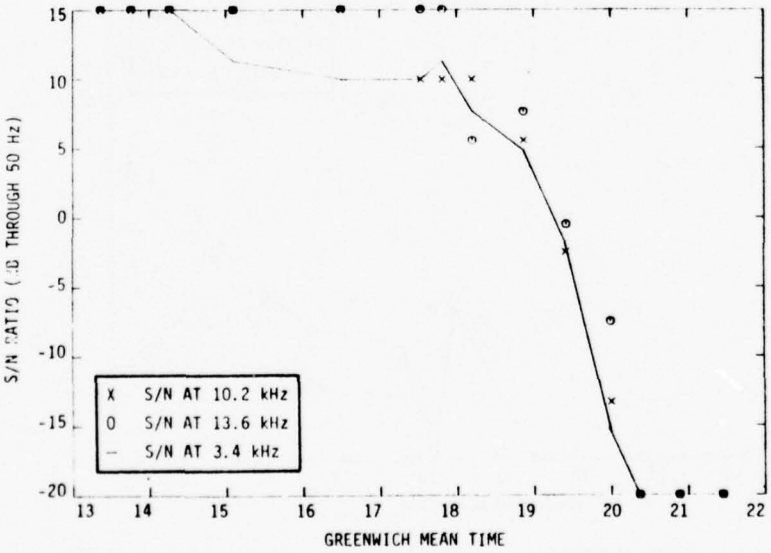

FIGURE B.46. S/N RATIOS, STATION A, FRANKFURT-CHICAGO, FLIGHT 59, SEPTEMBER 1, 1975

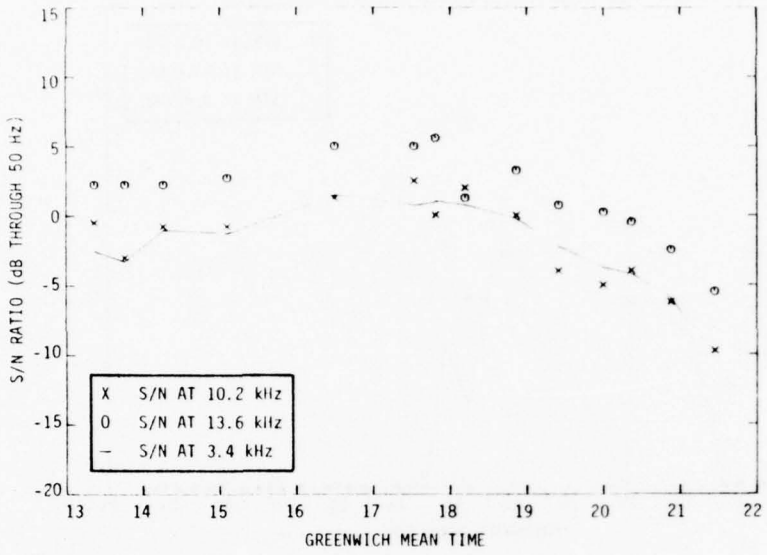

FIGURE 47. S/N RATIOS, STATION B (TRINIDAD), FRANKFURT-CHICAGO, FLIGHT 59, SEPTEMBER 1, 1975

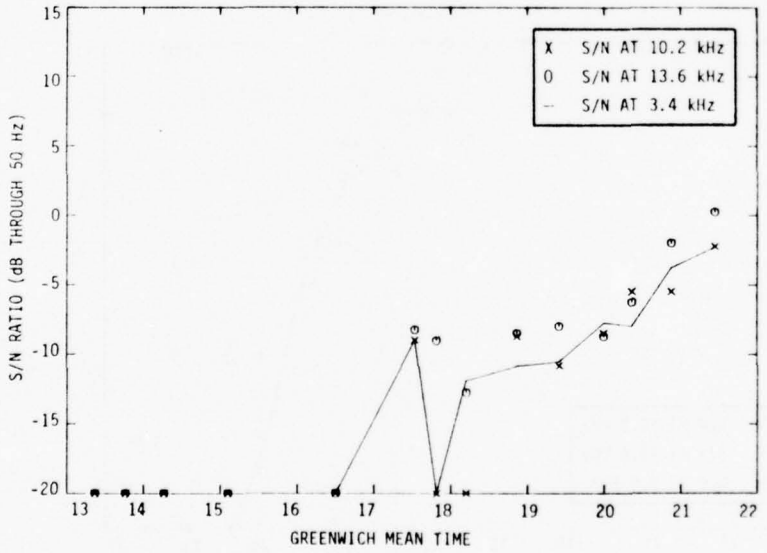

FIGURE B.48. S/N RATIOS, STATION C, FRANKFURT-CHICAGO, FLIGHT 59, SEPTEMBER 1, 1975

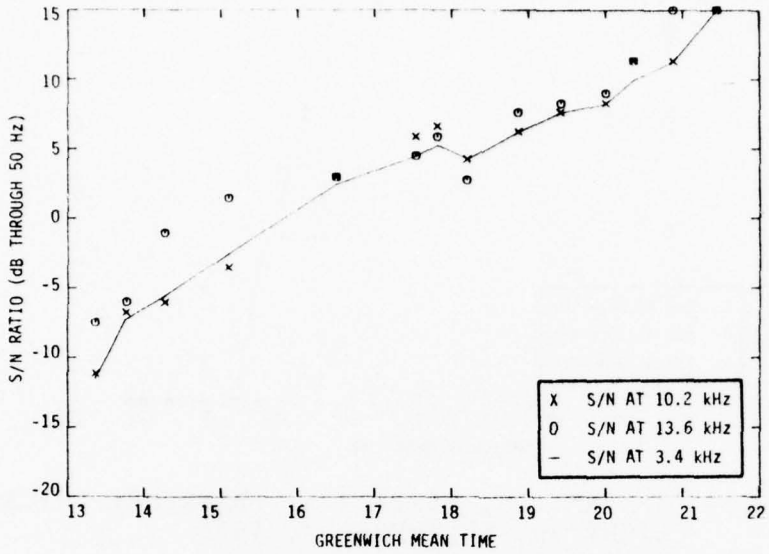

FIGURE B. 49. S/N RATIOS, STATION D, FRANKFURT-CHICAGO, FLIGHT 59, SEPTEMBER 1, 1975

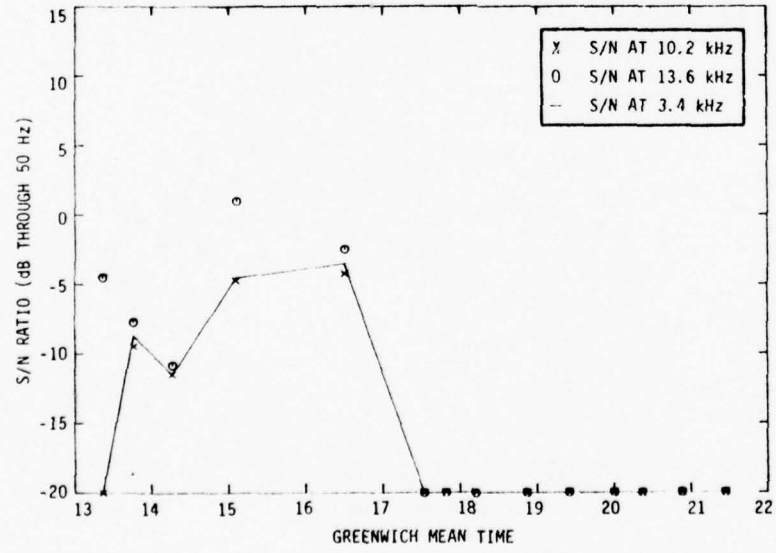

FIGURE B. 50. S/N RATIOS, STATION H, FRANKFURT-CHICAGO, FLIGHT 59, SEPTEMBER 1, 1975

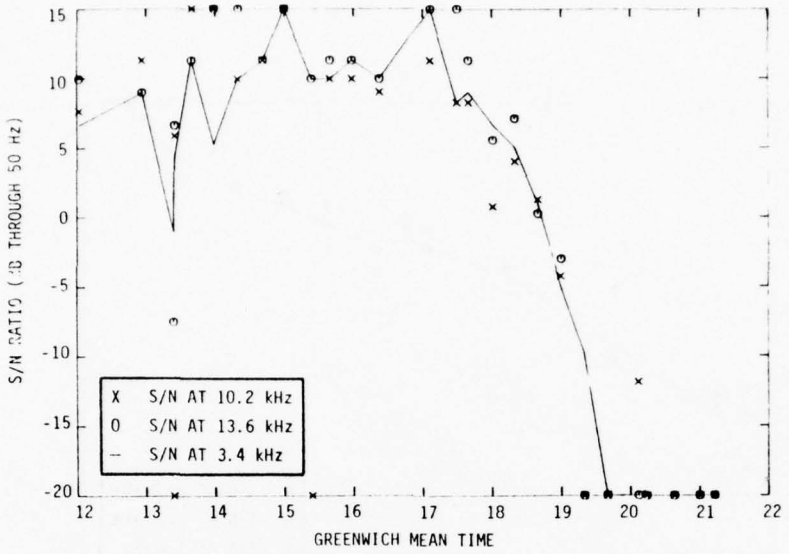

FIGURE B.51. S/N RATIOS, STATION A, FRANKFURT-CHICAGO, FLIGHT 59, SEPTEMBER 2, 1975

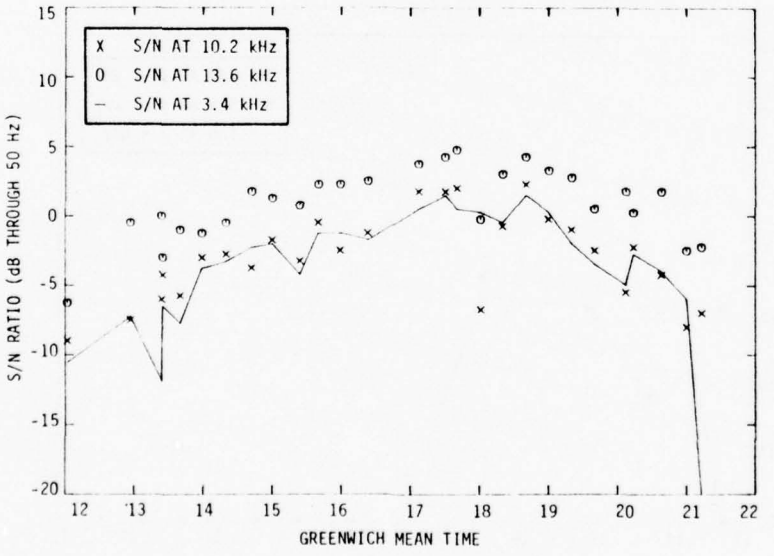

FIGURE B. 52. S/N RATIOS, STATION B (TRINIDAD), FRANKFURT-CHICAGO, FLIGHT 59, SEPTEMBER 2, 1975

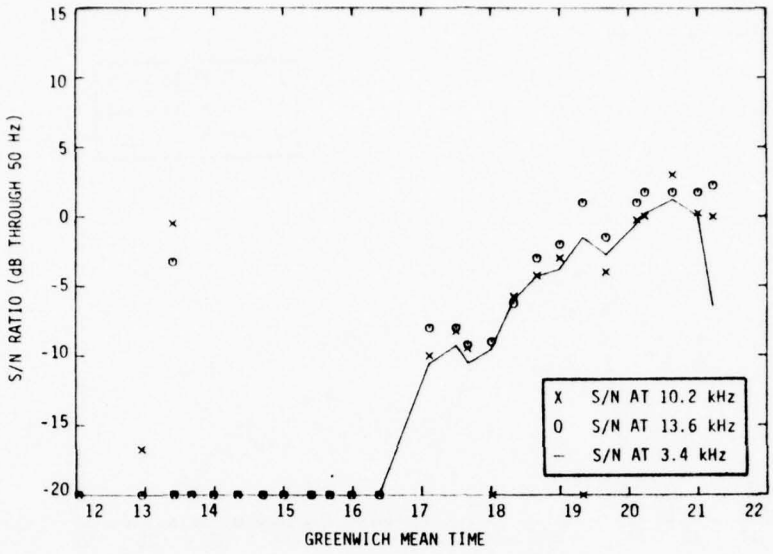

FIGURE B.53. S/N RATIOS, STATION C, FRANKFURT-CHICAGO, FLIGHT 59, SEPTEMBER 2, 1975

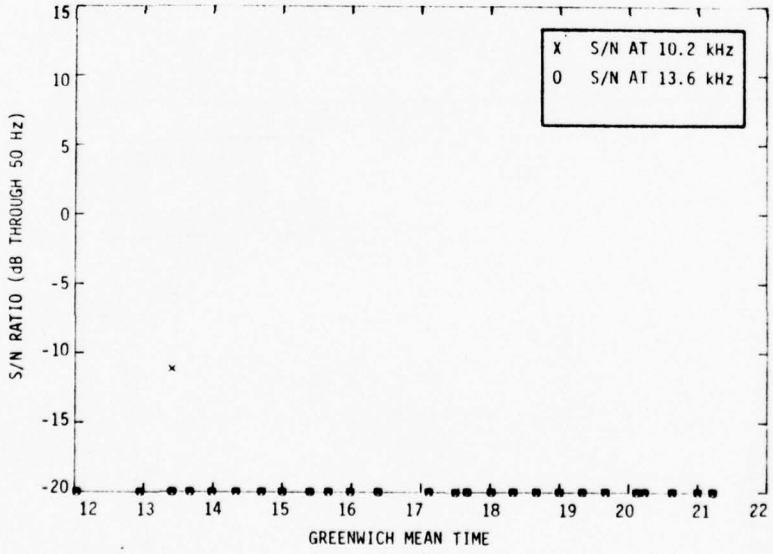

FIGURE B.54. S/N RATIOS, STATION D, FRANKFURT-CHICAGO, FLIGHT 59, SEPTEMBER 2, 1975

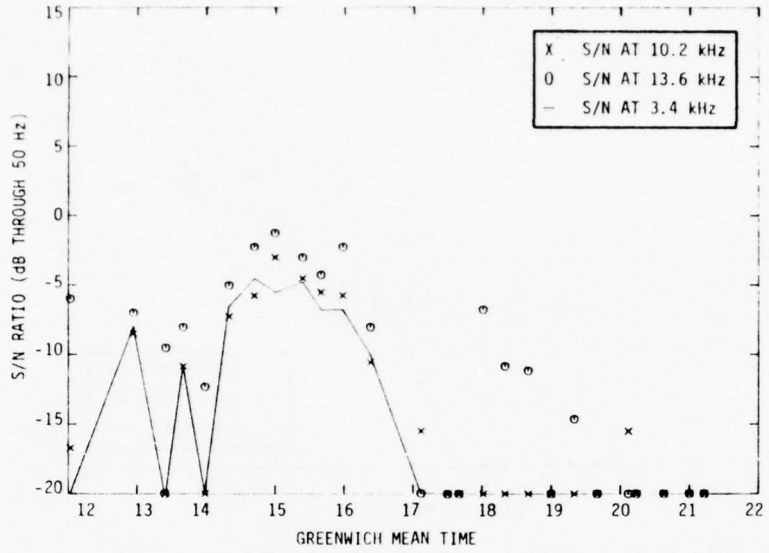

FIGURE B.55. S/N RATIOS, STATION H, FRANKFURT-CHICAGO, FLIGHT 59, SEPTEMBER 2, 1975

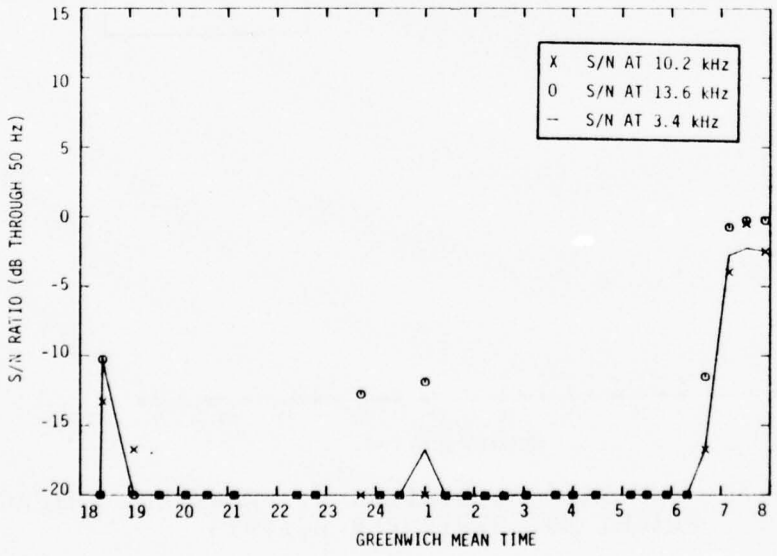

FIGURE B.56. S/N RATIOS, STATION A, NEW YORK-HONOLULU VIA DALLAS, FLIGHT 825, APRIL 8, 1976

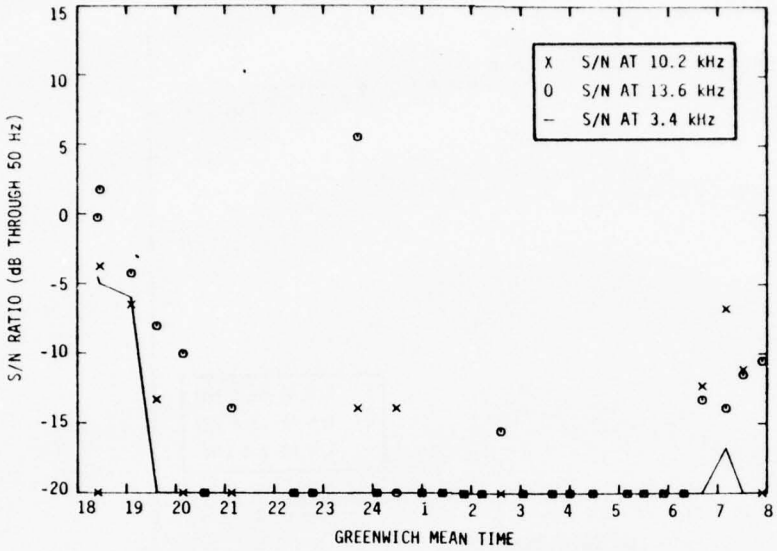

FIGURE B.57. S/N RATIOS, STATION B, NEW YORK-HONOLULU VIA DALLAS, FLIGHT 825, APRIL 8, 1976

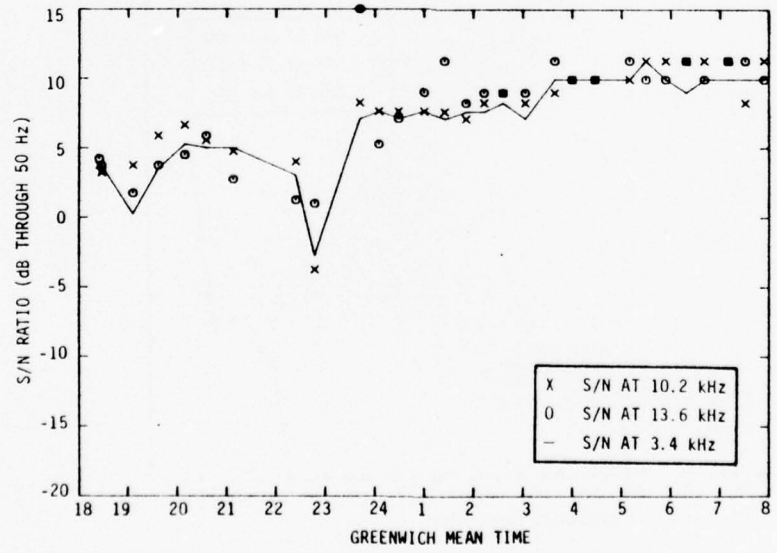

FIGURE B.58. S/N RATIOS, STATION C, NEW YORK-HONOLULU VIA DALLAS, FLIGHT 825, APRIL 8, 1976

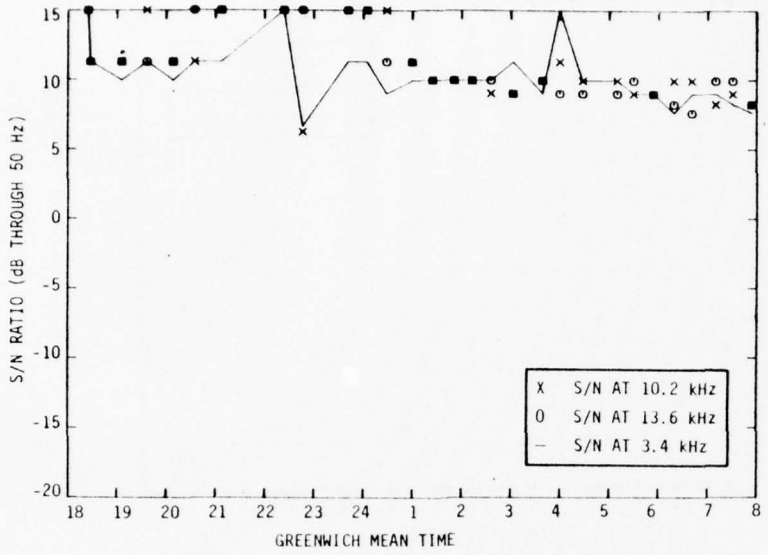

FIGURE B.59. S/N RATIOS, STATION D, NEW YORK-HONOLULU VIA DALLAS, FLIGHT 825, APRIL 8, 1976

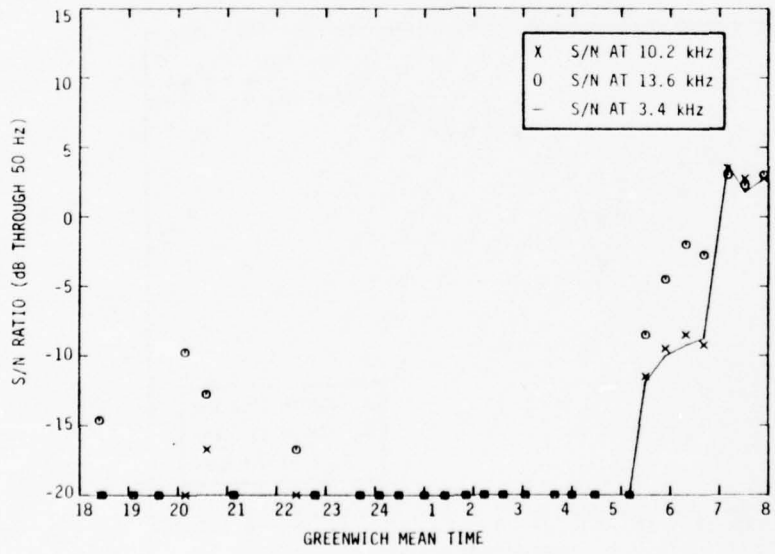

FIGURE B.60. S/N RATIOS, STATION E, NEW YORK-HONOLULU VIA DALLAS, FLIGHT 825, APRIL 8, 1976

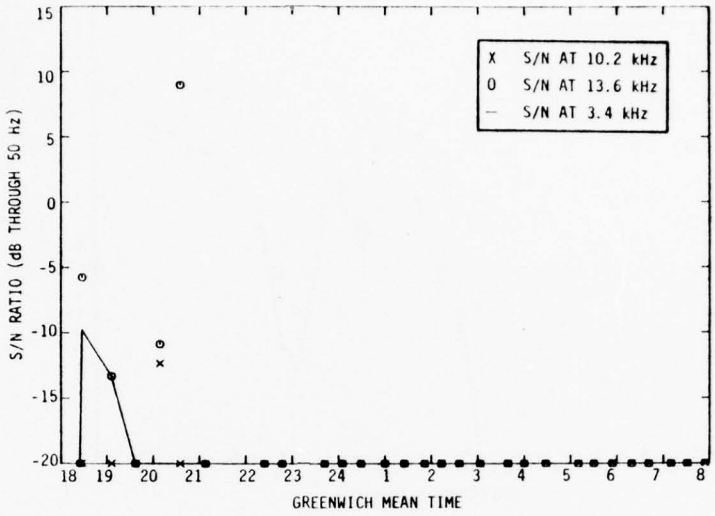

FIGURE B.61. S/N RATIOS, STATION F, NEW YORK-HONOLULU VIA DALLAS, FLIGHT 825, APRIL 8, 1976

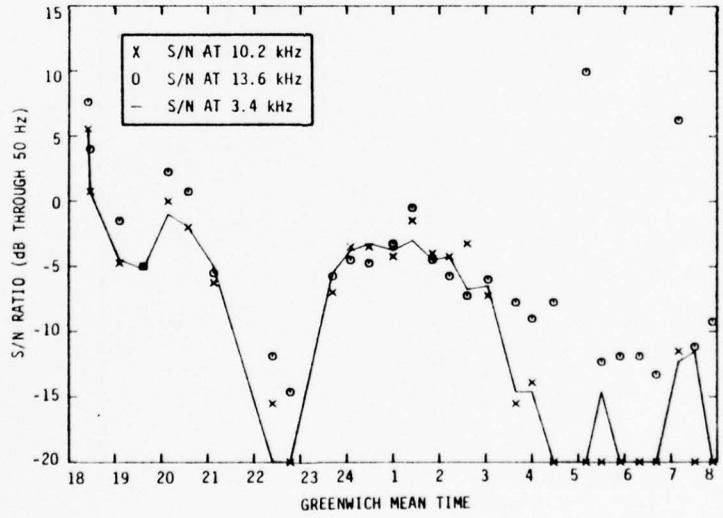

FIGURE B.62. S/N RATIOS, STATION G, NEW YORK-HONOLULU VIA DALLAS, FLIGHT 825, APRIL 8, 1976

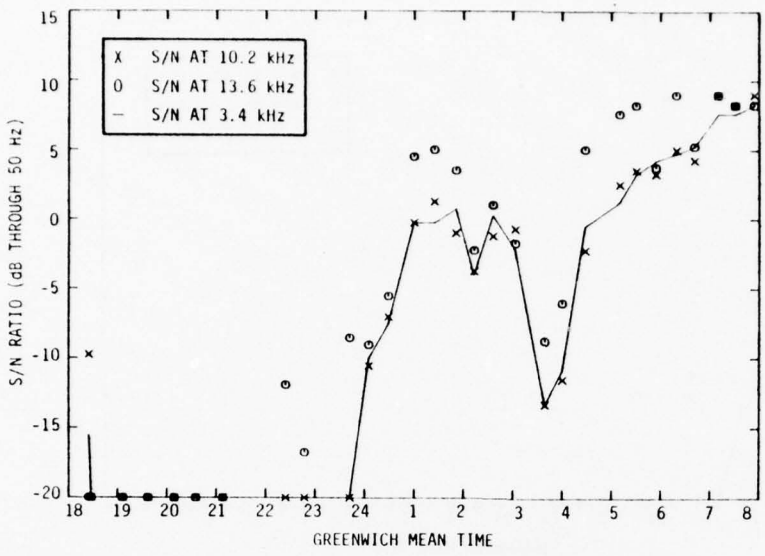

FIGURE B.63. S/N RATIOS, STATION H, NEW YORK-HONOLULU VIA DALLAS, FLIGHT 825, APRIL 8, 1976

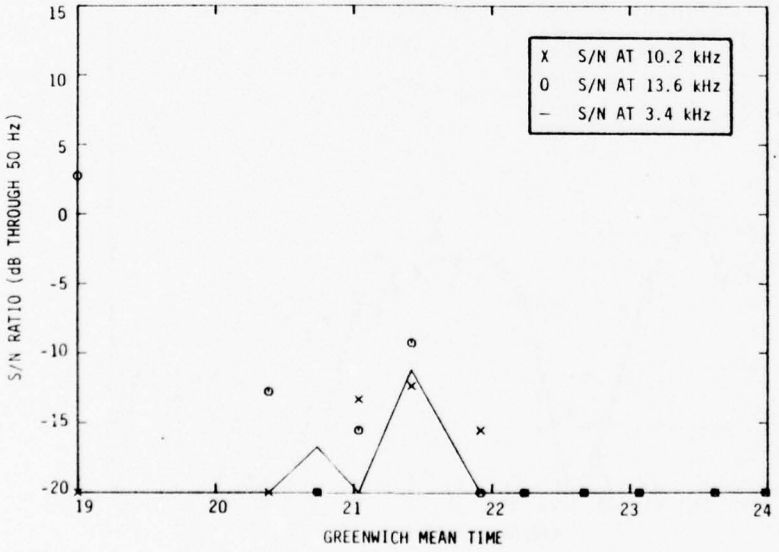

FIGURE B.64. S/N RATIOS, STATION A, HONOLULU-SAN FRANCISCO VIA LOS ANGELES, FLIGHT 818, APRIL 10, 1976

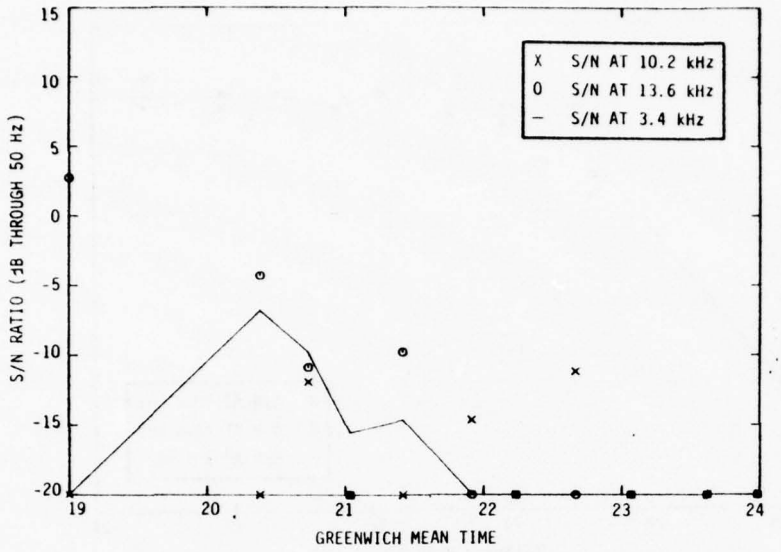

FIGURE B.65. S/N RATIOS, STATION B, HONOLULU-SAN FRANCISCO VIA LOS ANGELES, FLIGHT 818, APRIL 10, 1976

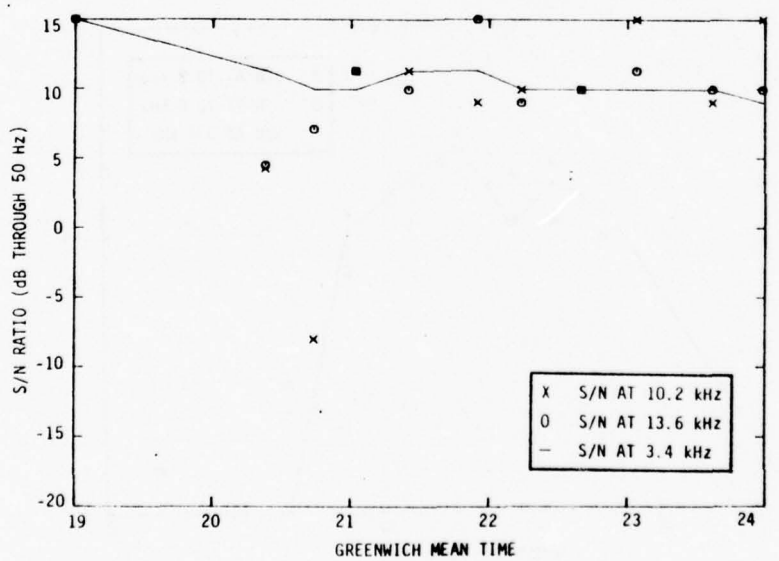

FIGURE B.66. S/N RATIOS, STATION C, HONOLULU-SAN FRANCISCO VIA LOS ANGELES, FLIGHT 818, APRIL 10, 1976

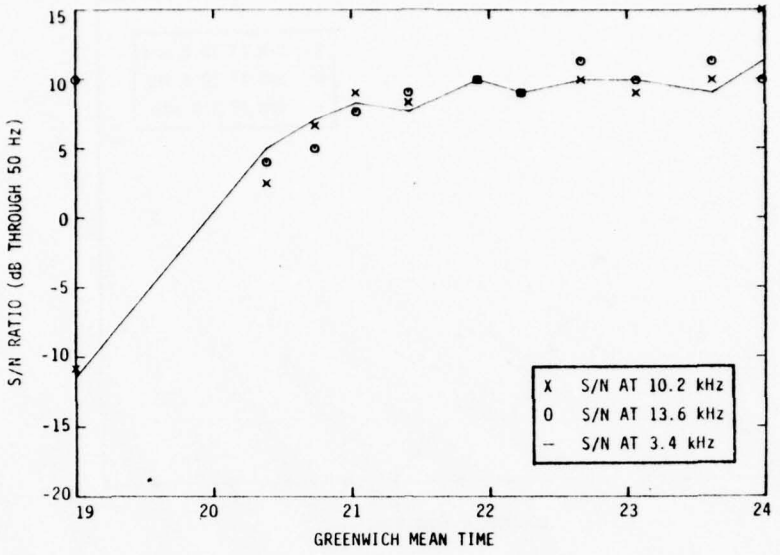

FIGURE B.67. S/N RATIOS, STATION D, HONOLULU-SAN FRANCISCO VIA LOS ANGELES, FLIGHT 818, APRIL 10, 1976

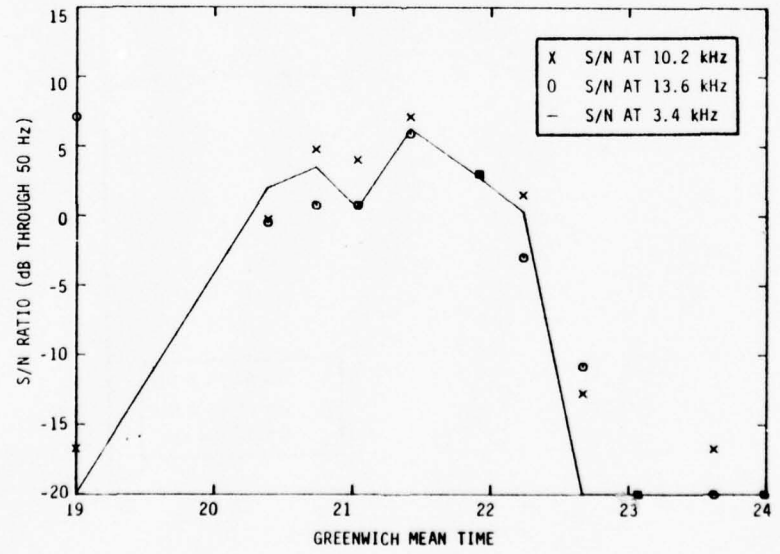

FIGURE B.68. S/N RATIOS, STATION E, HONOLULU-SAN FRANCISCO VIA LOS ANGELES, FLIGHT 818, APRIL 10, 1976

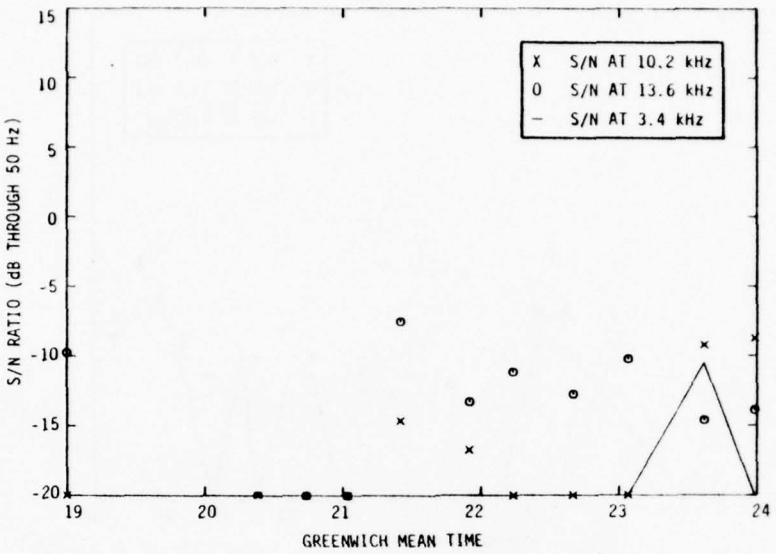

FIGURE B.69. S/N RATIOS, STATION G, HONOLULU-SAN FRANCISCO VIA LOS ANGELES, FLIGHT 818, APRIL 10, 1976

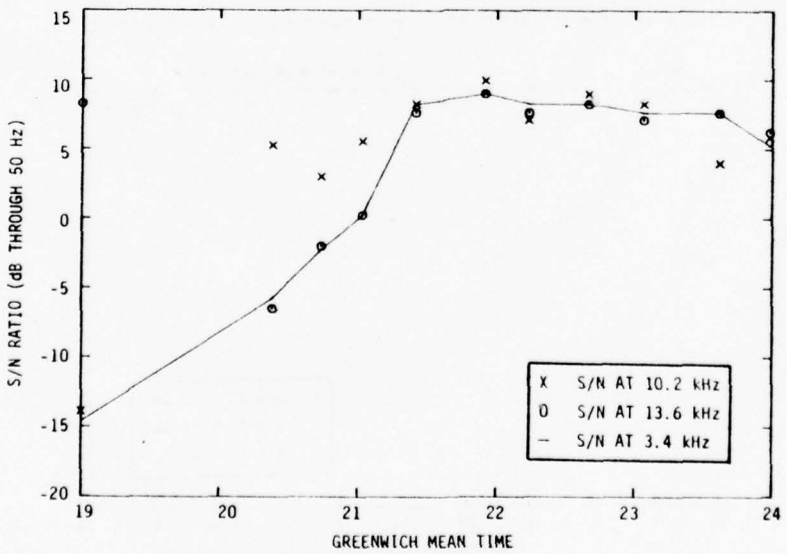

FIGURE B.70. S/N RATIOS, STATION H, HONOLULU-SAN FRANCISCO VIA LOS ANGELES, FLIGHT 818, APRIL 10, 1976

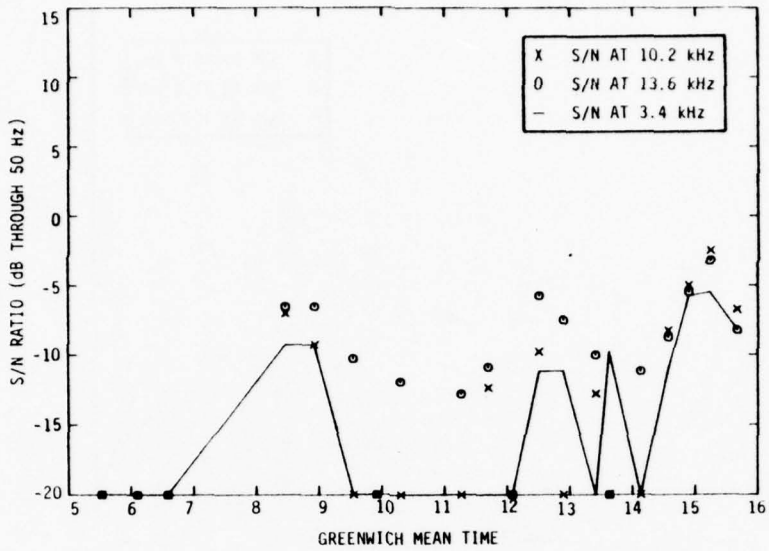

FIGURE B.71. S/N RATIOS, STATION B, SAN FRANCISCO-TAHITI VIA LOS ANGELES, FLIGHT 815, APRIL 11, 1976

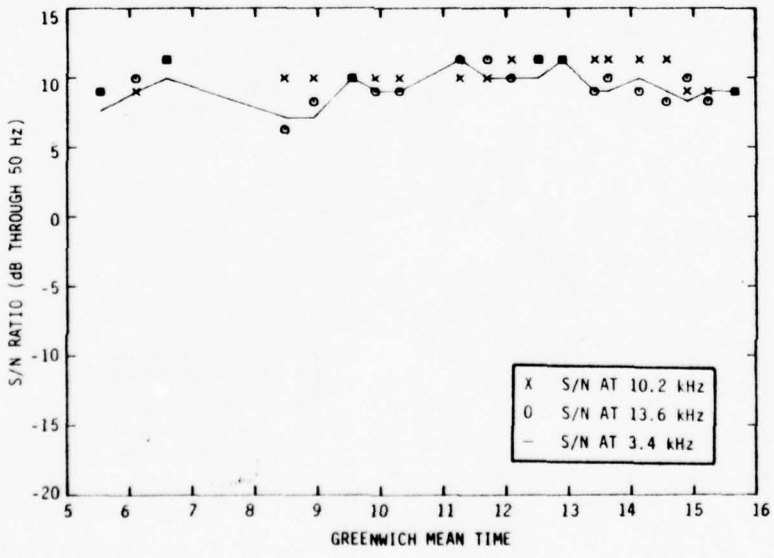

FIGURE B.72. S/N RATIOS, STATION C, SAN FRANCISCO-TAHITI VIA LOS ANGELES, FLIGHT 815, APRIL 11, 1976

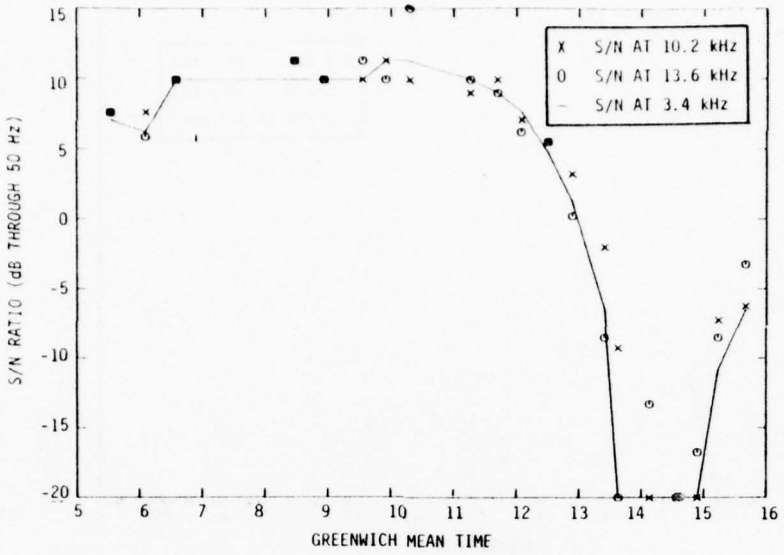

FIGURE B.73. S/N RATIOS, STATION D, SAN FRANCISCO-TAHITI VIA LOS ANGELES, FLIGHT 815, APRIL 11, 1976

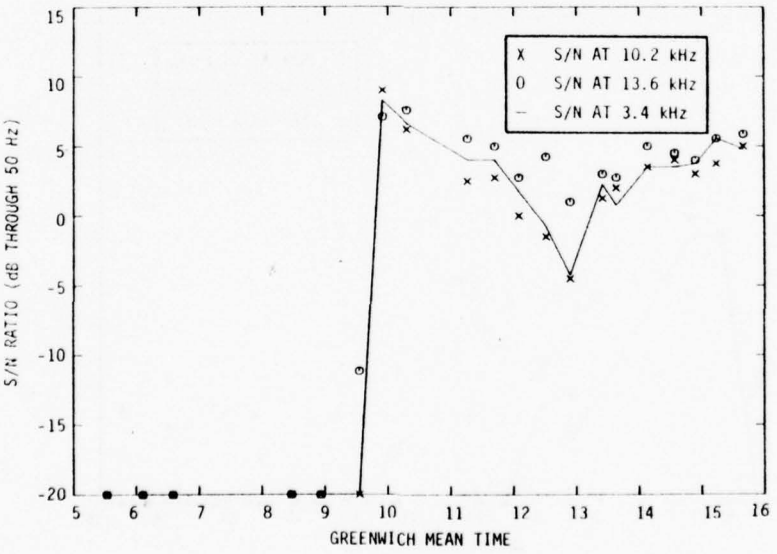

FIGURE B.74. S/N RATIOS, STATION E, SAN FRANCISCO-TAHITI VIA LOS ANGELES, FLIGHT 815, APRIL 11, 1976

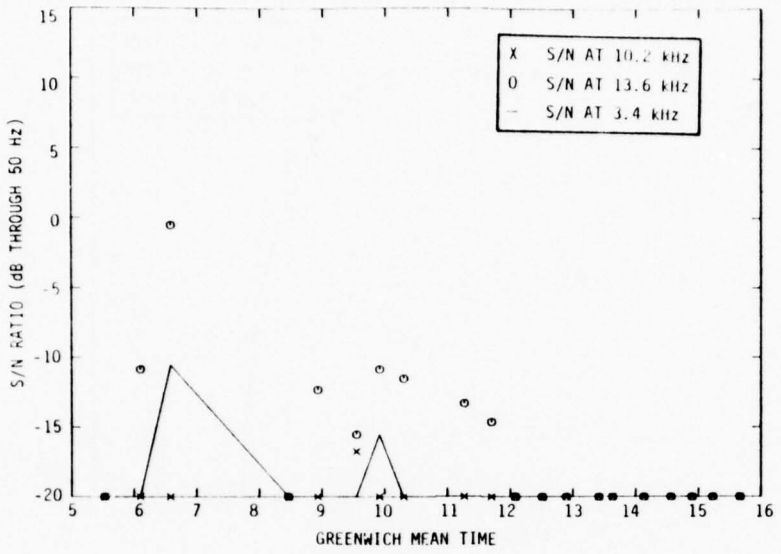

FIGURE B.75. S/N RATIOS, STATION F, SAN FRANCISCO-TAHITI VIA LOS ANGELES, FLIGHT 815, APRIL 11, 1976

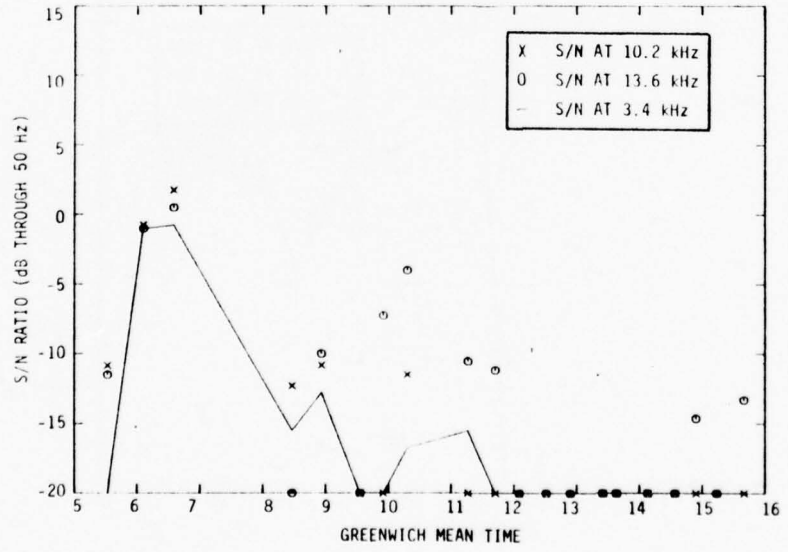

FIGURE B.76. S/N RATIOS, STATION G, SAN FRANCISCO-TAHITI VIA LOS ANGELES, FLIGHT 815, APRIL 11, 1976

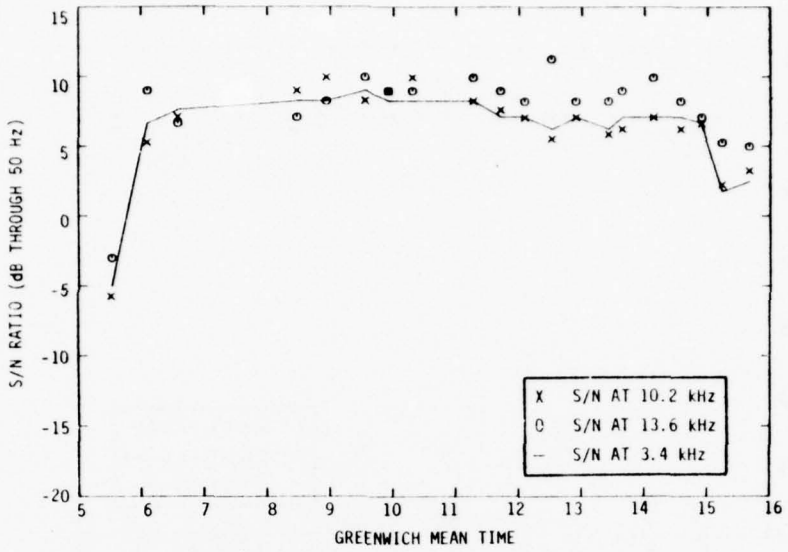

FIGURE B.77. S/N RATIOS, STATION H, SAN FRANCISCO-TAHITI VIA LOS ANGELES, FLIGHT 815, APRIL 11, 1976

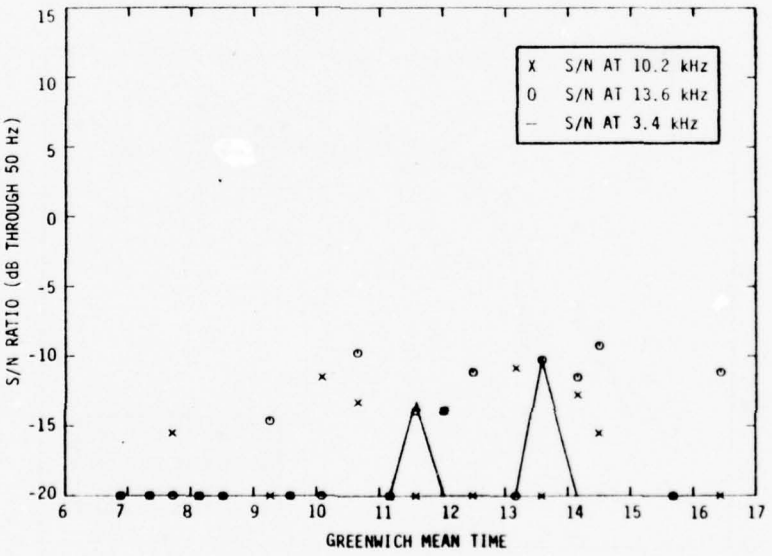

FIGURE B.78. S/N RATIOS, STATION B, TAHITI-SAN FRANCISCO VIA LOS ANGELES, FLIGHT 816, APRIL 12, 1976

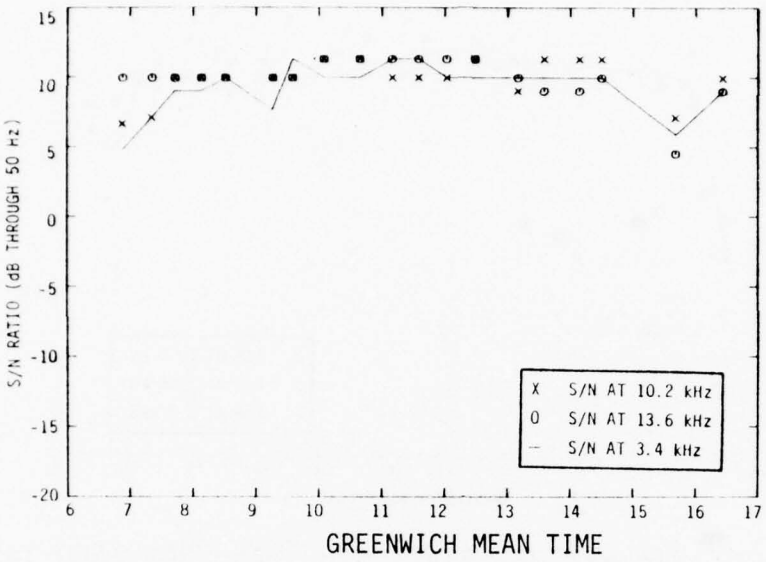

FIGURE B.79. S/N RATIOS, STATION C, TAHITI-SAN FRANCISCO VIA LOS ANGELES, FLIGHT 816, APRIL 12, 1976

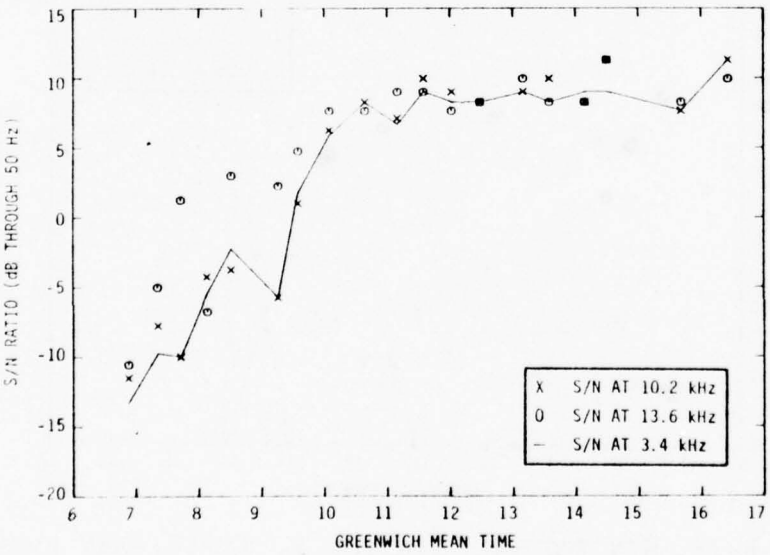

FIGURE B.80. S/N RATIOS, STATION D, TAHITI-SAN FRANCISCO VIA LOS ANGELES, FLIGHT 816, APRIL 12, 1976

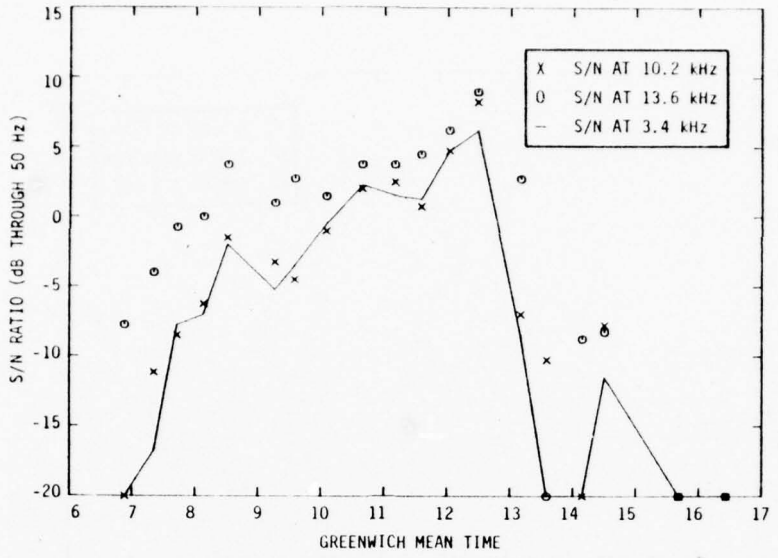

FIGURE B.81. S/N RATIOS, STATION E, TAHITI-SAN FRANCISCO VIA LOS ANGELES, FLIGHT 816, APRIL 12, 1976

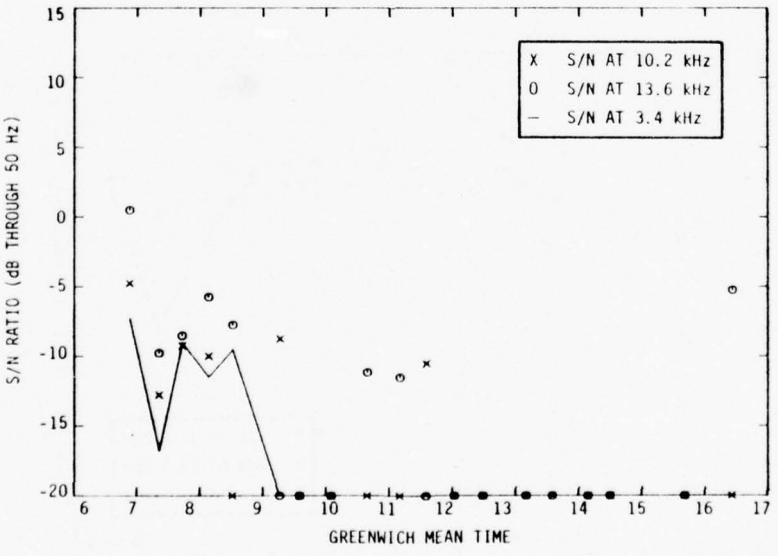

FIGURE B.82. S/N RATIOS, STATION F, TAHITI-SAN FRANCISCO VIA LOS ANGELES, FLIGHT 816, APRIL 12, 1976

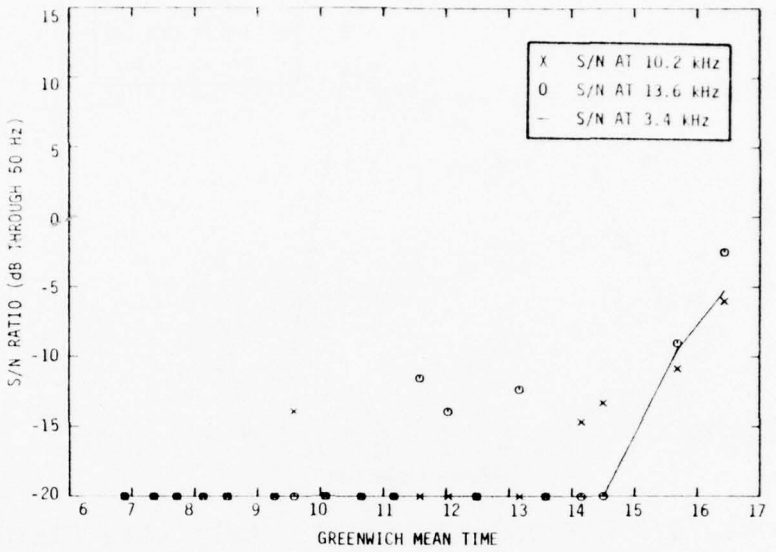

FIGURE B.83. S/N RATIOS, STATION G, TAHITI-SAN FRANCISCO VIA LOS ANGELES, FLIGHT 816, APRIL 12, 1976

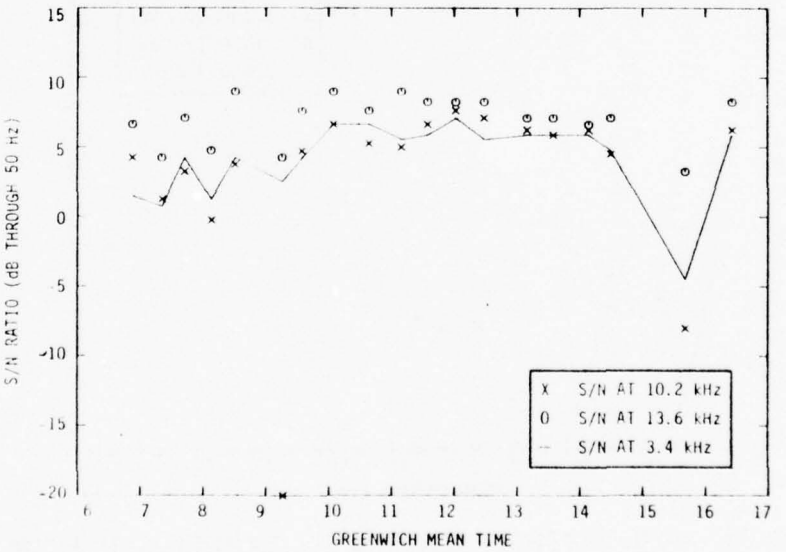

FIGURE B.84. S/N RATIOS, STATION H, TAHITI-SAN FRANCISCO VIA LOS ANGELES, FLIGHT 816, APRIL 12, 1976

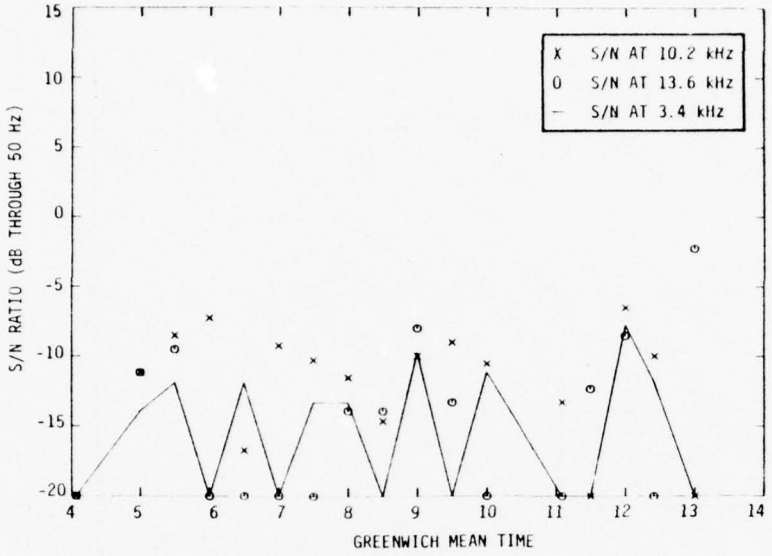

FIGURE B.85. S/N RATIOS, STATION B, SAN FRANCISCO-TAHITI VIA LOS ANGELES, FLIGHT 815, APRIL 25, 1976

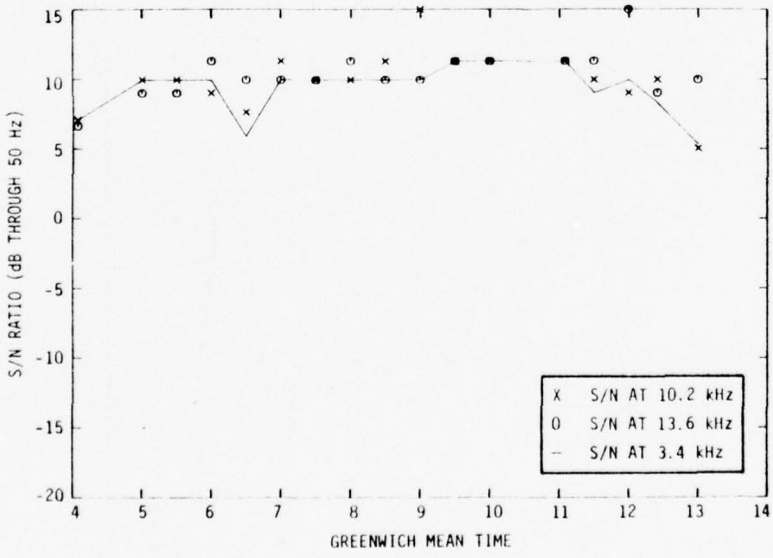

FIGURE B.86. S/N RATIOS, STATION C, SAN FRANCISCO-TAHITI VIA LOS ANGELES, FLIGHT 815, APRIL 25, 1976

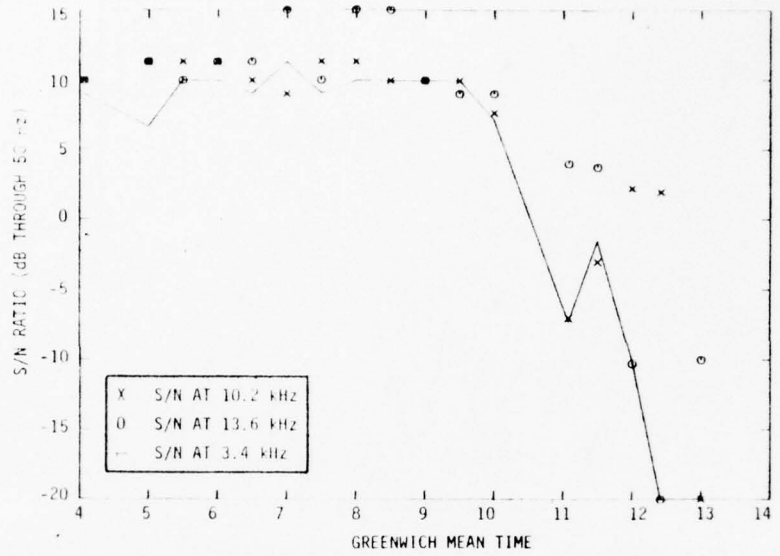

FIGURE B.87. S/N RATIOS, STATION D, SAN FRANCISCO-TAHITI VIA LOS ANGELES, FLIGHT 815, APRIL 25, 1976

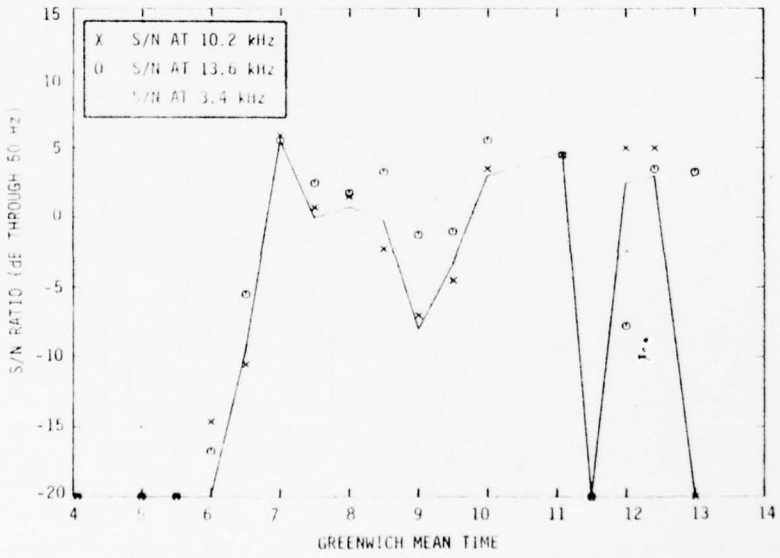

FIGURE B.88. S/N RATIOS, STATION E, SAN FRANCISCO-TAHITI VIA LOS ANGELES, FLIGHT 815, APRIL 25, 1976

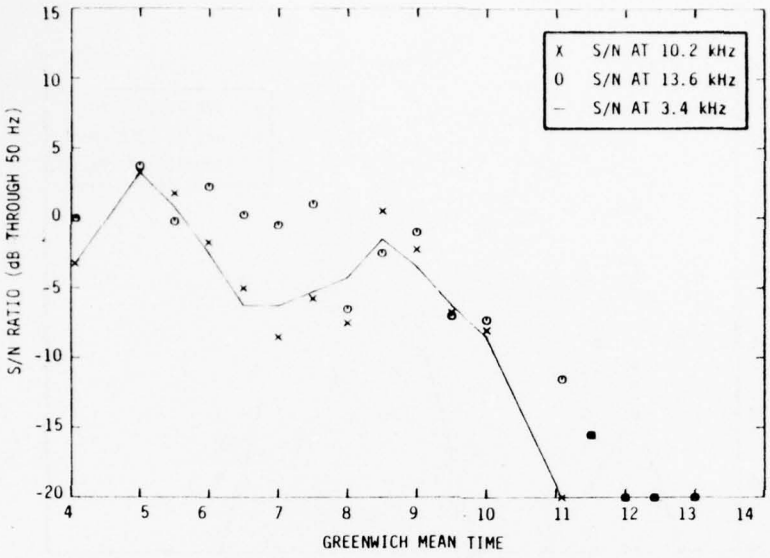

FIGURE B.89. S/N RATIOS, STATION G, SAN FRANCISCO-TAHITI VIA LOS ANGELES, FLIGHT 815, APRIL 25, 1976

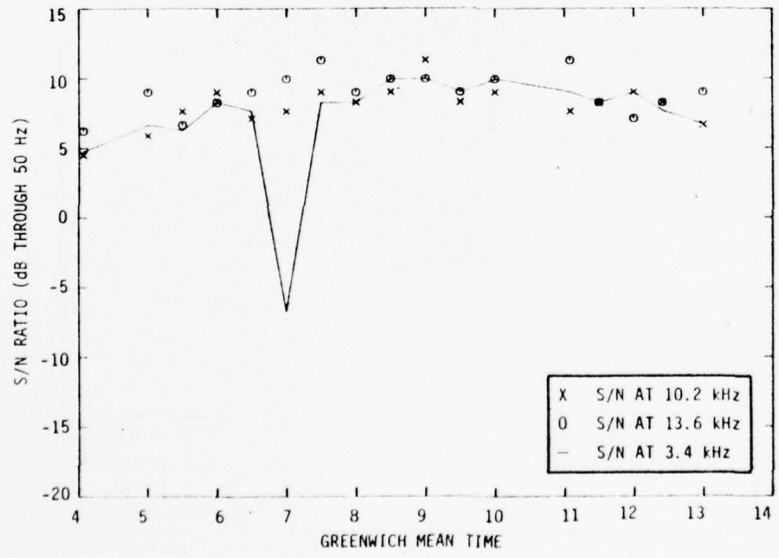

FIGURE B.90. S/N RATIOS, STATION H, SAN FRANCISCO-TAHITI VIA LOS ANGELES, FLIGHT 815, APRIL 25, 1976

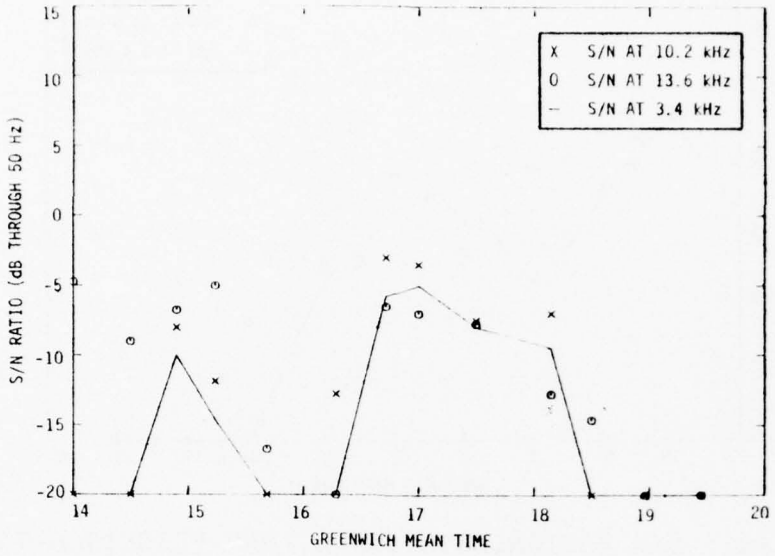

FIGURE B.91. S/N RATIOS, STATION B, TAHITI-AUCKLAND, FLIGHT 815, APRIL 25, 1976

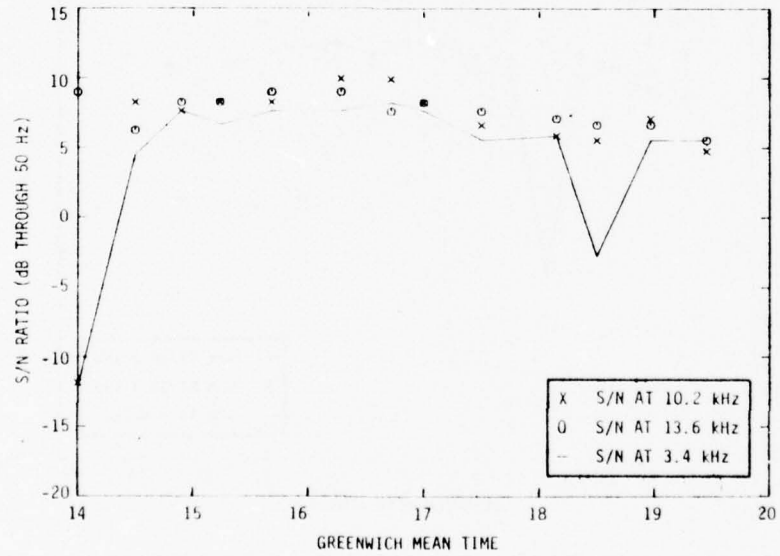

FIGURE B.92. S/N RATIOS, STATION C, TAHITI-AUCKLAND, FLIGHT 815, APRIL 25, 1976

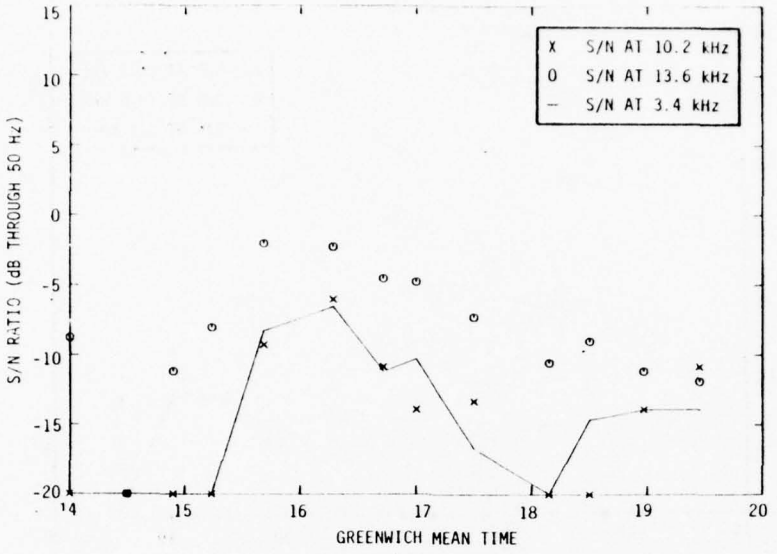

FIGURE B.93. S/N RATIOS, STATION D, TAHITI-AUCKLAND, FLIGHT 815, APRIL 25, 1976

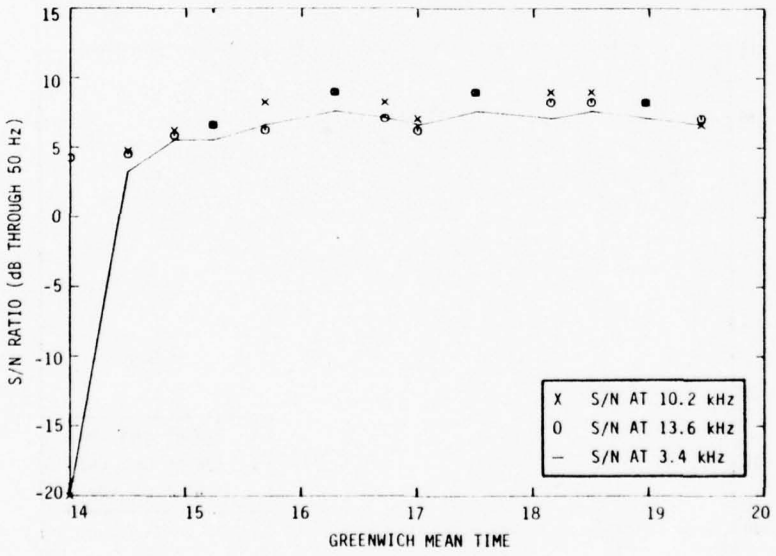

FIGURE B.94. S/N RATIOS, STATION E, TAHITI-AUCKLAND, FLIGHT 815, APRIL 25, 1976

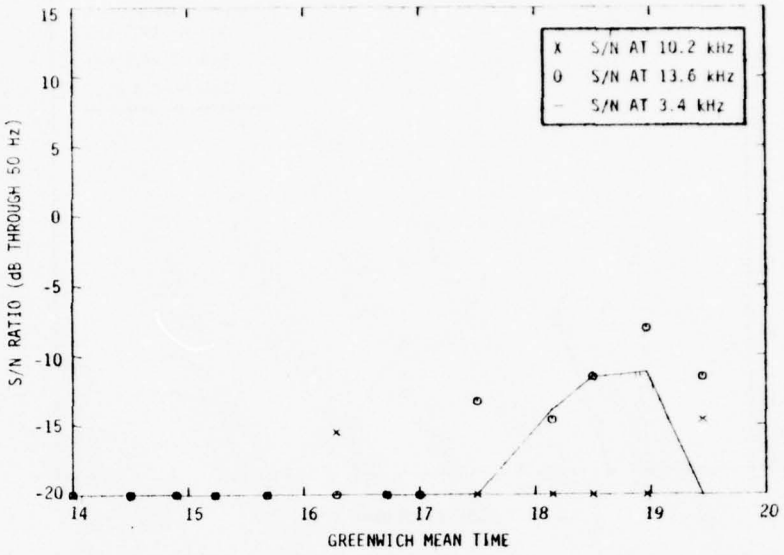

FIGURE B.95. S/N RATIOS, STATION G, TAHITI-AUCKLAND, FLIGHT 815, APRIL 25, 1976

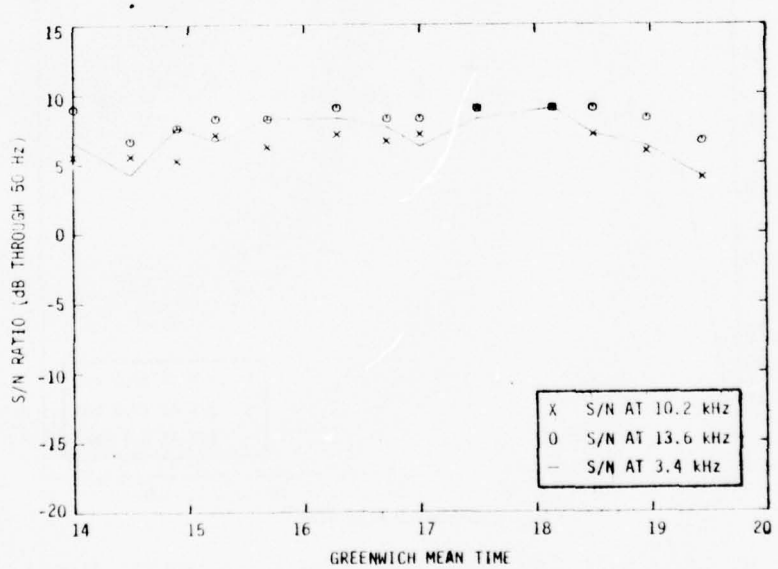

FIGURE B.96. S/N RATIOS, STATION H, TAHITI-AUCKLAND, FLIGHT 815, APRIL 25, 1976

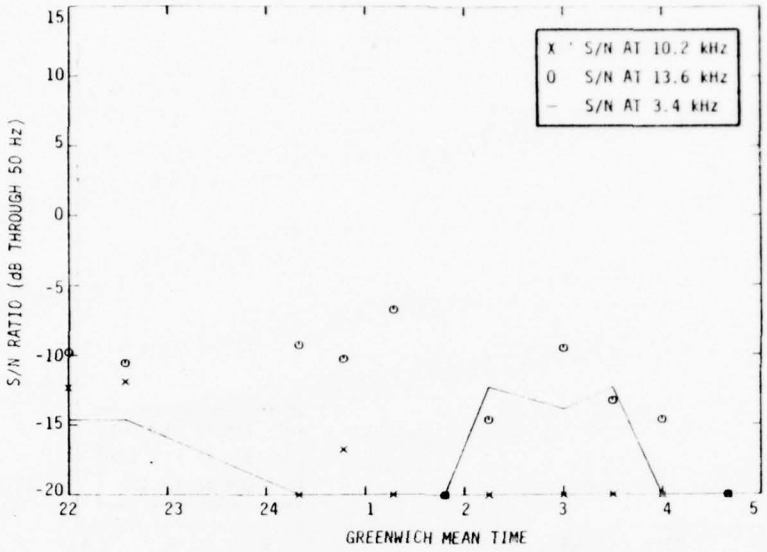

FIGURE B.97. S/N RATIOS, STATION A, AUCKLAND-TAHITI, FLIGHT 816, APRIL 29, 1976

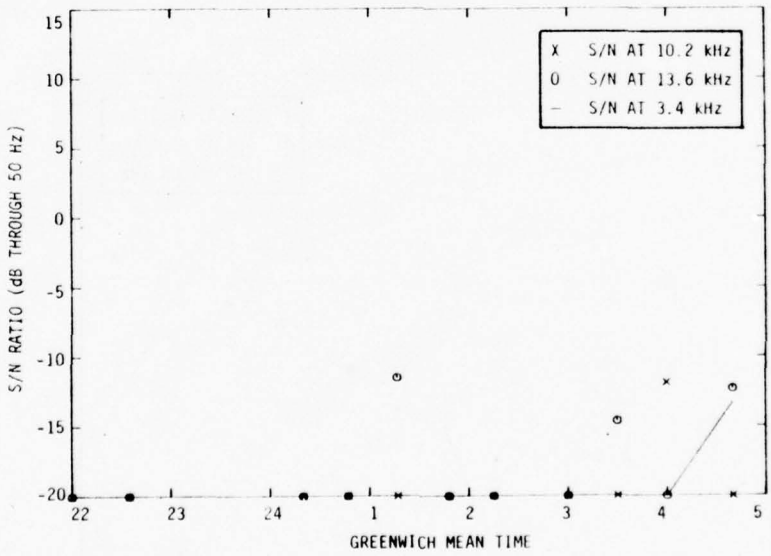

FIGURE B. 98. S/N RATIOS, STATION B, AUCKLAND-TAHITI, FLIGHT 816, APRIL 29, 1976

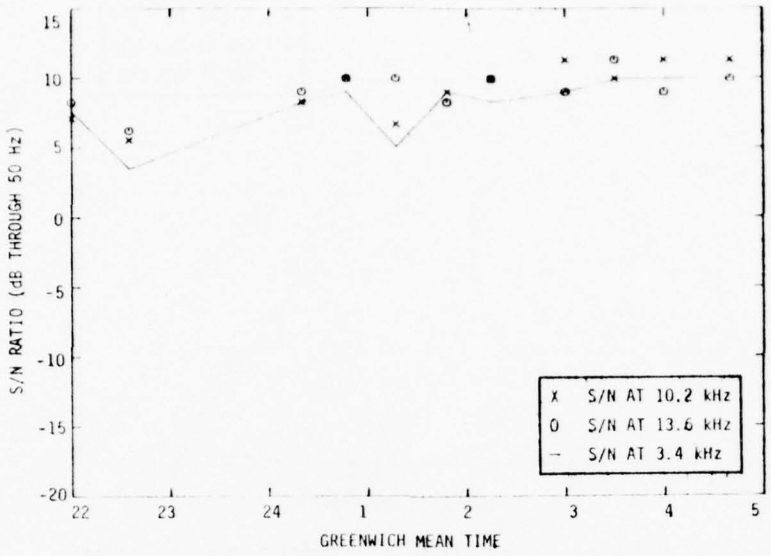

FIGURE B.99. S/N RATIOS, STATION C, AUCKLAND-TAHITI, FLIGHT 816, APRIL 29, 1976

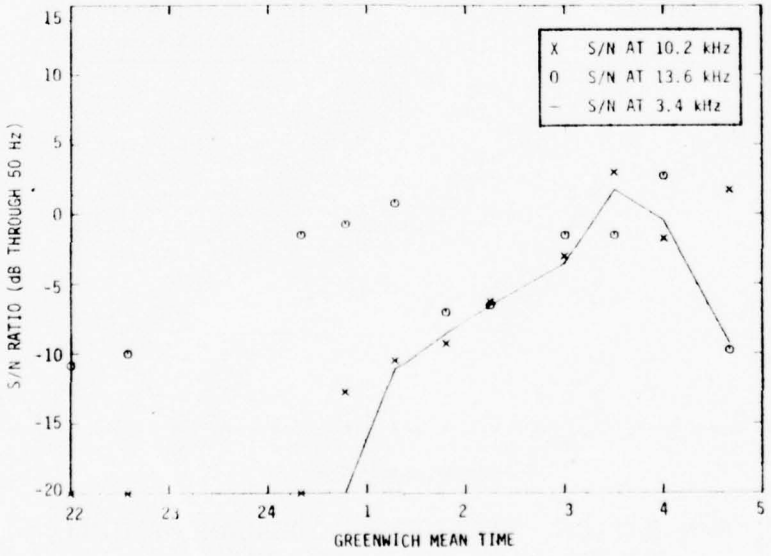

FIGURE B.100. S/N RATIOS, STATION D, AUCKLAND-TAHITI, FLIGHT 816, APRIL 29, 1976

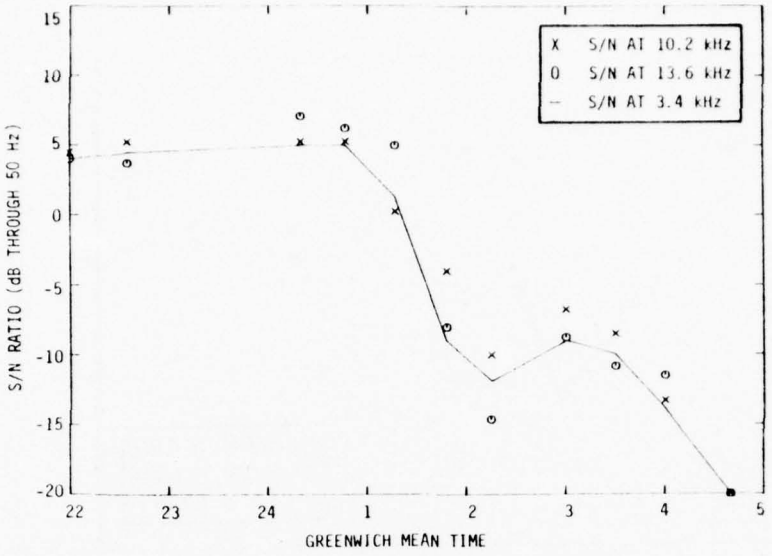

FIGURE B.101. S/N RATIOS, STATION E, AUCKLAND-TAHITI, FLIGHT 816, APRIL 29, 1976

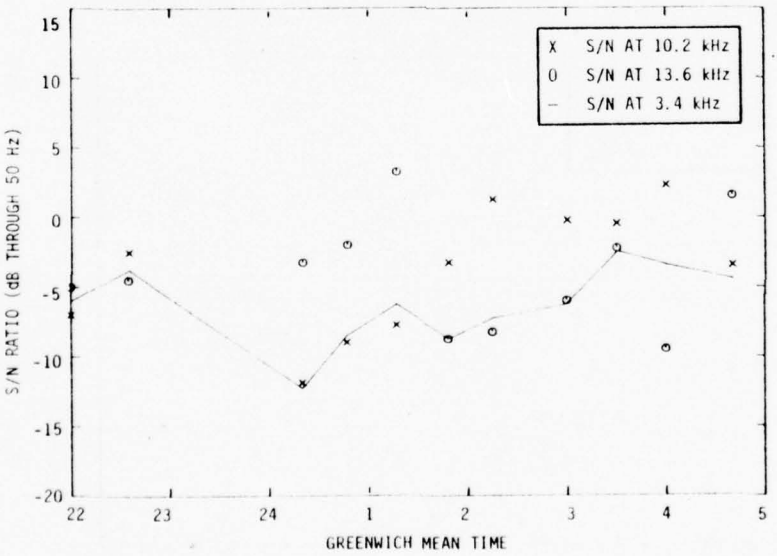

FIGURE B.102. S/N RATIOS, STATION F, AUCKLAND-TAHITI, FLIGHT 816, APRIL 29, 1976

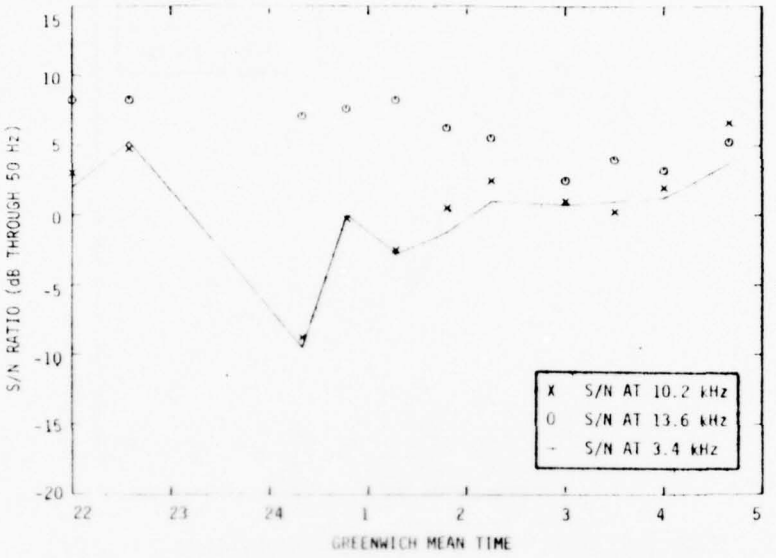

FIGURE B.103. S/N RATIOS, STATION H, AUCKLAND-TAHITI, FLIGHT 816, APRIL 29, 1976

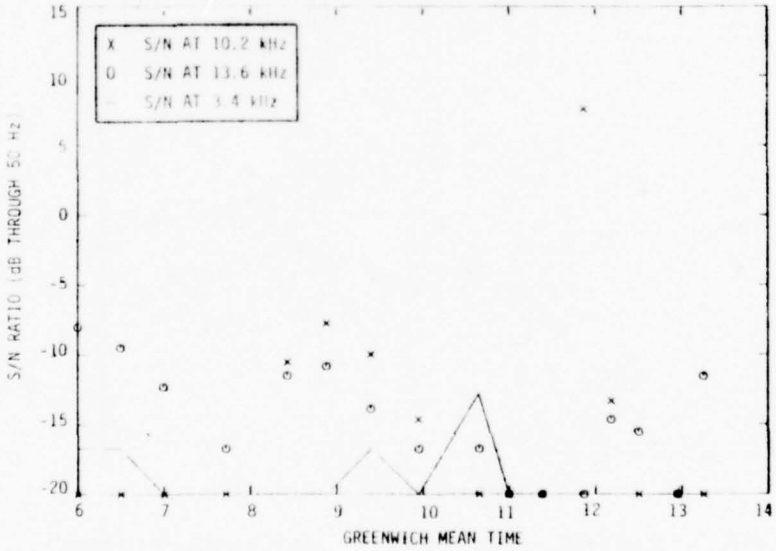

FIGURE B.104. S/N RATIOS, STATION B, TAHITI-LOS ANGELES, FLIGHT 816, APRIL 29, 1976

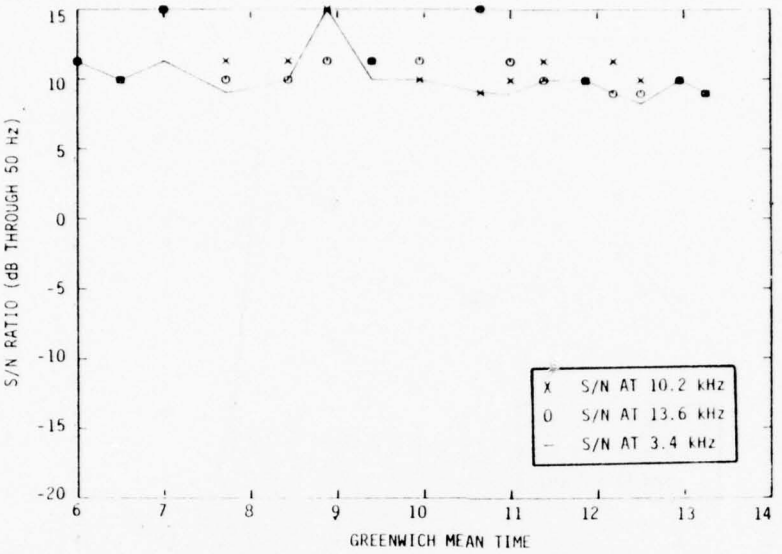

FIGURE B.105. S/N RATIOS, STATION C, TAHITI-LOS ANGELES, FLIGHT 816, APRIL 29, 1976

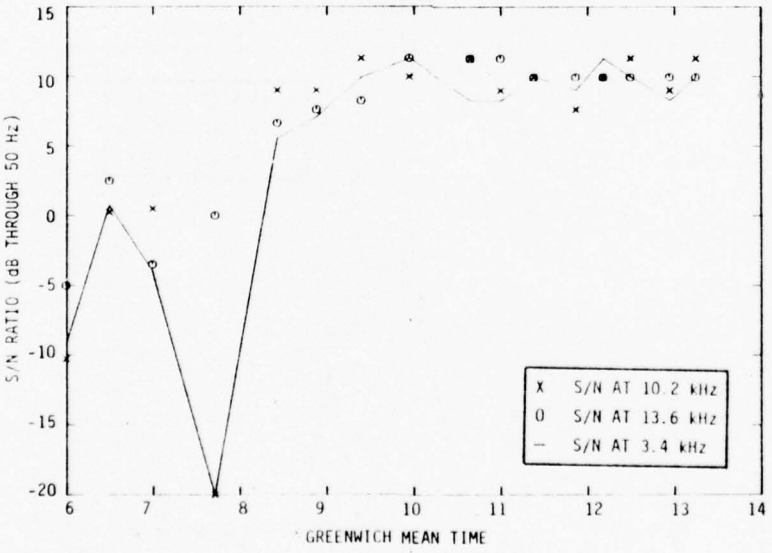

FIGURE B.106. S/N RATIOS, STATION D, TAHITI-LOS ANGELES, FLIGHT 816, APRIL 29, 1976

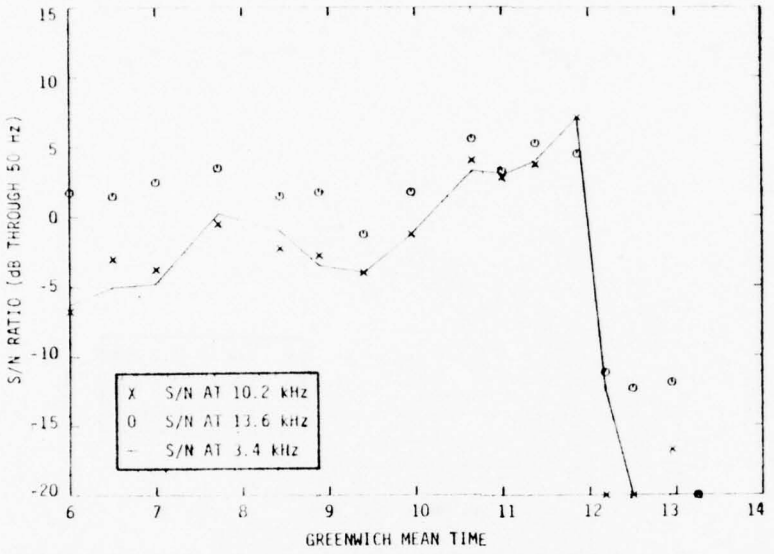

FIGURE B.107. S/N RATIOS, STATION E, TAHITI-LOS ANGELES, FLIGHT 816, APRIL 29, 1976

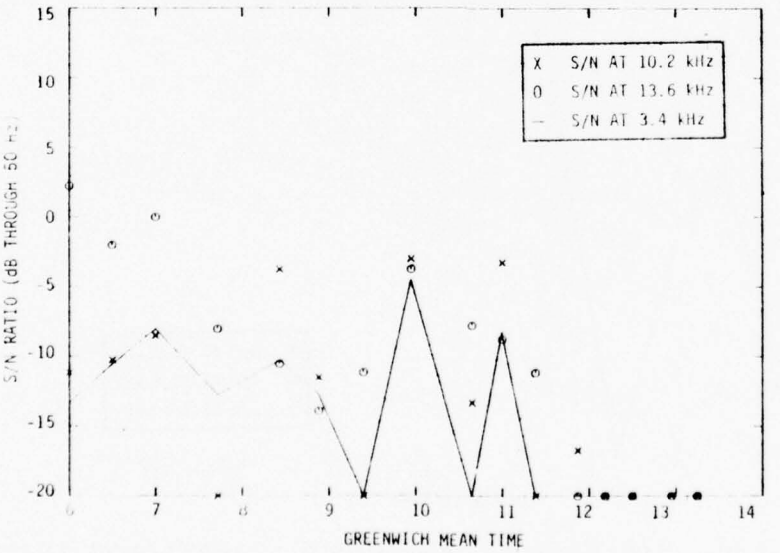

FIGURE B.108. S/N RATIOS, STATION F, TAHITI-LOS ANGELES, FLIGHT 816, APRIL 29, 1976

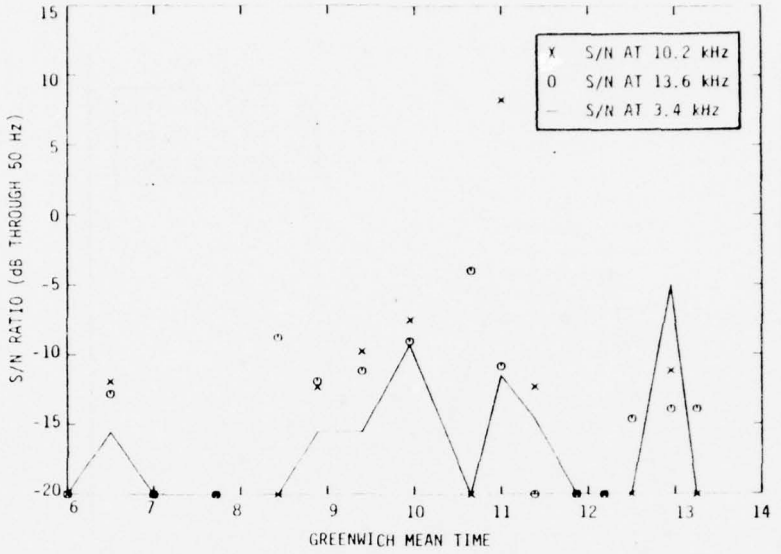

FIGURE B.109. S/N RATIOS, STATION G, TAHITI-LOS ANGELES, FLIGHT 816, APRIL 29, 1976

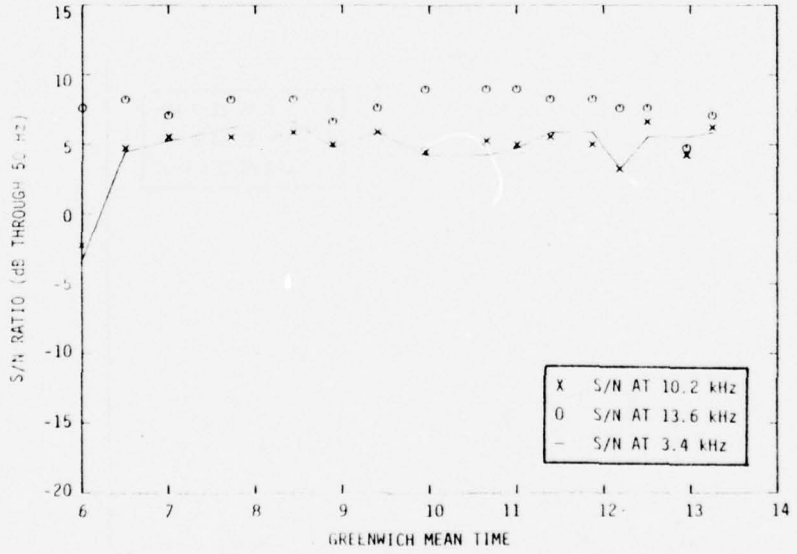

FIGURE B.110. S/N RATIOS, STATION H, TAHITI-LOS ANGELES, FLIGHT 816, APRIL 29, 1976

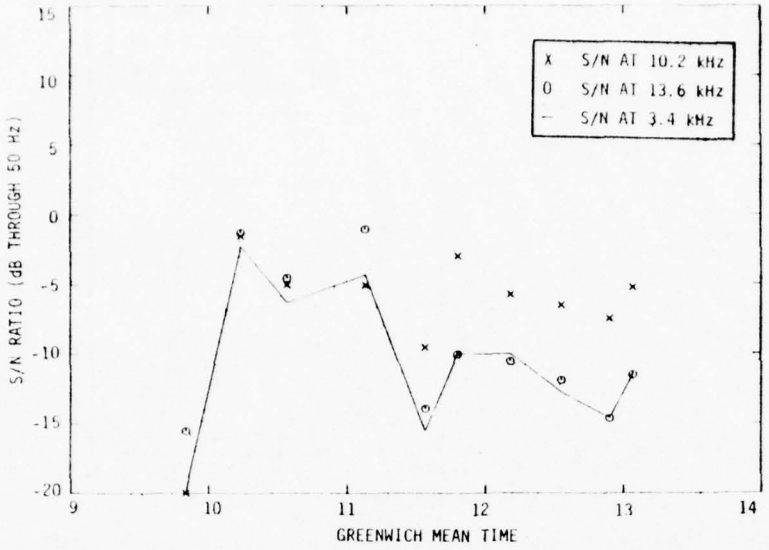

FIGURE B.111. S/N RATIOS, STATION A, TOKYO-GUAM, FLIGHT 803, MAY 17, 1976

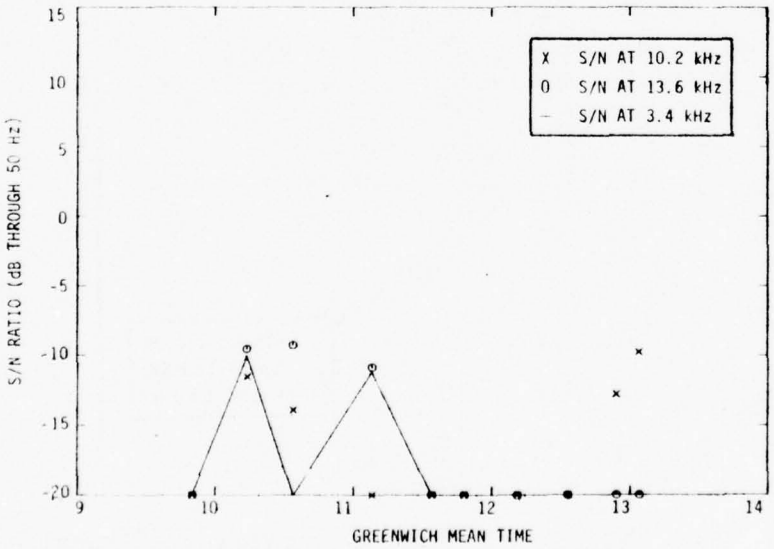

FIGURE B.112. S/N RATIOS, STATION B, TOKYO-GUAM, FLIGHT 803, MAY 17, 1976

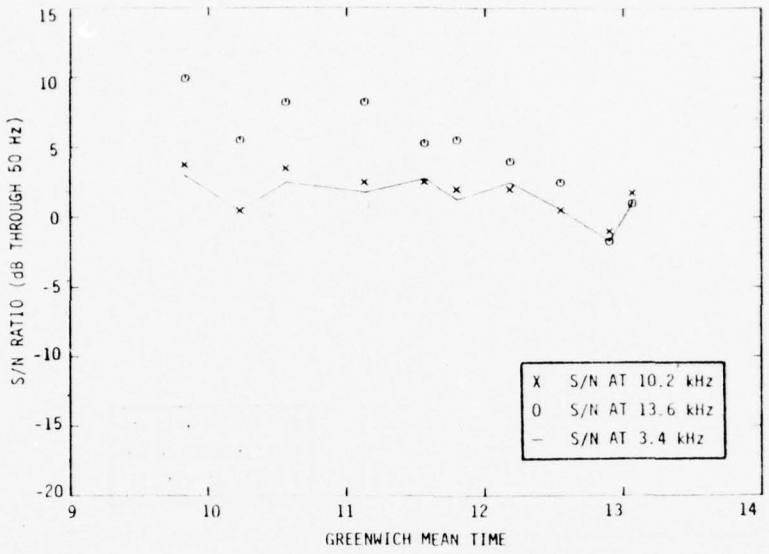

FIGURE B.113. S/N RATIOS, STATION C, TOKYO-GUAM, FLIGHT 803, MAY 17, 1976

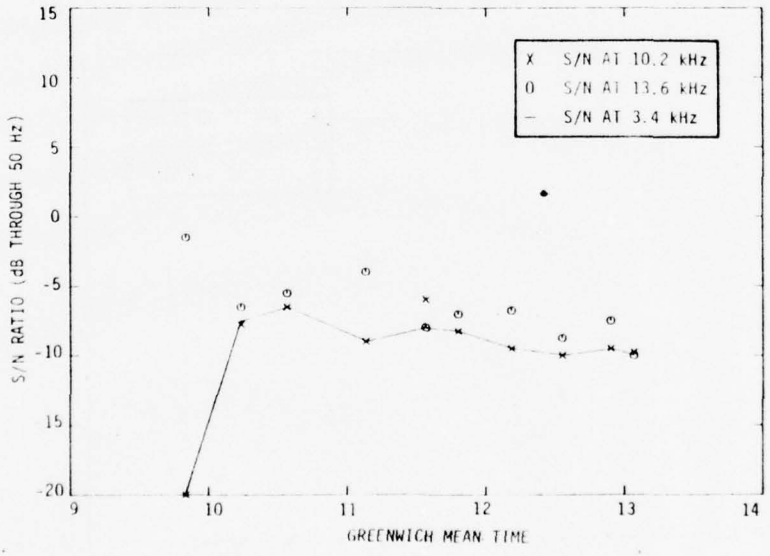

FIGURE B.114. S/N RATIOS, STATION D, TOKYO-GUAM, FLIGHT 803, MAY 17, 1976

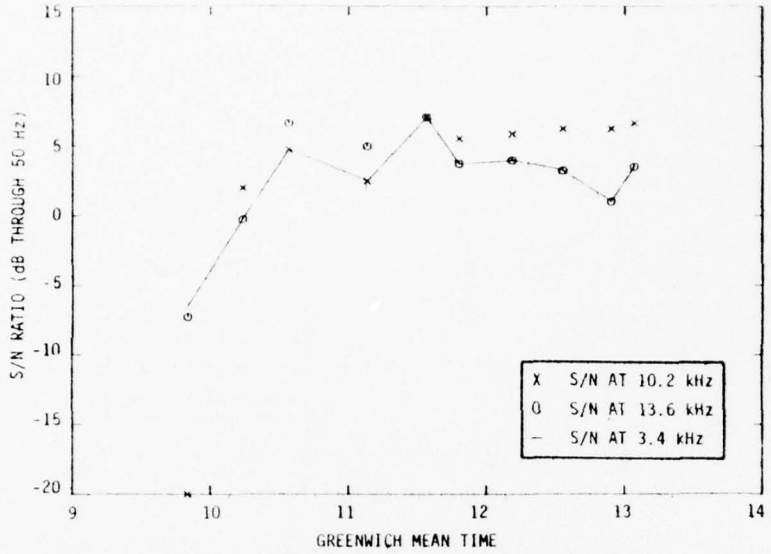

FIGURE B.115. S/N RATIOS, STATION E, TOKYO-GUAM, FLIGHT 803, MAY 17, 1976

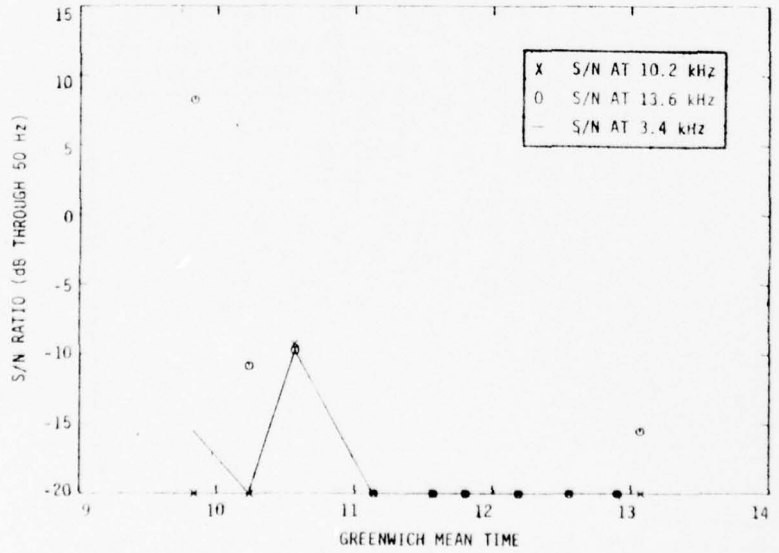

FIGURE B.116. S/N RATIOS, STATION F, TOKYO-GUAM, FLIGHT 803, MAY 17, 1976

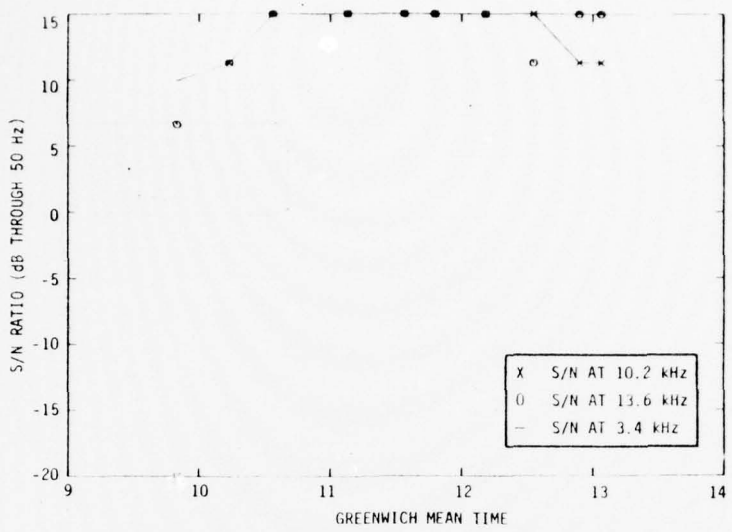

FIGURE B. 117. S/N RATIOS, STATION H, TOKYO-GUAM, FLIGHT 803, MAY 17, 1976

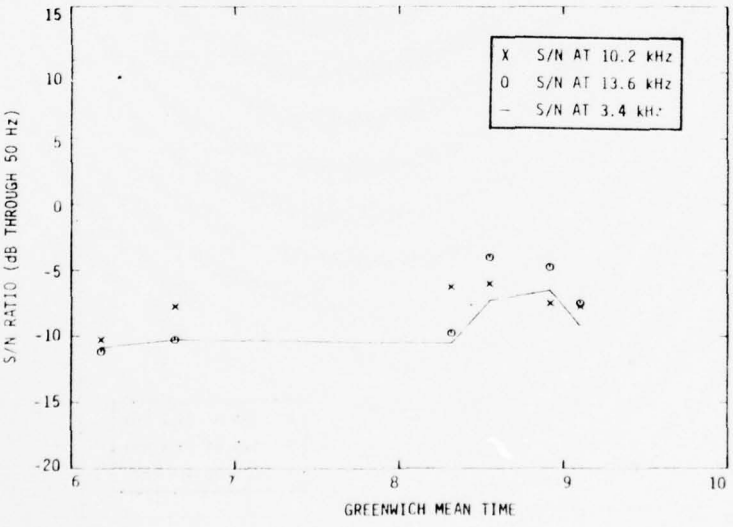

FIGURE B.118. S/N RATIOS, STATION A, GUAM-TOKYO, FLIGHT 802, MAY 17, 1976

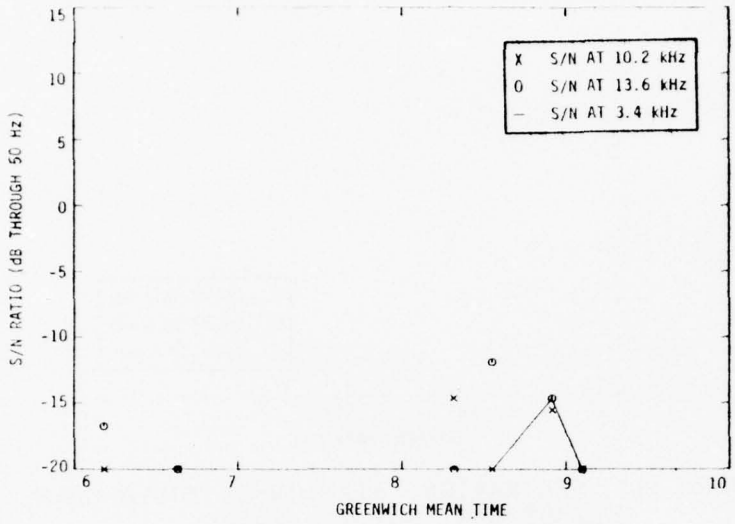

FIGURE B.119. S/N RATIOS, STATION B, GUAM-TOKYO, FLIGHT 802, MAY 17, 1976

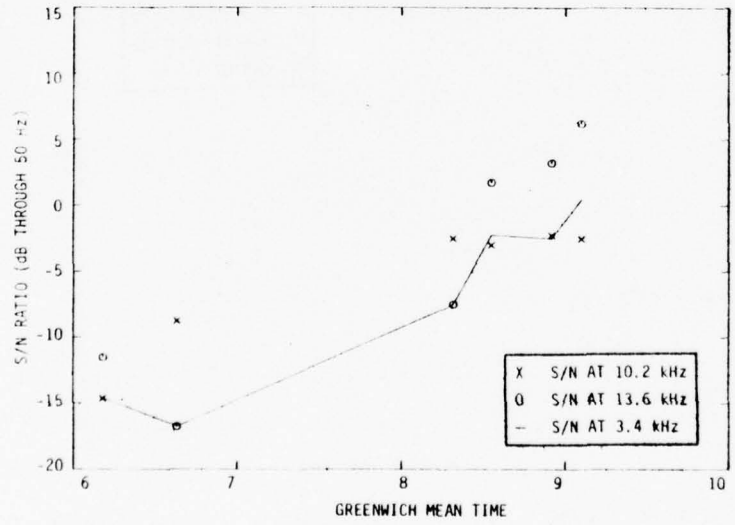

FIGURE B.120. S/N RATIOS, STATION C, GUAM-TOKYO, FLIGHT 802, MAY 17, 1976

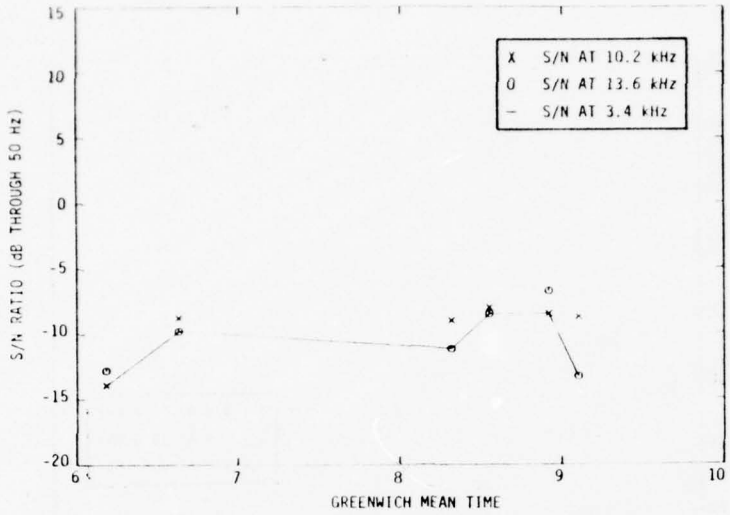

FIGURE B.121. S/N RATIOS, STATION D, GUAM-TOKYO, FLIGHT 802, MAY 17, 1976

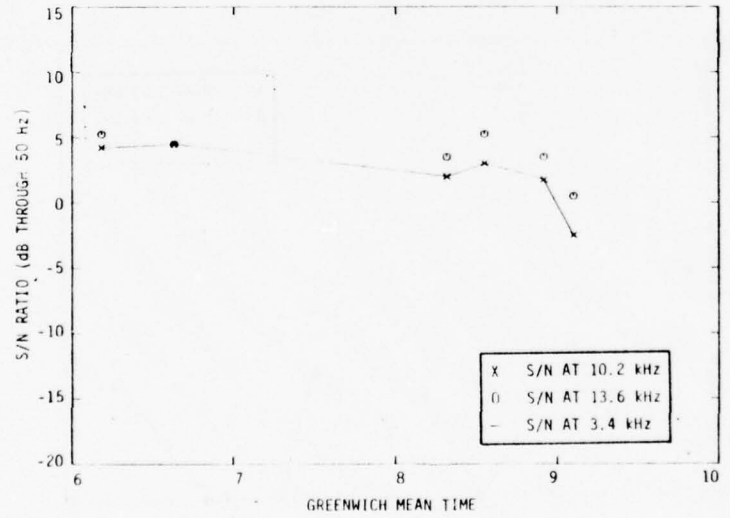

FIGURE B.122. S/N RATIOS, STATION E, GUAM-TOKYO, FLIGHT 802, MAY 17, 1976

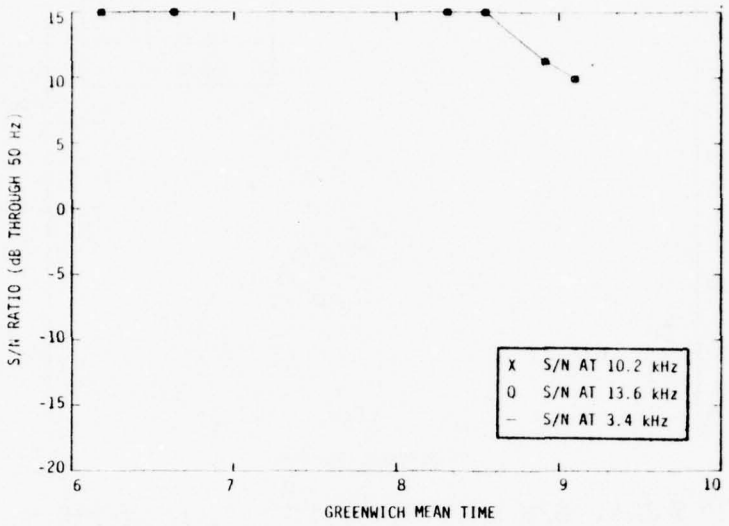

FIGURE B.123. S/N RATIOS, STATION H, GUAM-TOKYO, FLIGHT 802, MAY 17, 1976

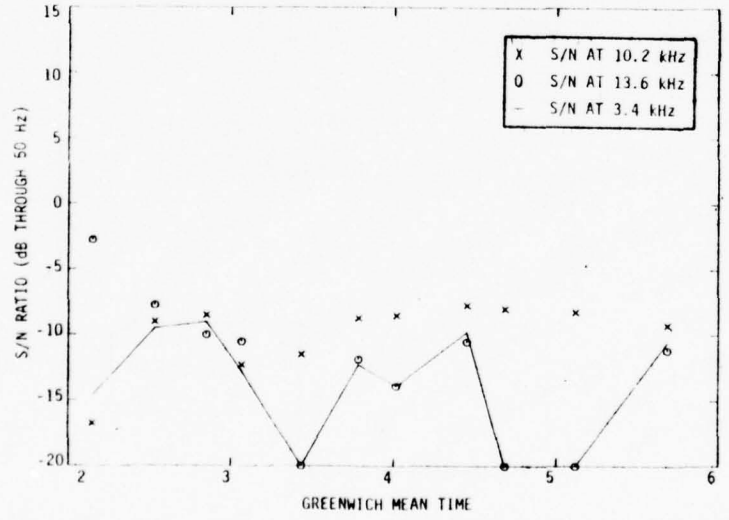

FIGURE B.124. S/N RATIOS, STATION A, TOKYO-HONG KONG, FLIGHT 003, MAY 18, 1976

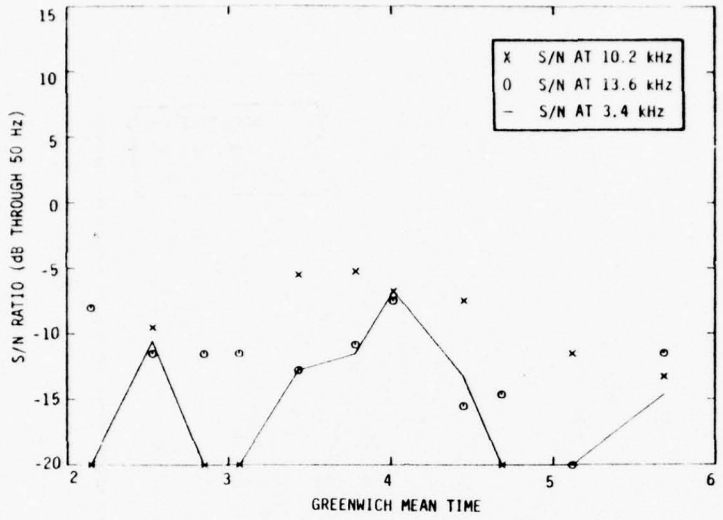

FIGURE B.125. S/N RATIOS, STATION B, TOKYO-HONG KONG, FLIGHT 003, MAY 18, 1976

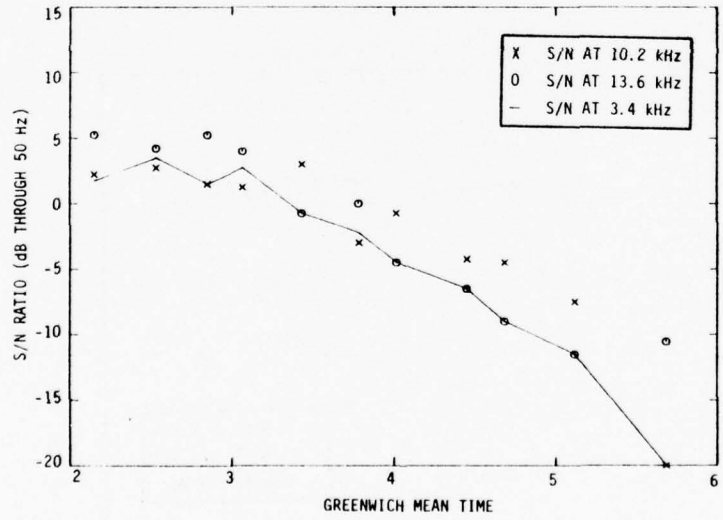

FIGURE B.126. S/N RATIOS, STATION C, TOKYO-HONG KONG, FLIGHT 003, MAY 18, 1976

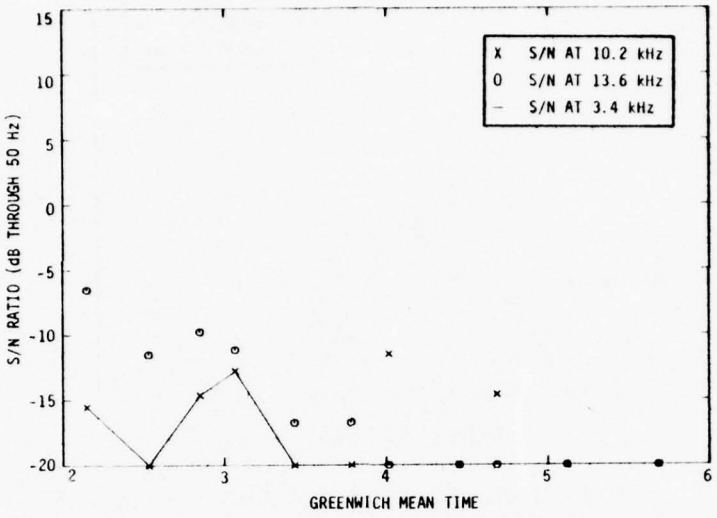

FIGURE B.127. S/N RATIOS, STATION D, TOKYO-HONG KONG, FLIGHT 003, MAY 18, 1976

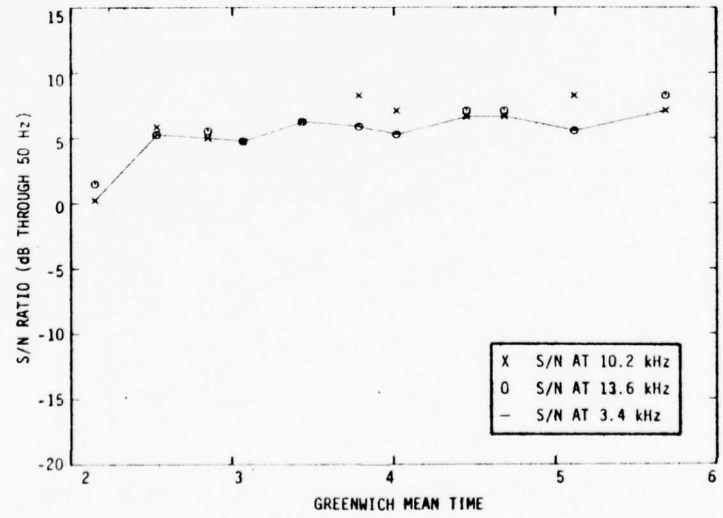

FIGURE B.128. S/N RATIOS, STATION E, TOKYO-HONG KONG, FLIGHT 003, MAY 18, 1976

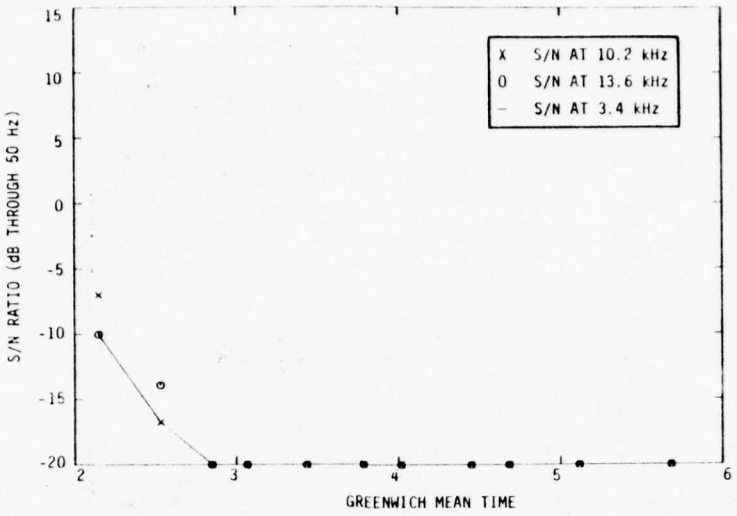

FIGURE B.129. S/N RATIOS, STATION F, TOKYO-HONG KONG, FLIGHT 003, MAY 18, 1976

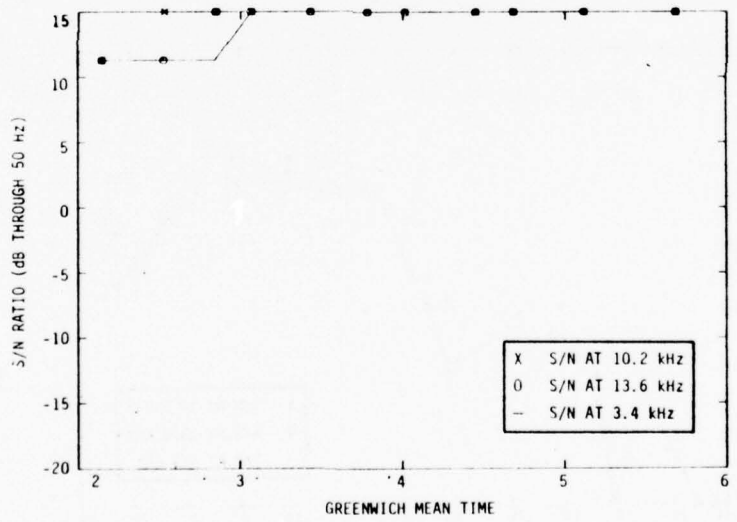

FIGURE B.130. S/N RATIOS, STATION H, TOKYO-HONG KONG, FLIGHT 003, MAY 18, 1976

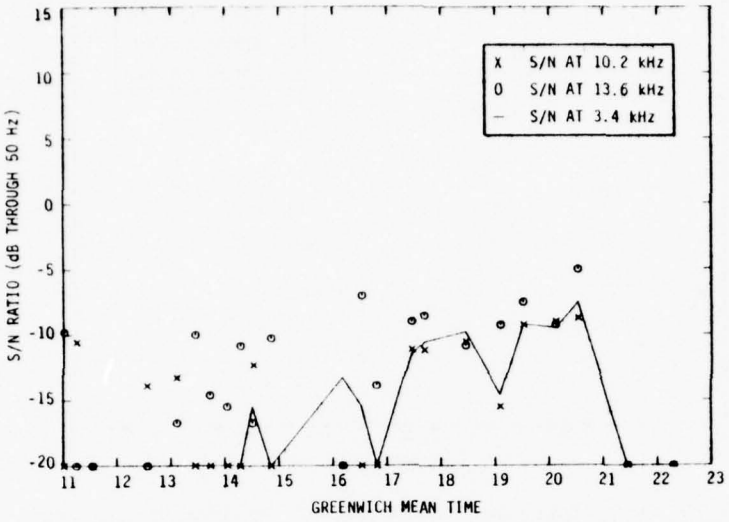

FIGURE B.131. S/N RATIOS, STATION A, HONG KONG-SYDNEY VIA DJAKARTA, FLIGHT 812, MAY 19, 1976

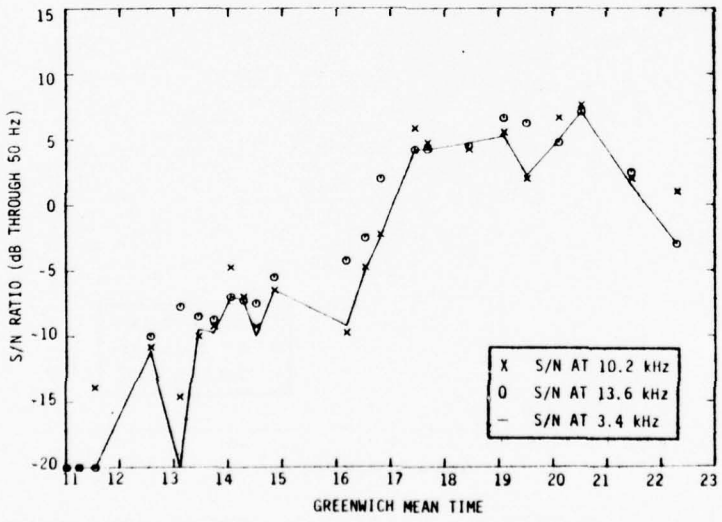

FIGURE B. 132. S/N RATIOS, STATION B, HONG KONG-SYDNEY VIA DJAKARTA, FLIGHT 812, MAY 19, 1976

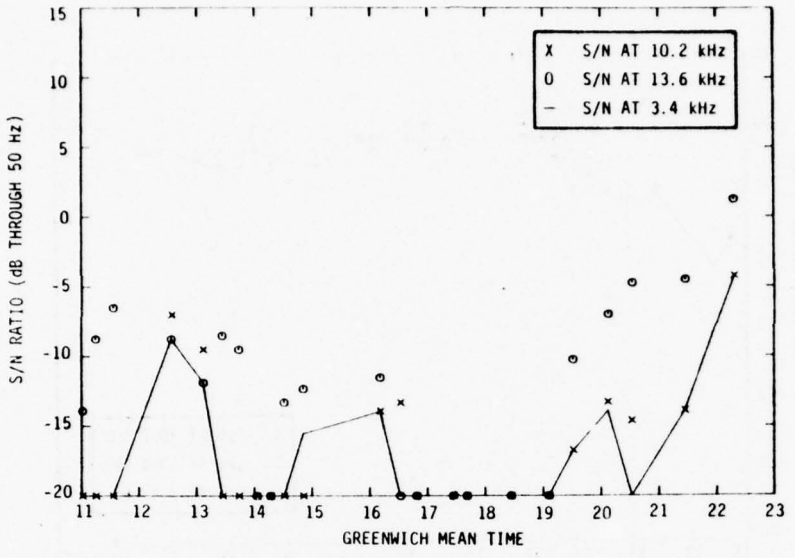

FIGURE B.133. S/N RATIOS, STATION C, HONG KONG-SYDNEY VIA DJAKARTA, FLIGHT 812, MAY 19, 1976

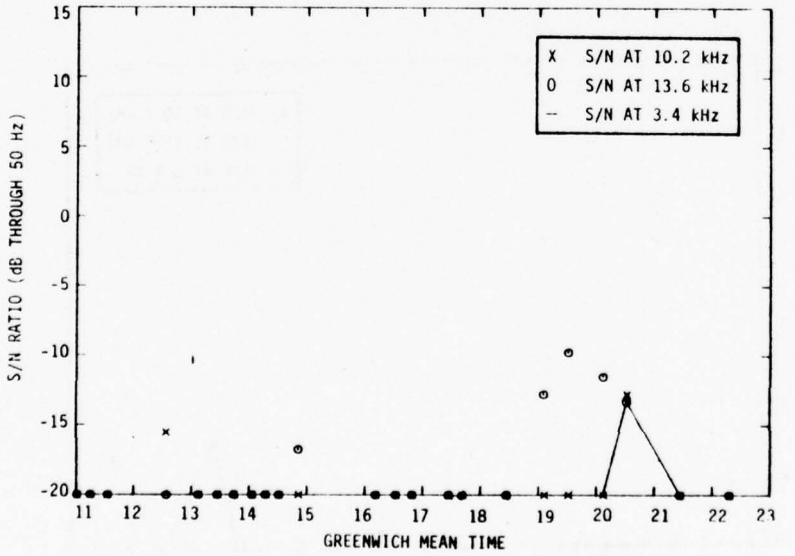

FIGURE B.134. S/N RATIOS, STATION D, HONG KONG-SYDNEY VIA DJAKARTA, FLIGHT 812, MAY 19, 1976

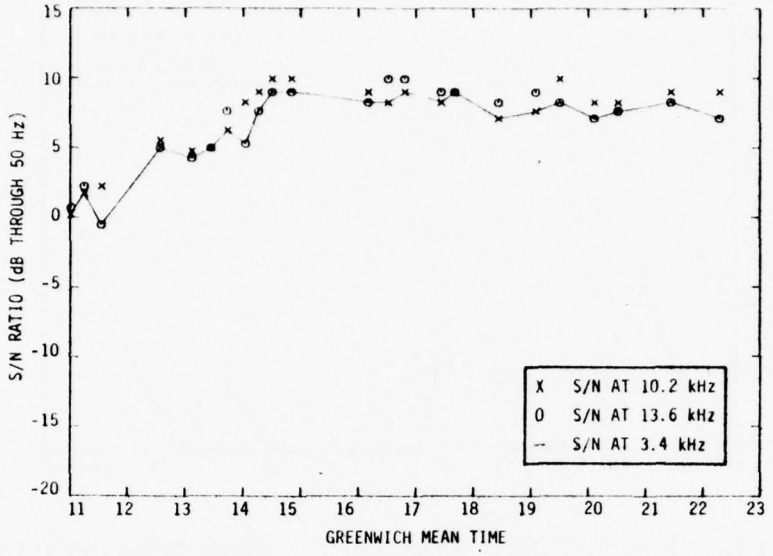

FIGURE B.135. S/N RATIOS, STATION E, HONG KONG-SYDNEY VIA DJAKARTA, FLIGHT 812, MAY 19, 1976

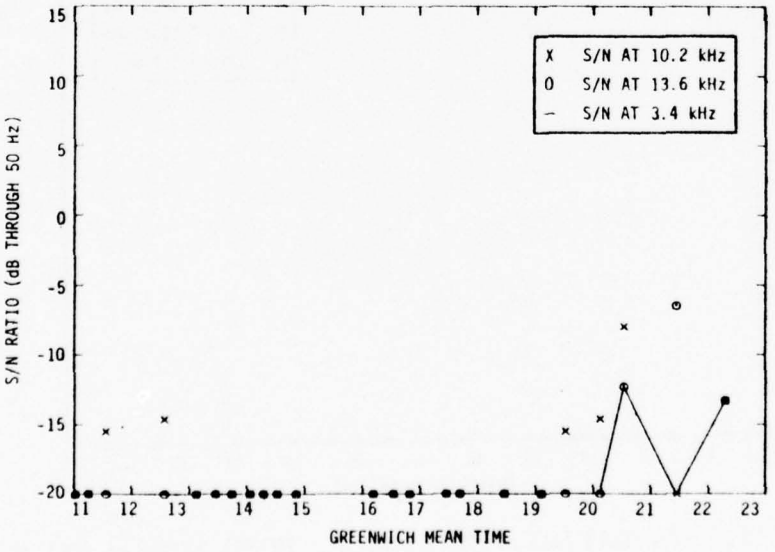

FIGURE B.136. S/N RATIOS, STATION F, HONG KONG-SYDNEY VIA DJAKARTA, FLIGHT 812, MAY 19, 1976

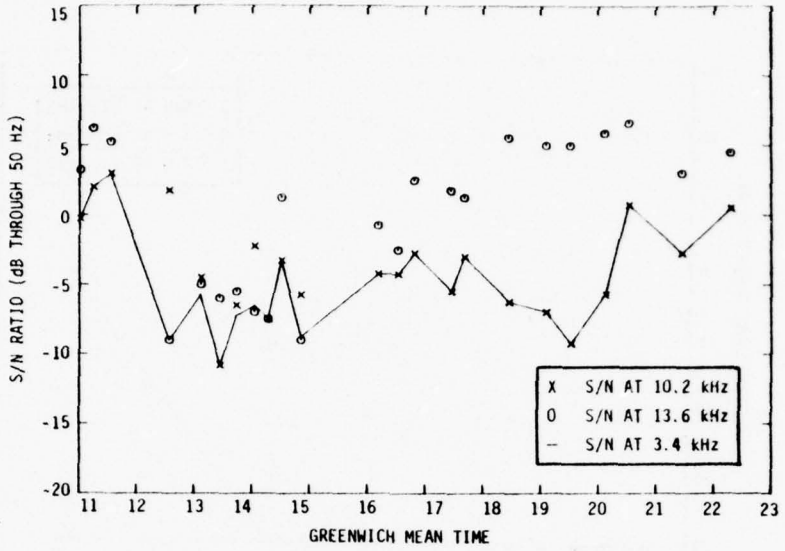

FIGURE B.137. S/N RATIOS, STATION H, HONG KONG-SYDNEY VIA DJAKARTA, FLIGHT 812, MAY 19, 1976

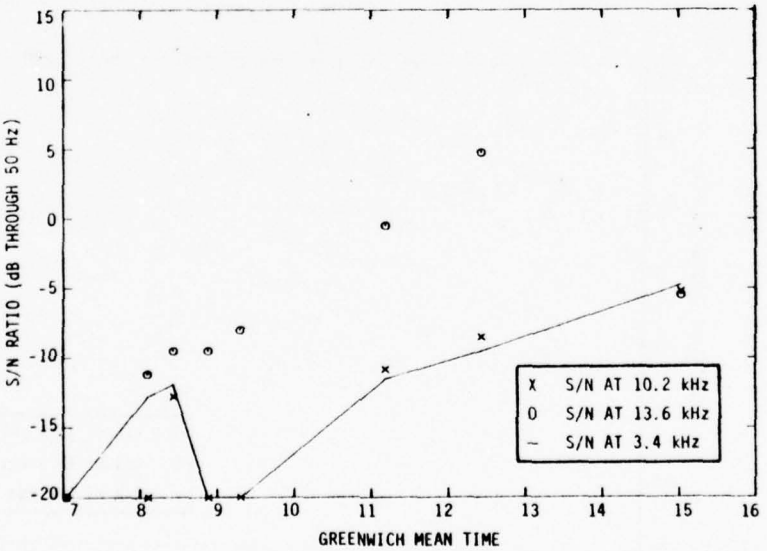

FIGURE B.138. S/N RATIOS, STATION A, SYDNEY-HONOLULU, FLIGHT 812, MAY 20, 1976

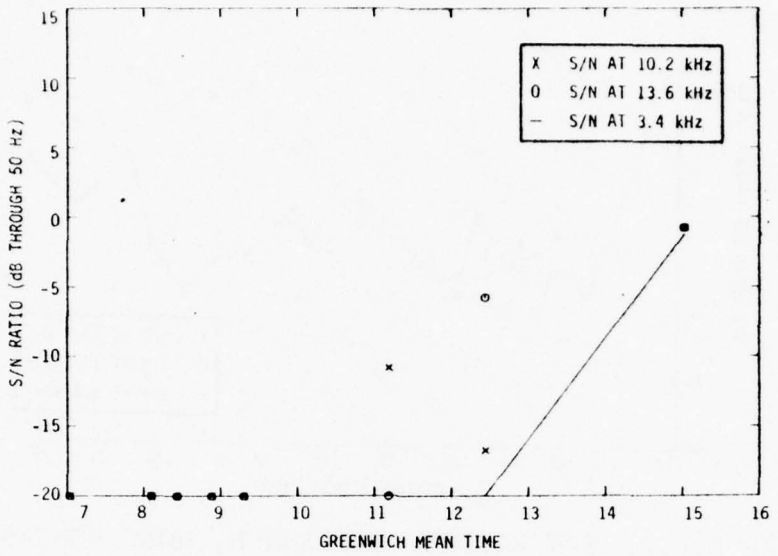

FIGURE B.139. S/N RATIOS, STATION B, SYDNEY-HONOLULU, FLIGHT 812, MAY 20, 1976

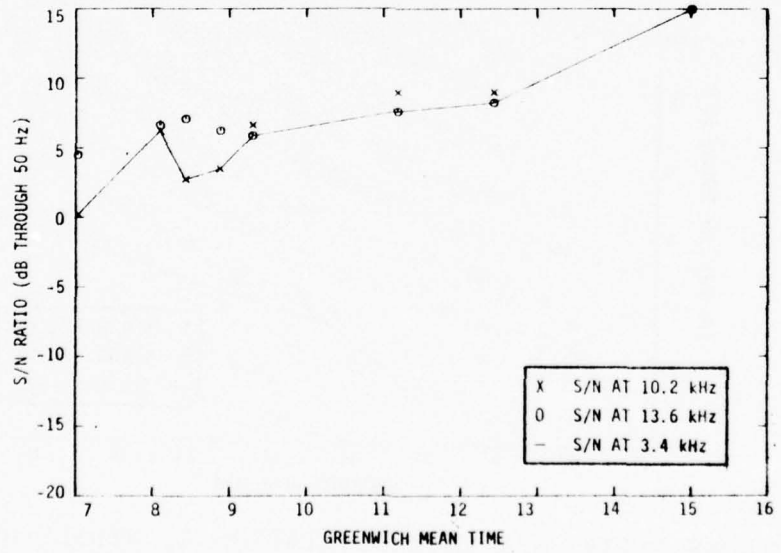

FIGURE B.140. S/N RATIOS, STATION C, SYDNEY-HONOLULU, FLIGHT 812, MAY 20, 1976

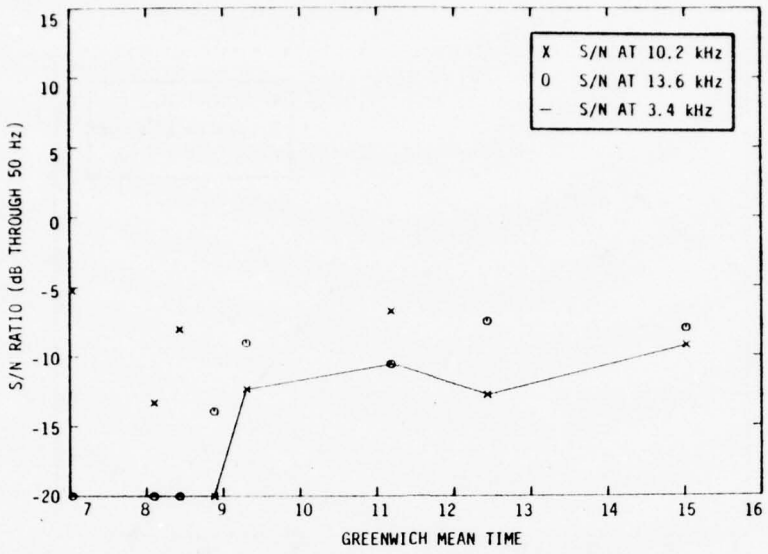

FIGURE B.141. S/N RATIOS, STATION D, SYDNEY-HONOLULU, FLIGHT 812, MAY 20, 1976

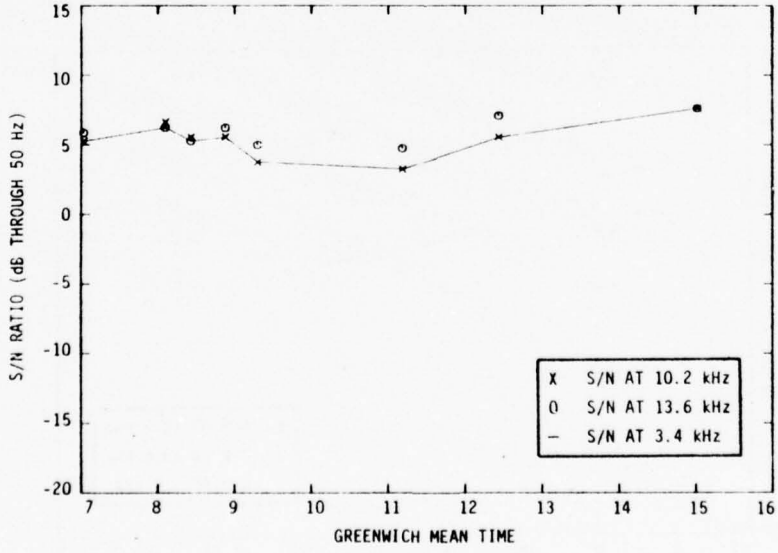

FIGURE B.142. S/N RATIOS, STATION E, SYDNEY-HONOLULU, FLIGHT 812, MAY 20, 1976

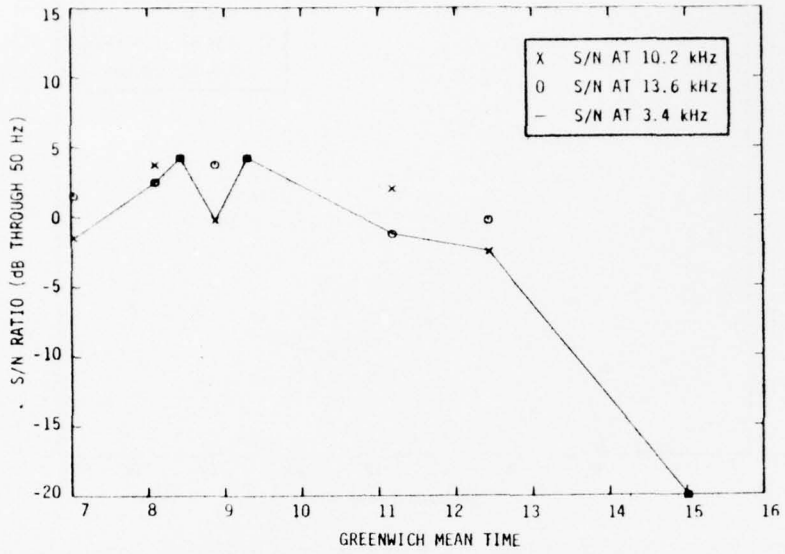

FIGURE B.143. S/N RATIOS, STATION F, SYDNEY-HONOLULU, FLIGHT 812, MAY 20, 1976

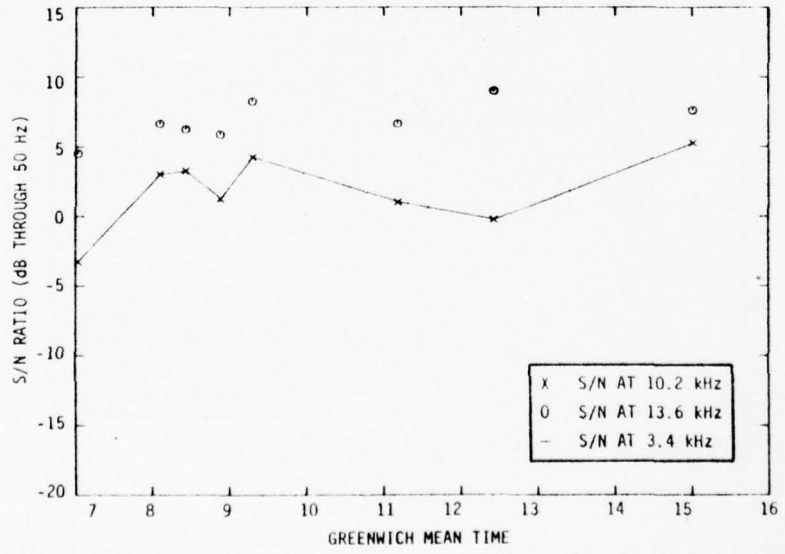

FIGURE B.144. S/N RATIOS, STATION H, SYDNEY-HONOLULU, FLIGHT 812, MAY 20, 1976

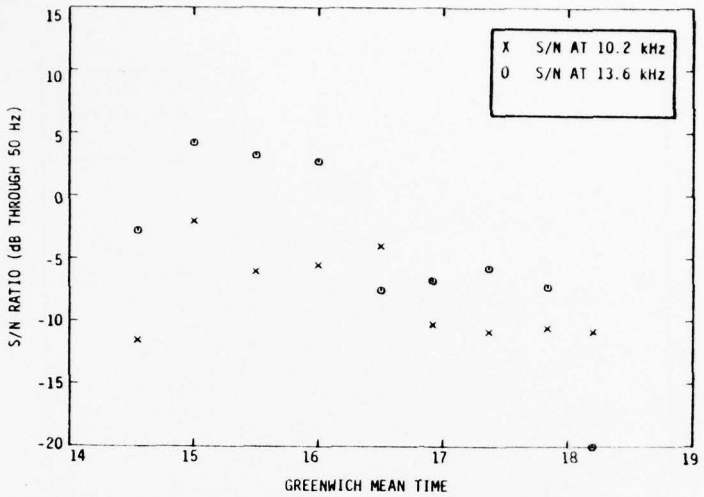

FIGURE B.145. S/N RATIOS, STATION A, NEW YORK-CARACAS, FLIGHT 217, JULY 22, 1976

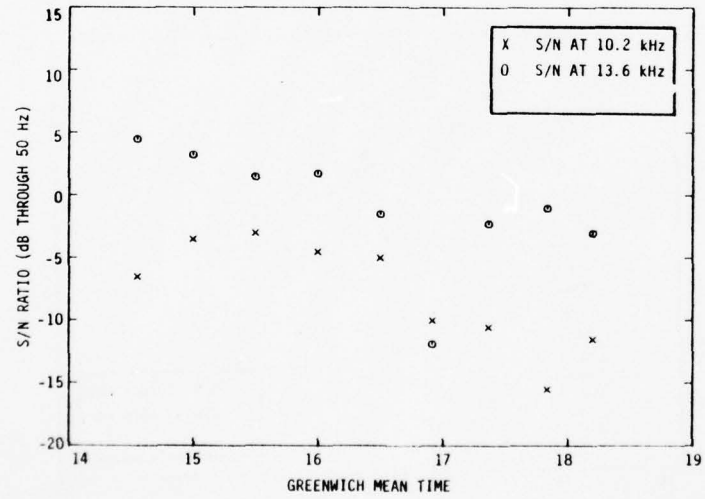

FIGURE B.146. S/N RATIOS, STATION B, NEW YORK-CARACAS, FLIGHT 217, JULY 22, 1976

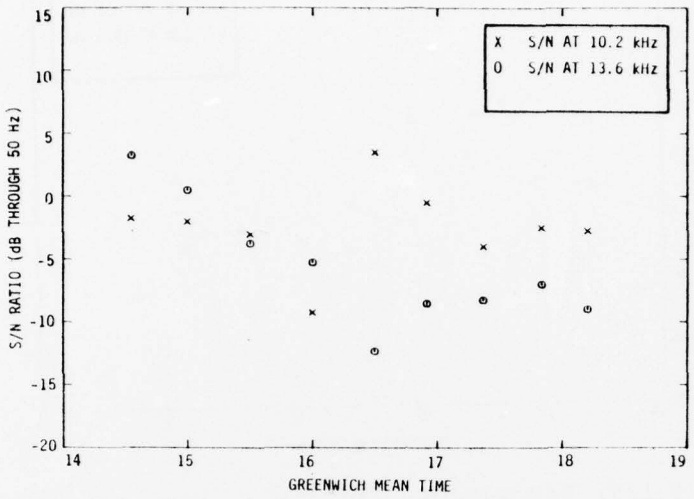

FIGURE B.147. S/N RATIOS, STATION C, NEW YORK-CARACAS, FLIGHT 217, JULY 22, 1976

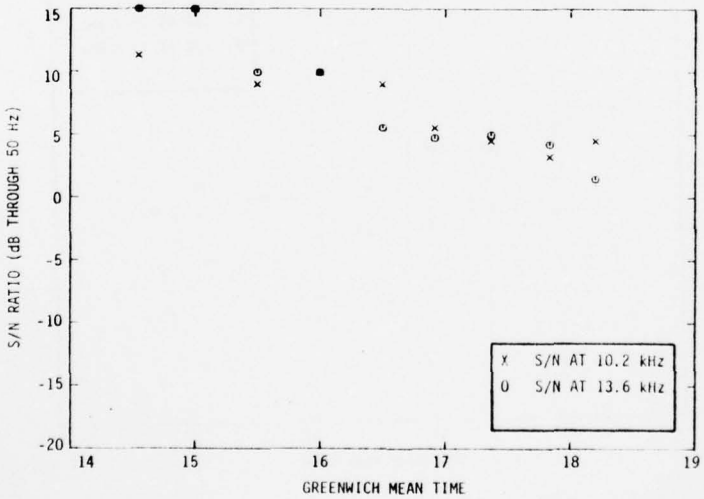

FIGURE B.148. S/N RATIOS, STATION D, NEW YORK-CARACAS, FLIGHT 217, JULY 22, 1976

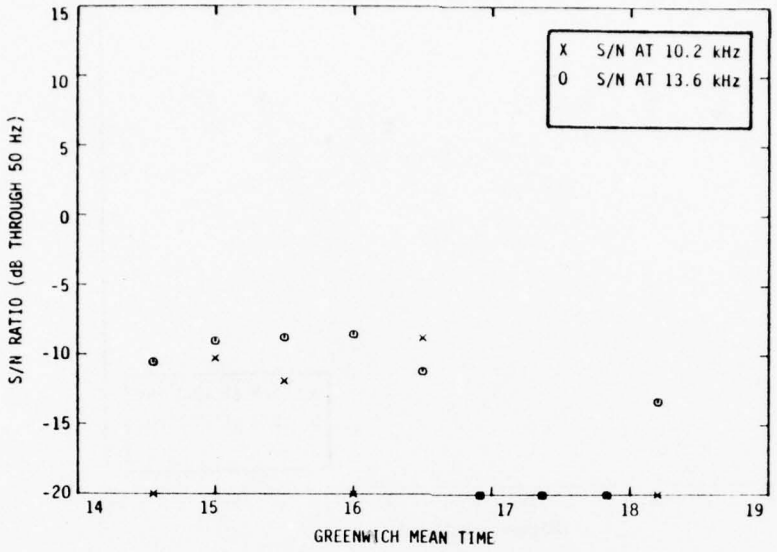

FIGURE B.149. S/N RATIOS, STATION E, NEW YORK-CARACAS, FLIGHT 217, JULY 22, 1976

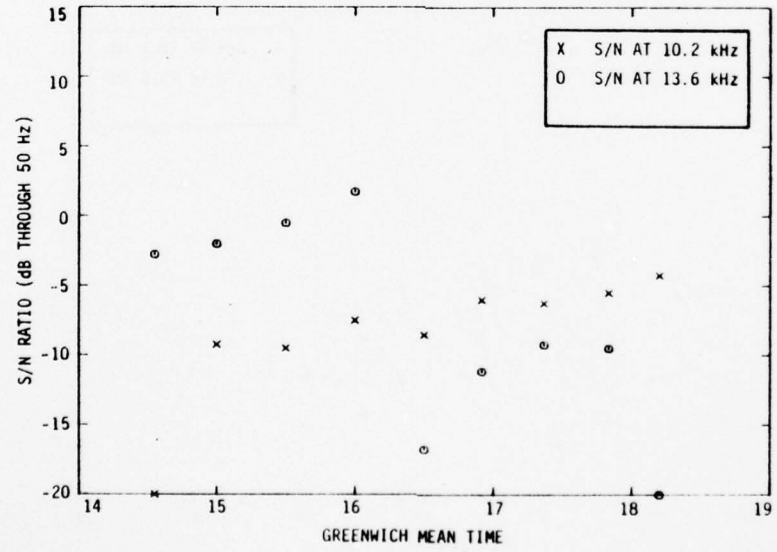

FIGURE B.150. S/N RATIOS, STATION F, NEW YORK-CARACAS, FLIGHT 217, JULY 22, 1976

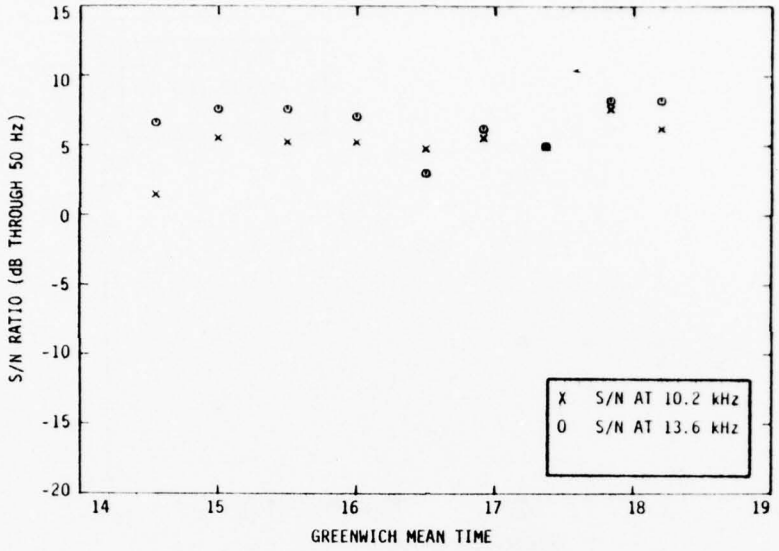

FIGURE B.151. S/N RATIOS, STATION G, NEW YORK-CARACAS, FLIGHT 217, JULY 22, 1976

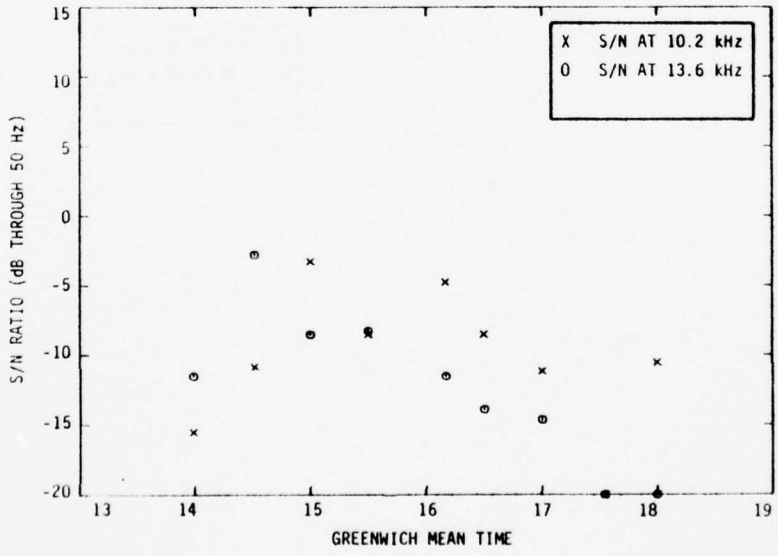

FIGURE B.152. S/N RATIOS, STATION A, NEW YORK-CARACAS, FLIGHT 217, AUGUST 12, 1976

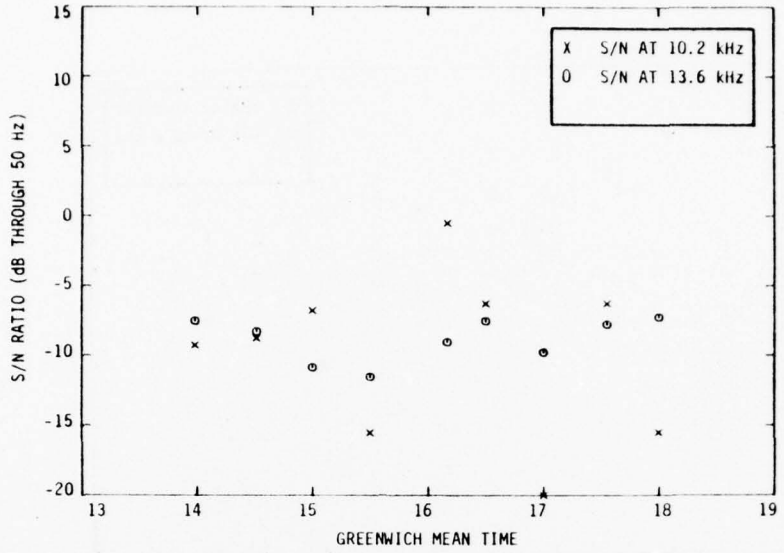

FIGURE B. 153. S/N RATIOS, STATION B, NEW YORK-CARACAS, FLIGHT 217, AUGUST 12, 1976

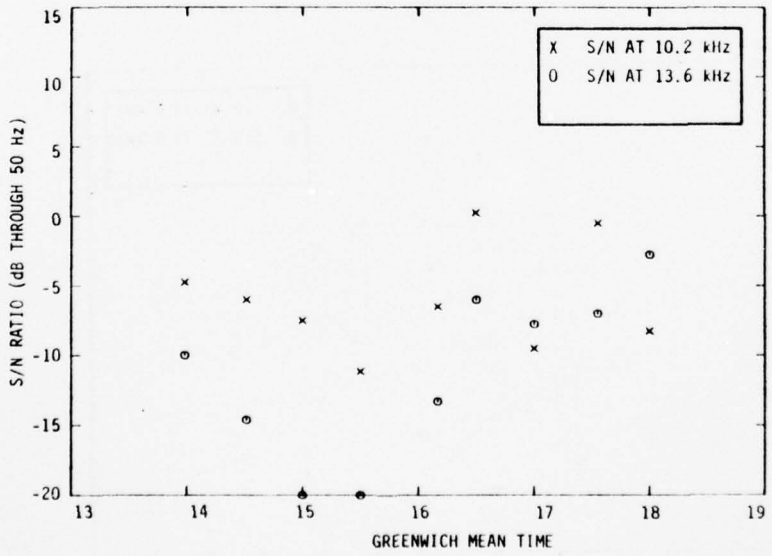

FIGURE B.154. S/N RATIOS, STATION C, NEW YORK-CARACAS, FLIGHT 217, AUGUST 12, 1976

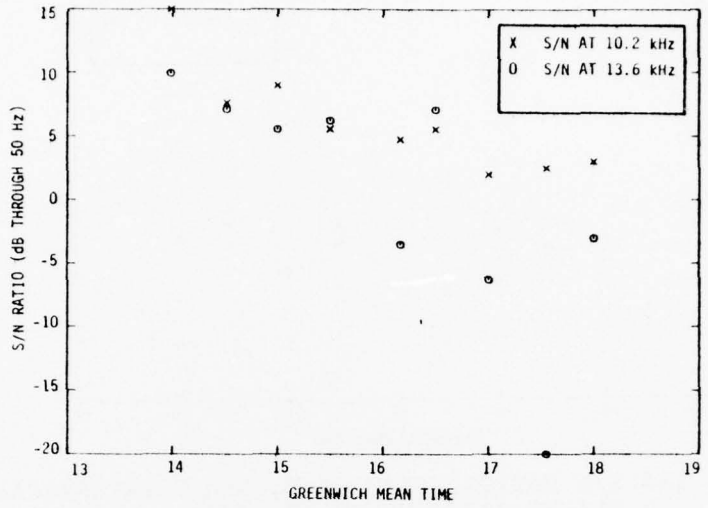

FIGURE B.155. S/N RATIOS, STATION D, NEW YORK-CARACAS, FLIGHT 217, AUGUST 12, 1976

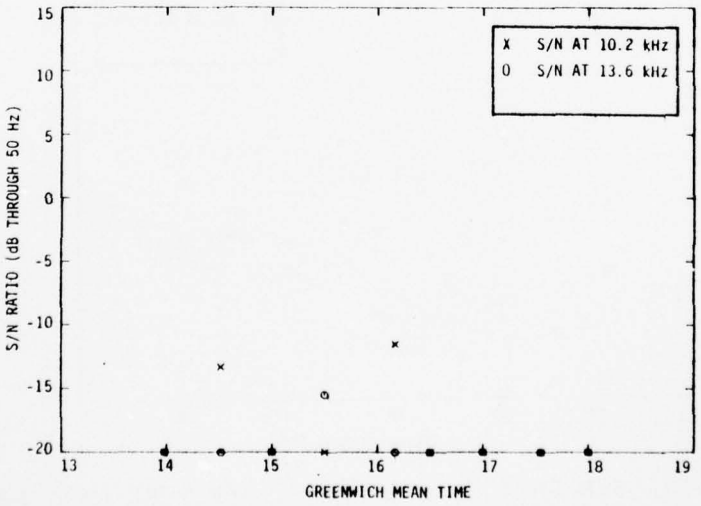

FIGURE B.156. S/N RATIOS, STATION E, NEW YORK-CARACAS, FLIGHT 217, AUGUST 12, 1976

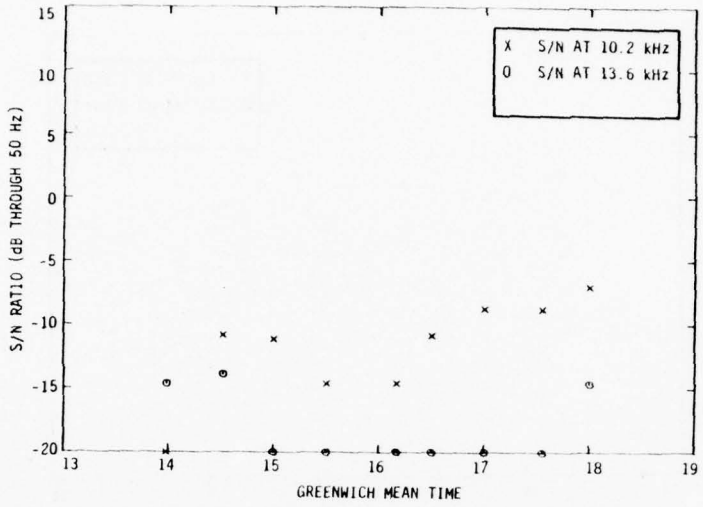

FIGURE B.157. S/N RATIOS, STATION F, NEW YORK-CARACAS, FLIGHT 217, AUGUST 12, 1976

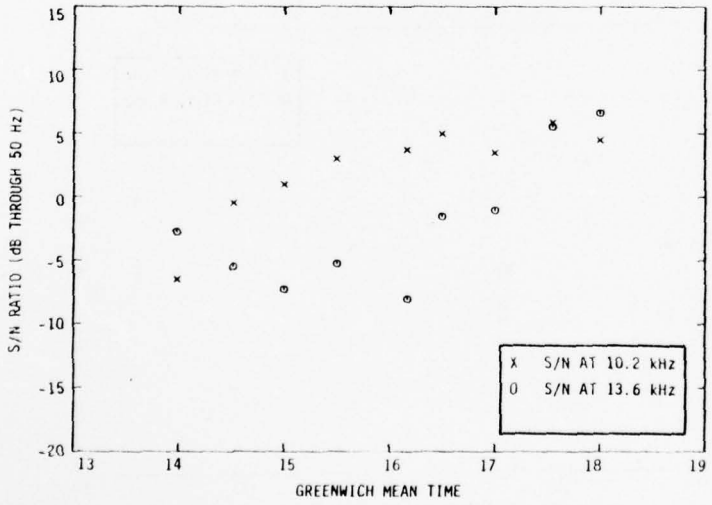

FIGURE B.158. S/N RATIOS, STATION G, NEW YORK-CARACAS, FLIGHT 217, AUGUST 12, 1976

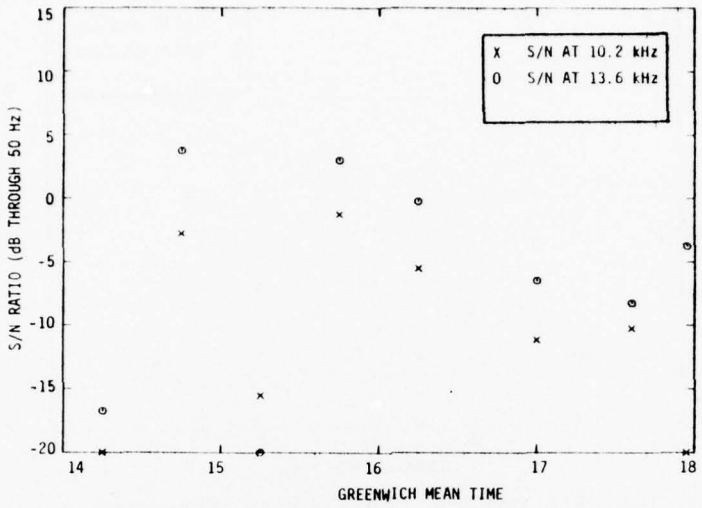

FIGURE B. 159. S/N RATIOS, STATION A, NEW YORK-CARACAS, FLIGHT 217, SEPT. 9, 1976

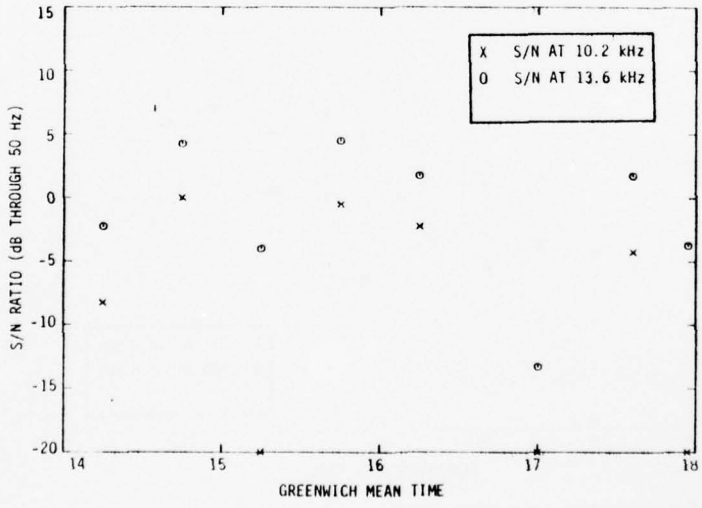

FIGURE B. 160. S/N RATIOS, STATION B, NEW YORK-CARACAS, FLIGHT 217, SEPT. 9, 1976

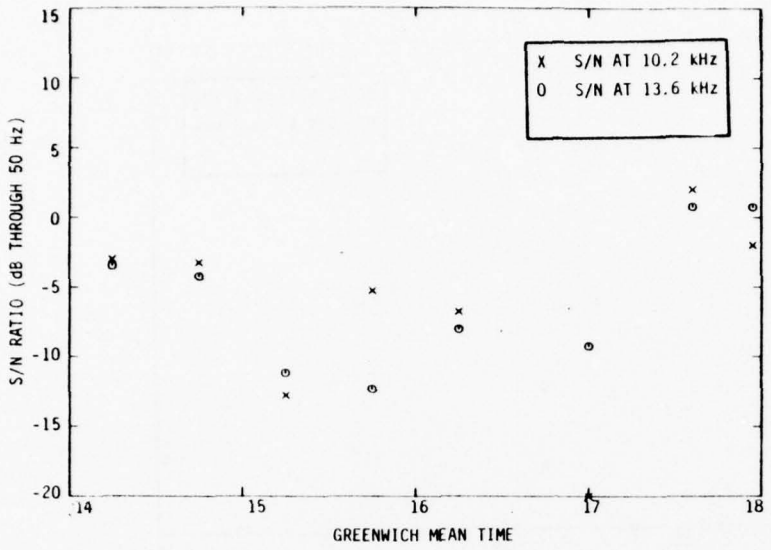

FIGURE B.161. S/N RATIOS, STATION C, NEW YORK-CARACAS, FLIGHT 217, SEPT. 9, 1976

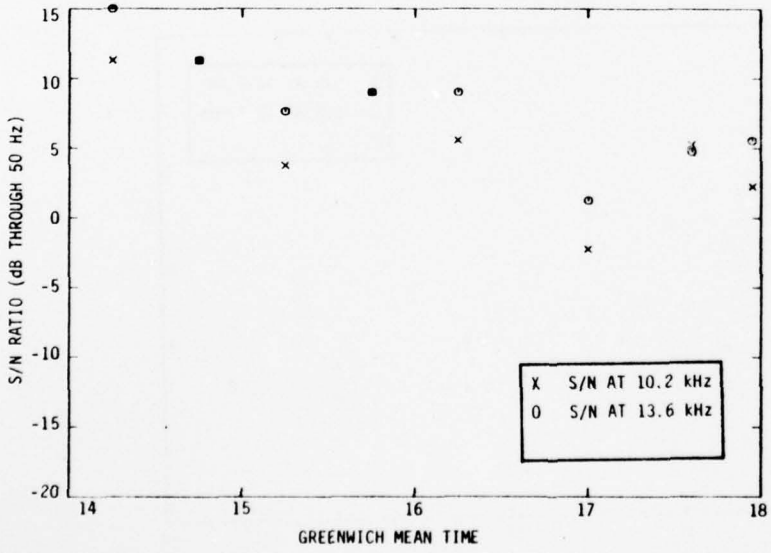

FIGURE B.162. S/N RATIOS, STATION D, NEW YORK-CARACAS, FLIGHT 217, SEPT. 9, 1976

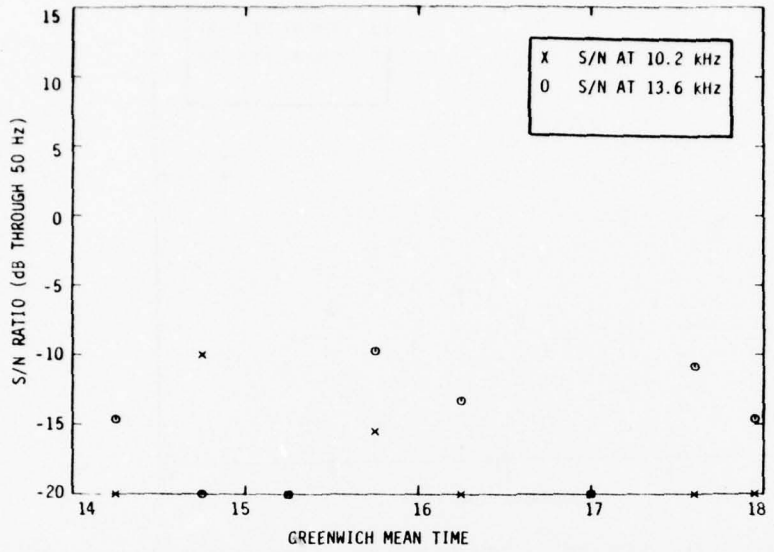

FIGURE B. 163. S/N RATIOS, STATION E, NEW YORK-CARACAS, FLIGHT 217, SEPT. 9, 1976

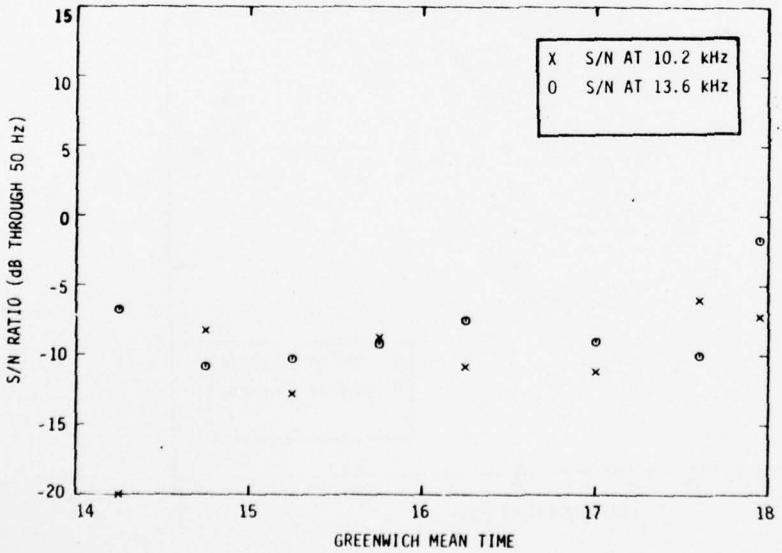

FIGURE B. 164. S/N RATIOS, STATION F, NEW YORK-CARACAS, FLIGHT 217, SEPT. 9, 1976

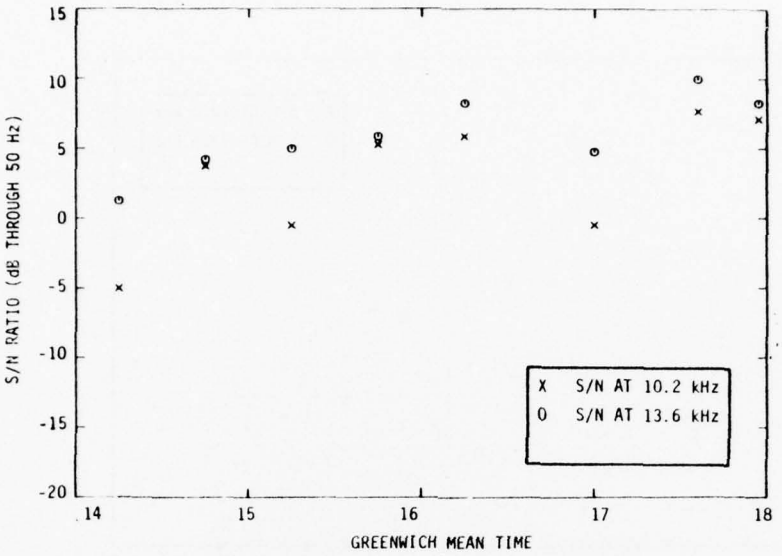

FIGURE B.165. S/N RATIOS, STATION G, NEW YORK-CARACAS, FLIGHT 217, SEPT. 9, 1976

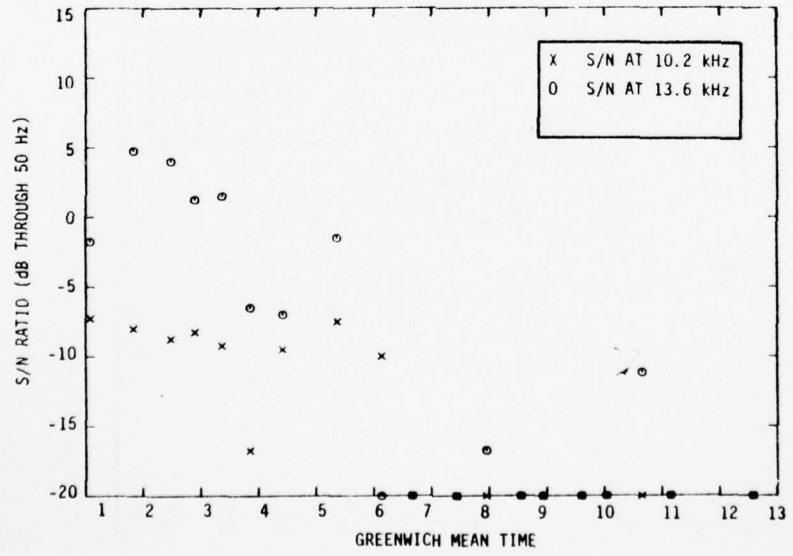

FIGURE B.166. S/N RATIOS, STATION A, NEW YORK-MONTEVIDEO, FLIGHT 203, JUNE 5, 1976

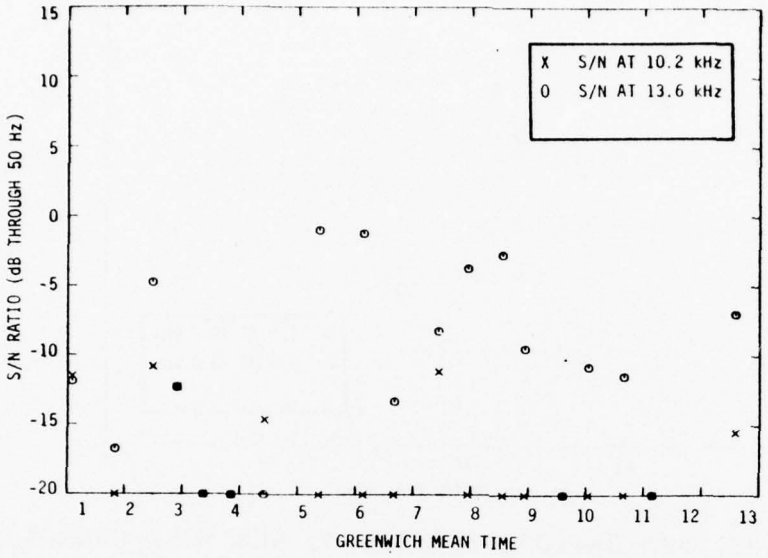

FIGURE B. 167. S/N RATIOS, STATION B, NEW YORK-MONTEVIDEO, FLIGHT 203, JUNE 5, 1976

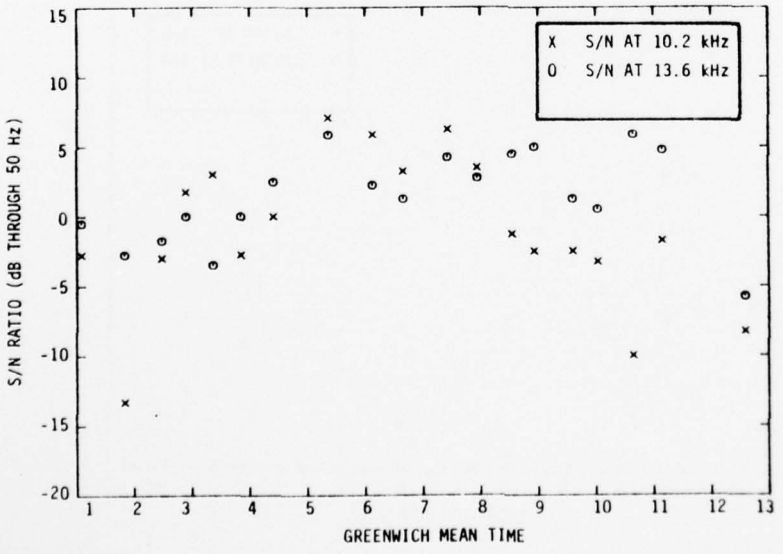

FIGURE B. 168. S/N RATIOS, STATION C, NEW YORK-MONTEVIDEO, FLIGHT 203, JUNE 5, 1976

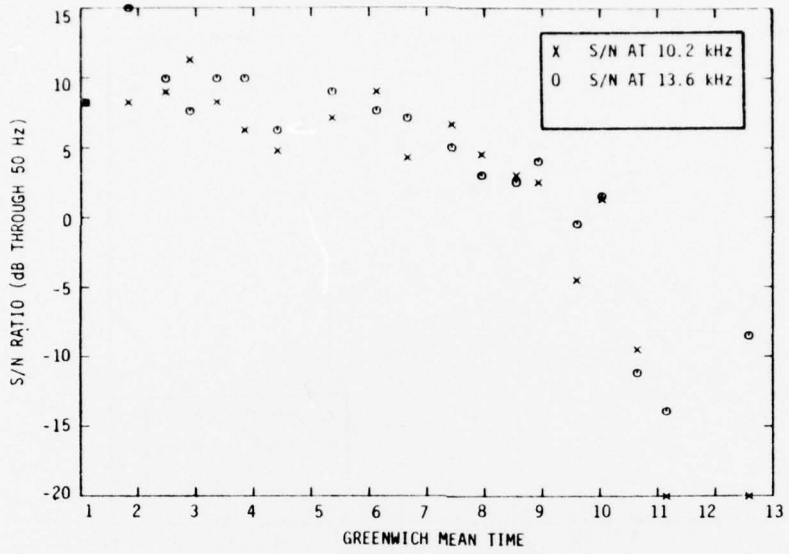

FIGURE B. 169. S/N RATIOS, STATION D, NEW YORK-MONTEVIDEO, FLIGHT 203, JUNE 5, 1976

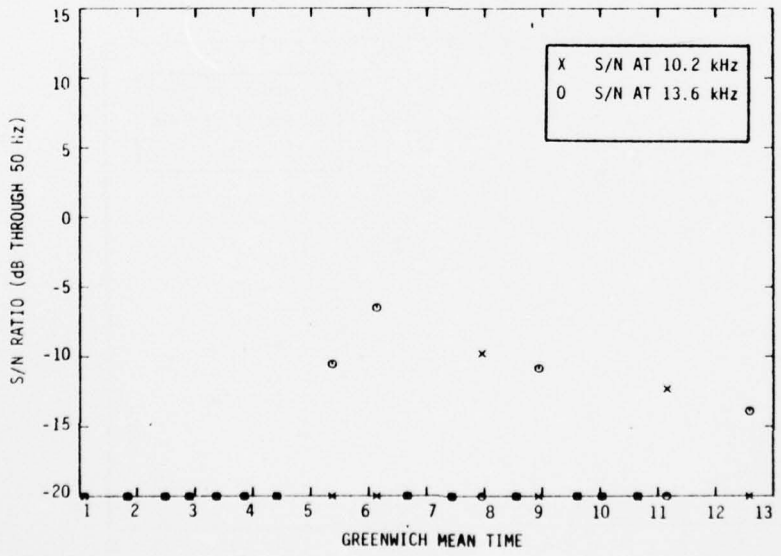

FIGURE B. 170. S/N RATIOS, STATION E, NEW YORK-MONTEVIDEO, FLIGHT 203, JUNE 5, 1976

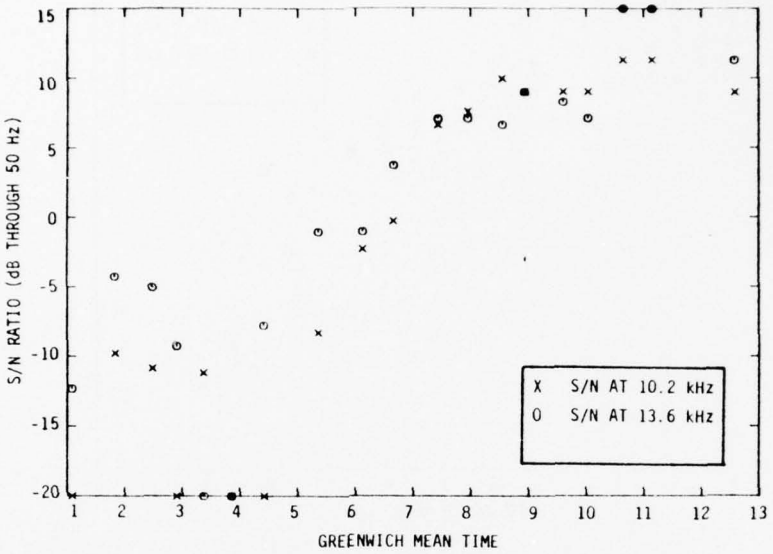

FIGURE B. 171. S/N RATIOS, STATION F, NEW YORK-MONTEVIDEO, FLIGHT 203, JUNE 5, 1976

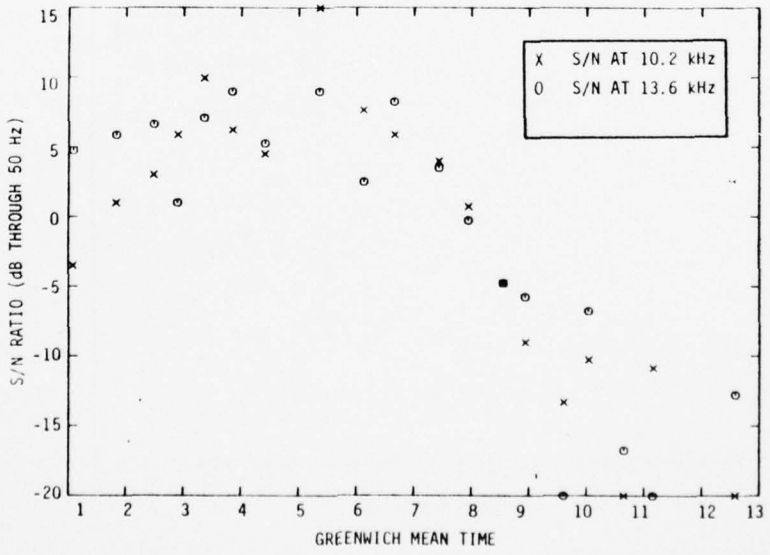

FIGURE B.172. S/N RATIOS, STATION G, NEW YORK-MONTEVIDEO, FLIGHT 203, JUNE 5, 1976

AD-A041 095 SYSTEMS CONTROL INC PALO ALTO CALIF F/G 17/7
AN OPERATIONAL EVALUATION OF OMEGA FOR CIVIL AVIATION OCEANIC N--ETC(U)
FEB 77 F KARKALIK, E WISCHMEYER DOT-FA75WA-3662
UNCLASSIFIED FAA-RD-77-65 NL

3 OF 3
AD
A041 095

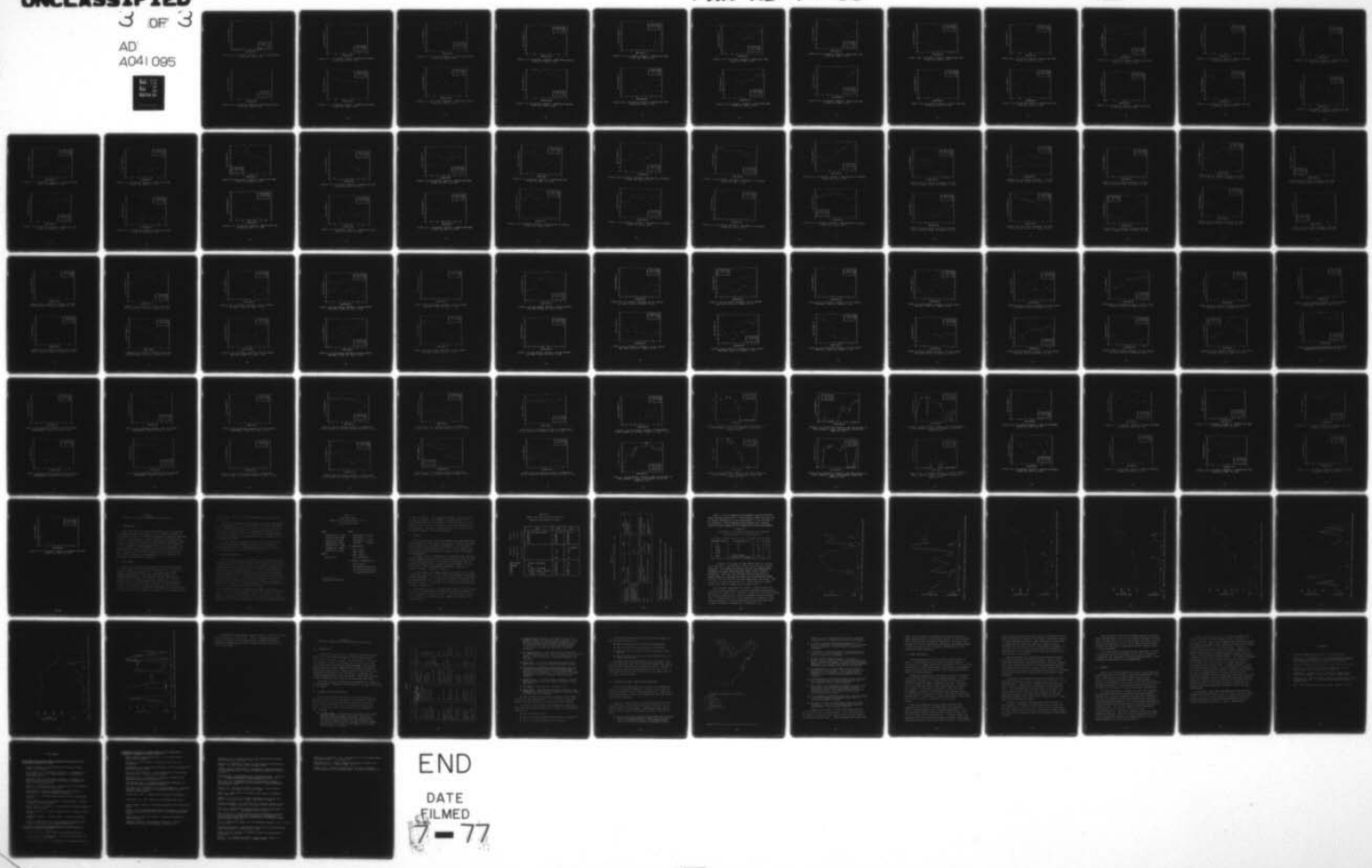

END

DATE
FILMED
7-77

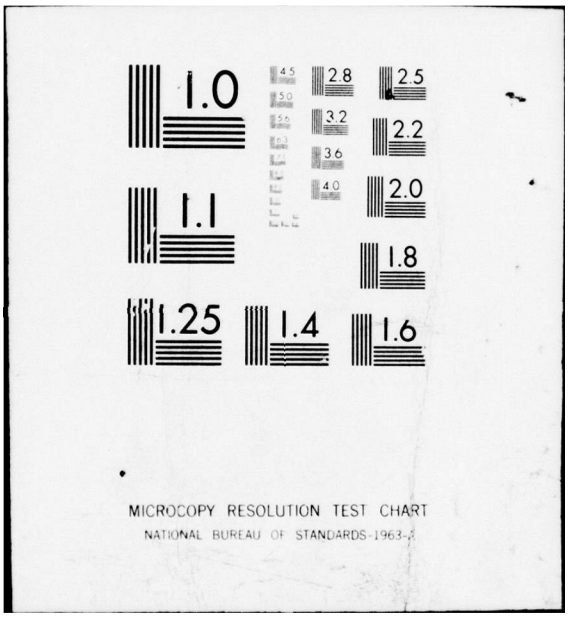
1.0
1.1
1.25
1.4
1.6
1.8
2.0
2.2
2.5
2.8
3.2
3.6
4.0
4.5
5.0
5.6
6.3
MICROCOPY RESOLUTION TEST CHART
NATIONAL BUREAU OF STANDARDS-1963-A

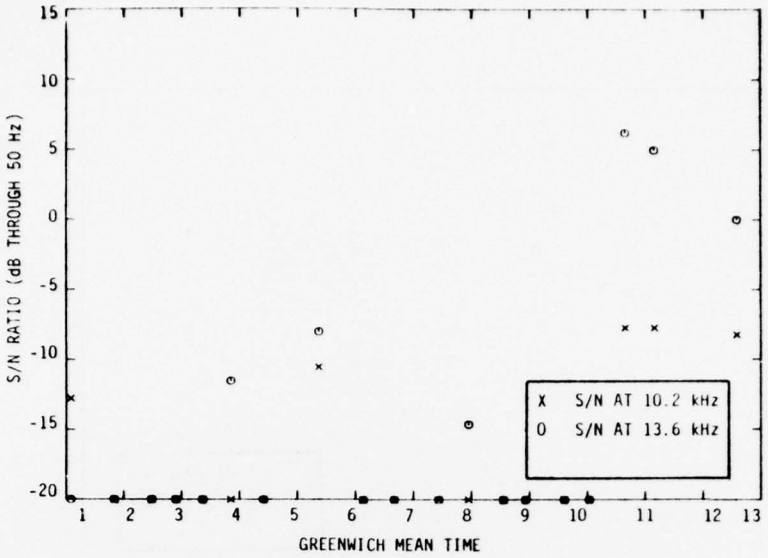

FIGURE B.173. S/N RATIOS, STATION H, NEW YORK-MONTEVIDEO, FLIGHT 203, JUNE 5, 1976

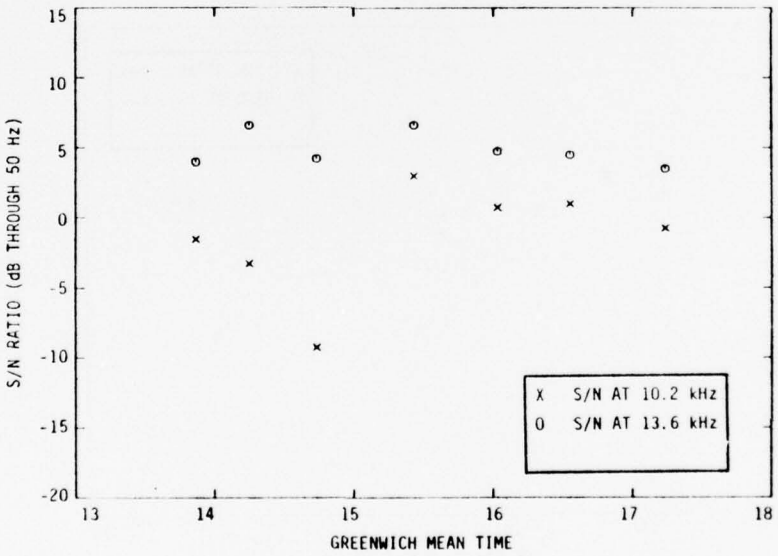

FIGURE B.174. S/N RATIOS, STATION A, MONTEVIDEO-CARACAS, FLIGHT 218, JUNE 6, 1976

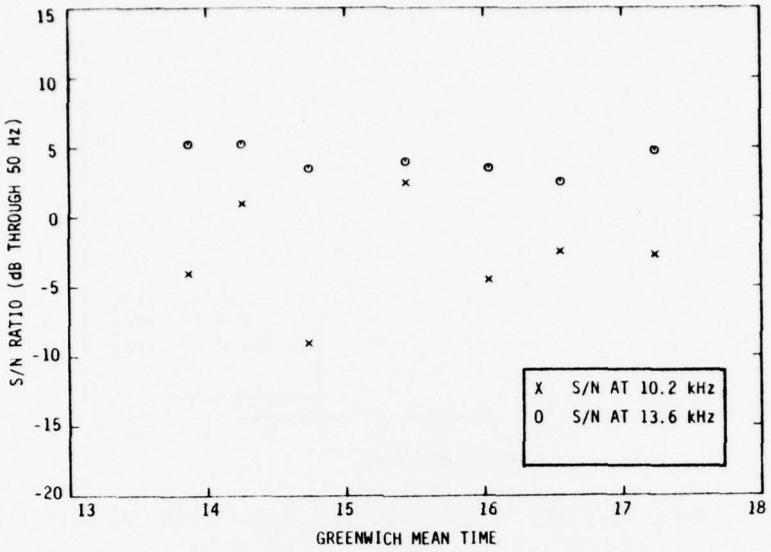

FIGURE B.175. S/N RATIOS, STATION B, MONTEVIDEO-CARACAS, FLIGHT 218, JUNE 6, 1976

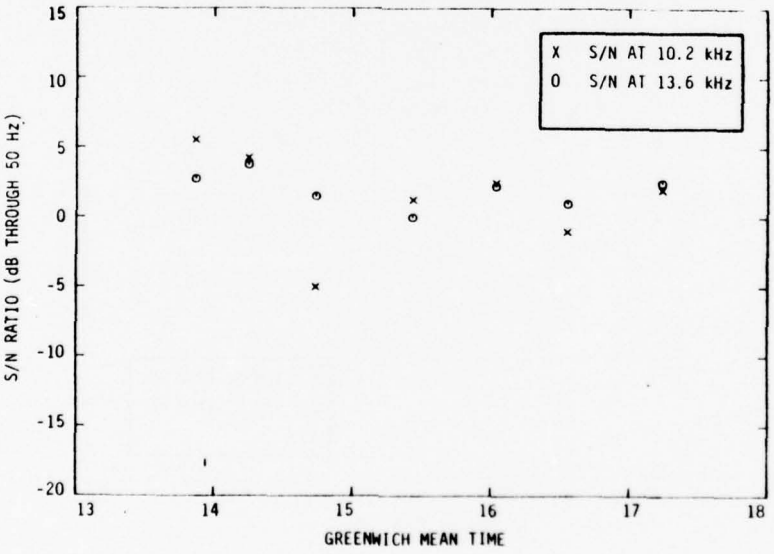

FIGURE B. 176. S/N RATIOS, STATION C, MONTEVIDEO-CARACAS, FLIGHT 218, JUNE 6, 1976

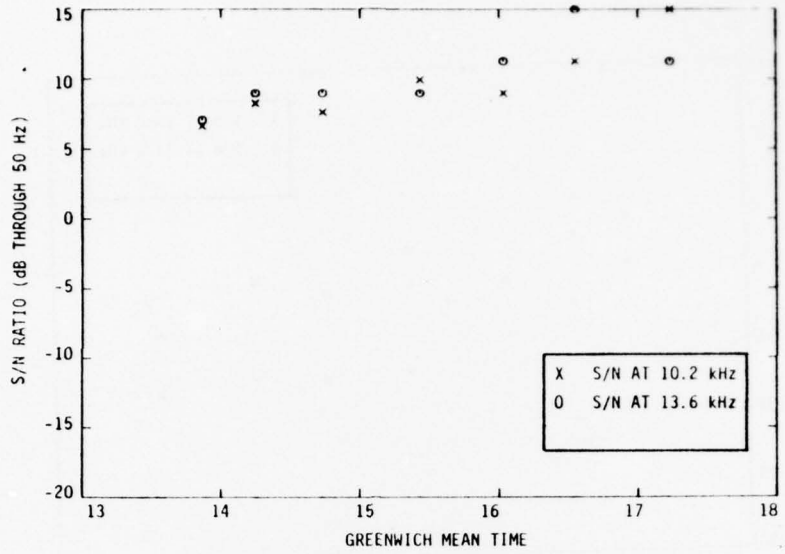

FIGURE B.177. S/N RATIOS, STATION D, MONTEVIDEO-CARACAS, FLIGHT 218, JUNE 6, 1976

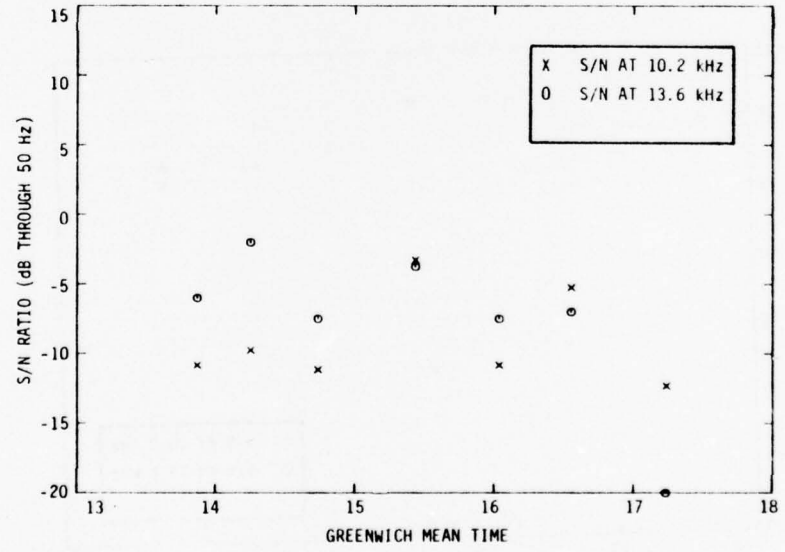

FIGURE B.178. S/N RATIOS, STATION E, MONTEVIDEO-CARACAS, FLIGHT 218, JUNE 6, 1976

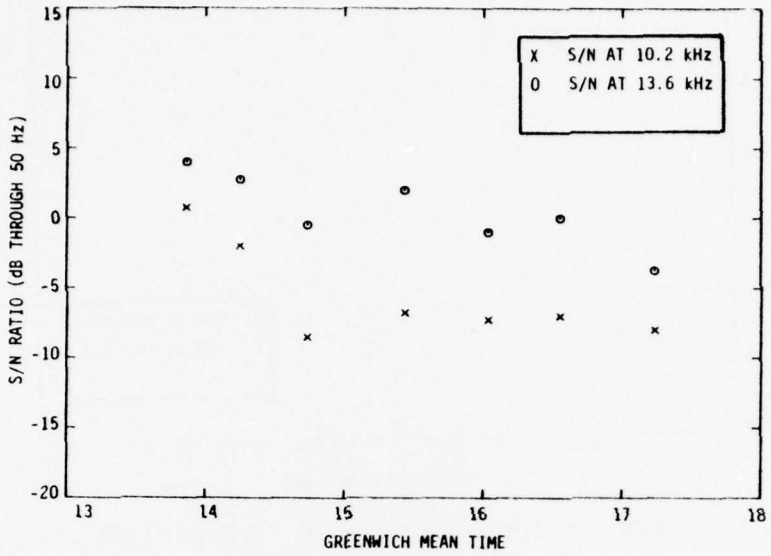

FIGURE B.179. S/N RATIOS, STATION F, MONTEVIDEO-CARACAS, FLIGHT 218, JUNE 6, 1976

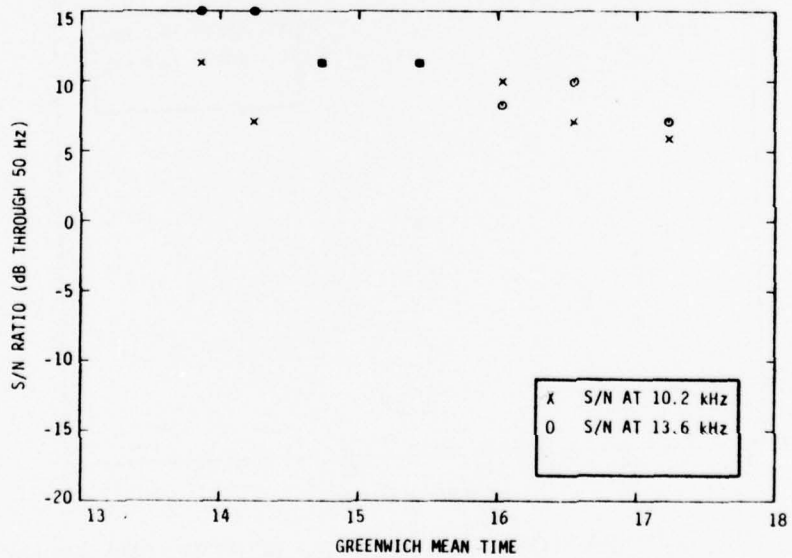

FIGURE B.180. S/N RATIOS, STATION G, MONTEVIDEO-CARACAS, FLIGHT 218, JUNE 6, 1976

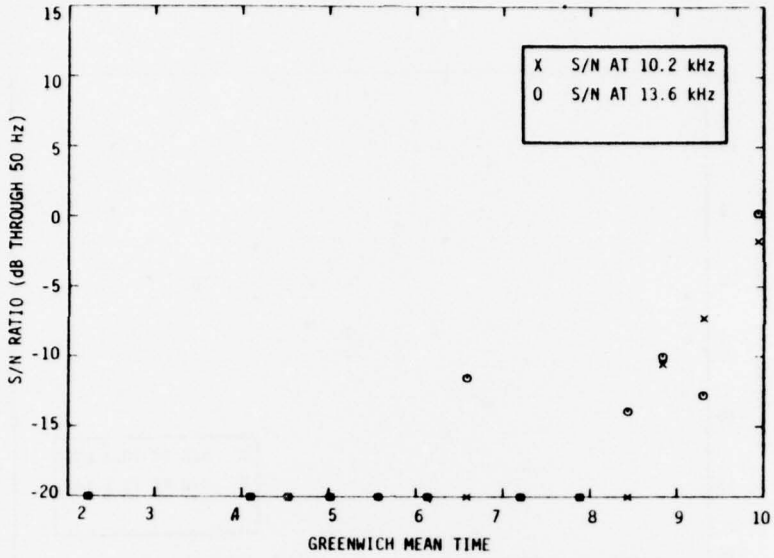

FIGURE B.181. S/N RATIOS, STATION A, CARACAS-NEW YORK, FLIGHT 218, JUNE 6, 1976

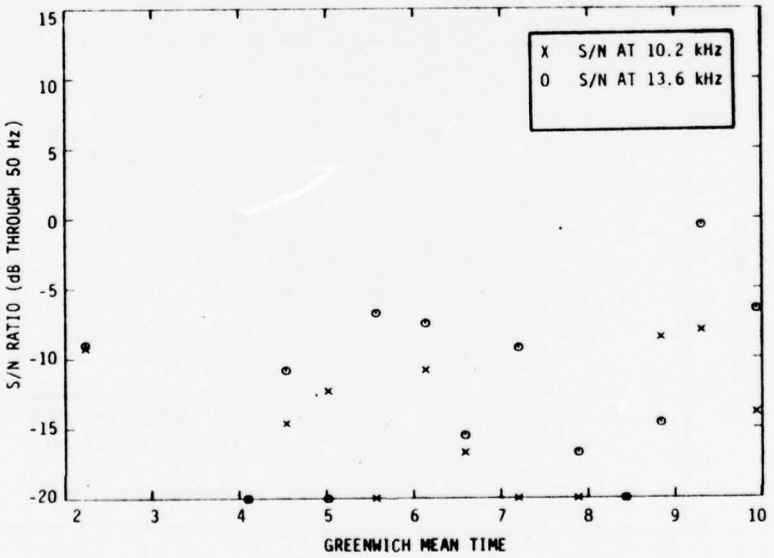

FIGURE B.182. S/N RATIOS, STATION B, CARACAS-NEW YORK, FLIGHT 218, JUNE 6, 1976

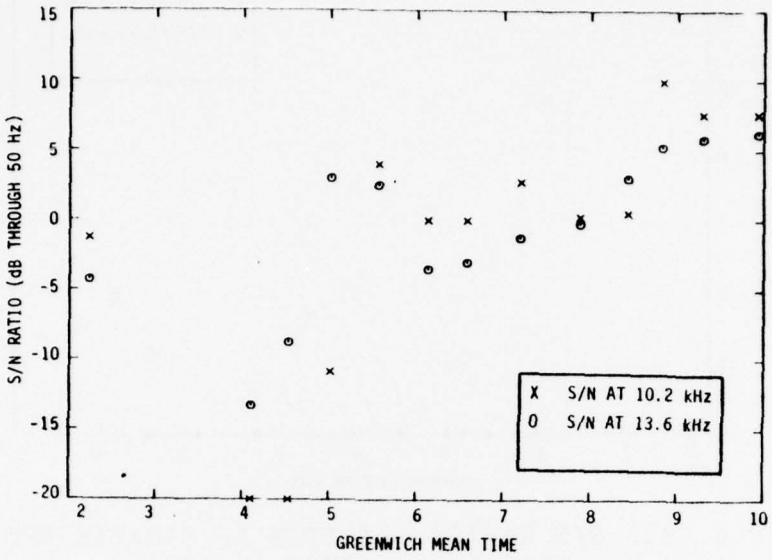

FIGURE B.183. S/N RATIOS, STATION C, CARACAS-NEW YORK, FLIGHT 218, JUNE 6, 1976

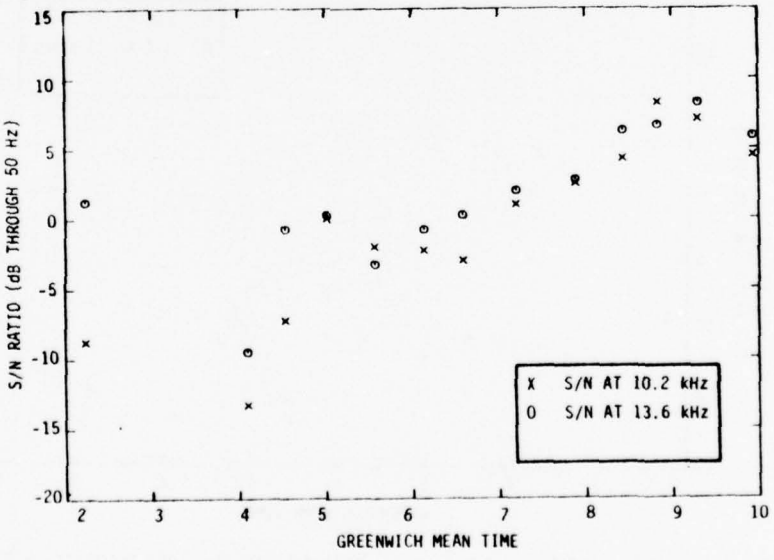

FIGURE B. 184. S/N RATIOS, STATION D, CARACAS-NEW YORK, FLIGHT 218, JUNE 6, 1976

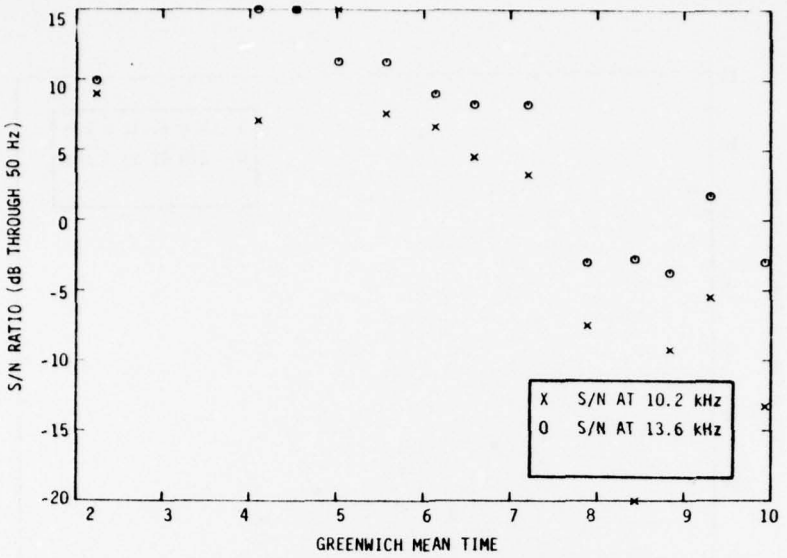

FIGURE B.185. S/N RATIOS, STATION F, CARACAS-NEW YORK, FLIGHT 218, JUNE 6, 1976

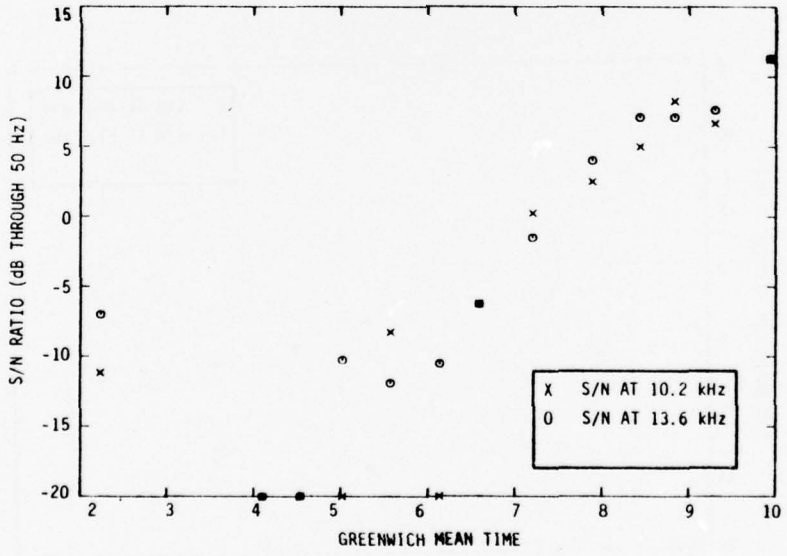

FIGURE B. 186. S/N RATIOS, STATION G, CARACAS-NEW YORK, FLIGHT 218, JUNE 6, 1976

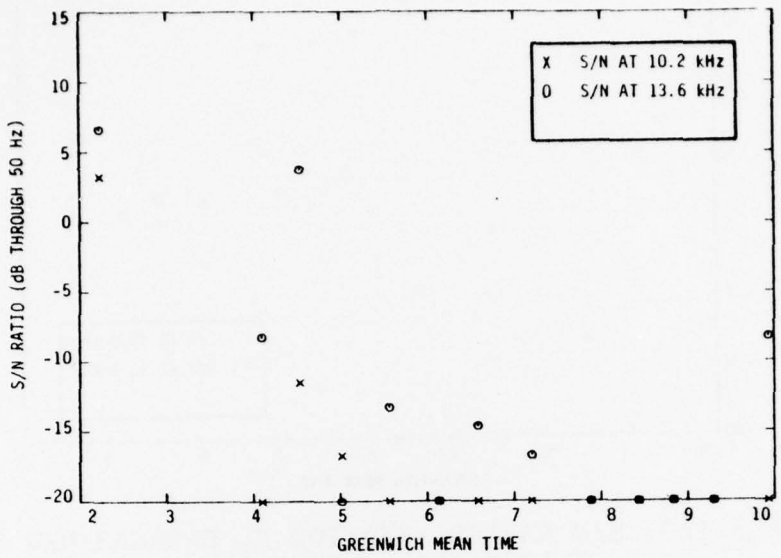

FIGURE B.187. S/N RATIOS, STATION H, CARACAS-NEW YORK, FLIGHT 218, JUNE 6, 1976

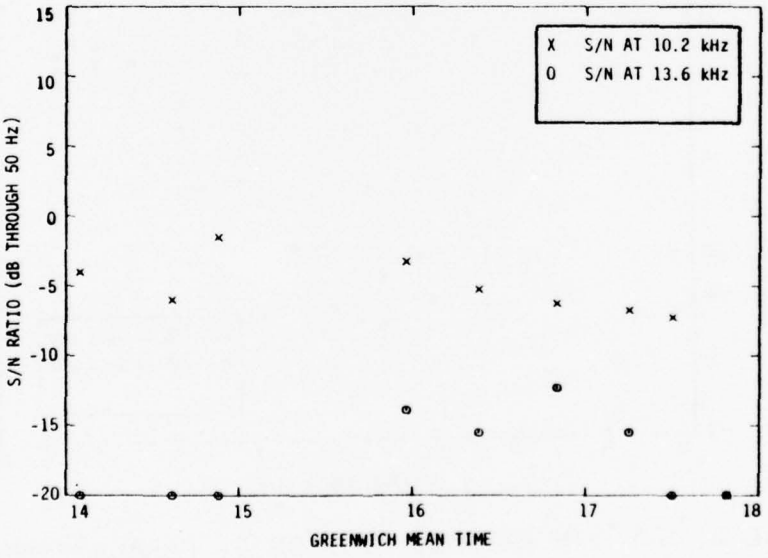

FIGURE B. 188. S/N RATIOS, STATION A, CARACAS-NEW YORK, FLIGHT 218, JULY 23, 1976

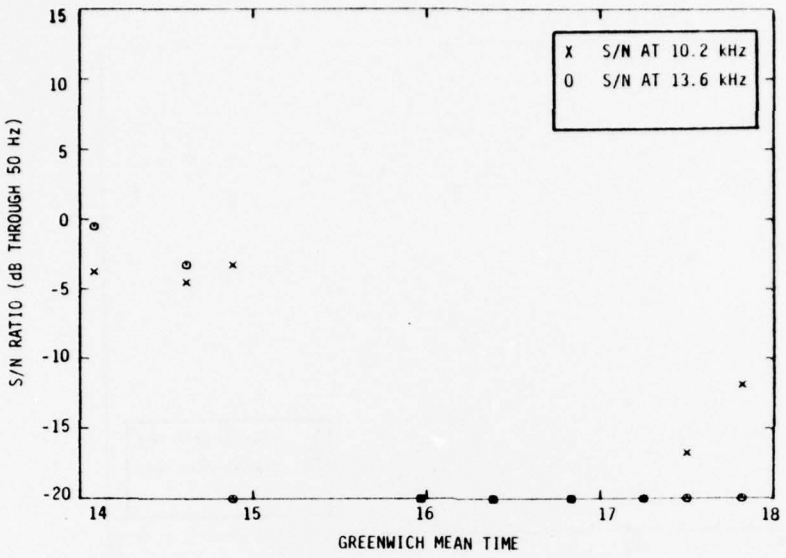

FIGURE B.189. S/N RATIOS, STATION B, CARACAS-NEW YORK, FLIGHT 218, JULY 23, 1976

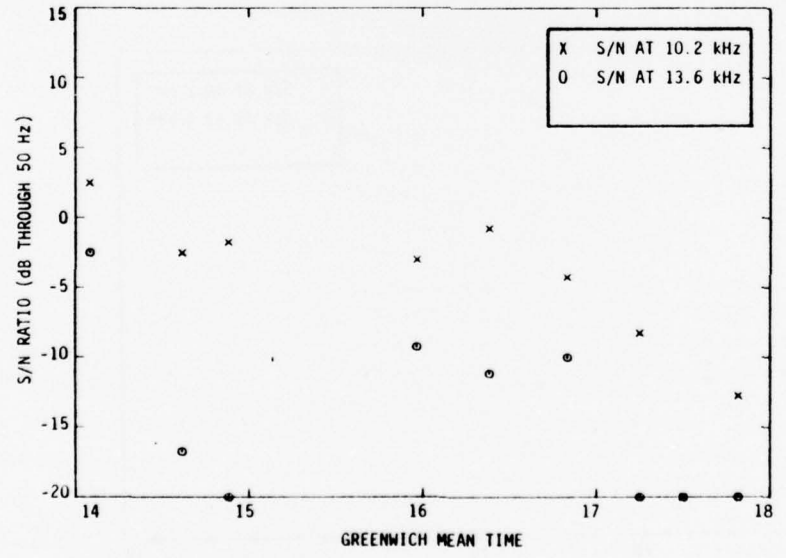

FIGURE B.190. S/N RATIOS, STATION C, CARACAS-NEW YORK, FLIGHT 218, JULY 23, 1976

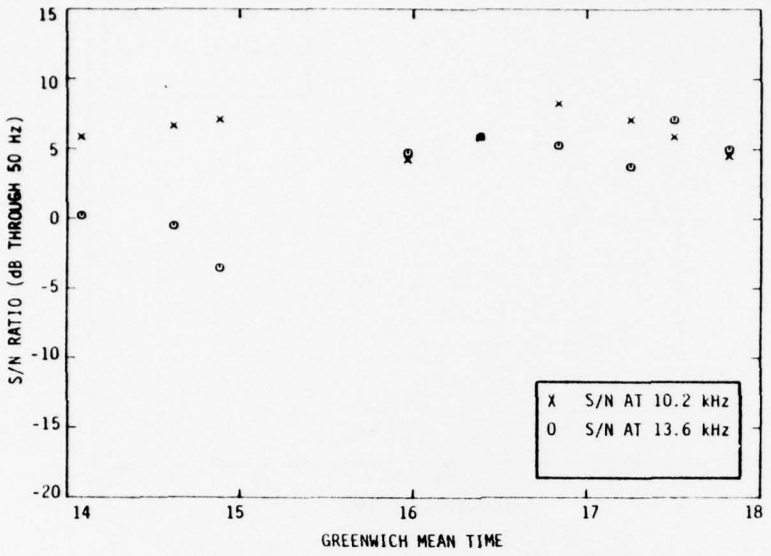

FIGURE B.191. S/N RATIOS, STATION D, CARACAS-NEW YORK, FLIGHT 218, JULY 23, 1976

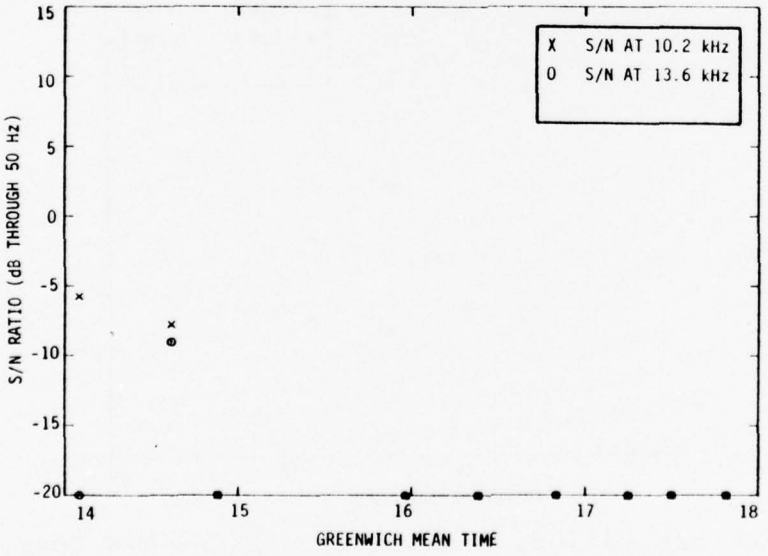

FIGURE B.192. S/N RATIOS, STATION E, CARACAS-NEW YORK, FLIGHT 218, JULY 23, 1976

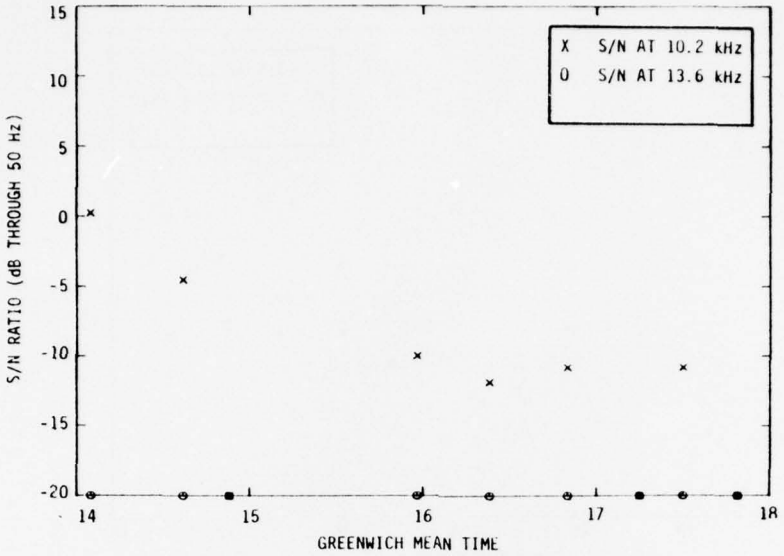

FIGURE B. 193. S/N RATIOS, STATION F, CARACAS-NEW YORK, FLIGHT 218, JULY 23, 1976

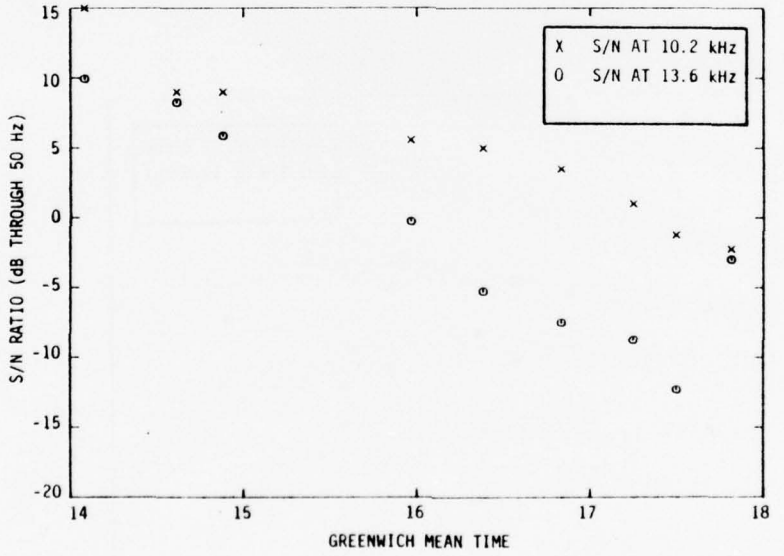

FIGURE B. 194. S/N RATIOS, STATION G, CARACAS-NEW YORK, FLIGHT 218, JULY 23, 1976

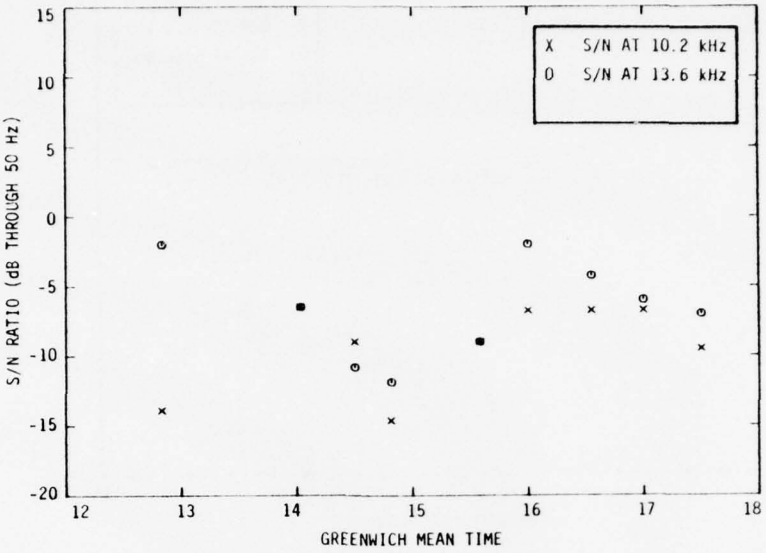

FIGURE B. 195. S/N RATIOS, STATION A, CARACAS-NEW YORK, FLIGHT 218, AUGUST 13, 1976

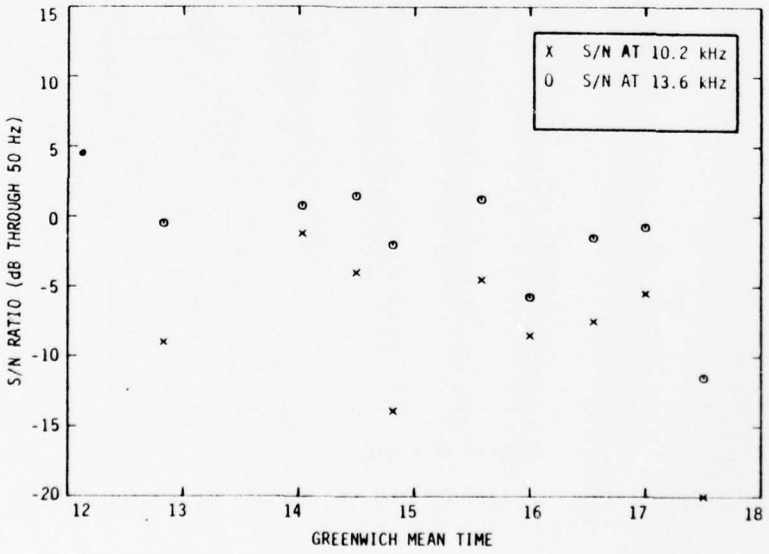

FIGURE B. 196. S/N RATIOS, STATION B, CARACAS-NEW YORK, FLIGHT 218, AUGUST 13, 1976

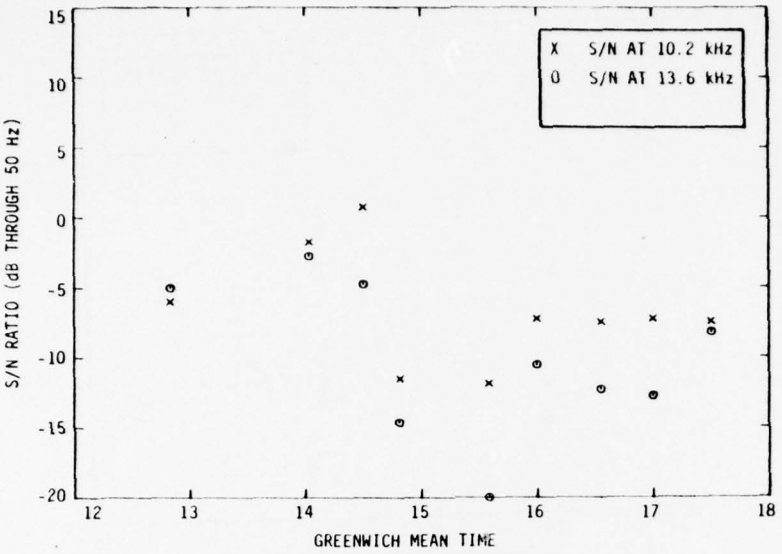

FIGURE B. 197. S/N RATIOS, STATION C, CARACAS-NEW YORK, FLIGHT 218, AUGUST 13, 1976

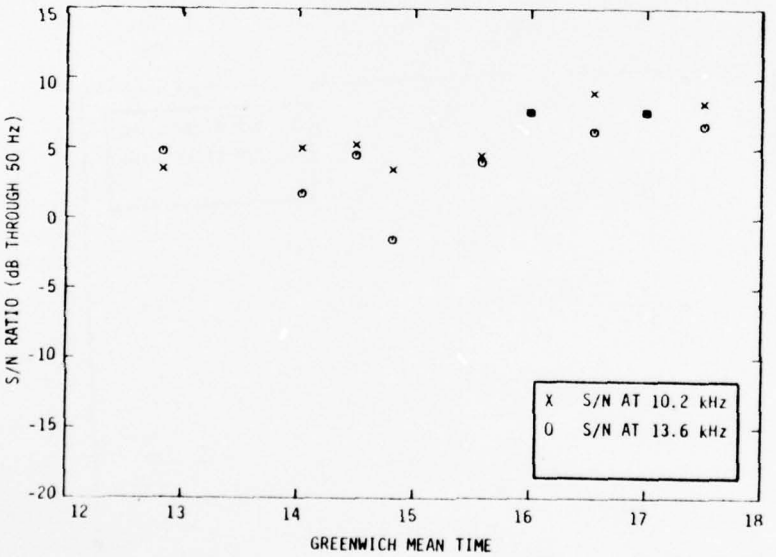

FIGURE B. 198. S/N RATIOS, STATION D, CARACAS-NEW YORK, FLIGHT 218, AUGUST 13, 1976

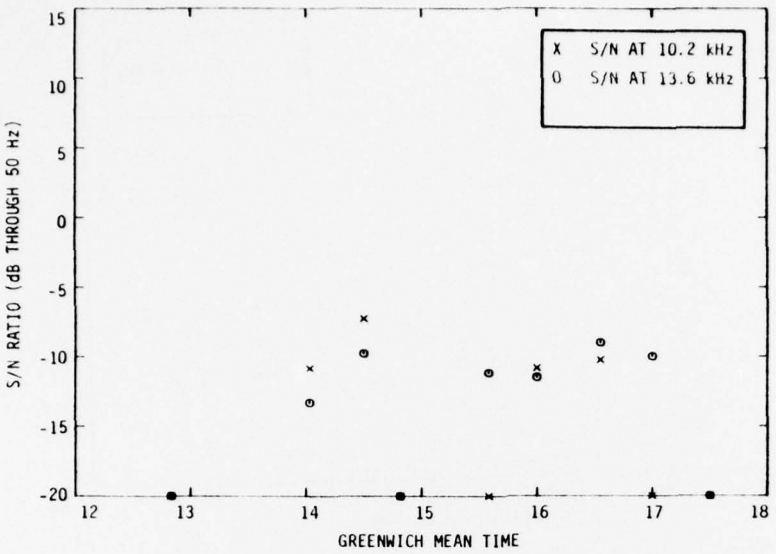

FIGURE B.199. S/N RATIOS, STATION E, CARACAS-NEW YORK, FLIGHT 218, AUGUST 13, 1976

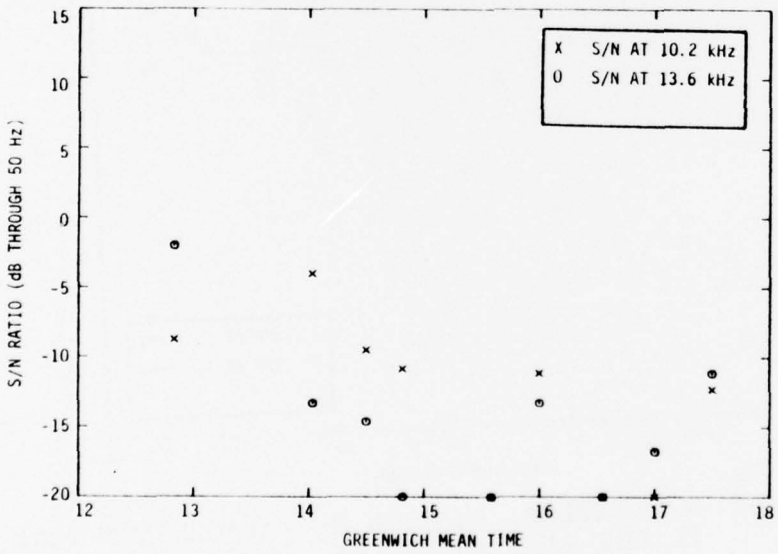

FIGURE B.200. S/N RATIOS, STATION F, CARACAS-NEW YORK, FLIGHT 218, AUGUST 13, 1976

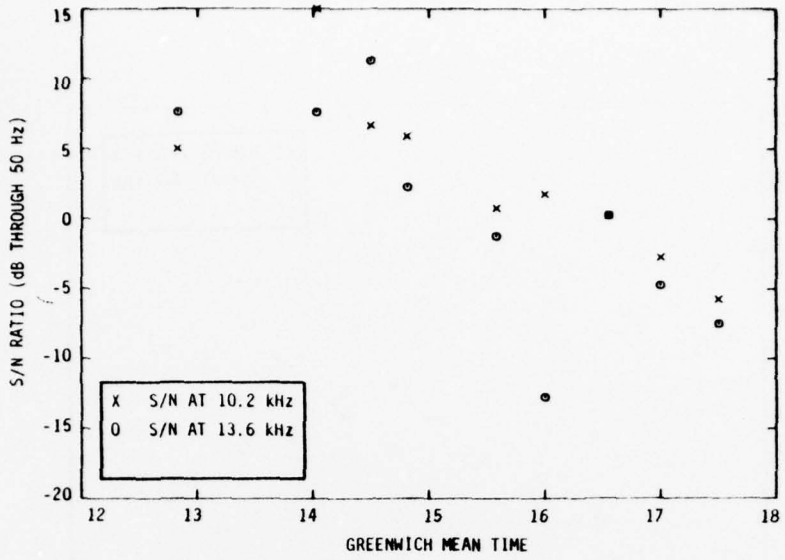

FIGURE B.201. S/N RATIOS, STATION G, CARACAS-NEW YORK, FLIGHT 218, AUGUST 13, 1976

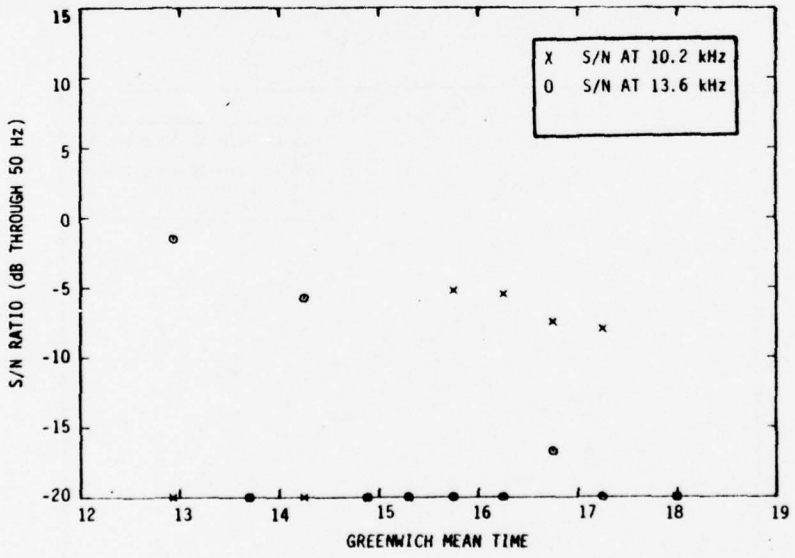

FIGURE B.202. S/N RATIOS, STATION A, CARACAS-NEW YORK, FLIGHT 218, SEPT. 10, 1976

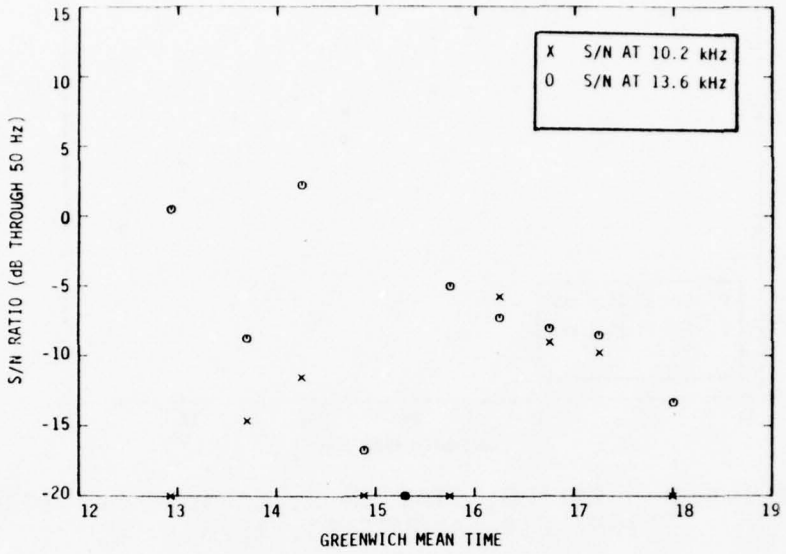

FIGURE B. 203. S/N RATIOS, STATION B, CARACAS-NEW YORK, FLIGHT 218, SEPT. 10, 1976

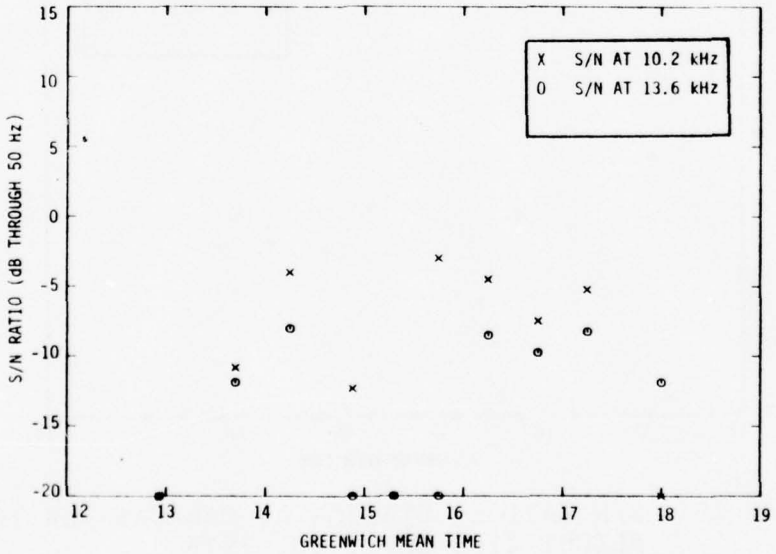

FIGURE B. 204. S/N RATIOS, STATION C, CARACAS-NEW YORK, FLIGHT 218, SEPT. 10, 1976

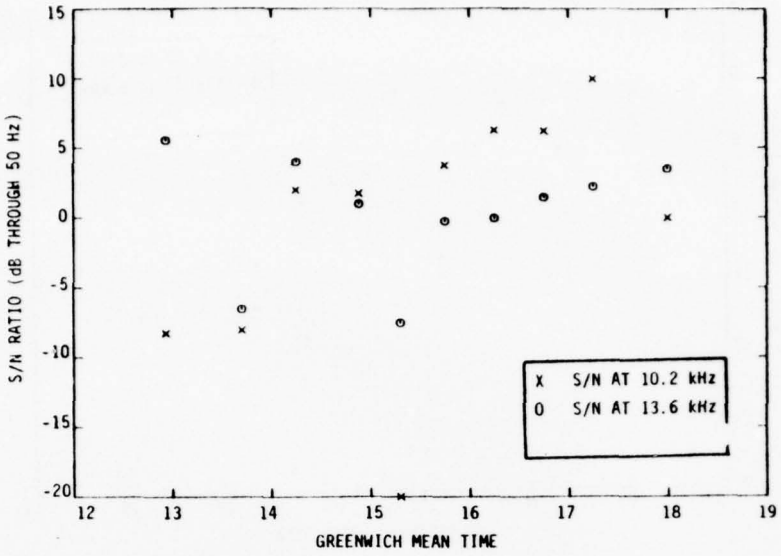

FIGURE B. 205. S/N RATIOS, STATION D, CARACAS-NEW YORK, FLIGHT 218, SEPT. 10, 1976

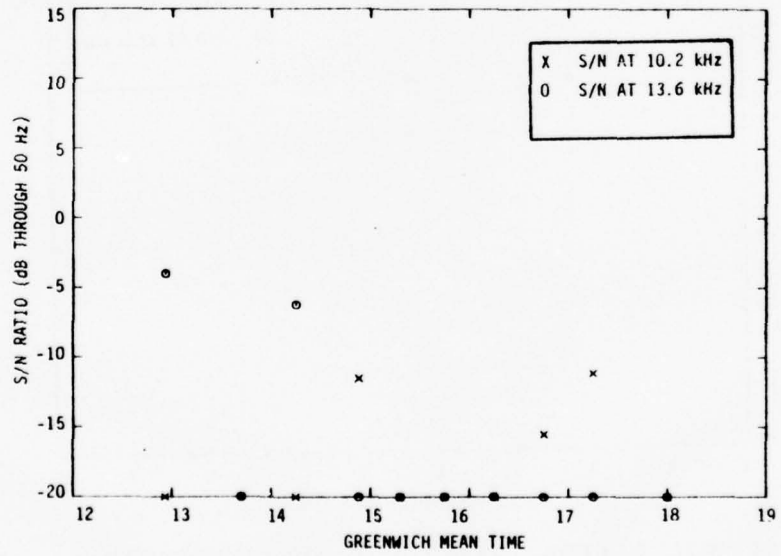

FIGURE B.206. S/N RATIOS, STATION F, CARACAS-NEW YORK, FLIGHT 218, SEPT. 10, 1976

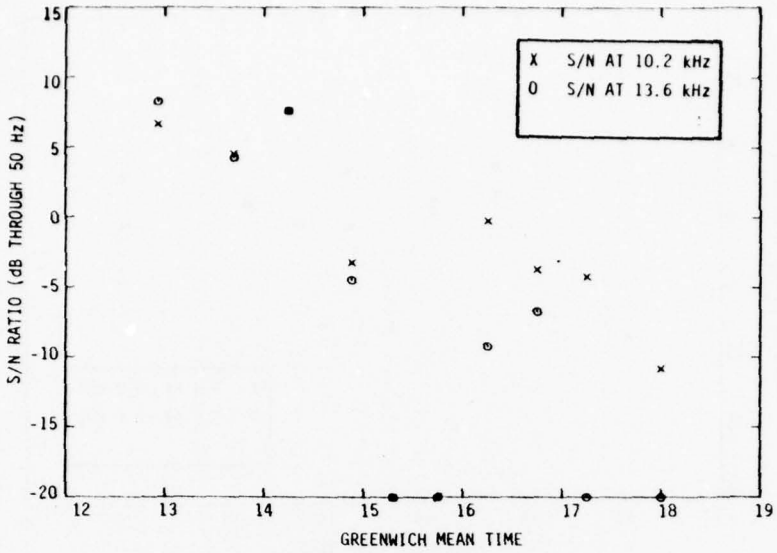

FIGURE B. 207. S/N RATIOS, STATION G, CARACAS-NEW YORK, FLIGHT 218, SEPT. 10, 1976

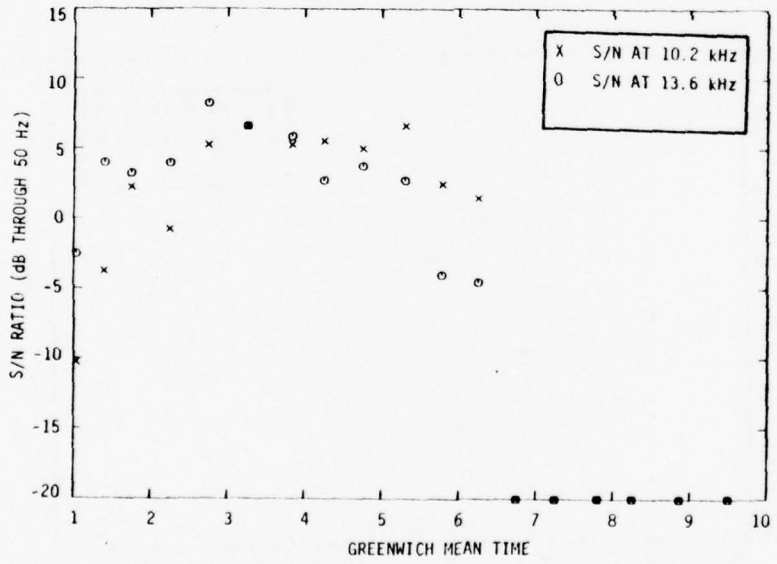

FIGURE B. 208. S/N RATIOS, STATION A, NEW YORK-RIO DE JANEIRO, FLIGHT 201, JULY 6, 1976

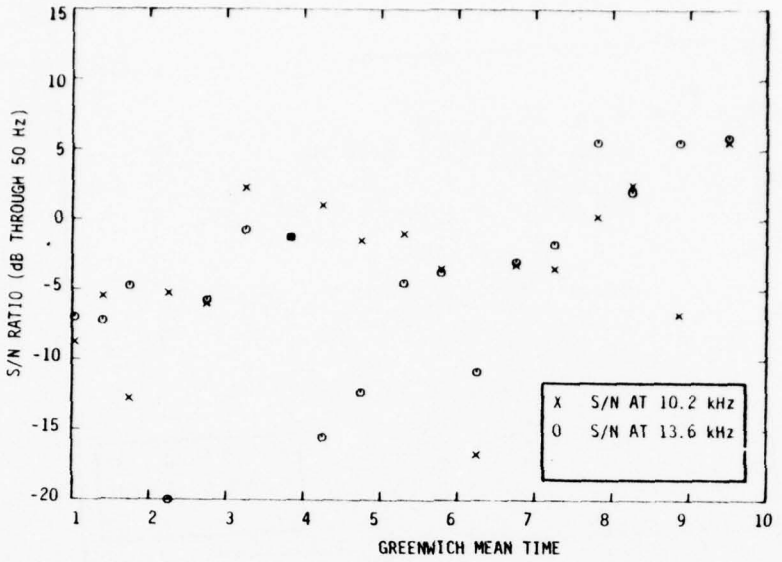

FIGURE B. 209. S/N RATIOS, STATION B, NEW YORK-RIO DE JANEIRO, FLIGHT 201, JULY 6, 1976

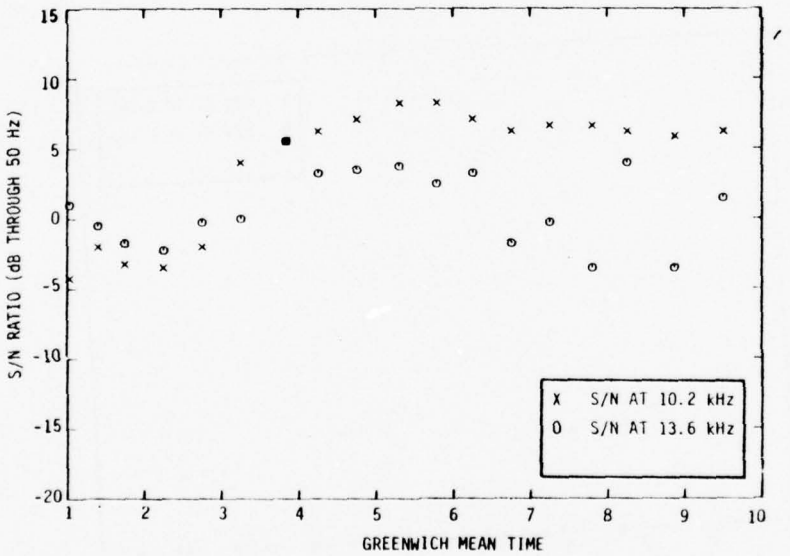

FIGURE B. 210. S/N RATIOS, STATION C, NEW YORK-RIO DE JANEIRO, FLIGHT 201, JULY 6, 1976

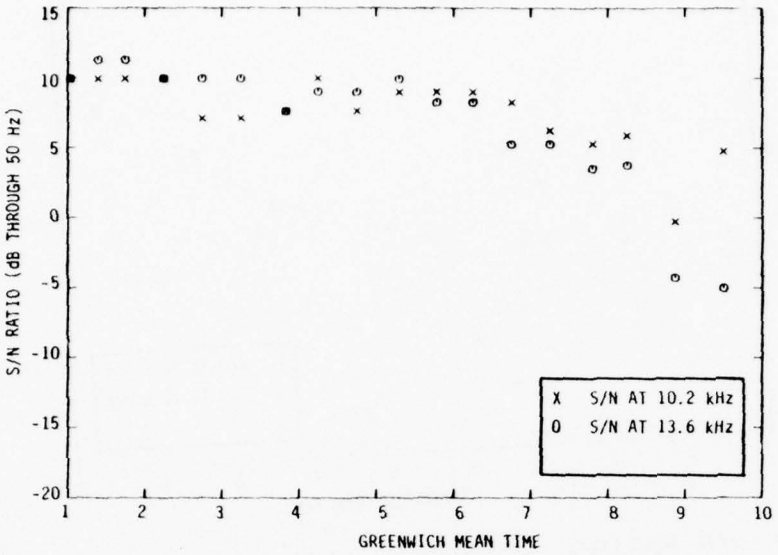

FIGURE B. 211. S/N RATIOS, STATION D, NEW YORK-RIO DE JANEIRO, FLIGHT 201, JULY 6, 1976

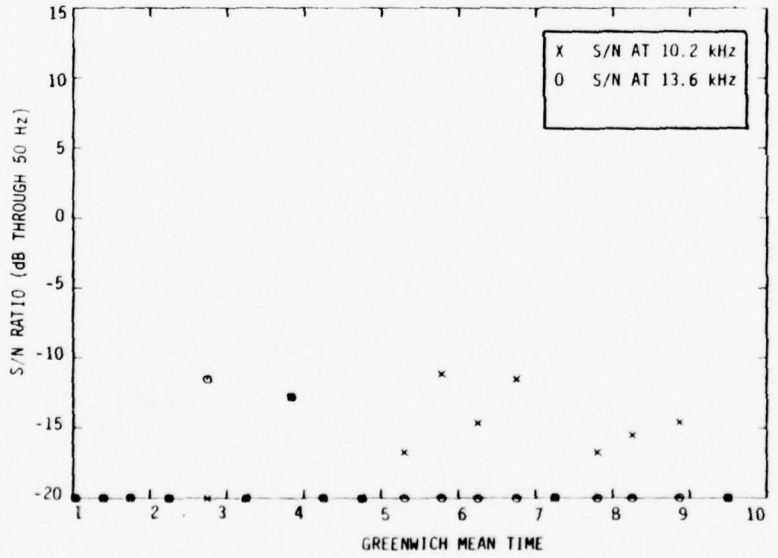

FIGURE B.212. S/N RATIOS, STATION E, NEW YORK-RIO DE JANEIRO, FLIGHT 201, JULY 6, 1976

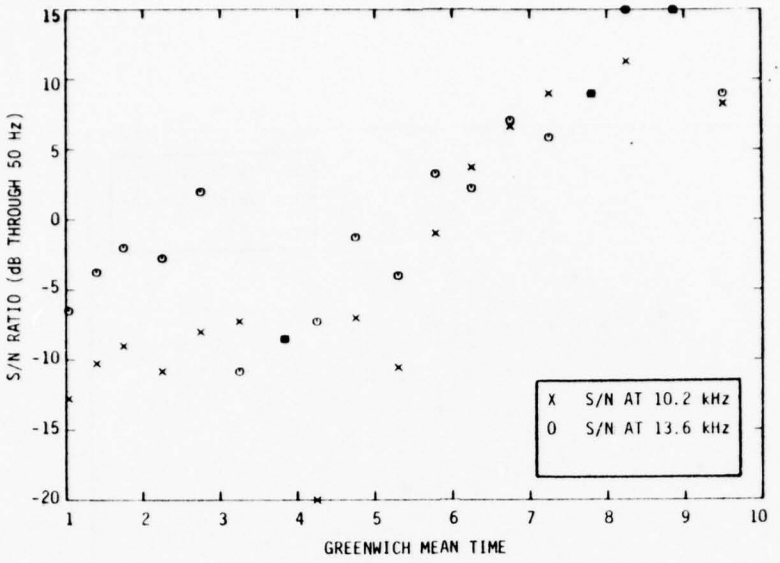

FIGURE B.213. S/N RATIOS, STATION F, NEW YORK-RIO DE JANEIRO, FLIGHT 201, JULY 6, 1976

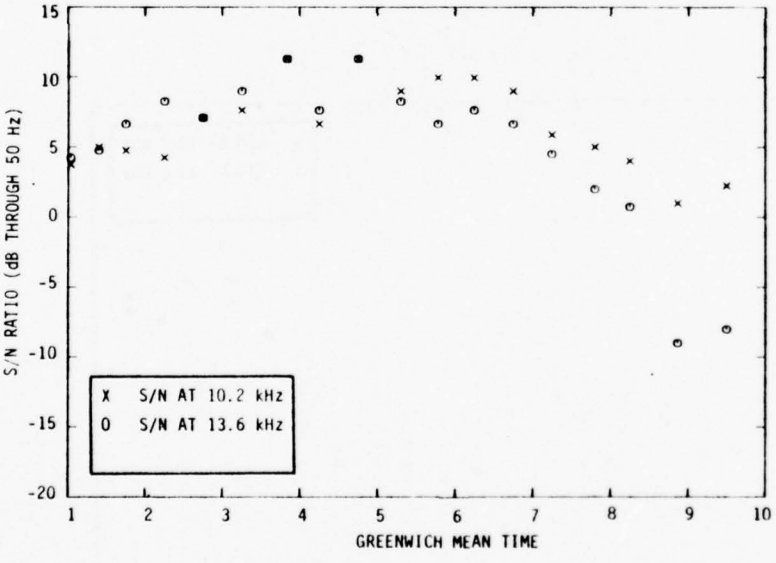

FIGURE B.214. S/N RATIOS, STATION G, NEW YORK-RIO DE JANEIRO, FLIGHT 201, JULY 6, 1976

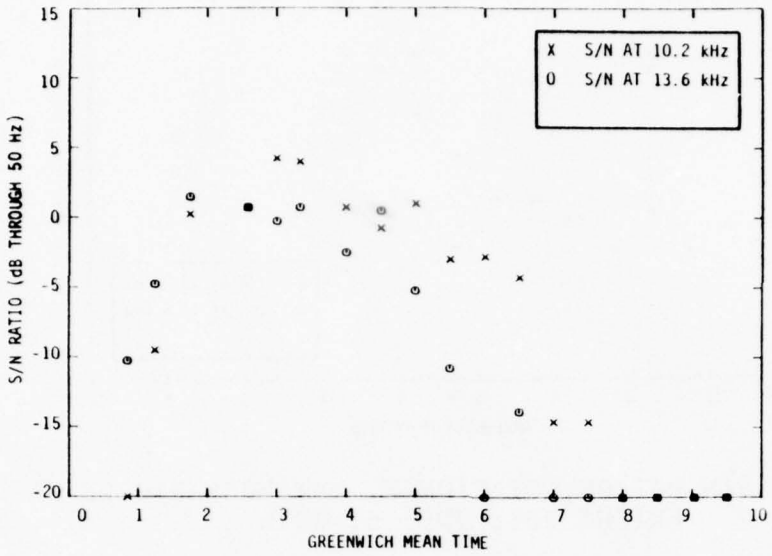

FIGURE B.215. S/N RATIOS, STATION A, NEW YORK-RIO DE JANEIRO, FLIGHT 201, AUGUST 2, 1976

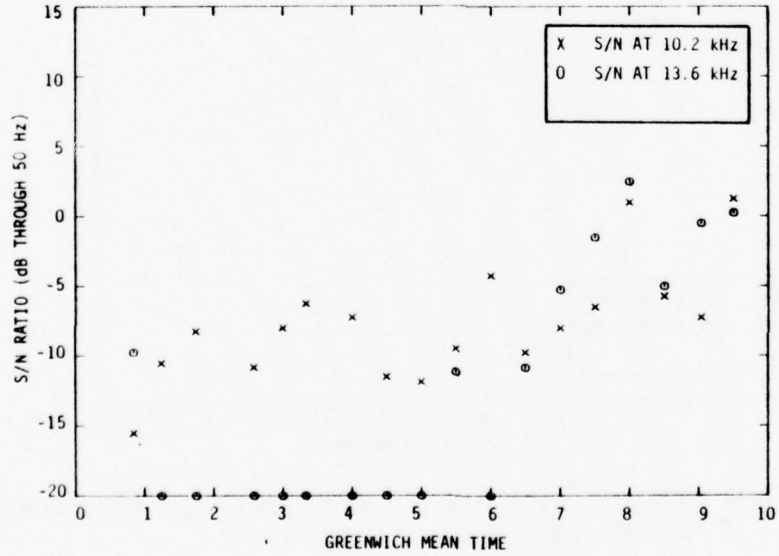

FIGURE B.216. S/N RATIOS, STATION B, NEW YORK-RIO DE JANEIRO, FLIGHT 201, AUGUST 2, 1976

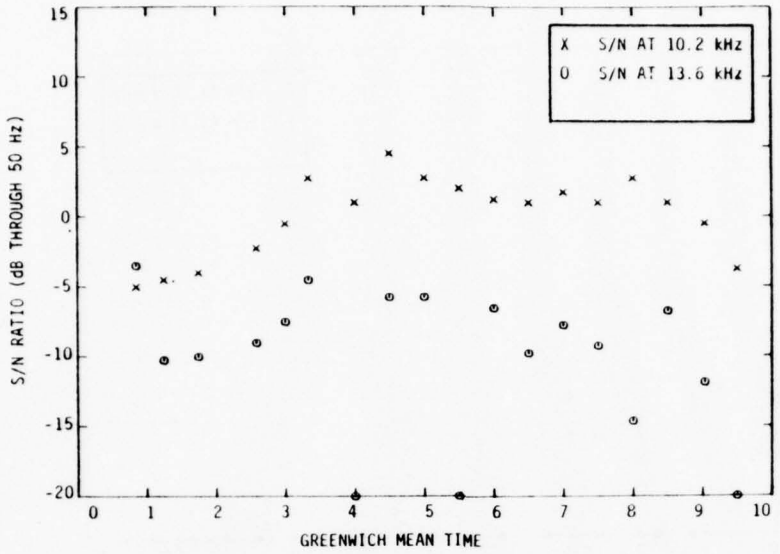

FIGURE B. 217. S/N RATIOS, STATION C, NEW YORK-RIO DE JANEIRO, FLIGHT 201, AUGUST 2, 1976

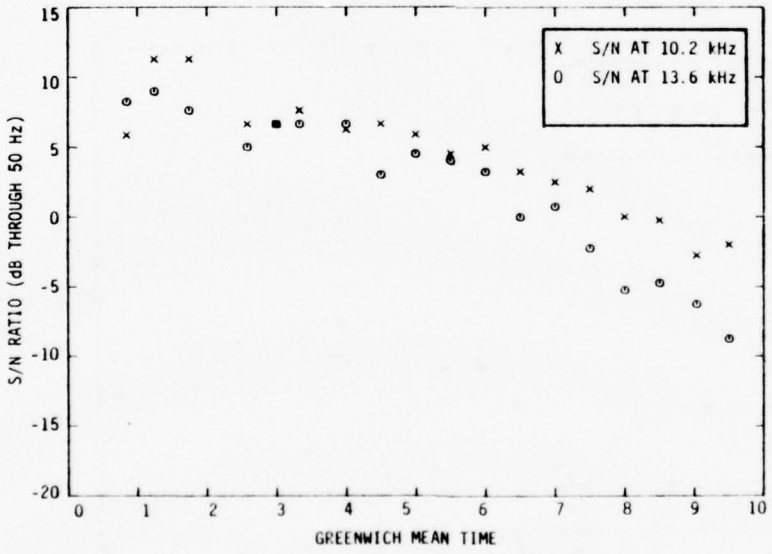

FIGURE B. 218. S/N RATIOS, STATION D, NEW YORK-RIO DE JANEIRO, FLIGHT 201, AUGUST 2, 1976

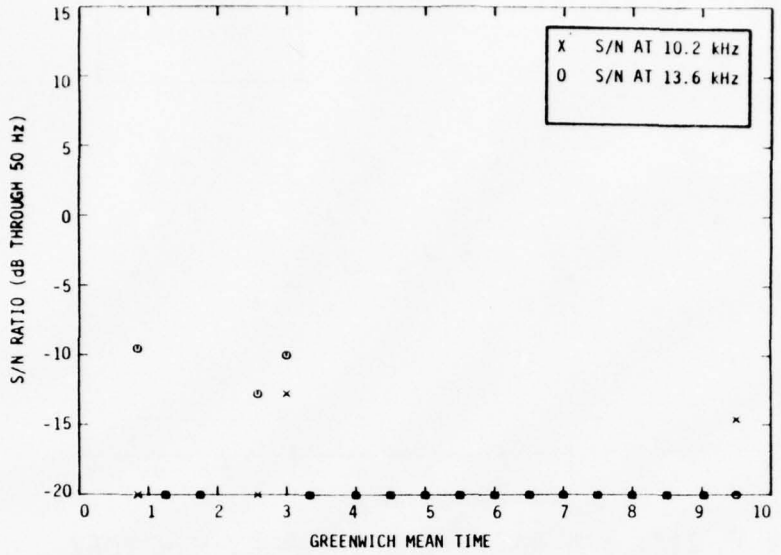

FIGURE B. 219. S/N RATIOS, STATION E, NEW YORK-RIO DE JANEIRO, FLIGHT 201, AUGUST 2, 1976

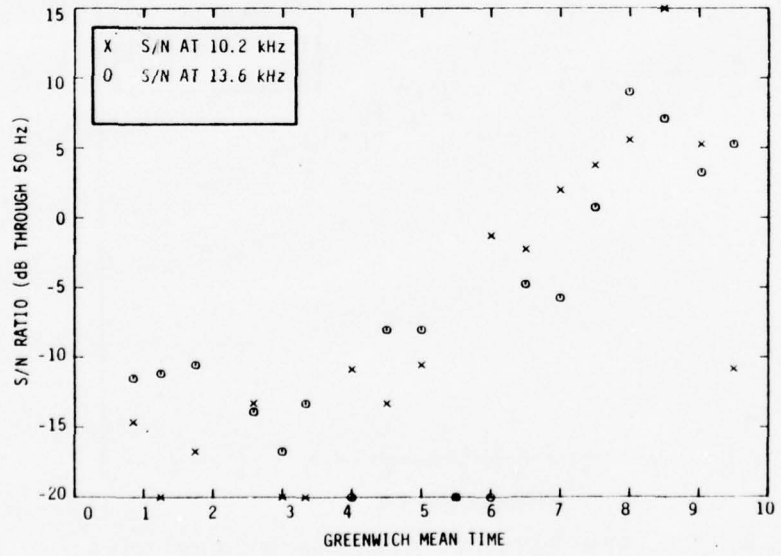

FIGURE B. 220. S/N RATIOS, STATION F, NEW YORK-RIO DE JANEIRO, FLIGHT 201, AUGUST 2, 1976

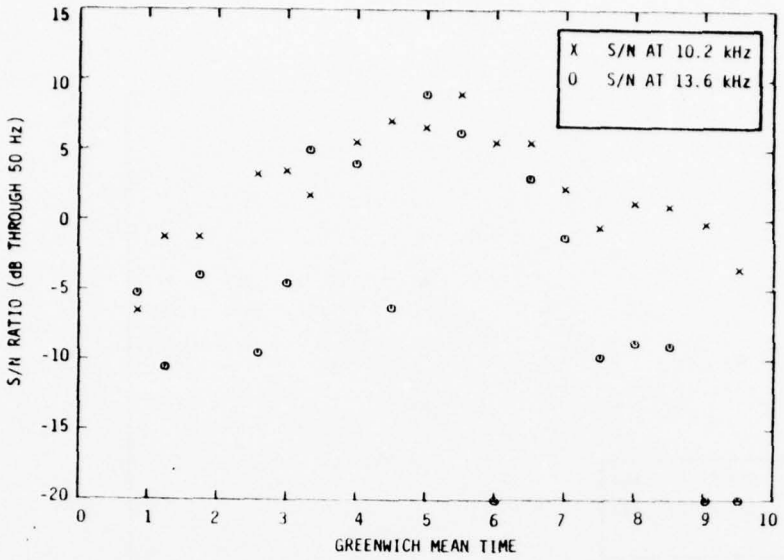

FIGURE B. 221. S/N RATIOS, STATION G, NEW YORK-RIO DE JANEIRO, FLIGHT 201, AUGUST 2, 1976

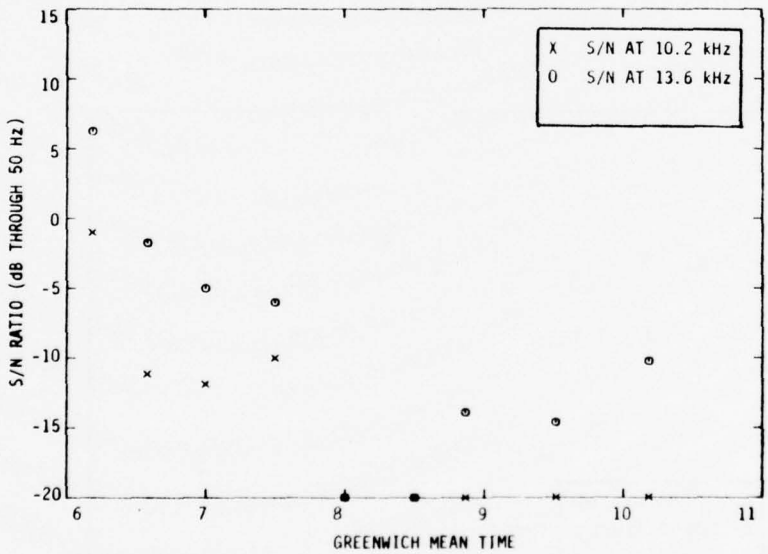

FIGURE B. 222. S/N RATIOS, STATION A, NEW YORK-RIO DE JANEIRO, FLIGHT 201, AUGUST 18, 1976

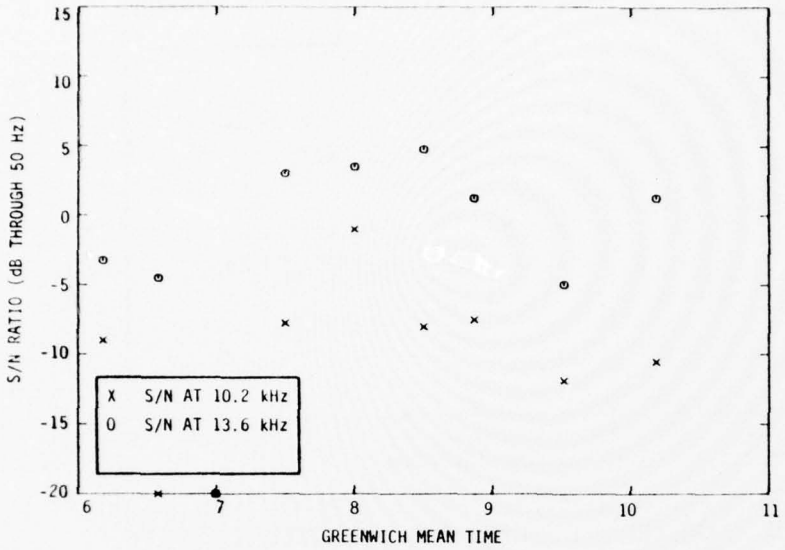

FIGURE B.223. S/N RATIOS, STATION B, NEW YORK-RIO DE JANEIRO, FLIGHT 201, AUGUST 18, 1976

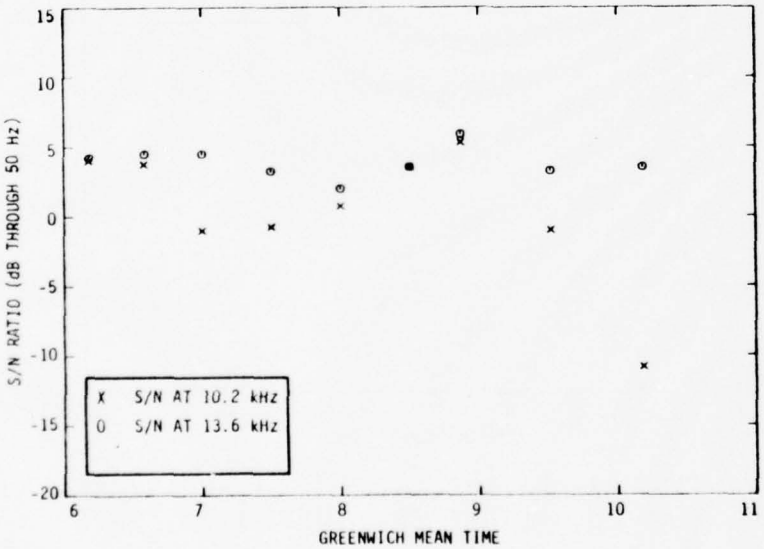

FIGURE B. 224. S/N RATIOS, STATION C, NEW YORK-RIO DE JANEIRO, FLIGHT 201, AUGUST 18, 1976

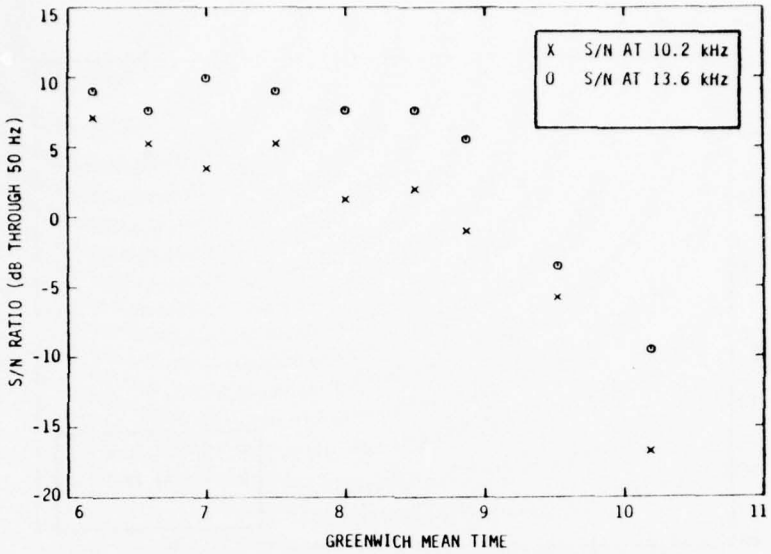

FIGURE B. 225. S/N RATIOS, STATION D, NEW YORK-RIO DE JANEIRO, FLIGHT 201, AUGUST 18, 1976

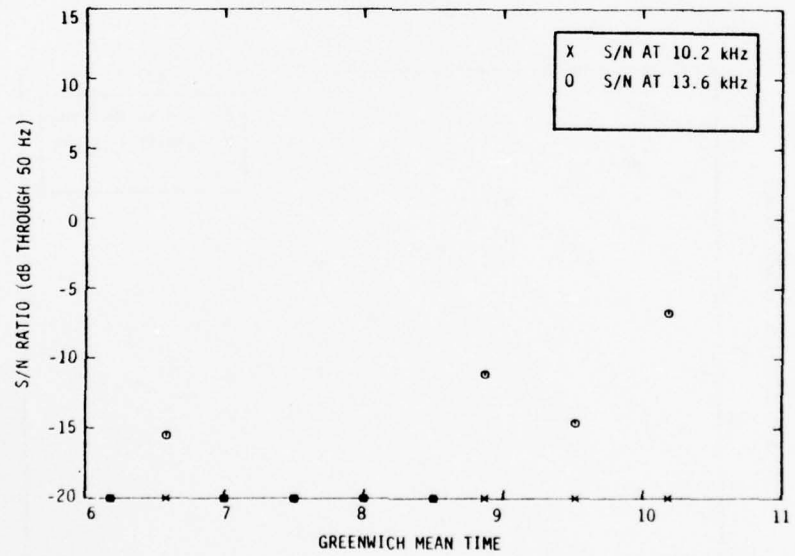

FIGURE B.226. S/N RATIOS, STATION E, NEW YORK-RIO DE JANEIRO, FLIGHT 201, AUGUST 18, 1976

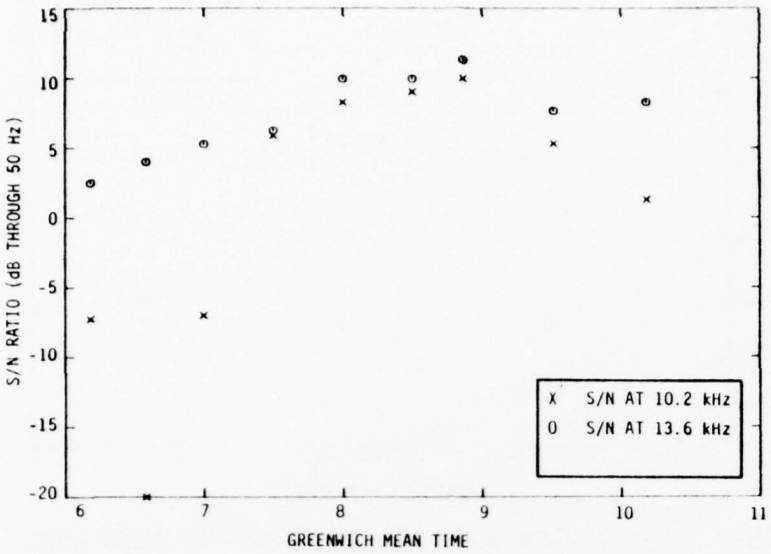

FIGURE B. 227. S/N RATIOS, STATION F, NEW YORK-RIO DE JANEIRO, FLIGHT 201, AUGUST 18, 1976

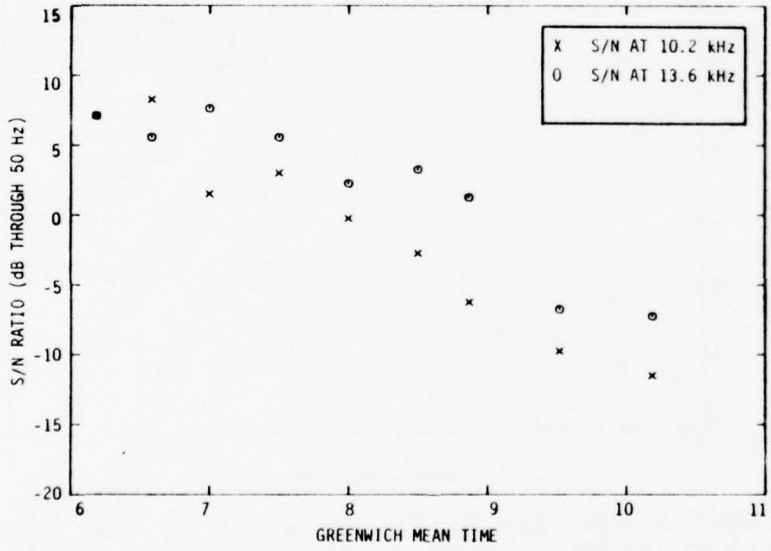

FIGURE B.228. S/N RATIOS, STATION G, NEW YORK-RIO DE JANEIRO, FLIGHT 201, AUGUST 18, 1976

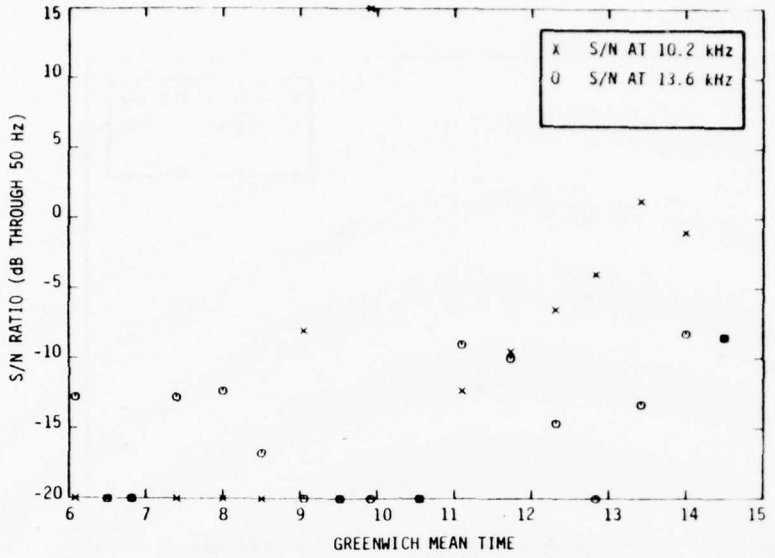

FIGURE B.229. S/N RATIOS, STATION A, RIO DE JANEIRO-NEW YORK, FLIGHT 202, JULY 7, 1976

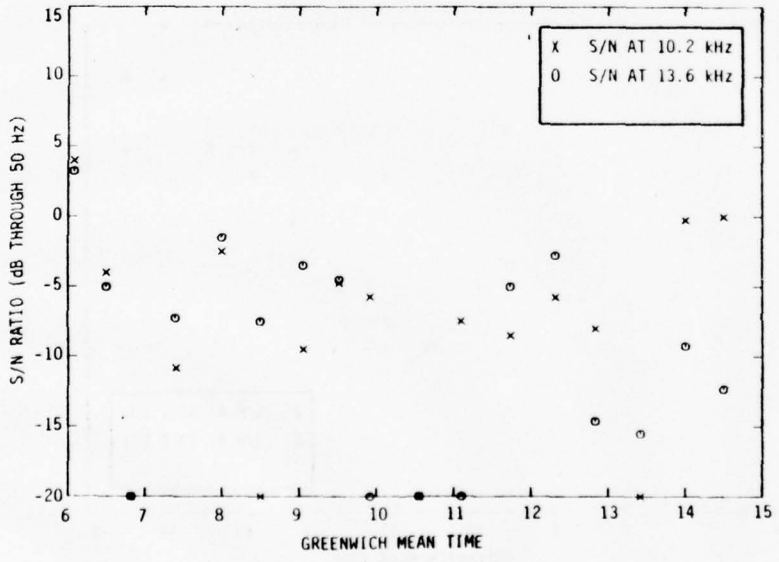

FIGURE B. 230. S/N RATIOS, STATION B, RIO DE JANEIRO-NEW YORK, FLIGHT 202, JULY 7, 1976

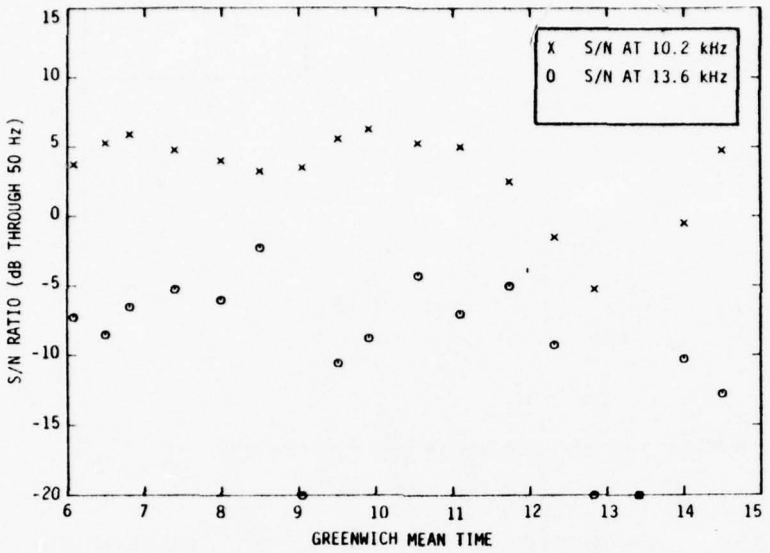

FIGURE B. 231. S/N RATIOS, STATION C, RIO DE JANEIRO-NEW YORK, FLIGHT 202, JULY 7, 1976

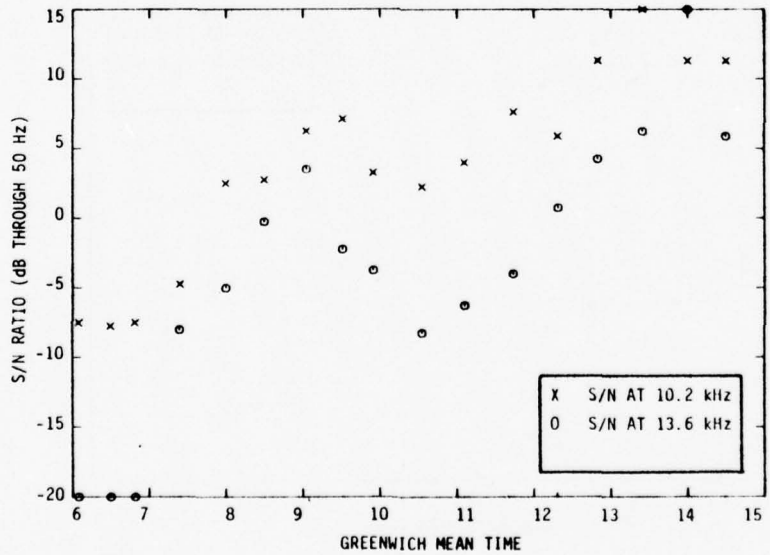

FIGURE B. 232. S/N RATIOS, STATION D, RIO DE JANEIRO-NEW YORK, FLIGHT 202, JULY 7, 1976

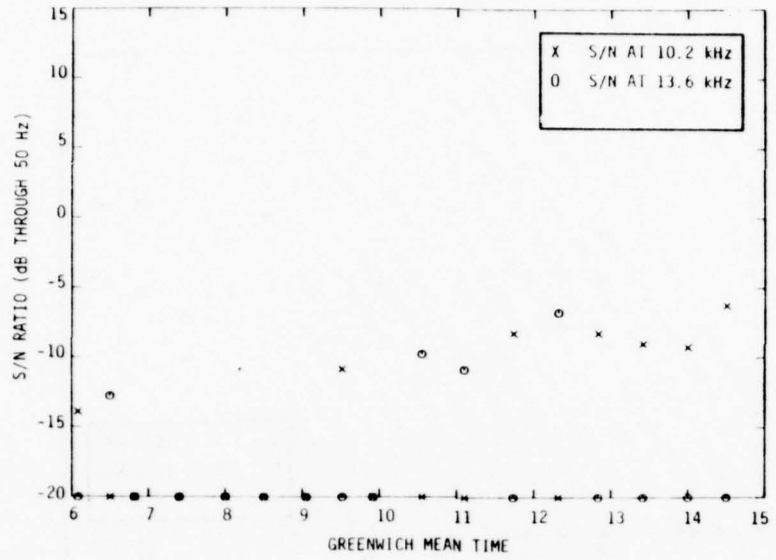

FIGURE B. 233. S/N RATIOS, STATION E, RIO DE JANEIRO-NEW YORK, FLIGHT 202, JULY 7, 1976

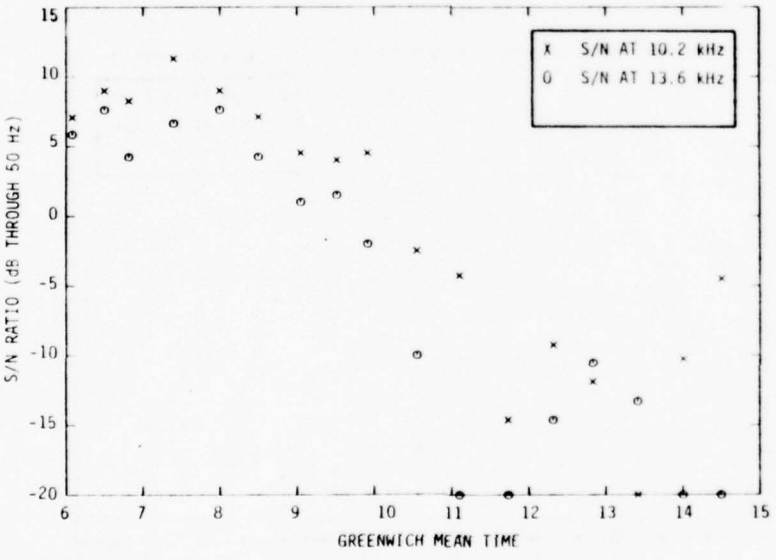

FIGURE B. 234. S/N RATIOS, STATION F, RIO DE JANEIRO, NEW YORK, FLIGHT 202, JULY 7, 1976

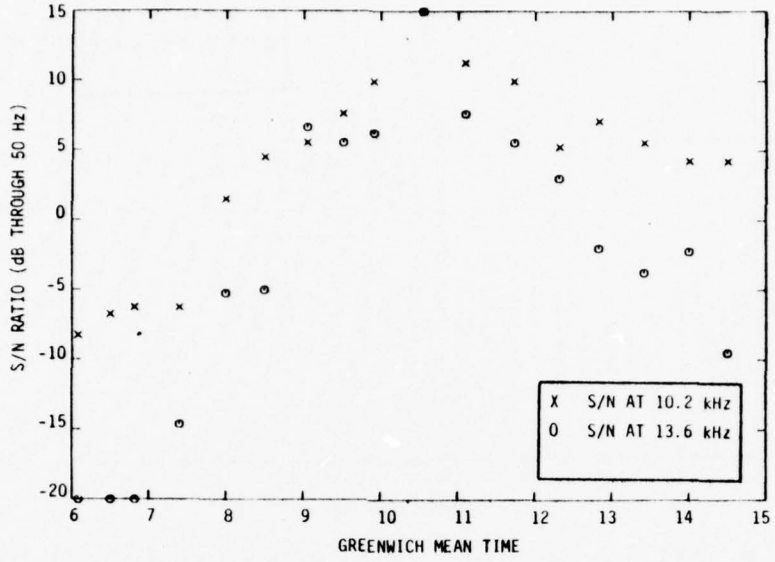

FIGURE B. 235. S/N RATIOS, STATION G, RIO DE JANEIRO-NEW YORK, FLIGHT 202, JULY 7, 1976

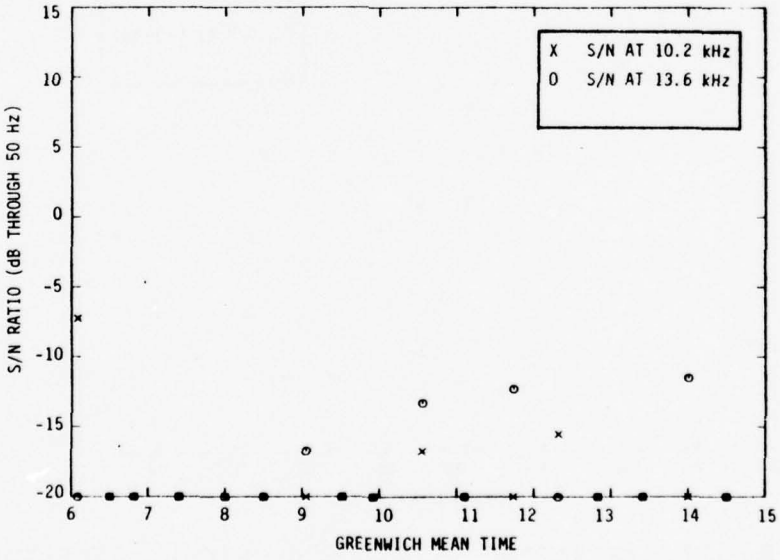

FIGURE B. 236. S/N RATIOS, STATION H, RIO DE JANEIRO-NEW YORK, FLIGHT 202, JULY 7, 1976

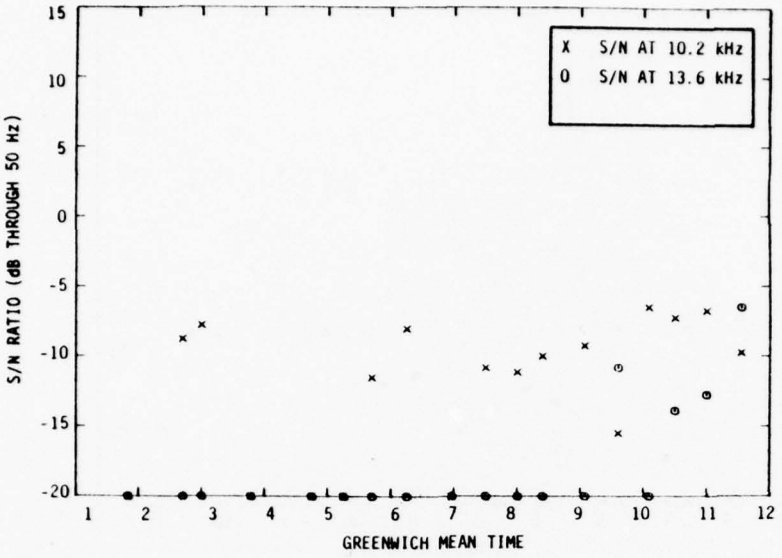

FIGURE B.237. S/N RATIOS, STATION A, RIO DE JANEIRO-NEW YORK, FLIGHT 202, AUGUST 3, 1976

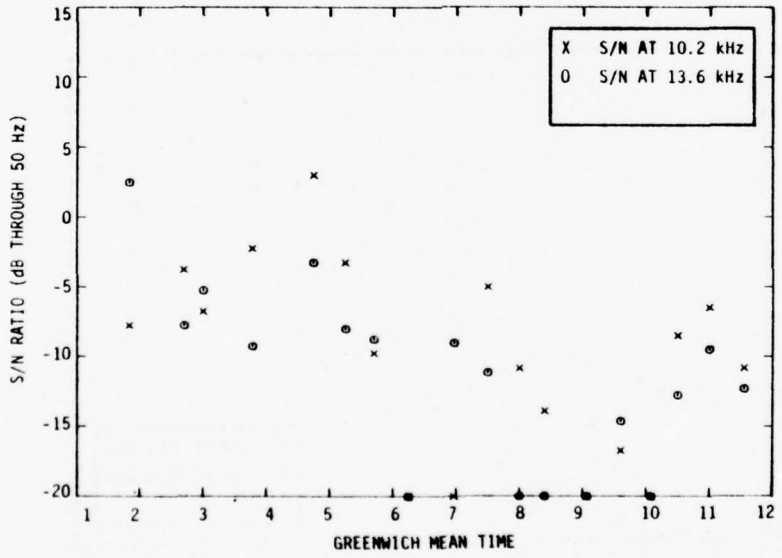

FIGURE B.238. S/N RATIOS, STATION B, RIO DE JANEIRO-NEW YORK, FLIGHT 202, AUGUST 3, 1976

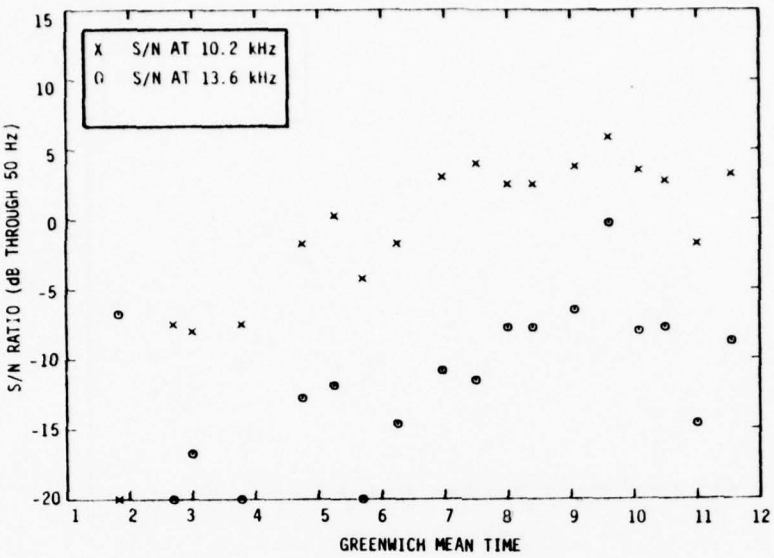

FIGURE B. 239. S/N RATIOS, STATION C, RIO DE JANEIRO-NEW YORK, FLIGHT 202, AUGUST 3, 1976

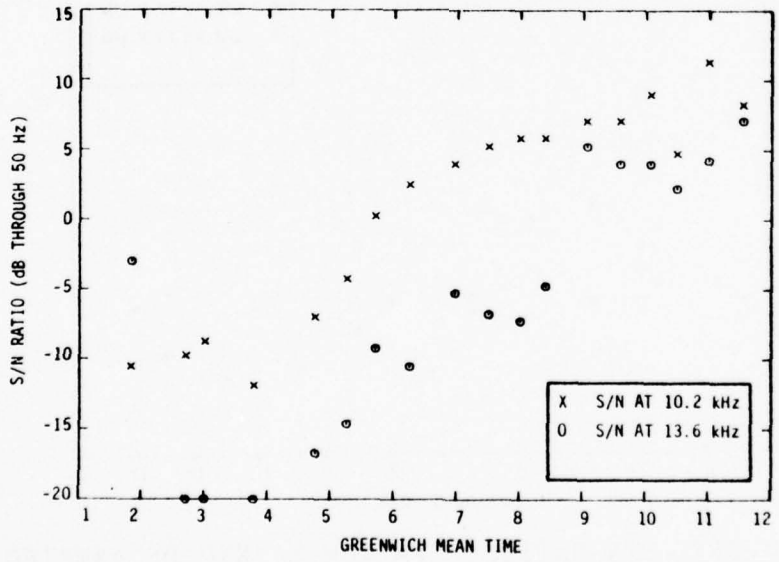

FIGURE B. 240. S/N RATIOS, STATION D, RIO DE JANEIRO-NEW YORK, FLIGHT 202, AUGUST 3, 1976

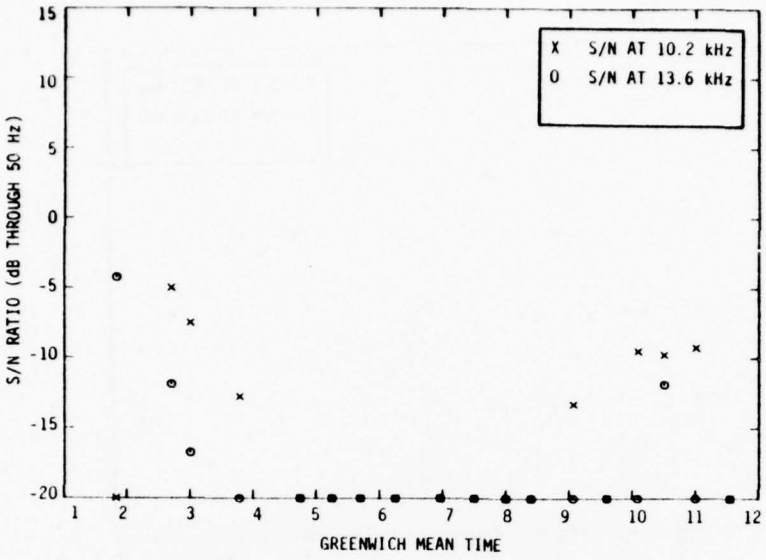

FIGURE B.241. S/N RATIOS, STATION E, RIO DE JANEIRO-NEW YORK, FLIGHT 202, AUGUST 3, 1976

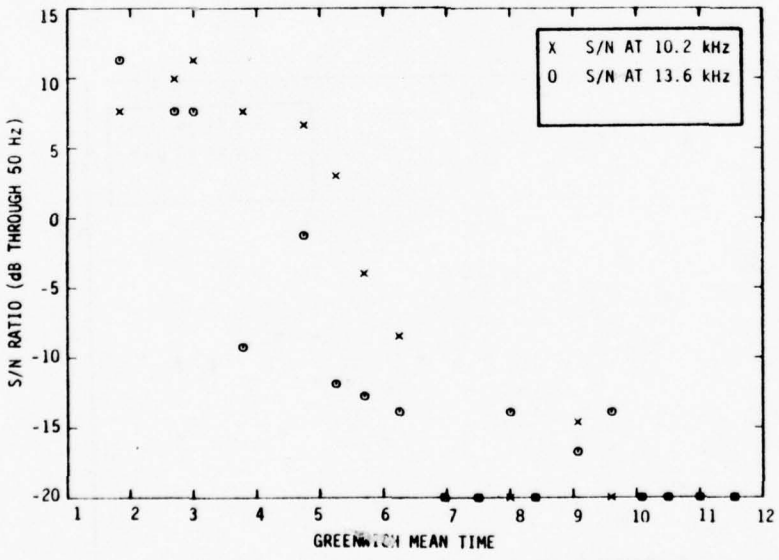

FIGURE B.242. S/N RATIOS, STATION F, RIO DE JANEIRO-NEW YORK, FLIGHT 202, AUGUST 3, 1976

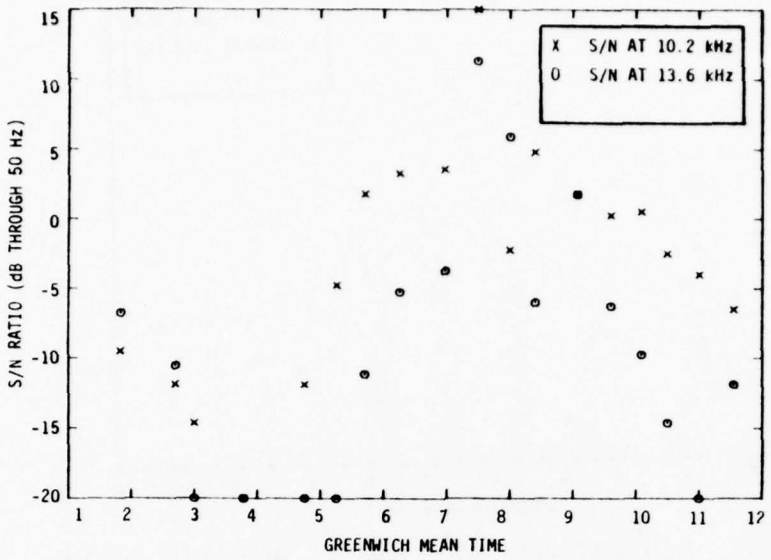

FIGURE B. 243. S/N RATIOS, STATION G, RIO DE JANEIRO-NEW YORK, FLIGHT 202, AUGUST 3, 1976

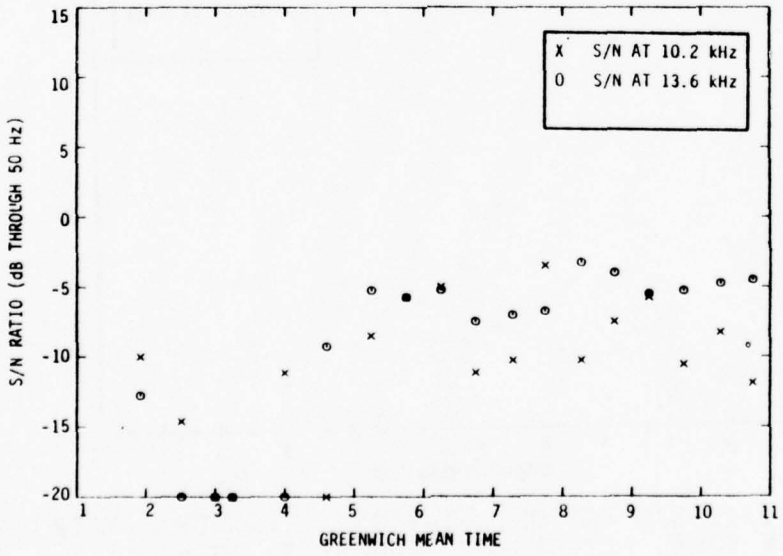

FIGURE B. 244. S/N RATIOS, STATION A, RIO DE JANEIRO-NEW YORK, FLIGHT 202, AUGUST 19, 1976

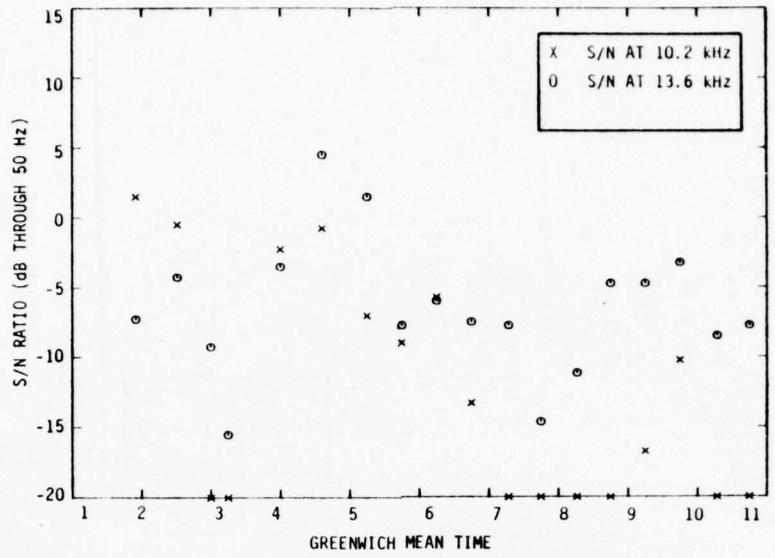

FIGURE B. 245. S/N RATIOS, STATION B, RIO DE JANEIRO-NEW YORK, FLIGHT 202, AUGUST 19, 1976

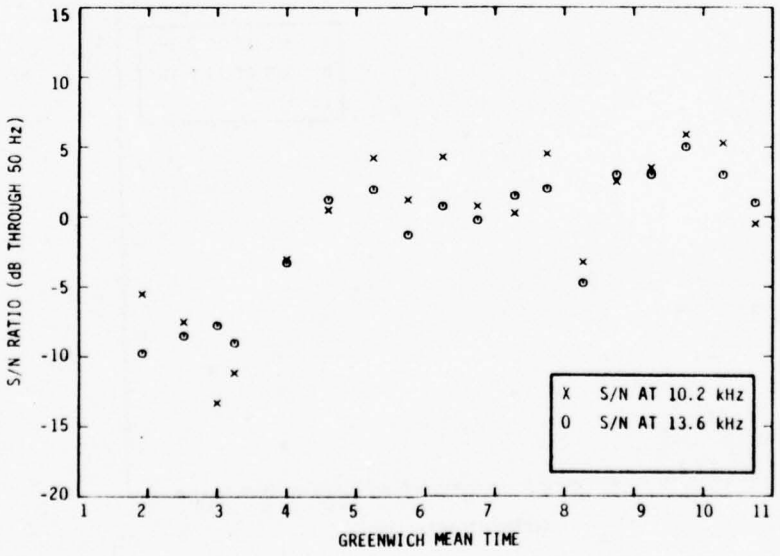

FIGURE B. 246. S/N RATIOS, STATION C, RIO DE JANEIRO-NEW YORK, FLIGHT 202, AUGUST 19, 1976

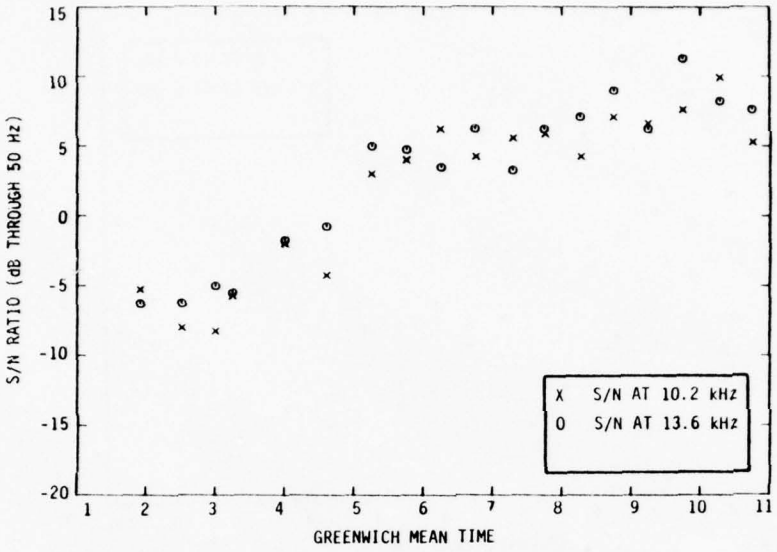

FIGURE B. 247. S/N RATIOS, STATION D, RIO DE JANEIRO-NEW YORK, FLIGHT 202, AUGUST 19, 1976

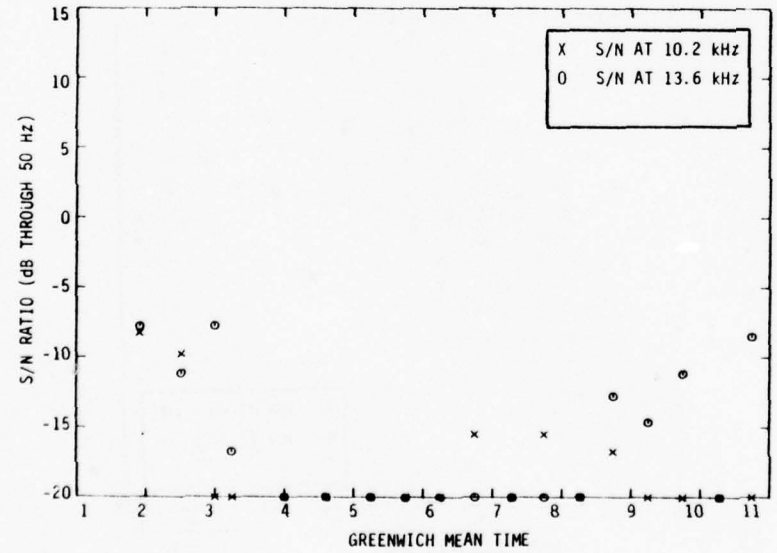

FIGURE B. 248. S/N RATIOS, STATION E, RIO DE JANEIRO-NEW YORK, FLIGHT 202, AUGUST 19, 1976

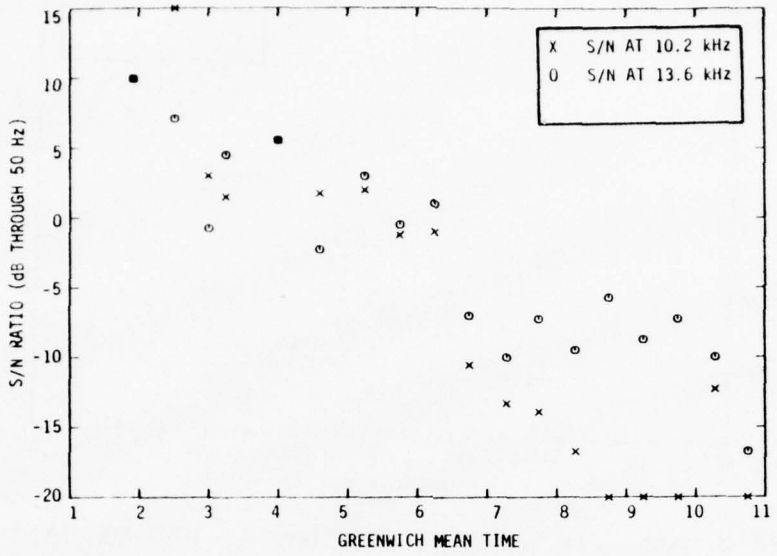

FIGURE B.249. S/N RATIOS, STATION F, RIO DE JANEIRO-NEW YORK, FLIGHT 202, AUGUST 19, 1976

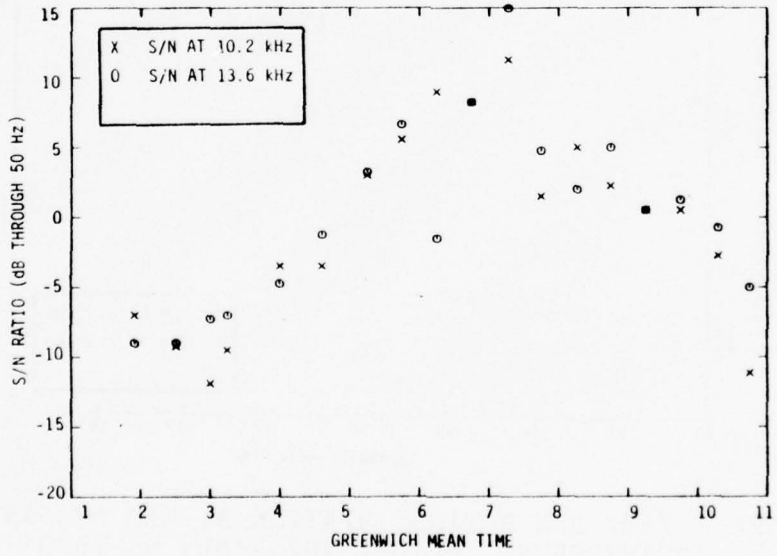

FIGURE B.250. S/N RATIOS, STATION G, RIO DE JANEIRO-NEW YORK, FLIGHT 202, AUGUST 19, 1976

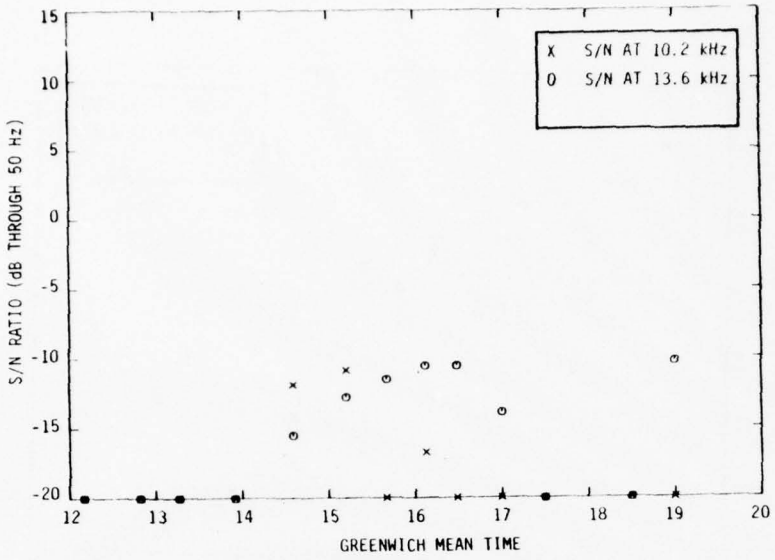

FIGURE B. 251. S/N RATIOS, STATION A, RIO DE JANEIRO-JOHANNESBURG, FLIGHT 201, JULY 6, 1976

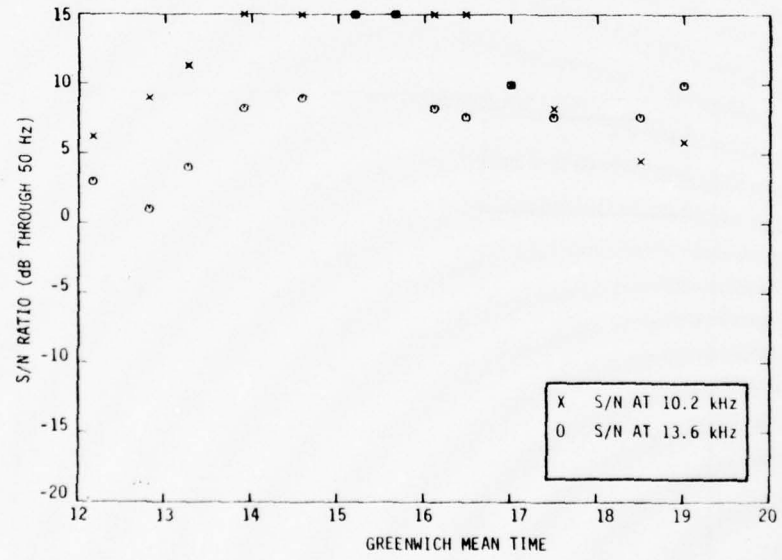

FIGURE B. 252. S/N RATIOS, STATION B, RIO DE JANEIRO-JOHANNESBURG, FLIGHT 201, JULY 6, 1976

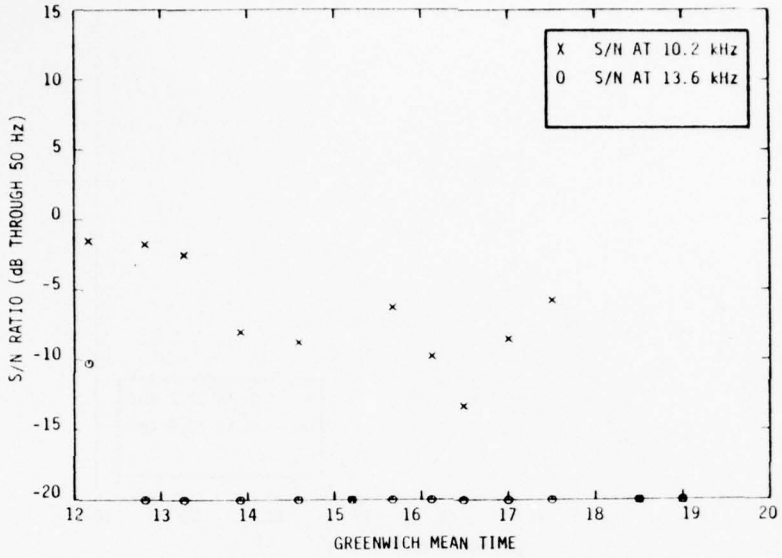

FIGURE B. 253. S/N RATIOS, STATION C, RIO DE JANEIRO-JOHANNESBURG, FLIGHT 201, JULY 6, 1976

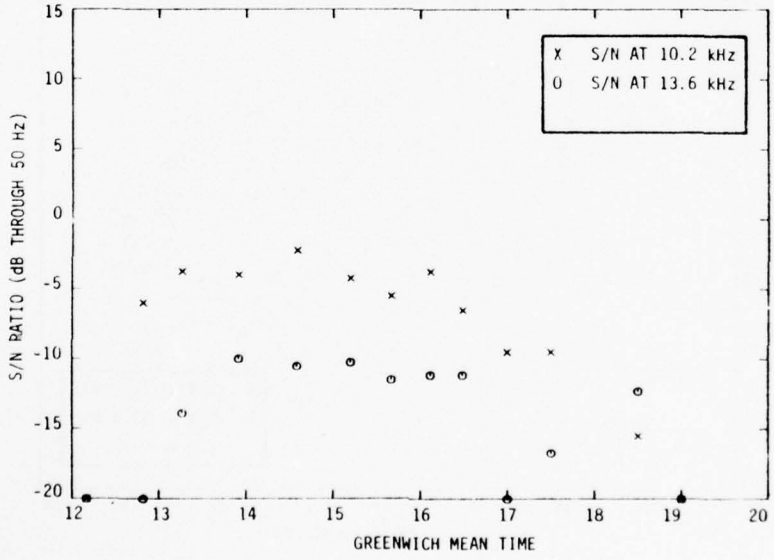

FIGURE B. 254. S/N RATIOS, STATION D, RIO DE JANEIRO-JOHANNESBURG, FLIGHT 201, JULY 6, 1976

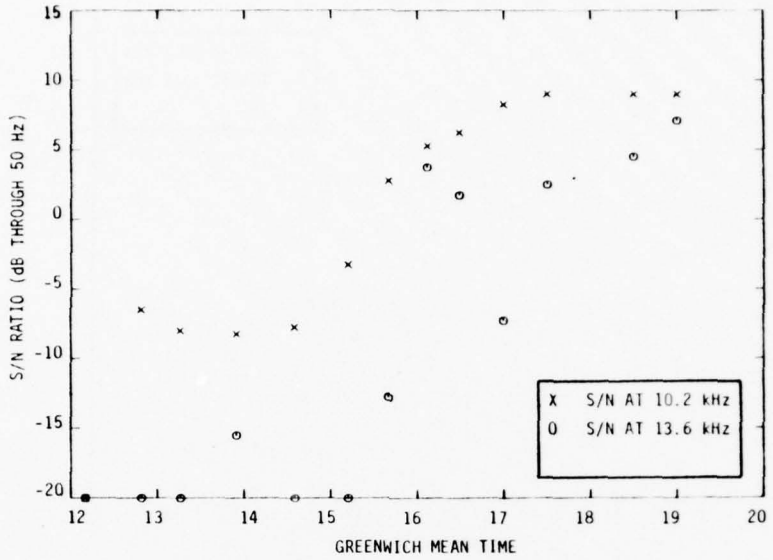

FIGURE B. 255. S/N RATIOS, STATION E, RIO DE JANEIRO-JOHANNESBURG, FLIGHT 201, JULY 6, 1976

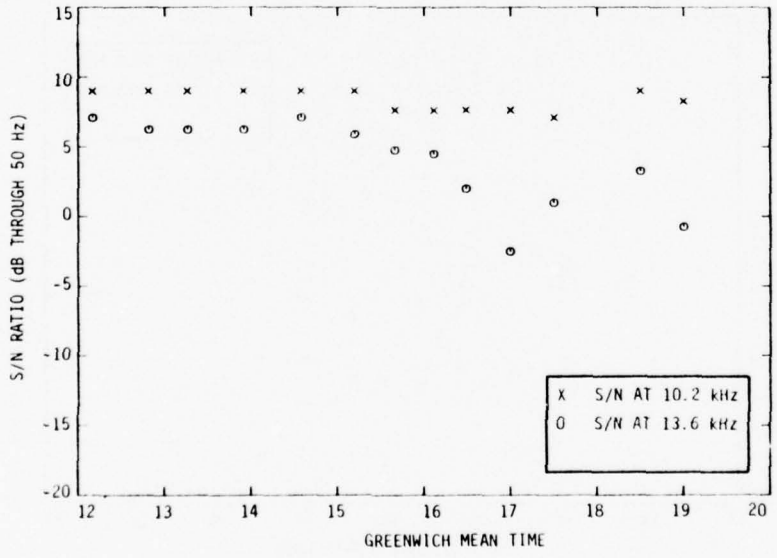

FIGURE B. 256. S/N RATIOS, STATION F, RIO DE JANEIRO-JOHANNESBURG, FLIGHT 201, JULY 6, 1976

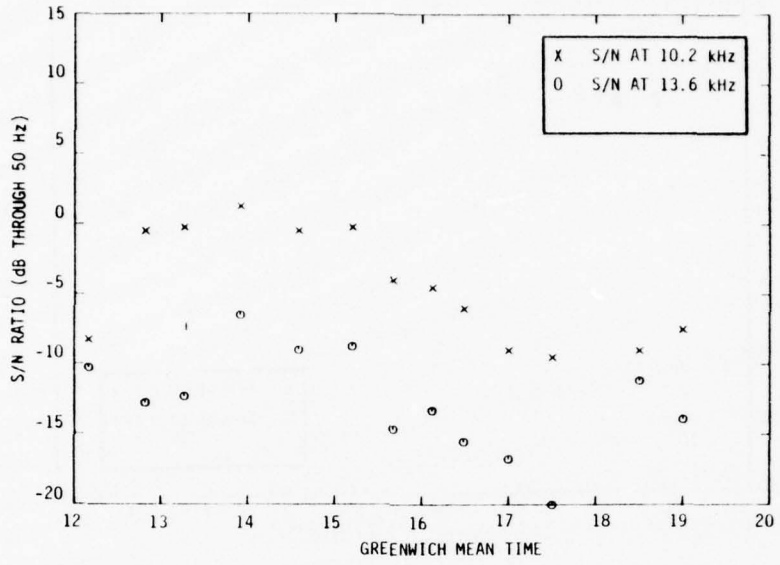

FIGURE B.257. S/N RATIOS, STATION G, RIO DE JANEIRO-JOHANNESBURG, FLIGHT 201, JULY 6, 1976

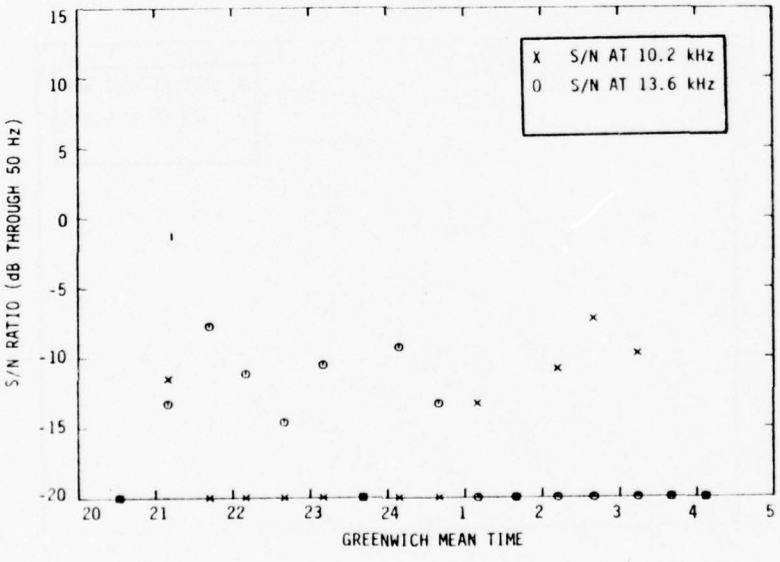

FIGURE B.258. S/N RATIOS, STATION A, JOHANNESBURG-RIO DE JANEIRO VIA CAPETOWN, FLIGHT 202, JULY 7, 1976

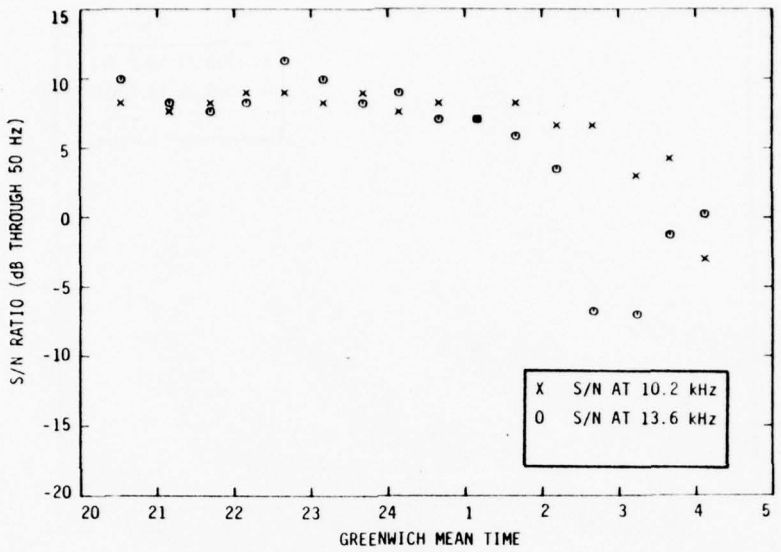

FIGURE B. 259. S/N RATIOS, STATION B, JOHANNESBURG-RIO DE JANEIRO VIA CAPETOWN, FLIGHT 202, JULY 7, 1976

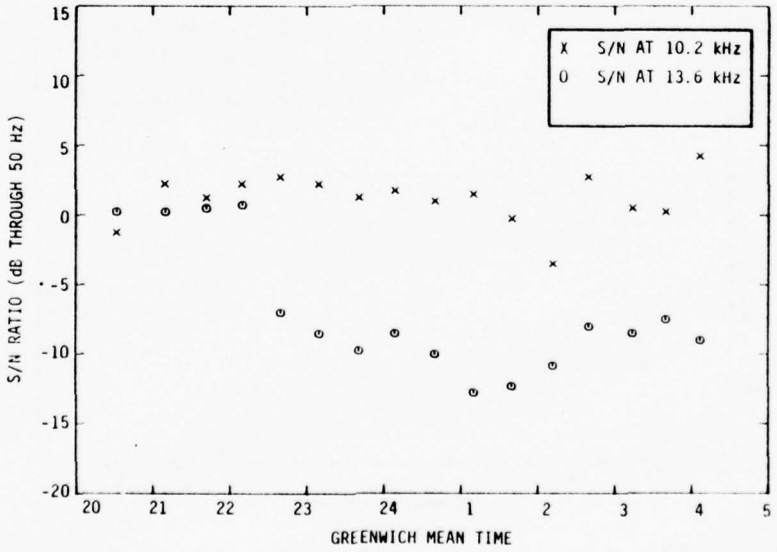

FIGURE B. 260. S/N RATIOS, STATION C, JOHANNESBURG-RIO DE JANEIRO VIA CAPETOWN, FLIGHT 202, JULY 7, 1976

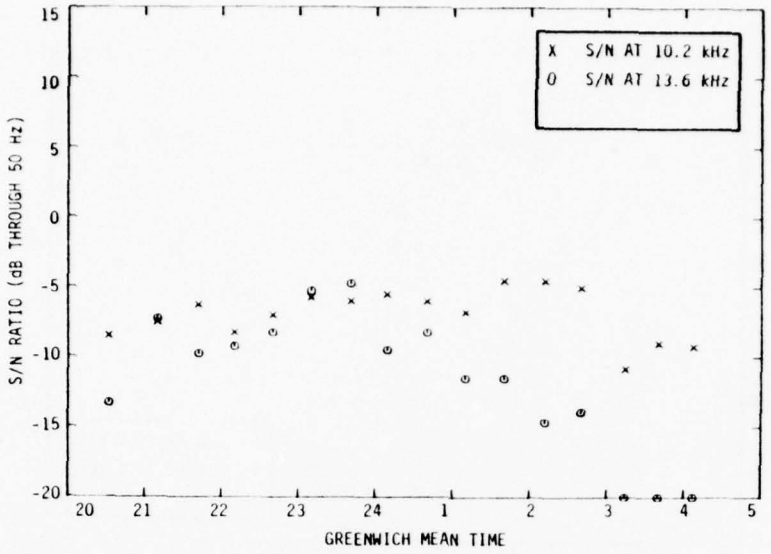

FIGURE B.261. S/N RATIOS, STATION D, JOHANNESBURG-RIO DE JANEIRO VIA CAPETOWN, FLIGHT 202, JULY 7, 1976

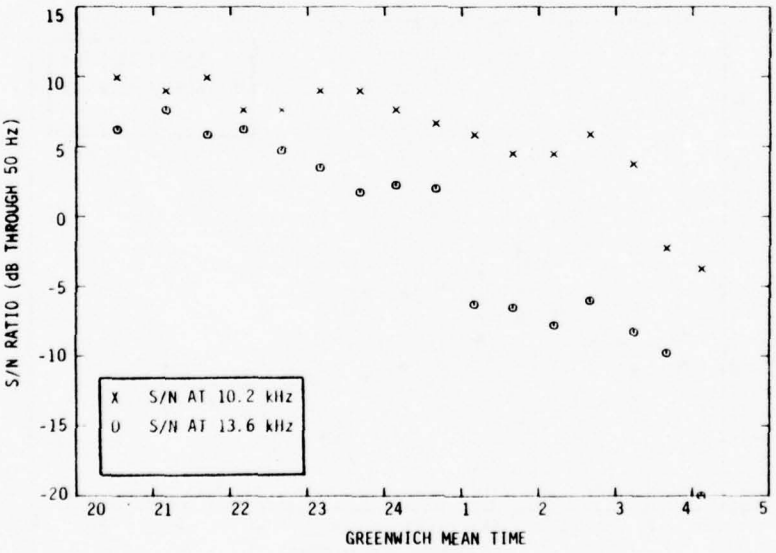

FIGURE B.262. S/N RATIOS, STATION E, JOHANNESBURG-RIO DE JANEIRO VIA CAPETOWN, FLIGHT 202, JULY 7, 1976

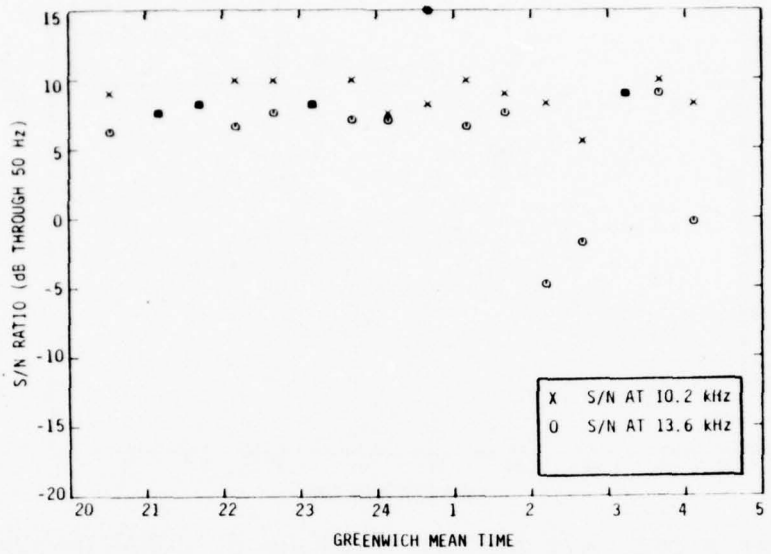

FIGURE B.263. S/N RATIOS, STATION F, JOHANNESBURG-RIO DE JANEIRO VIA CAPETOWN, FLIGHT 202, JULY 7, 1976

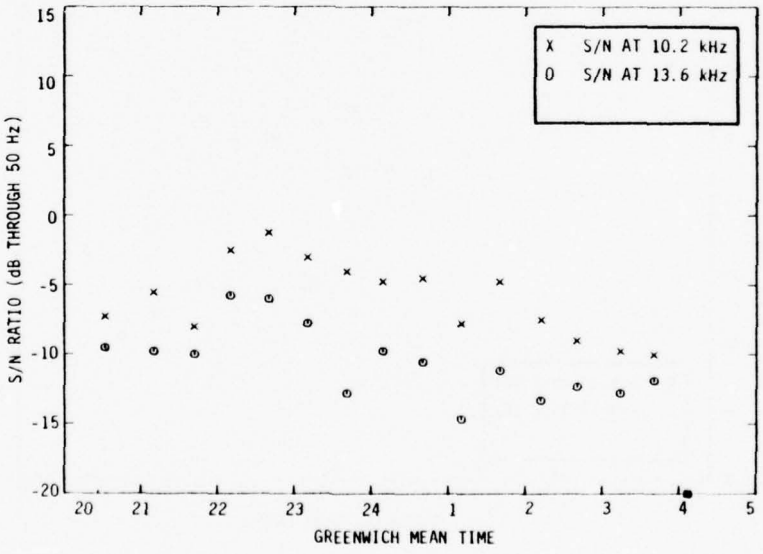

FIGURE B. 264. S/N RATIOS, STATION G, JOHANNESBURG-RIO DE JANEIRO VIA CAPETOWN, FLIGHT 202, JULY 7, 1976

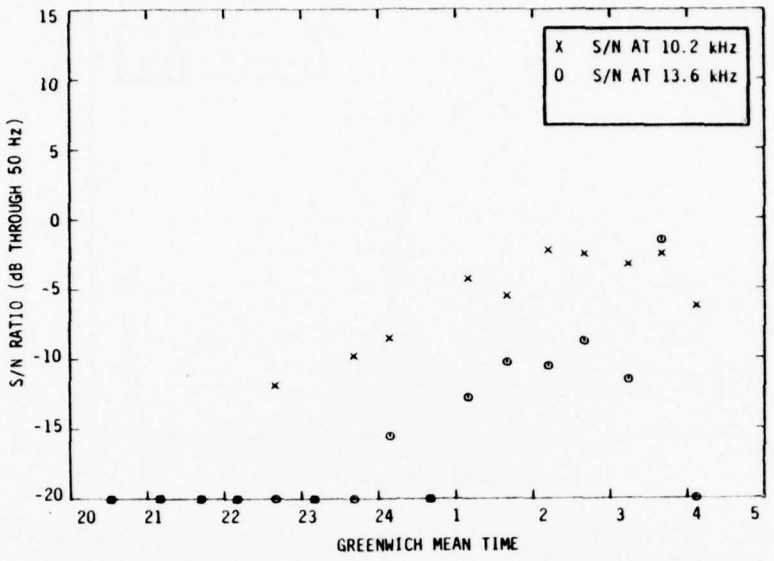

FIGURE B. 265. S/N RATIOS, STATION H, JOHANNESBURG-RIO DE JANEIRO VIA CAPETOWN, FLIGHT 202, JULY 7, 1976

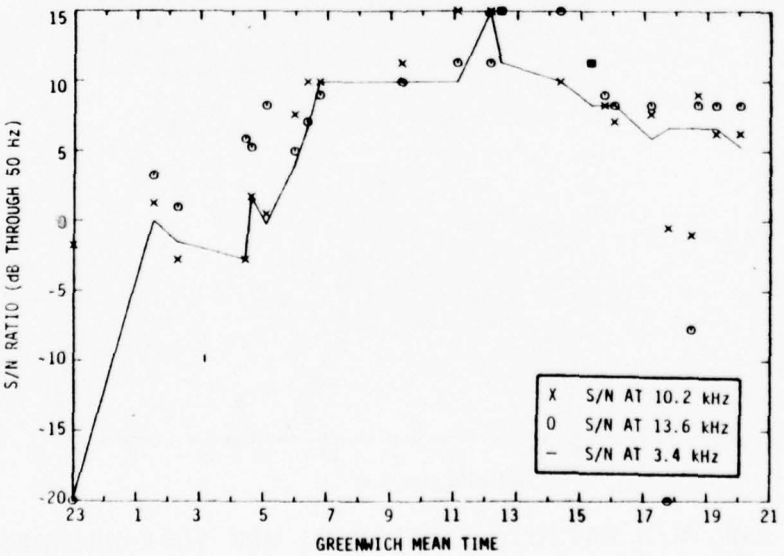

FIGURE B. 266. S/N RATIOS, STATION B, NEW YORK-NAIROBI VIA DAKAR, MONROVIA, LAGOS, AND KINSHASA, FLIGHT 190, MARCH 16, 1976

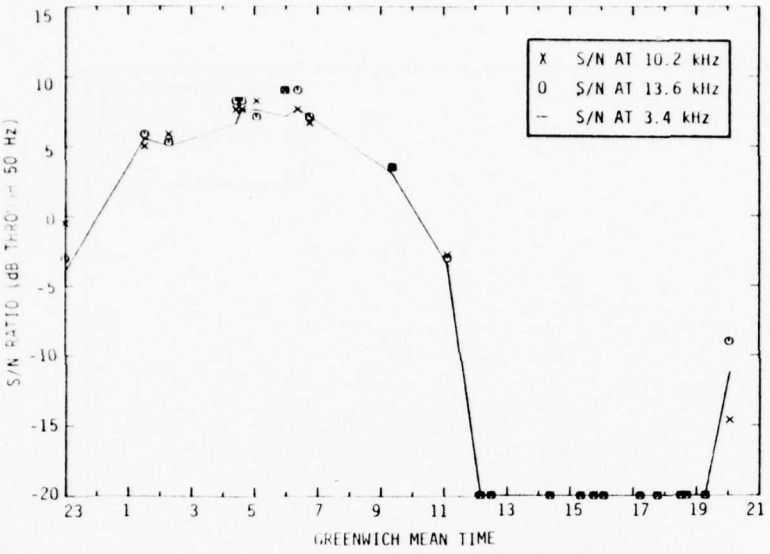

FIGURE B. 267. S/N RATIOS, STATION C, NEW YORK-NAIROBI VIA DAKAR, MONROVIA, LAGOS, AND KINSHASA, FLIGHT 190, MARCH 16, 1976

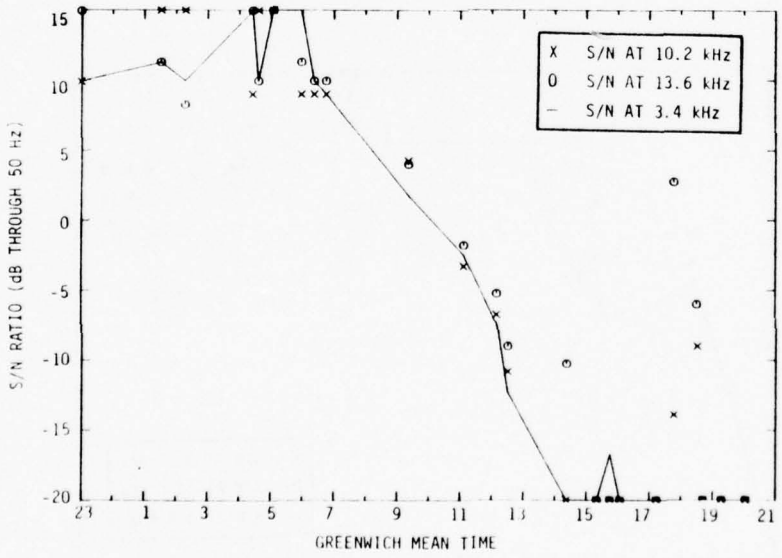

FIGURE B.268. S/N RATIOS, STATION D, NEW YORK-NAIROBI VIA DAKAR, MONROVIA, LAGOS, AND KINSHASA, FLIGHT 190, MARCH 16, 1976

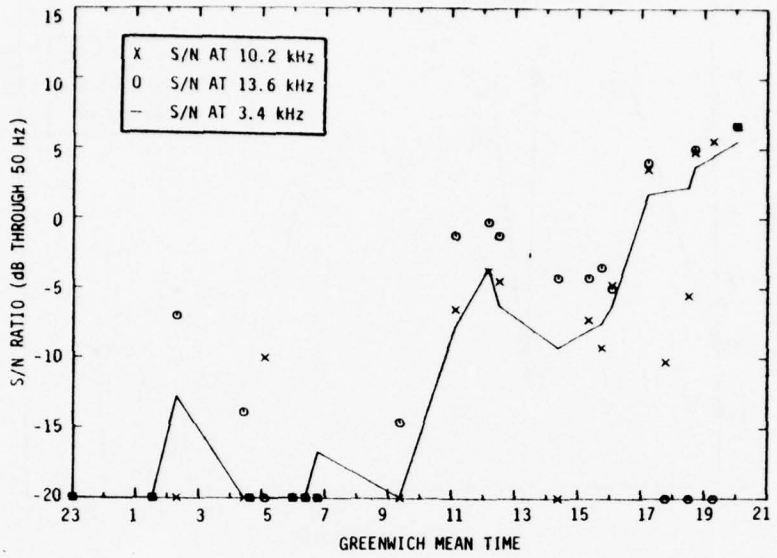

FIGURE B.269. S/N RATIOS, STATION E, NEW YORK-NAIROBI VIA DAKAR, MONROVIA, LAGOS, AND KINSHASA, FLIGHT 190, MARCH 16, 1976

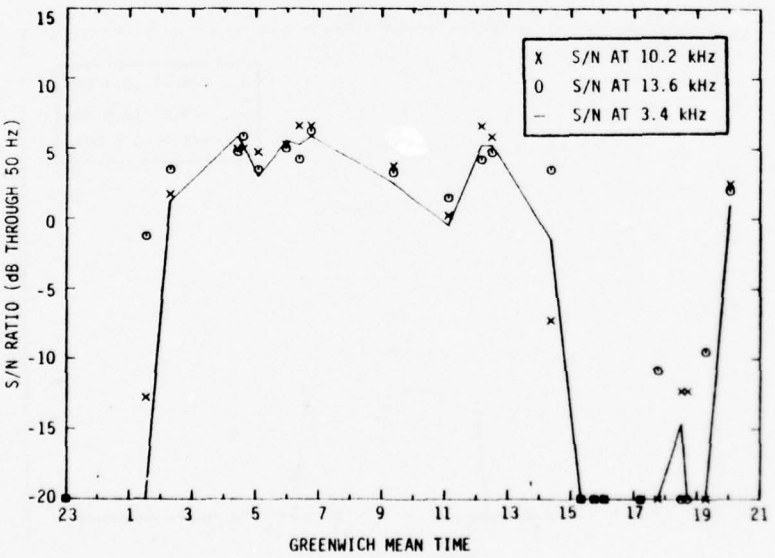

FIGURE B.270. S/N RATIOS, STATION F, NEW YORK-NAIROBI VIA DAKAR, MONROVIA, LAGOS, AND KINSHASA, FLIGHT 190, MARCH 16, 1976

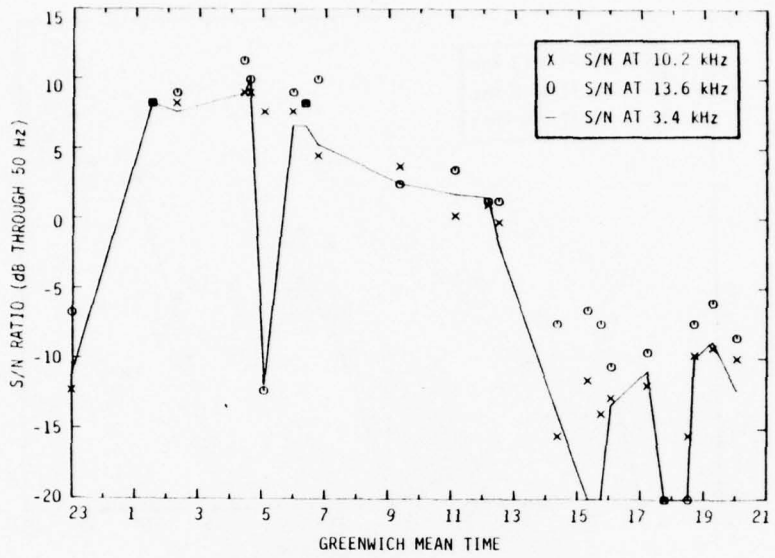

FIGURE B. 271. S/N RATIOS, STATION G, NEW YORK-NAIROBI VIA DAKAR, MONROVIA, LAGOS, AND KINSHASA, FLIGHT 190, MARCH 16, 1976

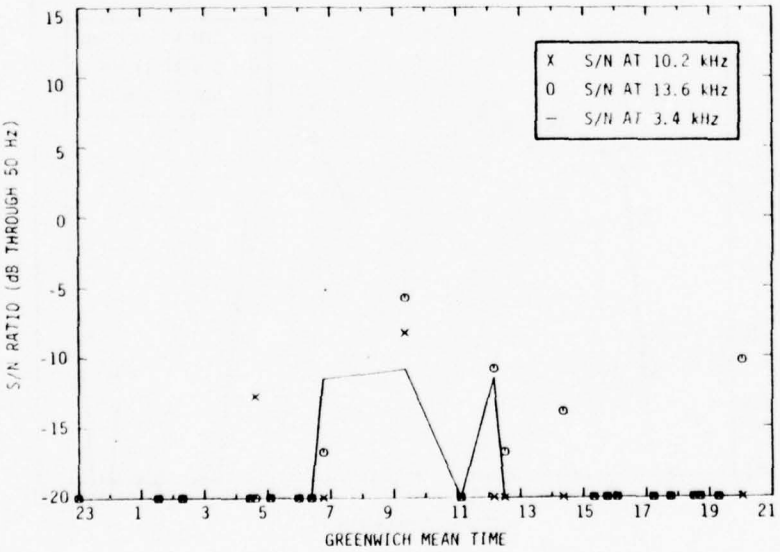

FIGURE B. 272. S/N RATIOS, STATION H. NEW YORK-NAIROBI VIA DAKAR, MONROVIA, LAGOS, AND KINSHASA, FLIGHT 190, MARCH 16, 1976

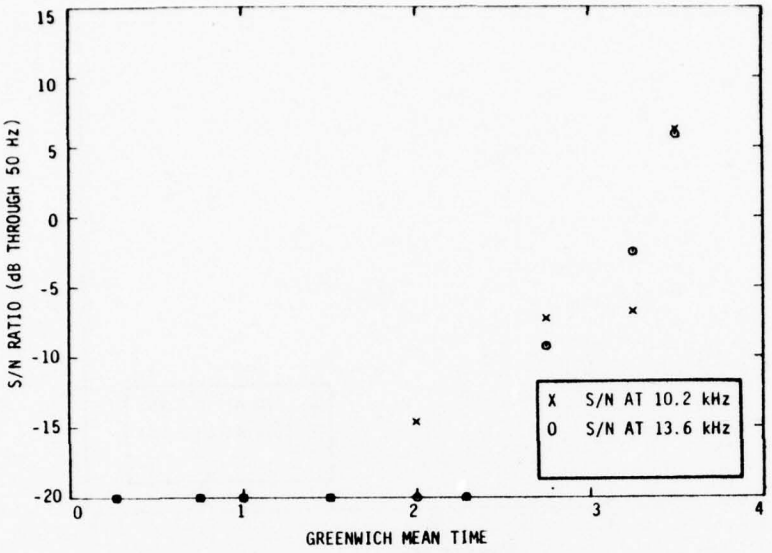

FIGURE B.273. S/N RATIOS, STATION A, SEATTLE-FAIRBANKS, FLIGHT 903, SEPT. 20, 1976

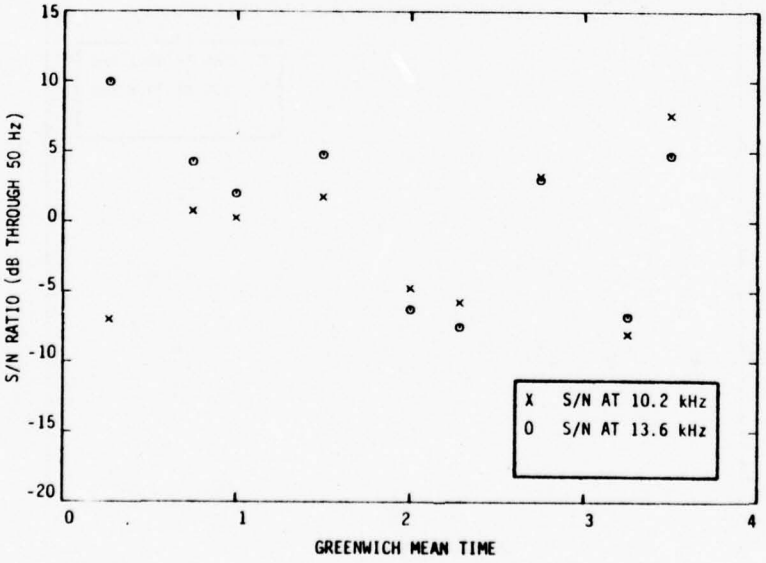

FIGURE B.274. S/N RATIOS, STATION C, SEATTLE-FAIRBANKS, FLIGHT 903, SEPT. 20, 1976

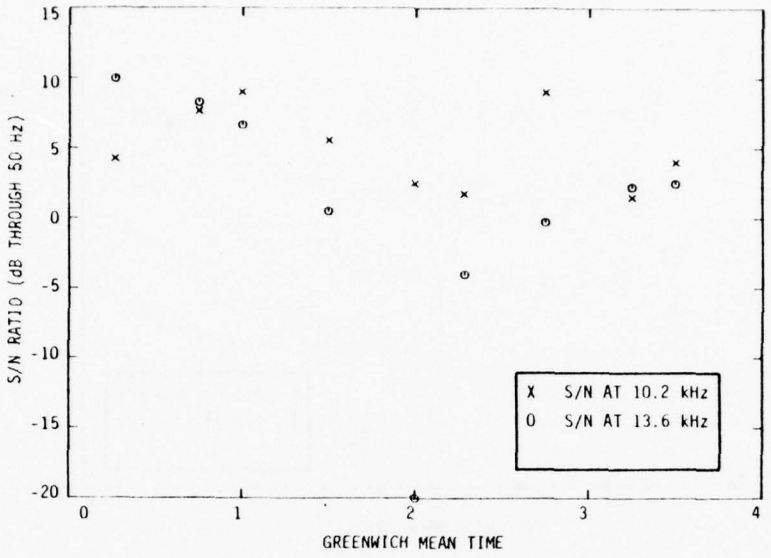

FIGURE B.275. S/N RATIOS, STATION D, SEATTLE-FAIRBANKS, FLIGHT 903, SEPT. 20, 1976

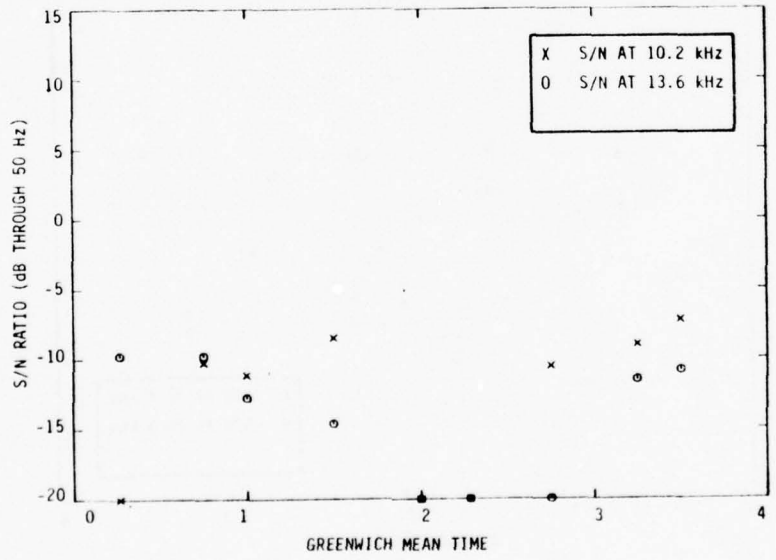

FIGURE B.276. S/N RATIOS, STATION H, SEATTLE-FAIRBANKS, FLIGHT 903, SEPT. 20, 1976

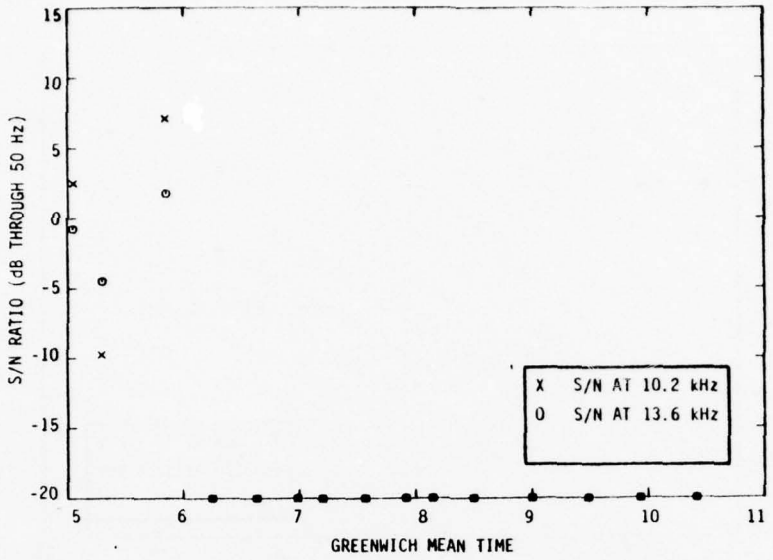

FIGURE B. 277. S/N RATIOS, STATION A, FAIRBANKS-NEW YORK, FLIGHT 912, SEPT. 20, 1976

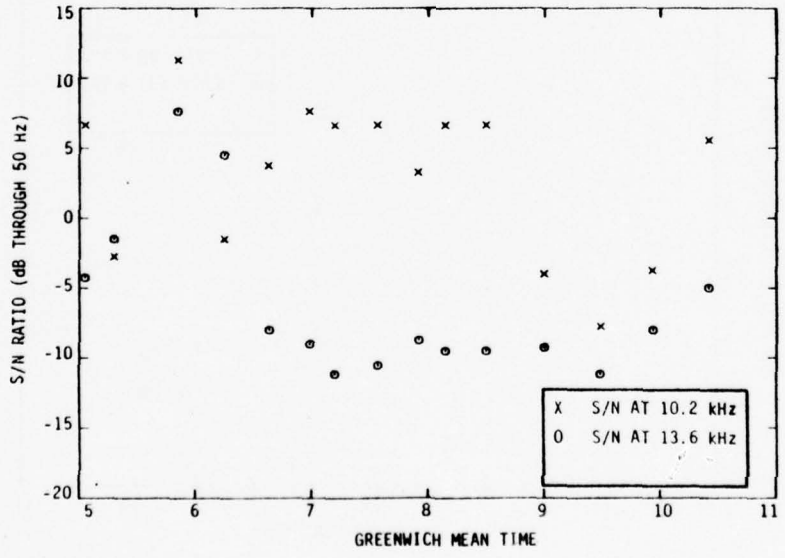

FIGURE B. 278. S/N RATIOS, STATION C,, FAIRBANKS-NEW YORK, FLIGHT 912, SEPT. 20, 1976

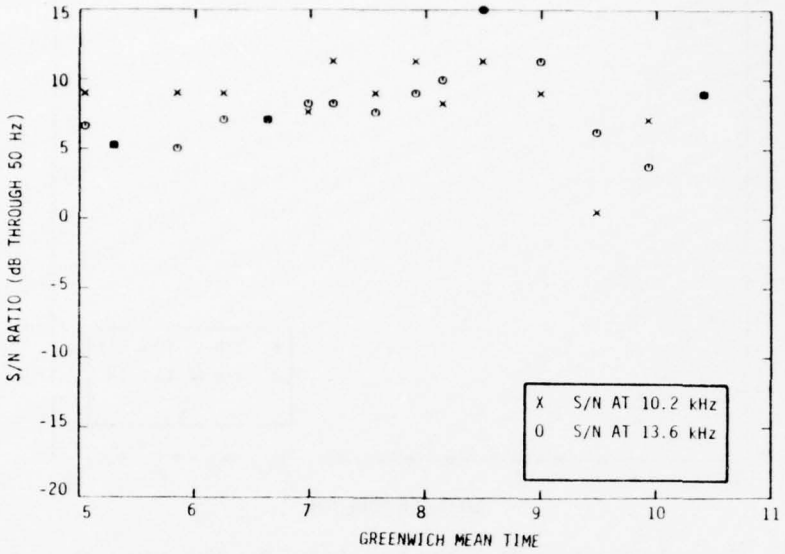

FIGURE B.279. S/N RATIOS, STATION D, FAIRBANKS-NEW YORK, FLIGHT 912, SEPT. 20, 1976

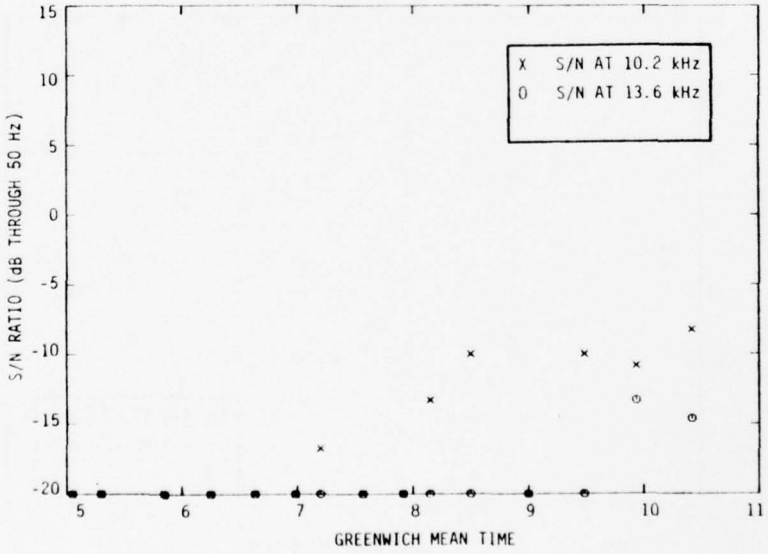

FIGURE B. 280. S/N RATIOS, STATION G, FAIRBANKS-NEW YORK, FLIGHT 912, SEPT. 20, 1976

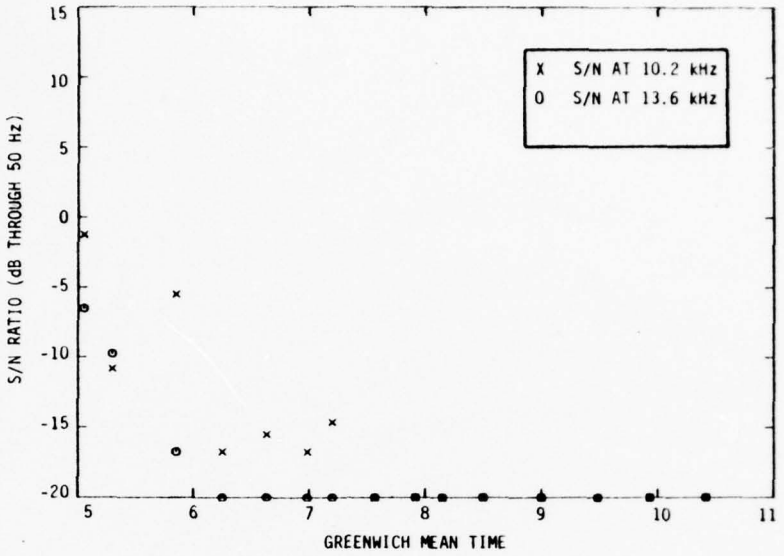

FIGURE B. 281. S/N RATIOS, STATION H, FAIRBANKS-NEW YORK, FLIGHT 912, SEPT. 20, 1976

APPENDIX C
ANALYSIS OF US NAVAL OBSERVATORY TIME SERIES DATA

C.1 INTRODUCTION

Time series data from the US Naval Observatory were analyzed to determine frequency and duration of VLF, LORAN, and Omega off-air periods, as well as information concerning transmitter long-term stability. The objectives of this research were to determine on a first cut basis those factors in the transmitter/antenna systems of VLF/LF navigation systems which would limit overall system accuracy, reliability and performance for aircraft navigation. To accomplish these goals, tabular data was copied in different formats, plotted, and subjected to elementary statistical analysis. This method of analysis was comparatively easy to perform, and thoroughly utilized the data available.

C.2 DATA SOURCES

Data for this analysis was supplied by the US Naval Observatory Daily Phase Values and Time Differences Series 4, from late February 1973 until November 1975. This weekly publication supplied information to those users of LORAN, Omega, Navy communications stations, and commercial TV for timing purposes. Specifically, the publication provides "differences, in microseconds, between the USNO Master Clock and the arriving phase of the carrier frequencies of the VLF stations as affected by the daylight phase delay and between the USNO Master Clock and the time reference pulses of the LORAN C, D stations, and TV transmission"[7].

Stations and/or chains for which information is given are listed in Table C-1.

Additionally, propagation disturbances measured in Washington during daylight hours are listed by time of occurrence and magnitude. Magnitude information is given by a code which relates the phase delay, in microseconds, to a single digit between 1 and 9. Station off-air times, periods of instability, scheduled maintenance times, correction of typographical errors, and other notes are included in the report.

The Time Service Information Letter of August 15, 1973 was used as a key for understanding of time service information. Additionally, Time Series Announcements Series 14 were studied for information about time-keeping notes for USNO.

C.3 METHOD OF ANALYSIS

For this appendix, three VLF stations, a total of three Omega frequencies from two stations, and two LORAN-C chains were selected to give information as shown in Table C-1. Because the information is supplied on a weekly basis, this information was compiled into tables for each station and each year. In this format, data was plotted to provide quick comprehension of transmitter performance over the course of a year. These plots provided a quick reference on which station drift, signal jumps, and scattering of the received signal on a day-to-day basis were easily observed. In addition, station off-air periods, excluding regularly scheduled maintenance, and steps in transmitted signal were tabulated.

Statistical analysis of station performance was also performed. For each station, monthly average and standard deviation of received signals were calculated, and these statistics were then plotted. The standard deviation of the received phase was used as a handy measure of station performance, although the limitations of this

Table C-1

USNO Daily Phase

Values and Time Differences, Series 4

Stations Monitored

LORAN-C

- Northwest Pacific (9970)
- Central Pacific (4990)
- East Coast US* (9930)
- Norwegion Sea (7970)
- North Atlantic* (7930)
- Southeast Asia (5970)
- North Pacific (5930)

LORAN-D

- West Coast US

OMEGA

North Dakota*	10.2 kHz
North Dakota	13.1 kHz
North Dakota*	13.6 kHz
Trinidad*	13.6 kHz

VLF COMMUNICATION

- GBR (Rugby)
- NAA* (Maine)
- NBA* (Balboa)
- NLK* (Washington)

TV STATIONS (WASHINGTON, D.C.)

- WTTG, Channel 5
- NBC Network Measured Twice
- ABC Network Measured Twice
- CBS Network Measured Twice

---

* Analyzed for this study.

statistic were noted. The standard deviation is more sensitive to jumps in signals in the middle of the month than it is to jumps towards the end of the month. It does not identify drifts in phase, and it does not isolate day-to-day scattering of the received phase. However, it does provide a well defined, easily implemented measure of station performance.

IV. RESULTS

Based upon the daily phase measurements and other USNO data, LORAN appeared to be the "best" navigation system and VLF communication the "worst", with Omega in the middle. Justification follows, with consideration given to off-air time, monthly mean and standard deviation, occurrence of jumps, steps, and propagation disturbances.

In terms of off-air/transmitters(s) unstable time, the North Atlantic LORAN-C chain has had an excellent record, with the sum of off-air/unstable times for the whole system better than any single VLF communication or Omega station performance in 1973, 1974 or 1975. East Coast LORAN-C performance, however, is markedly inferior, as shown in Table C-2.

In 1973, there were enough extended periods of off-air time to make this statistic of little value in describing VLF and Omega system performance. In 1974 and 1975, however, VLF stations averaged approximately twice as much off-air time per station as did the Omega stations. In addition, VLF stations required regularly scheduled maintenance.

With regard to steps in transmissions, Table C-3 shows clearly that the VLF communication stations are far more susceptible to steps than Omega or LORAN-C stations. Using occurrence of steps as a criterion for performance, VLF communication stations are clearly inferior.

Table C-2

Minutes Per Year Off the Air/Unstable

Scheduled Maintenance Excluded

		1973	1974	1975
LORAN EAST COAST	M	470 + 66 (whole system)	25 + 101	941 + 6
	W	664	422	181
	X	1359	468	390
	Y	396	928	297
	Z	1793	276	266
LORAN NORTH ATLANTIC	M	-	-	12 (system)
	W	-	36	20
	X	-	36	79
	Y	-	-	-
	Z	-	105	28
NORTH DAKOTA		15 days + 120 events	625	757
TRINIDAD		366	403	116
NAA		8 days + 96 events	1307	411
NBA		18 days (sched.) + 445 mins.	1389	1685
NLK		5 days + 32 events	174	891

Table C-3

Occurrence of Steps in Transmissions - μSec

	1973	1974	1975
EAST COAST LORAN	6.9	-	6.1 (scheduled), 6.9
NORTH ATLANTIC LORAN	-0.5, 6.0 (scheduled)	A	6.4 (scheduled)
OMEGA NORTH DAKOTA 10.2	-	-	-4
OMEGA NORTH DAKOTA 13.6	-	-5,+5	-
OMEGA TRINIDAD 13.6	-	-	-
NAA	-11,-20,-10,+10,+2,-2 -16,+16,+15.5,-15,-162 (65 mins. drift)	+14,-14,+17,-17,+12,-12 +13,-13	-13,+13,+14,-14,+12,-5 -13,+12,-7,-13,+13,+13,+12
NBA	-1,-0.5,+1.5-1.0,+1.0 +2,+2	-2,+2,+13,-17 B	-4,-11,-10,+3,+6
NLK	+24,+23,+21,-4,+13,-14,-7,-27,+14	-10,-7,+5,-13 +22,-10,+12	+25,+12,-27,-22,-8,+5 +3,+6,+21

A Two jumps due to new measurement of chain position, plus 2.4 μs jump after an off air period.

B Three instances of instability with cycle jump or slippage, plus period of off frequency

C Stepped During diurnal shift. Also an off frequency period.

Table C-4 lists propagation disturbances observed in Washington during dayling hours. Cycle matching LORAN receivers will be largely unaffected by these disturbances, as the sky wave is not measured. These propagation disturbances will, however, adversely affect Omega and VLF communication phase measurements.

Table C-4

Occurrences of Propagation Anomalies as Measured in Washington, D.C., during Daylight

MAGNITUDE (μSEC)	1973 (MID-APRIL, ff.)	1974	1975
2-4	75	213	84
5-10	37	84	11
10-20	4	13	3
20-40	-	2	-
Other	1 PCA, 1 Strong ionospheric disturbance	2 PCA	-

Figures C-1 through C-8 show monthly mean of received phase relative to the USNO Master Clock, and also the standard deviation. The standard deviations for the VLF communication standards are larger than Omega and LORAN station standard deviations. Note that the vertical scale of the plots of monthly mean is 2 sec/inch for Loran-C, 10 μsec/inch for Omega, and 10 or 100 μsec/inch for the VLF communication stations. Thus, in terms of signal repeatability on a long term basis, LORAN-C appears best and VLF communication stations worst.

For aircraft navigation use, however, system reliability is critical because failure of a single transmitter may eliminate coverage over a wide area. Similarly, a jump in a particular station may induce a large error or cause an airborne receiver to break lock. In other words, for a wide-coverage air navigation system without redundancy, a single transmitter failure may mean that no usable navigation information is available at all.

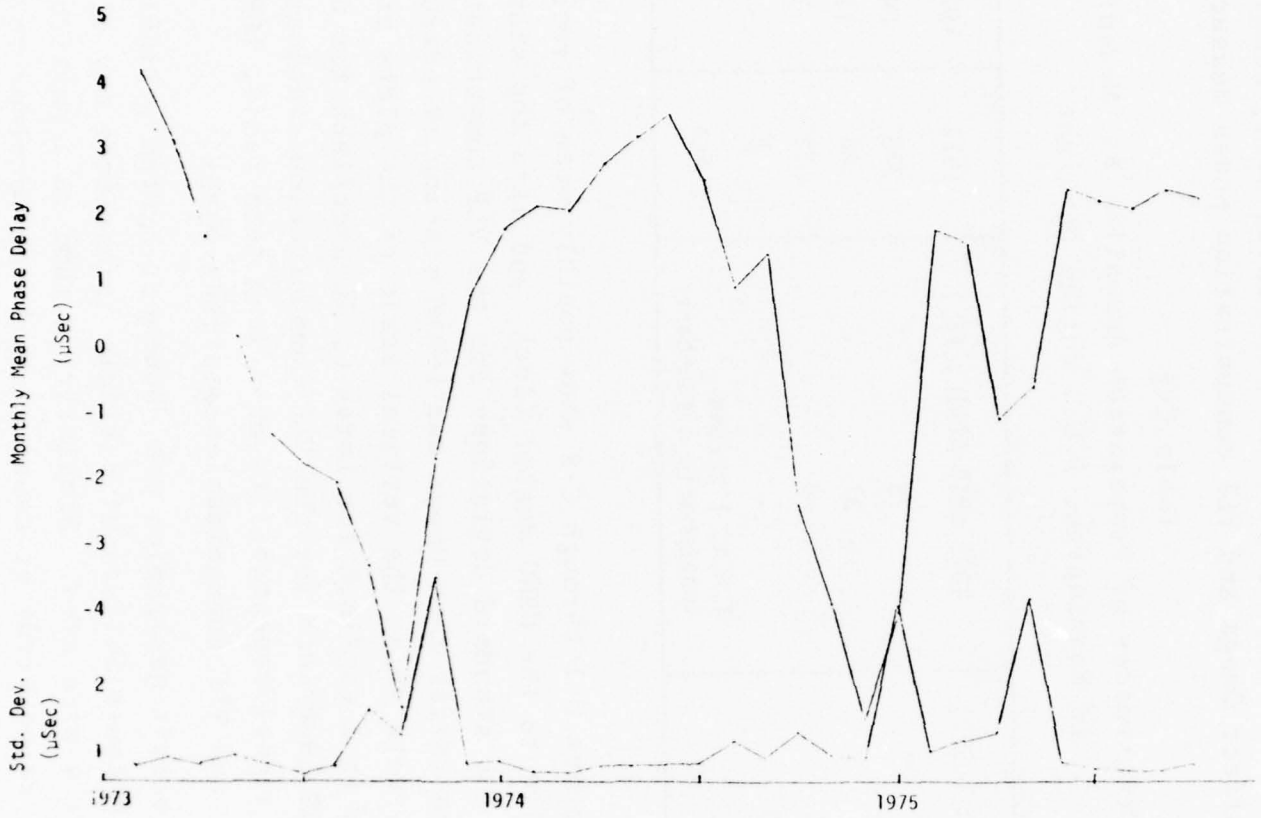

Figure C-1 East Coast LORAN-C Monthly Mean Timing Error and Standard Deviation

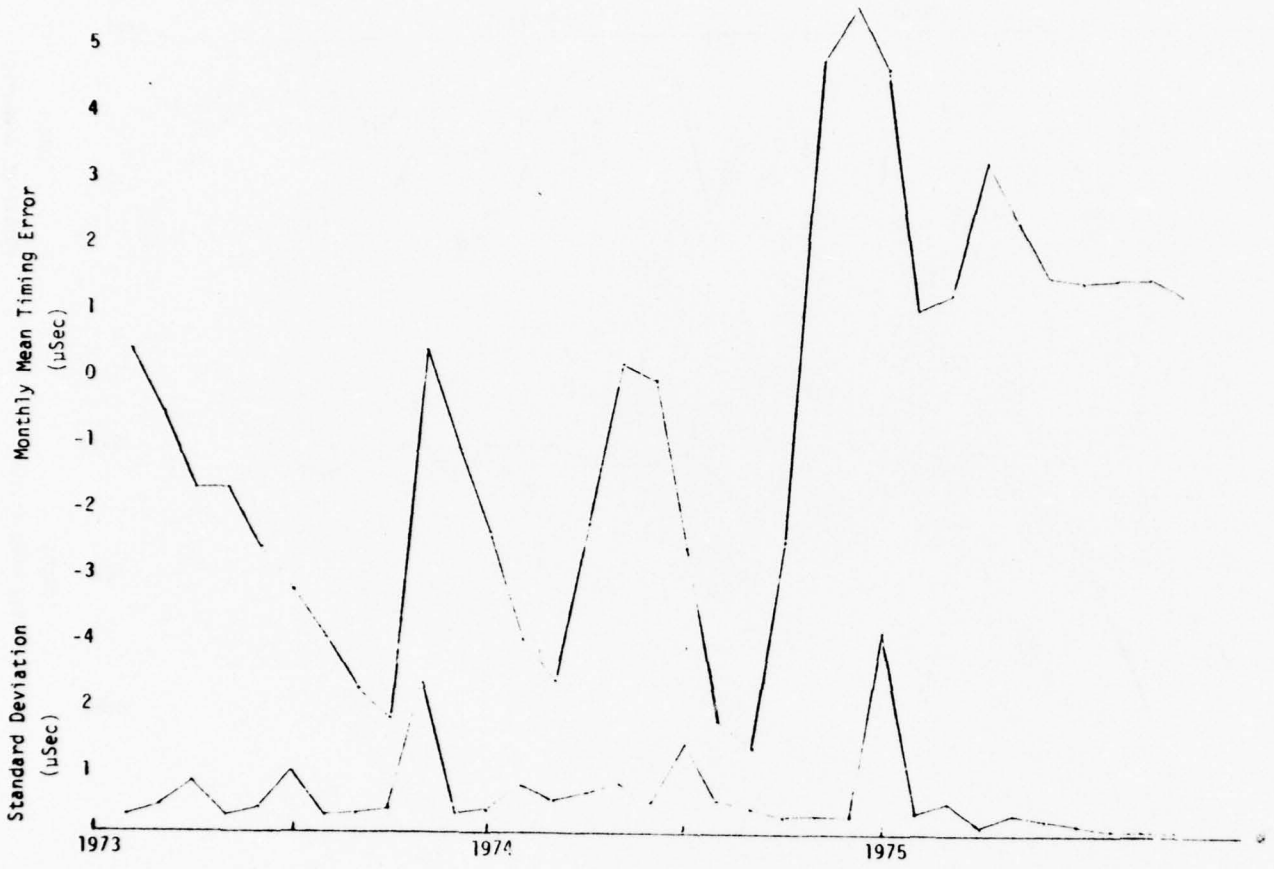

Figure C-2 North Atlantic LORAN-C Monthly Mean Timing Error and Standard Deviation

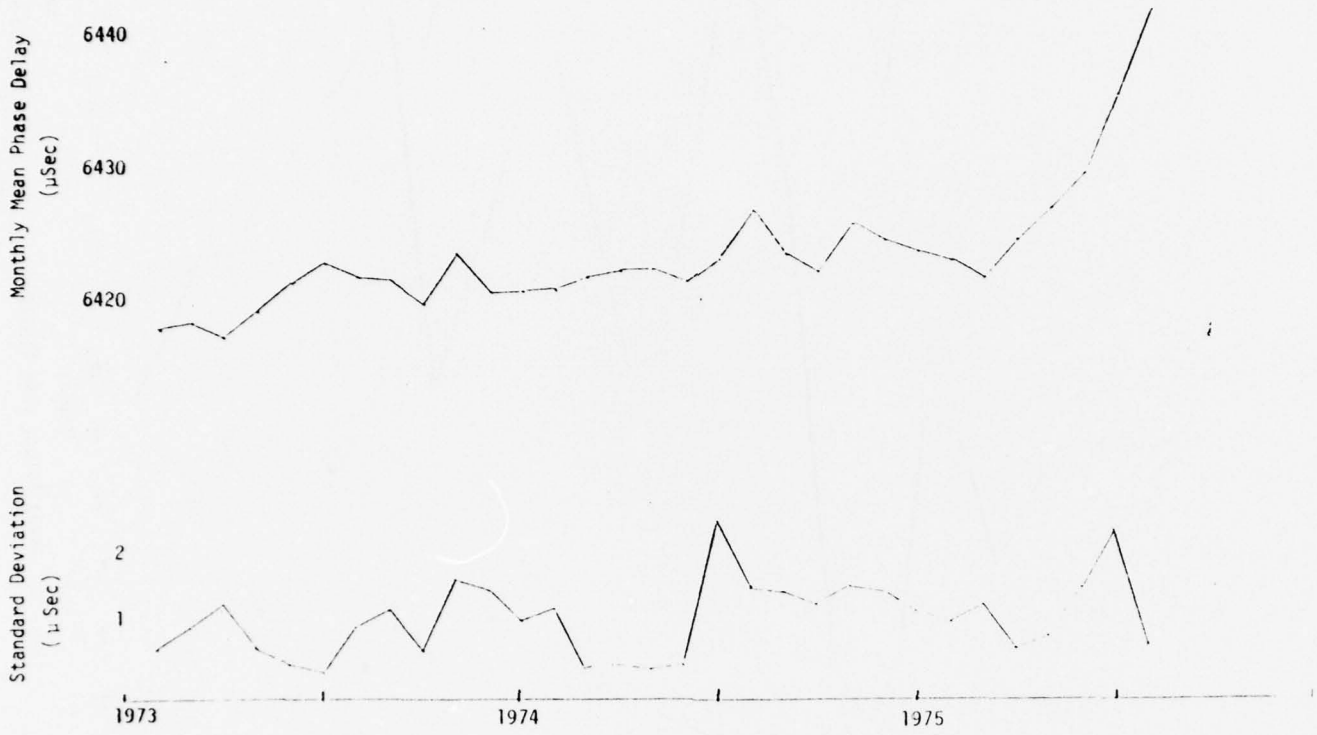

Figure C-3 Omega North Dakota (10.2 kHz) Mean Monthly Phase Delay Standard Deviation

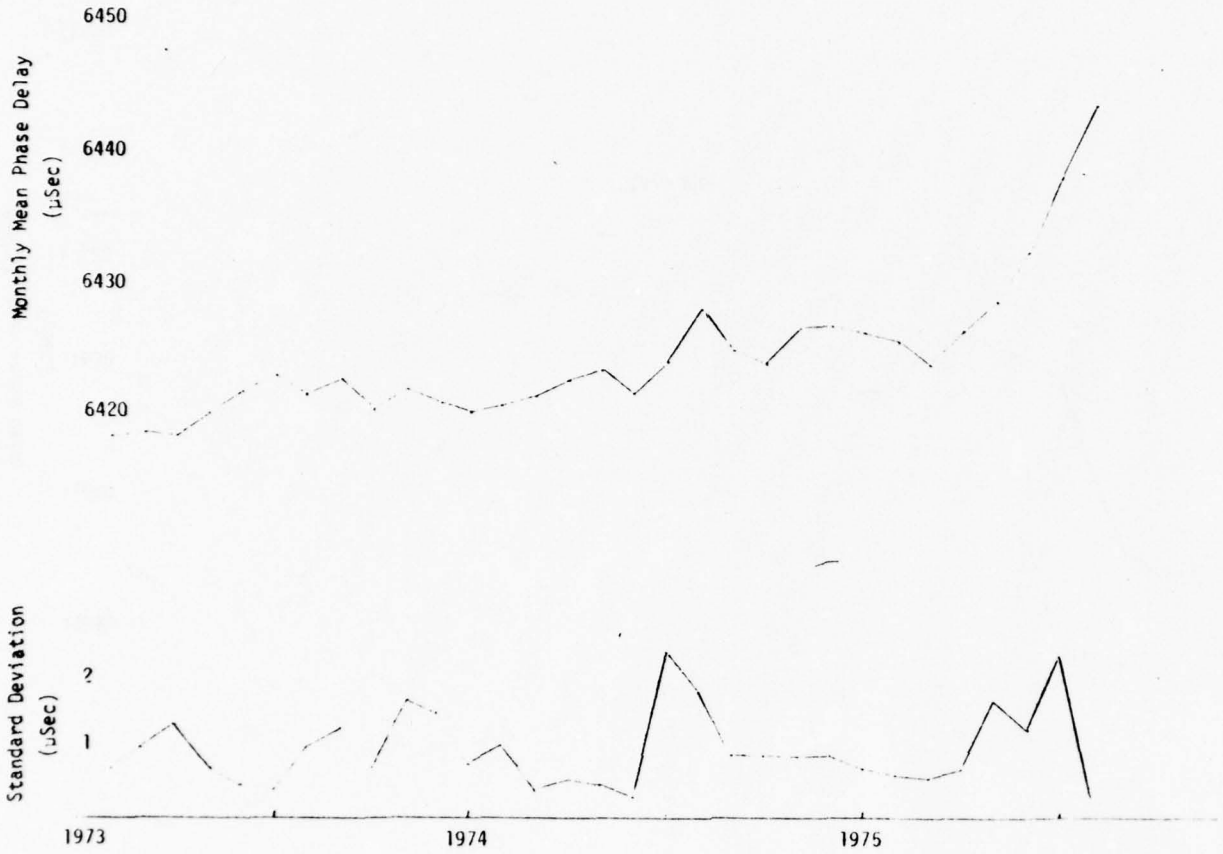

Figure C-4 Omega North Dakota (13.6 kHz) Monthly Mean Phase Delay and Standard Deviation

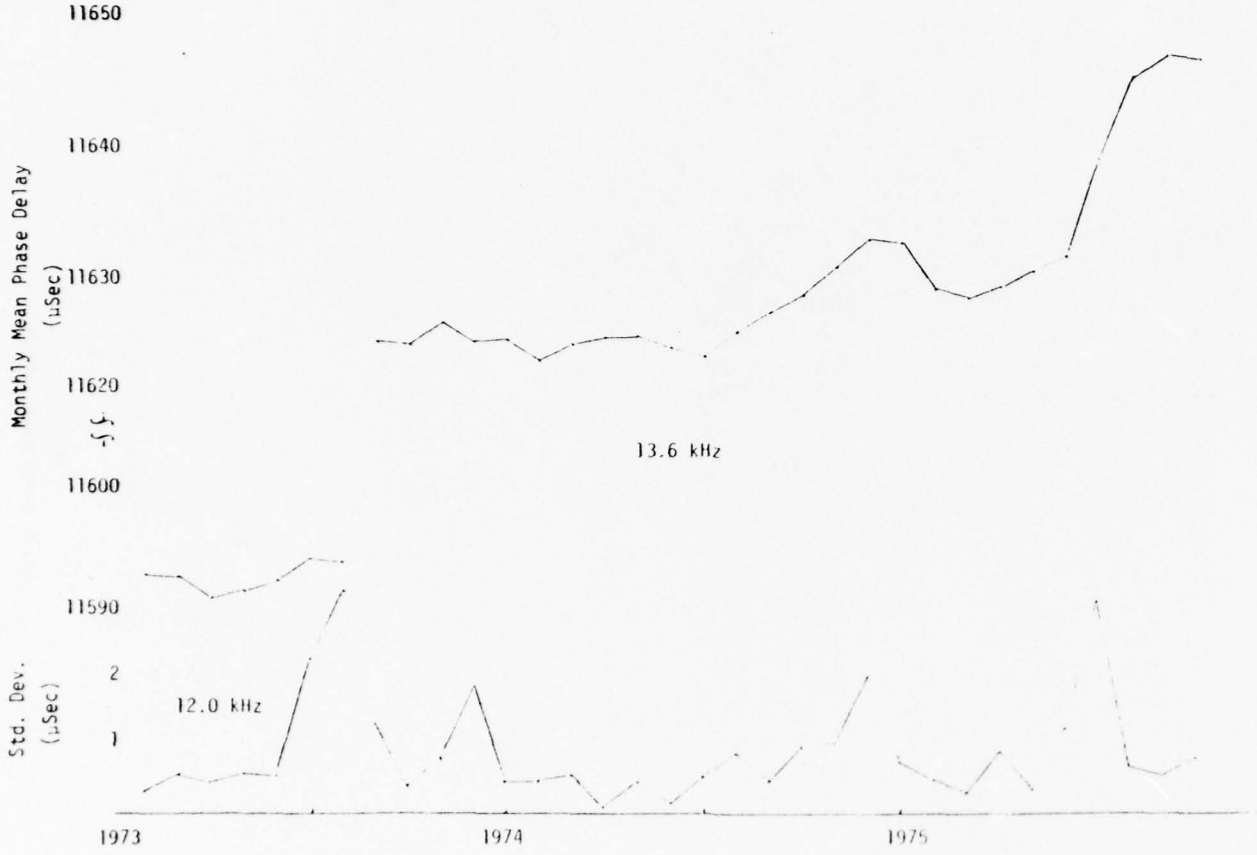

Figure C-5 Omega Trinidad Monthly Mean Phase Delay and Standard Deviation

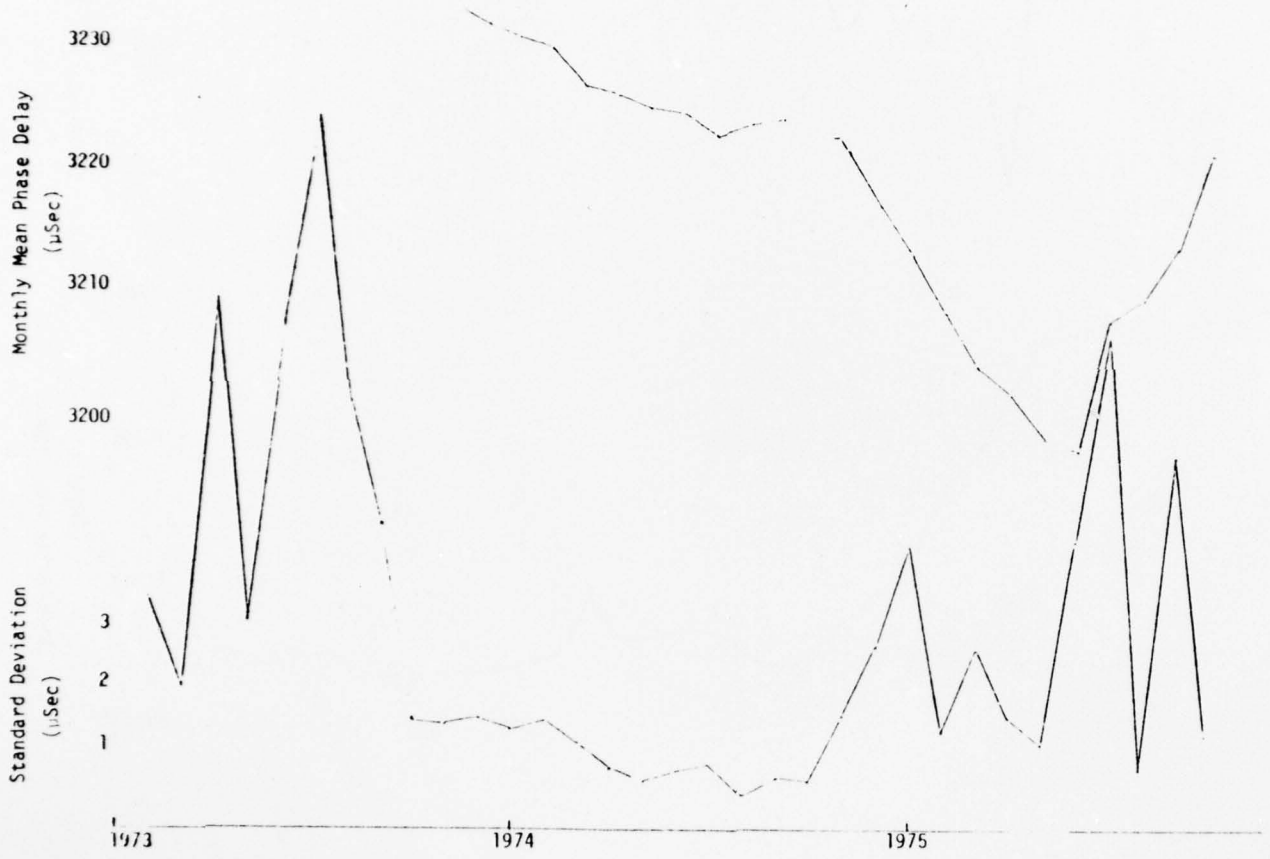

Figure C-6 NAA (Maine) (17.8 kHz) Monthly Mean Phase Delay and Standard Deviation

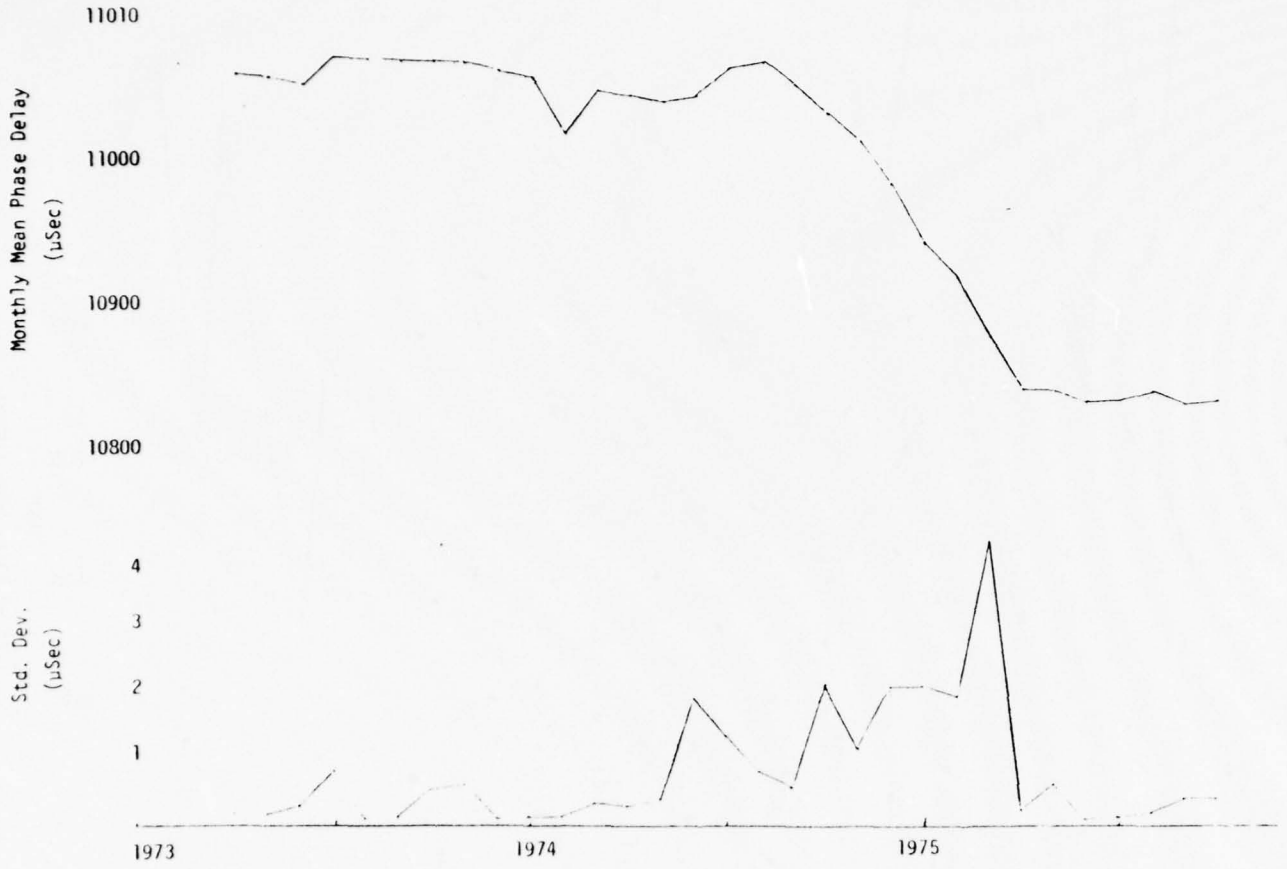

Figure C-7 NBA (Balboa) Monthly Mean Phase Delay and Standard Deviation (24.0 kHz)

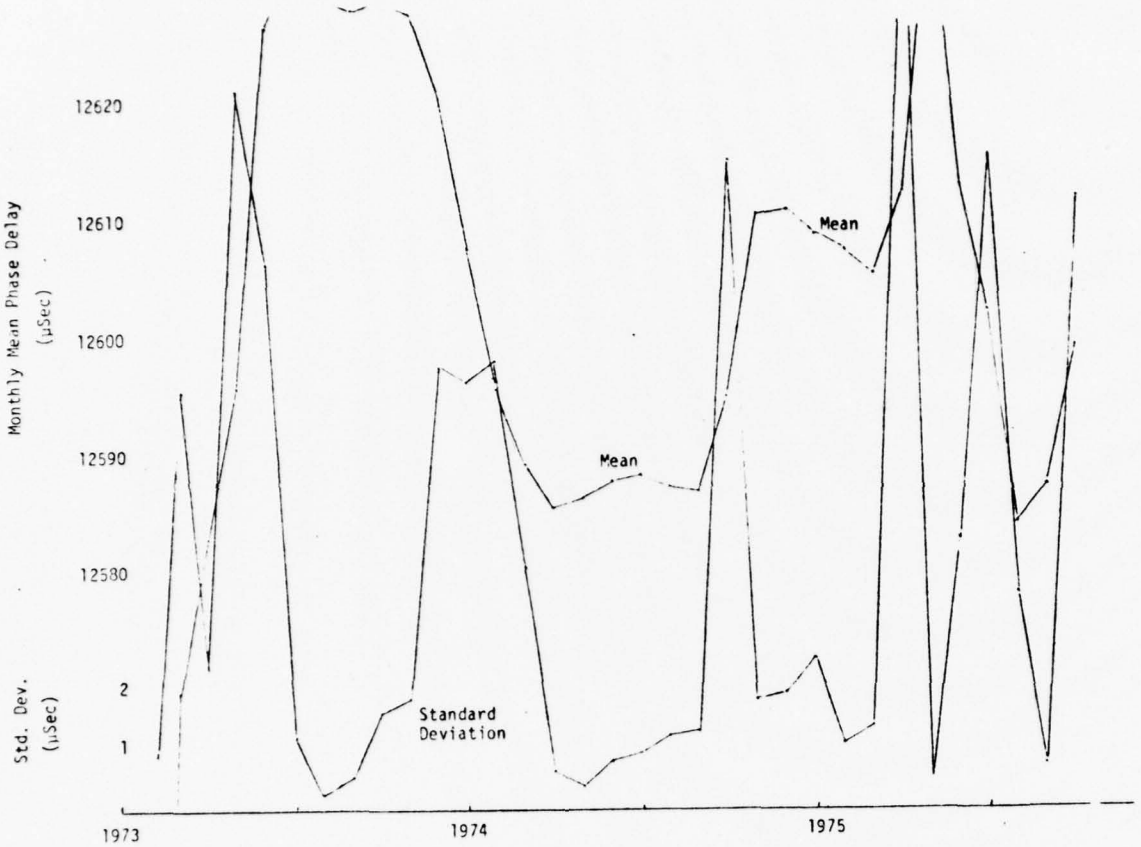

Figure C-8 NLK (Washington) Monthly Mean Phase Delay and Standard Deviation (18.6 kHz)

A limitation of the analysis of this appendix is that the measurements are made only once per day. Thus, no implications can be made as to signal quality through the day. Diurnal variations, propagation anomaly characteristics, and phase noise are not subject to this analysis.

APPENDIX D
REVIEW OF PREVIOUS OMEGA EVALUATIONS AND FIELD TESTS

D.1 INTRODUCTION

A literature search has been conducted to identify reports and articles involving measurement of actual Omega signals. The objectives, methods, results, and conclusions of each work were studied in detail to determine the contribution of each work to the body of operational Omega knowledge. The various reports are very briefly summarized to document the state of Omega evaluations to-date. However, most of these reports were based on data gathered before the Liberia, La Reunion, and Argentina Omega stations began operations. Many areas of Omega system performance remain open for investigation and study.

The works reviewed to formulate this appendix are listed in the Bibliography. Reference is made herein by the name of the work or its author.

D.2 AIRBORNE RECEIVER EVALUATIONS

Many of the documents reviewed dealt with evaluations of Omega/VLF receivers in an operational environment, or a specific Omega receiver and its initial flight evaluation following design and/or integration into a new operating configuration. Table D.1 shows the various programs which were documented. These included:

- Northrop ARN-99 - This unit was one of the first modern automatic Omega receivers, and it has been used in many applications, primarily military. These have included Omega/INS configurations for AWACS and P-3 aircraft, evaluation in an F-4, high latitude flights in a KC-135, North Atlantic crossings in a DC-8, flight evaluation in a P-3, and initial flight test results from a variety of aircraft.

Table D.1

Receiver Evaluations

RECEIVER	MODES	TEST AREAS	TEST BED	DATE
NRL/LSI MK I, II, III	**Mk I & II single frequency, Mk II Included ρ , ρ mode**	Pacific, Atlantic, Europe, Western Hemisphere	C-54, EC-121, KC-135, UH-34D	1961-1969
NRL/LSI MK III	10.2, 11 1/3 kHz Difference Frequency	Western Hemisphere	EC-121	1968
Northrop ARN-99	Three Frequency	Eglin AFB	P-3	1969
NRL/LSI MK III	Three Frequency	High Latitudes	KC-135	1970
Northrop ARN-99	Three Frequency	High Latitudes	KC-135	1970
Westinghouse C813A	10.2, 13.6 kHz		Ships, buoys	1971
Global GNS-200	VLF	Western Hemisphere	Various General Aviation	1971
ITT ARN-88	w/INS	Atlantic Undersea Test & Evaluation Center	P-3	1971
Canadian Marconi CMA-719	Three Frequency	North Sea, North Atlantic	Comet	9/71--
Global GNS-200	VLF	Canadian Arctic	Twin Otter	1972--
Northrop ARN-99	Three Frequency	Western Hemisphere	P-3	1972-1973
Canadian Marconi ARN-115	Three Frequency	Western Hemisphere	P-3	1972-1973
Northrop ARN-99	Three Frequency	Patuxent, MD	F-4	7/74
Northrop ARN-99	w/INS	Eastern US, West Africa	P-3	8,9/74
Litton ONS-21	Three Frequency	East Coast	Navaho	
Dynell Mk III	10.2 kHz Only	Northeast US	Cherokee	Spring 1975
Dynell Mk5	10.2, 13.6 kHz	North Atlantic, Carribean	B-707	June 1975--
Canadian Marconi CM-740P	Three Frequency	North Atlantic, Carribean	B-707	June 1975--

- Canadian Marconi CMA-719 - The CMA-719 receiver was another of the first automatic Omega receivers. Documentation included initial flight evaluations across the North Atlantic and in Europe, evaluations on a P-3 aircraft, and flights across the North Atlantic in both three-frequency and difference frequency operation.

- The Global GNS-200 - This unit navigates with Navy VLF communication station signal and Omega unique frequency signals. Operational use in the Canadian Arctic and numerous flight evaluations in general aviation were described.

- Dynell Mk-3 - MIT flight evaluation programs used a Dynell Mk-3 receiver in a general aviation aircraft.

- Naval Research Laboratory/Lear Siegler Mk I, II, and III Omega receivers - These early airborne Omega receivers are documented as to their performance and operational characteristics. The Mk III was evaluated extensively in various programs, including polar flights.

- Litton ONS-21 - A three frequency automatic receiver, this unit received initial flight evaluations on the East Coast.

- ITT-ARN-88 - This unit was tested on a P-3.

- Dynell Mk-5 - Although not designed specifically for airborne use, this unit was evaluated on Pan Am flights to Europe and the Carribean.

The U.S. Air Force has recently evaluated several Omega receivers in the 2041 Program. The final reports from this project were not available for inclusion in this appendix.

In general, the in-flight Omega evaluations above have been first-cut evaluations designed to answer such fundamental questions as:

- Does the receiver work?

- Where are signals available and usable for navigation?

- What are the approximate error statistics?

The above flight evaluations did not seek to answer the more detailed questions of:

- What individual noise sources were encountered?
- What was the magnitude and cause of the noises?
- When and where can these effects be expected in the future?
- Which stations exhibit best signal characteristics in particular regions?

Helicopter Omega evaluations have been performed. The Army has apparently done some differential Omega work, and the NRL/LSI MK III receiver was evaluated on a UH-34. The ARN-99 Omega receiver front end has been utilized as part of the navigation systems for the CH-46 and CH-47 helicopters at the U.S. Naval Air Test Center.

D.3 DIFFERENTIAL OMEGA SIMULATIONS/EVALUATIONS

Differential Omega shows great promise for reducing the effects of propagation anomalies. As such, it has been the subject of extensive field experimentation, with a remote monitor station used to correct other Omega data after the conclusion of the experiment.

Figure D.1 shows monitor station locations used for differential Omega. Not shown on the map are monitor sites in France, Malta, and the Bahamas. Differential Omega studies are discussed in order of geographic location, from east to west:

- In 1971, the Royal Aircraft Establishment was concerned with airborne measurement of Omega signal characteristics, and conducted flights in the Mediterranean and in Norway for evaluation of differential Omega

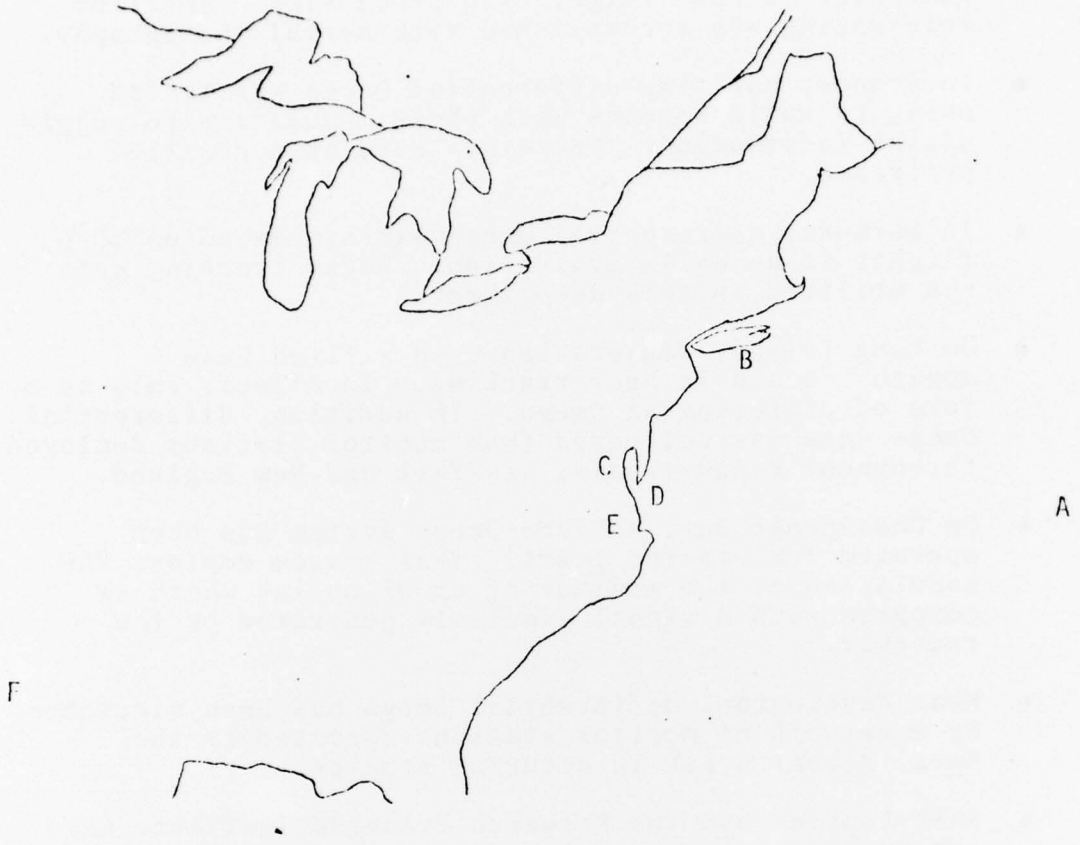

DIFFERENTIAL OMEGA SIMULATION/EVALUATIONS

A. Bermuda
B. Long Island
C. Washington, D.C.
D. Chesapeake Bay
E. NASA-Langley Area
F. Texas

Figure D-1 Differential Omega Simulation/Evaluation Sites

simulated in post-flight data processing. Position referencing was accomplished with aerial photography.

- In France, maritime differential Omega was tested using LF radio beacons with phase modulation to supply uplink information. Decca was used as a position reference.

- In Bermuda, differential Omega was simulated on DC-6 flights in an early evaluation. Radar tracking data was utilized in this experiment.

- On Long Island, Beukers Lab used a fixed base monitor to aid in buoy tracking. In effect, this is a form of differential Omega. In addition, differential Omega data was collected from monitor stations deployed throughout Pennsylvania, New York and New England.

- On Chesapeake Bay, a Micro-Omega system has been operated for several years. This system employs VLF modulation at the monitor of an HF uplink which is compared with a signal similarly generated by the receiver.

- Near Washington, differential Omega has been simulated by a network of monitor stations operated by the Naval Research Lab in accuracy studies.

- NASA-Langley and the Research Triangle Institute have extensively analyzed data from monitor stations sequentially deployed throughout Maryland, Virginia, and North Carolina. This analysis has included differential Omega studies.

- In the Bahamas, differential Omega was simulated during a series of shipboard experiments run by the U.S. Naval Oceanographic Institute.

- In Texas, a series of differential Omega tests were simulated by Tracor with the monitor data obtained simultaneously from different locations.

In summary, the concept of differential Omega has been well proven by these initial studies. Error characteristics are known for different ranges and bearings from the station for several different cases. Further ground-based studies can

supply new and valuable information concerning differential Omega characteristics in mountainous terrain, at high latitudes, and in other unusual propagation conditions. Of course, the evaluation of actual aeronautical and marine differential Omega will be necessary to give definitive information on system capabilities and limitations.

D.4 OTHER EVALUATIONS

Other Omega evaluations have covered a wide variety of topics, from integration with a ship's inertial system to feasibility of a single Omega line of position, and from in-flight measurements of modal interference to estimates of groundspeed accuracy derived from monitor data. These investigations and others are discussed below.

Fundamental measurements and analyses of Omega characteristics have been done by Pierce, Swanson and Rupp. At Harvard, measurements of phase at 10.2 and 13.6 kHz led to Pierce's concept of composite Omega. Swanson of the Naval Electronic Center has done field tests across North America to evaluate the accuracy of 1969 Skywave corrections. Rupp has made measurements at Dallas of experimental four-frequency Omega for enhanced lane resolution for use in the Global Rescue Alarm Network (GRAN). In addition to signal measurements, there have been extensive analyses conducted as part of these efforts.

Additional fundamental Omega studies have been done concerning noise sources, including Polar Cap Absorptions (PCS's), precipitation static, and modal interference. Under NRL sponsorship, monitor stations were operated on the east coast of Canada and in Washington, D.C. A proton counter was included in the high-latitude instrumentation, and showed good correlation between solar proton events and PCA's. Precipitation

static effects and occurrence have been well documented at the NOAA Environmental Research Labs in Miami by experience obtained on flights through hurricanes. Many significant contributions to Omega experience have been made by R. Burgess and his colleagues at the Royal Aircraft Establishment in England. Of particular note are flights made over the North Atlantic in 1966 and 1967, in which modal interference was detected out to 5000 km from the transmitter.

Many papers have been prepared by the Research Triangle Institute in conjunction with NASA-Langley. These reports, based upon monitor data from North Carolina, Virginia, and Maryland, have covered many aspects of Omega propagation appropriate to monitor data analysis, such as signal characteristics and sensitivity to receiver and propagation parameters, simulated differential Omega error characteristics, and composite Omega statistics.

Integration with shipboard navigation equipment has been performed to provide navigation between satellite fixes. On the USNS Redstone, a space vehicle tracking ship, satellite pass data was used to remove biases encountered in Omega transmissions. The augmented Omega data was then used to detect and remove Schuler drifts from the ship's inertial system. The NOAA ship Discoverer had similar requirements for accurate navigation between, and as back-up for, satellite fixes. These needs were satisfied with Omega.

Velocity measurement characteristics have been done at two locations. Navidyne in Virginia and Tracor in Texas have both done studies of monitor data to measure the groundspeeds of their (fixed) monitor stations. The errors of these schemes have shown that groundspeed should be measurable to approximately one knot.

Other published studies have included reports by Westinghouse and Hazeltine on the use of retransmitted Omega for tracking of various objects such as ships, buoys, balloons, aircraft, and cars. Retransmission was by HF for the Westinghouse Unit, and VHF to a satellite for the Hazeltine OPLE (Omega Position Location Experiment).

In an early work by McFarland of Ohio University, a light aircraft was flown directly along various lines of position to determine the "flyability" of this navigational mode. Thus, coordinate conversation was not accomplished.

D.5 SUMMARY

Based upon literature published to date, experimental and operational trials of the Omega system have demonstrated such basic characteristics as Omega system feasibility and accuracy in various operational modes. Experimentation in Omega system operations is now ready to move into more detailed, in-depth evaluation of signal propagation characteristics as the Omega system attains its final transmitter configuration.

In-flight evaluations of Omega, with very few exceptions, have not been concerned with detailed signal measurements. Phenomena not yet fully documented include modal interference from all of the Omega stations in different areas; terrain-related propagation anomalies; and even detailed information on signal availabilities and qualities from different stations in different areas. For use as a domestic enroute navigation system, Omega has received but a fraction of the evaluation required. Similarly, airborne differential Omega remains unevaluated. There is a strong requirement for extensive and detailed evaluations of airborne Omega in order to mature knowledge of system characteristics.

Monitor station programs have similarly provided a preliminary assessment of Omega characteristics, but much is still to be done. Most monitor programs have utilized receivers with long time constants, thus filtering out much of the dynamic information of interest to the airborne user. Similarly, monitor station locations to-date have largely ignored such inhospitable terrain as mountainous regions and the state of Alaska. Further monitor studies should be conducted, but with an emphasis on aviation related problems. For example, anomalous propagation events need not only to be measured in terms of μsec of delay, but also in terms of accuracy degradation encountered by the airborne user. In rugged terrain, it must be determined whether Omega is accurate enough for navigation in valleys or only above all terrain. Omega has great potential for use as a navigational aid in Alaska, but has not yet received an evaluation in this state characterized by wide variations in topography, surface conductivity, and meteorological conditions. Monitor data must not only be collected, but also correlated with data from other stations to satisfactorily document anomalous propagation, atmospheric noise, and other interference.

To summarize, basic Omega characteristics have been well documented for some specific areas and earlier station configurations. For use in aerial navigation, however, the detailed and extensive work of complete system evaluation remains to be done, especially with the new station configuration.

REFERENCES

1. Personal communication with Mr. Eric Swanson, NELC.

2. Scull, D.C., and Kasper J.F., Jr. "Omega Operational Development Status". Proceedings of First Annual Meeting, International Omega Association, Arlington, VA, July 1976.

3. Personal communication with Mr. Roy Farmer, Delco Electronics.

4. Pierce, J.A., "The Use of Composite Signals at Very Low Radio Frequencies", February 1968, AD 666 567.

5. Papousek, W., and Reder, F.H., "A Modified Composite Wave Technique for Omega". Navigation 20, No.2, Summer 1973.

6. Baltzer, O.J., "Use of Composite Omega in Aircraft Applications", Proceedings of the First ION Omega Symposium, Washington, D.C., November, 1971.

7. USNO, "Time Services Information Letter, "August 15, 1973.

BIBLIOGRAPHY

Proceedings of the Second Omega Symposium of the Institute of Navigation, November 5-7, 1974.

Rupp Jr., Walter E., "Experimental Four Frequency Omega Extends Lane Ambiguity."

Lytle, Carroll D. and Bradshaw, Edward S., "A Comprehensive Experimental Program for Investigation of Various Omega Operational Modes."

Comstock, Allen L. and Rounion, William A., "Report on the Results of more than Five Years of Testing Micro-Omega, a form of Differential Omega."

Baxa, E.G. and Piserchia, P.V., "Recent Results on Parametric Analysis of Differential Omega Error."

Nard, Georges, "State of Experimentation and Program of Development of Differential Omega in France."

Fischer, R.L., "Airborne Omega Navigation System Integration and Test."

Steyle, David A., "Mix and Match: A Hybrid Omega - Inertial Airborne Navigation System."

Smith, Edgar J., "Flight Test of an ARN-99(V)2 Omega Navigation Set in F-4 Aircraft."

Barker, Clifford, A., "Error Characteristics of Omega Derived Velocity."

Dickerson, Norman C., "Airborne ONS - A Low Cost Alternate to INS."

Baxa, E.G. and Lytle, C.D., "On Observations of Model Interference of the North Dakota Omega Transmission."

Proceedings of the First Omega Symposium of the Institute of Navigation, November 9-11, 1971.

Leslie, Frank, R., "Omega Short Term Ranging Precision."

Linfield R.F. and Jackson E.J., "A Digital Omega Sensor for Remote Platform Positioning."

Courtwood, Willard M., "An Evaluation of Differential Omega."

Proceedings of the First Omega Symposium of the Institute of Navigation, November 9-11, 1971. (Cont'd.)

Luken, Konrad, "Omega Phase Shifts in the Auroral Region due to Solar Phenomena."

Couzens, R., "The Accuracy of Connected Omega Close to a Transmitter."

MacTaggart, Don, "Design and Performance of CMA-719 Computerized Airborne Omega Receiver."

Rey, J.A. and Sakran, F.C., "The AN/ARN-99(v) Airborne Omega Navigation Set: Capabilities and Status."

Lawrence, Lt. J.G., and Lake, L., "Report on Omega System Operation aboard NOAA Ship Discover."

Tymerzaynym, Jos. J., "Potential Operational Advantages of Low Cost VLF/Omega Navigation Equipment."

Eisenberg, R.L., Thornbill, A.F., and Williams, M.F., "Development and Flight-Testing of Pre-production Omega Aircraft Receivers and Antennas."

Leaver, Maj. Carl A., "Omega Polar Navigation Performance."

McFarland, R.H., "The Flyability of Raw Omega Phase Data."

Nard, Georges, "Results of Recent Experiments with Differential Omega."

Hawkes, Keith M. and Birnbaum, David, "Integration and Flight Test of an Omega Receiver with the P-3C Aircraft Navigation System."

Lubin, Jack S. and Lewis Billy M., "Effects of Weather on Airborne Omega."

Hastings, Charles E. and Rounion, William A., "Test of Combination of Omega, Micro-Omega, and Raychist."

Reynolds, P.R.J., "Interim Report on Pan American World Airways Omega Navigation Evaluation," June 1975.

Burgess,B., "Propagation Effects and Lane Ambiguity Resolution in Omega," RAE Tech. Report 68151, November 1966.

Hoffman, Howell, Howoschinsky, & Wischmeyer, "Flight Evaluation of Omega Navigation in a General Aviation Aircraft" NASA CR-132720, April 1975.

McLarnon, R.P., "VLF Navigation in the Canadian Arctic - A Pilot's View," Canadian Aeronautics & Space Journal, September 1975.

Baxa, E.G. Jr., "Implementation of an Experimental Program to Investigate the Performance Characteristics of Omega Navigation," NASA CR-132516, 1973

Pierce, J.A., "The Use of Composite Signals at Very Low Radio Frequencies," ONR Report No.552, Feb., 1968.

Sage, F.G., "NRL/LST Mk III Airborne Omega System," Navigation, Winter 1969-1970

Swanson, E.R., "Accuracy of Omega Navigation System using 1969 Skywave Corrections," NELC Report 1675, Dec. 31, 1969.

Luken, K., Brogden, J.W. & Meyers, W.D., "Accuracy Studies of the Differential Omega Technique," NRL Report 7102, June 29, 1970.

Enge, F.J., "Application of Omega Position Location Experiment to Mass Transportation," Navigation, Winter 1969-1970.

Baxa, Britt, et al, "Investigation into the Propagation of Omega Very Low Frequency Signals and Techniques for Improvement of Navigational Accuracy including Differential and Composite Omega," NASA CR-132276, 1970-1971.

Tracor, "Differential Omega Test and Evaluation Program," Doc. 67-135-U, Jan. 18, 1967.

Northrop Corporation, "Operational Evaluation of an Airborne Omega Navigation System." FAA-RD-74-10,1, 1971.

Wright, Julian, "Accuracy of Omega/VLF Range-Rate Measurements," Navigation, Spring 1969.

Baltzer, O.J., "Omega test Result - DG-6 Aircraft Flight to Bermuda," (Unpublished Report), September 1968.

Sakran, F.C. and Birch, P.B., "Flight Tests of Two Airborne Omega Navigation Systems," Navigation, 1974.

Hwoschinsky, P.V., "Flight Evaluation of Omega Navigation for General Aviation," NASA CR 132611, 1975.

Beukers, J.M., "Accuracy Limitations of the Omega Navigation System Employed in the Different Mode.", Navigation, Spring 1973.